Title: Cutin as a key player in plant immunity: from the polymer chemistry to the biological function of its composing oligomers

Dissertation presented to obtain the Ph.D. degree in Plants for Life

Author: Carlos Jorge da Silva Moreira

Supervisors: Professor Cristina Silva Pereira
Professor Cyril Zipfel

Applied and Environmental Mycology Laboratory
Instituto de Tecnologia Química e Biológica (ITQB NOVA)
Universidade Nova de Lisboa
Av. da República, Quinta do Marquês
Estação Agronómica Nacional
2780-157 Oeiras
Portugal

I declare that the work presented in this thesis, except where otherwise stated, is based on my own research. It was supervised by Professor Cristina Silva Pereira (ITQB NOVA) and Professor Cyril Zipfel (IPMB UZH). The work was performed at *Instituto de Tecnologia Química e Biológica António Xavier, Universidade Nova de Lisboa;* and *Institute of Plant and Microbial Biology, University of Zurich*, between March 2017 and September 2021.

I am grateful for the financial support provided by ARALAB Equipamentos de Laboratório e Electromecânica Geral Lda, through the PhD contract 06/PlantsLife/2017, within the scope of the Plants for Life PhD program; by EMBO through the short-term fellowship 8003; and by the European Research Council through the grant ERC 2014-CoG-647928 to Cristina Silva Pereira and the University of Zurich to Cyril Zipfel. I also thank the CERMAX unit of ITQB-NOVA, Oeiras, Portugal, where the NMR data was acquired with equipment funded by FCT. I acknowledge the PhD program Plants for Life and the members of the thesis committee Dr. Elena Baena and Dr. Paula Duque for their valuable contributions.

“The absence of evidence is not the evidence of absence.”

Carl Sagan (1934-1996)

TABLE OF CONTENTS

CHAPTER III

CHAPTER IV

CHAPTER V

Acknowledgements

My PhD was an unforgettable journey in which I was constantly challenged and had the opportunity to learn in very distinct research environments, confirming that research fulfils me and is the career I want to pursue in the near future.

First, I wish to thank my wife Clévia for always believing in me, for her patience, motivation and constant support. Also, for the sacrifices that she and my beautiful son Gonçalo passed so that I could follow my dream. I thank my parents António and Eva, my sister Sónia and my godfather Raúl for their support at every step of the path that brought me to this moment.

Friends always gave me strength in difficult moments. Thank you very much Celso Martins and Rúben Rodrigues (Powerpuff trio) for the constant encouragement. A big thank you to all members of Confraria do Chouriço for the social gatherings. I also need to acknowledge the members of the cutin gang: Artur Bento, Vanessa Correia, Rita Escórcio, Ana Tomé and Ricardo Barras for all the things they taught me and for all the help, without you this moment would not be possible. A big thank you for all the members of both teams in which I developed my project for the amazing work environment. A sincere thank you to my dear friends Isabel Monte, Priya Pimprikar, Julien Gronnier and Samy Carbonnel that were my family in Zurich.

Finally, I want to thank both my supervisors. Cristina Silva Pereira was the first person believing in my potential and I am very glad for all the moments passed under her supervision. I have learned a lot with our conversations, brainstorming exercises, and guidance moments. More than an amazing leader, Cristina became a good friend. Cyril Zipfel inspired me for the way he thinks about science and immediately I knew I wanted to work and learn with such an amazing leader. Thank you for also believing in me and for all the guidance that impacted positively the development of my scientific skills. More than supervisors, I have chosen both as mentors for my scientific career.

Summary

The cuticle is the outermost defensive barrier in land plants, constituting a shield that protects against both biotic and abiotic stresses. It is comprised by a group of organic solvent soluble lipids that are commonly referred to as waxes and the plant polyester cutin.

Several functions have been assigned to cutin over the years including prevention of water loss, protection against UV radiation, proper organ formation, mechanical support and restriction of pathogen invasion. The last has been studied over the last decades, exploring how specific alterations of the cutin polymeric structure influence plant susceptibility to infection. An alternative angle is to understand if cutin degradation by pathogens constitutes a source of signals able to elicit plant immunity. It was demonstrated in several plant species that cutin monomers are able to induce immune responses such as reactive oxygen species accumulation, induction of specific defense genes and production of antimicrobial compounds. Nevertheless, a gap in the knowledge remained on the role of oligomeric molecules released during the early stages of degradation of the cutin barrier during infection.

Over the last decades, a wealth of knowledge was gathered on cutin composition and biosynthesis; nevertheless, deciphering cutin's structural organization continues to be a challenge The main difficulties hindering the acquisition of molecular-level structural information of cutin *in planta* result from its insoluble nature, association with other cuticular components (waxes and polysaccharides), and intrinsic complexity. Traditional cutin isolation techniques involve a subtractive approach consisting of an enzymatic removal of polysaccharides and an extensive dewaxing process exploring different organic solvents with different polarities. Most attempts to solve the puzzle of cutin structure have focused on solid state-based analysis of the whole polymer through spectroscopic techniques. An alternative approach was to study the products of the total and partial depolymerization of cutin through mass spectrometry-based methods.

In this thesis, I used cutin isolated from tomato as a model. We generated an original approach to create an *ex situ* platform to study cutin chemistry, structure and physical properties. At the same time, I used chemical depolymerization to mimic cutin degradation during infection and study the resulting hydrolysates. Finally, I systematically characterized the potential of these mixtures to activate plant immunity in model plants.

In Chapter I, I describe the main motivations behind the PhD project developed on this thesis and the objectives that were defined as measures of success. An extensive literature review is then presented, exploring *Solanum lycopersicum* and *Arabidopsis thaliana* as models for the study of cutin chemistry. Advances in the analytical tools available are then presented, guiding the reader to the major advances in the knowledge on cutin structure. The last sections focus on the biosynthetic pathway of this plant polyester, how proper cutin formation influences its biological roles and to which extent cutin derived molecules may influence plant immunity. Along the chapter, relevant contributions of the work developed on this thesis to the current state of the art are highlighted.

Chapter II describes the establishment of an original ionic liquid-based methodology to isolate cutin from the peels of tomato fruits. Moreover, a novel approach combining this isolation methodology with cryogenic milling of the recovered polyester allowed for the first time to obtain solution-state NMR spectra of cutin. Quantitative analyses are presented confirming the high level of preservation of the recovered polymer and new chemical features, such as presence of free acid groups, are assigned to cutin. To further validate the importance of the findings resulting from this chapter, a systematic characterization of cutin isolated from the miniature cultivar Micro-Tom is presented. Analysis of cutins isolated from wild type and mutants of important biosynthetic genes (*GPAT6* and *CUS1*), highlight the potential of cutin for biotechnological exploitation, namely due to its thermal resistant characteristics.

Chapter III deepens the characterization of cutin's chemical and physical signatures, by exploring the suitability of the established methodology to isolate cutin from a different plant source (red pepper). Moreover, powerful quantification strategies were employed, taking advantage of the possibility to perform solution-state NMR analyses. A comparison between the recovered cutins is then performed with suberin extracted by either cork or potato peels. Moreover, the thermal behavior of each plant polyester is evaluated through DSC and features of its structural architecture, namely degree of crystallinity, assessed by WAXS. Due to its proved thermal resistance, cutin from tomato is then further characterized by exploring cutin extracted from the model tomato Micro-Tom from the same genotypes explored in the previous chapters. This characterization allows to understand that specific mutations lead to alterations on the chemistry and structural arrangement of cutin, directly influencing its thermal resistance, rendering materials that are highly attractive for further biotechnological exploitation. The data collected in this chapter allowed to propose the rules of thumb for the quantification of the structure-property relationship that constitute a guide for future selection of bio-based polymers for the development of novel materials.

Chapter IV describes how the ionic liquid isolated cutins are useful for the study of its biological roles, namely activation of plant immunity. Using a highly preserved cutin recovered from tomato pomace, we were able to generate cutin oligomeric mixtures (COMs) that have proven induction of immune responses in model plants. We also describe that a highly preserved cutin, mimicking the polymer state in the initial stages of degradation by pathogens is also able to initiate activation of the plant immune system. Hallmark immune outputs, such as Ca^{2+} influx and MAP kinase activation, were triggered by both cutin and COMs. Moreover, a unique transcriptional reprogramming was described as the result of the treatment of *Arabidopsis thaliana* plants with COM. We propose in this chapter cutin-derived oligomers as novel DAMPs, able to activate plant immunity during the initial stages of pathogen infection. Initial studies, still ongoing, on the chemical

characterization of these oligomeric mixtures are also presented in the last section of the chapter, further confirming the oligomeric and lipidic nature of the active molecules.

To finalize this dissertation, Chapter V presents an integrative discussion on the main findings and original contributions to the current state of the art made by this thesis. More than just presenting the main achievements, new questions arose generating parallel projects that are also highlighted in this chapter. To end, future steps to solve the remaining mysteries on the mechanism of action of COM are presented.

Sumário

A cutícula é a barreira defensiva mais externa das plantas terrestres, constituindo um escudo protetor contra stress biótico e abiótico. É constituída por um grupo de lípidos solúveis em solventes orgânicos, normalmente designados de ceras, e pelo poliéster vegetal cutina.

Inúmeras funções têm sido atribuídas à cutina ao longo dos anos, incluindo prevenção da perda de água, proteção contra radiação UV, formação adequada dos órgãos da planta, suporte mecânico e restrição da invasão por agentes patogénicos. Esta última, tem sido estudada ao longo das últimas décadas, explorando o modo como alterações específicas da estrutura polimérica da cutina influenciam a suscetibilidade da planta à infeção. Um ângulo alternativo consiste em perceber se a degradação da cutina pelos agentes patogénicos constitui uma fonte de sinais capazes de ativar a imunidade nas plantas. Foi demonstrado, em várias espécies de plantas, que os monómeros de cutina são capazes de induzir respostas imunitárias tais como: acumulação de espécies reativas de oxigénio, indução de genes específicos de defesa e produção de compostos antimicrobianos. Ainda assim, um vazio no nosso conhecimento permanece, no que diz respeito ao papel de moléculas oligoméricas, libertadas durante os estágios iniciais de degradação da barreira de cutina durante a infeção.

Ao longo das últimas décadas, um manancial de conhecimento foi recolhido acerca da composição e biossíntese de cutina, no entanto, decifrar a organização estrutural da cutina continua a ser um desafio. Os maiores obstáculos à obtenção de informação estrutural, ao nível molecular, da cutina na planta, resultam da sua natureza insolúvel, da associação com outros componentes cuticulares (ceras e polissacáridos), bem como da sua intrínseca complexidade. As técnicas tradicionais usadas no isolamento de cutina envolvem uma abordagem subtrativa, consistindo na remoção enzimática de polissacáridos e remoção extensiva das ceras através do uso de diferentes solventes orgânicos com polaridades distintas. A maioria das tentativas de resolver o puzzle da estrutura da cutina focaram-se em análises

de estado sólido do polímero como um todo, através de técnicas de espectroscopia. Abordagens alternativas consistiram no estudo dos produtos resultantes da despolimerização total ou parcial da cutina, através de métodos baseados em espectrometria de massa.

Nesta tese, a cutina isolada das peles de tomate foi usada como modelo. Geramos uma abordagem original, de modo a criar uma plataforma *ex-situ* que possibilita o estudo da composição química da cutina, bem como da sua estrutura e propriedades físicas. A despolimerização química foi também usada como ferramenta para recriar a degradação da cutina que ocorre durante a infeção, e estudar os hidrolisados resultantes. Por fim, uma caracterização sistemática do potencial destas misturas para ativar a imunidade em plantas foi realizada, recorrendo a plantas modelo.

No capítulo I, comecei por descrever as principais motivações por detrás deste projeto de doutoramento, bem como dos objetivos definidos como medidas de sucesso do mesmo. Uma revisão extensiva da literatura é apresentada, explorando duas plantas modelo para o estudo da composição química da cutina, *Solanum lycopersicum* e *Arabidopsis thaliana*. São depois apresentados os principais avanços nas técnicas analíticas disponíveis, guiando o leitor para os avanços na compreensão da estrutura da cutina. As últimas secções focam-se na biossíntese deste poliéster vegetal, na forma como a formação apropriada da cutina influencia as suas funções biológicas e, até que ponto, moléculas derivadas de cutina podem influenciar a imunidade da planta. Ao longo do capítulo as contribuições relevantes, que resultam do trabalho desenvolvido nesta tese, para o avanço do conhecimento no estudo de cutina são destacadas.

O capítulo II descreve o estabelecimento de uma metodologia original, baseada em líquidos iónicos, para isolar cutina da pele de tomate. Para além disso, uma nova abordagem que combina este método de isolamento com moagem criogénica do polímero recuperado permitiu, pela primeira vez, a obtenção de um espectro de cutina em solução através de ressonância magnética nuclear (RMN). Análises quantitativas são apresentadas,

confirmando o elevado grau de preservação do polímero recuperado e, novas assinaturas químicas, como a presença de grupos ácidos livres, são atribuídas à cutina. Para validar a importância das descobertas apresentadas neste capítulo, uma caracterização sistemática de cutinas isoladas do tomate miniatura Micro-Tom é apresentada. A análise das cutinas isoladas das plantas de tipo selvagem e de mutantes de genes importantes para a biossíntese da cutina (*GPAT6* e *CUS1*), destaca o potencial da cutina para exploração biotecnológica, nomeadamente devido à sua resistência térmica.

O capítulo III aprofunda a caracterização das assinaturas química e física da cutina, através da exploração da adequabilidade do método de isolamento estabelecido para fontes vegetais alternativas, nomeadamente a pele do pimento. Para além disso, tirando partido da possibilidade de realizar RMN em solução, estratégias de quantificação robustas foram aplicadas neste estudo. Uma comparação entre as cutinas recuperadas de fontes distintas e suberina extraída da cortiça e da pele da batata é realizada. Adicionalmente, o comportamento térmico de cada poliéster é avaliado através de varredura diferencial de calorimetria (DSC) e, características da sua arquitetura estrutural, nomeadamente o grau de cristalinidade, avaliado por difração de raios-X a grandes ângulos (WAXS). Devido à sua comprovada resistência térmica, a cutina de tomate é então detalhadamente caracterizada, explorando cutina extraída do tomate modelo Micro-Tom e utilizando os mesmos genótipos do capítulo anterior. Esta caracterização permite perceber que mutações específicas conduzem a alterações na composição química e organização estrutural da cutina, influenciando diretamente a sua resistência térmica. Tais características permitem obter materiais que são altamente atrativos para futura exploração biotecnológica. Os dados recolhidos neste capítulo permitiram propor as regras para a quantificação da relação entre estrutura e propriedades, as quais constituem um guião para a futura seleção de biopolímeros para o desenvolvimento sustentável de novos materiais.

O capítulo IV descreve a utilidade de cutinas isoladas usando líquidos iónicos para o estudo das suas funções biológicas, nomeadamente a ativação da imunidade das plantas. O uso de uma cutina altamente preservada, isolada do bagaço do tomate, permitiu gerar misturas oligoméricas de cutina (COMs) que possuem atividade comprovada de indução de respostas imunitárias em plantas modelo. Também é descrito neste capítulo que uma cutina altamente preservada, representativa do estado do polímero nas fases iniciais de degradação por agentes patogénicos, é também capaz de iniciar a ativação do sistema imunitário da planta. Respostas imunitárias chave tais como influxo de cálcio e ativação de MAP quinases são atribuídas tanto à ação da cutina como das COMs. Para além disso, uma reprogramação transcricional única é descrita como resultado do tratamento das plantas de *Arabidopsis thaliana* com COM. Apresentamos neste capítulo oligómeros derivados de cutina como novos padrões moleculares associados a dano (DAMPs), capazes de ativar a imunidade da planta durantes os estágios iniciais de infeção por agentes patogénicos. Estudos iniciais, ainda a decorrer, relacionados com a caracterização química destas misturas oligoméricas são também apresentados na última secção deste capítulo, comprovando a natureza oligomérica e lipídica das moléculas ativas.

Para finalizar esta dissertação, o capítulo V apresenta uma discussão integrada das principais descobertas e contribuições originais para o avanço do conhecimento no estudo de cutina, feitas por esta tese. Mais do que uma simples apresentação dos principais avanços alcançados, novas questões surgiram, gerando projetos paralelos que são destacados neste capítulo. Por fim, os passos seguintes a dar para tentar solucionar os mistérios que subsistem, acerca do mecanismo de ação das COM são apresentados.

Thesis publications

Carlos J.S. Moreira[#], Artur Bento[#], Joana Pais, Johann Petit, Rita Escórcio, Vanessa G. Correia, Ângela Pinheiro, Łukasz P. Haliński, Oleksandr O. Mykhaylyk, Christophe Rothan, and Cristina Silva Pereira. "An Ionic Liquid Extraction That Preserves the Molecular Structure of Cutin Shown by Nuclear Magnetic Resonance", *Plant Physiology*, 2020, Volume 184, 592-606. (https://doi.org/10.1104/pp.20.01049) [#]equally contributing authors

Artur Bento, **Carlos J. S. Moreira,**[±] Vanessa G. Correia,[±] Rita Escórcio, Rúben Rodrigues, Ana S. Tomé, Nathalie Geneix, Johann Petit, Bénédicte Bakan, Christophe Rothan, Oleksandr O. Mykhaylyk and Cristina Silva Pereira. "Quantification of structure-property relationships for plant polyesters reveals suberin and cutin idiosyncrasies", *ACS Sustainable Chemistry & Engineering*, 2021.
(https://doi.org/10.1021/acssuschemeng.1c04733) [±]equally contributing authors.

List of acronyms

^{13}C MAS NMR	Carbon Magic Angle Spinning Nuclear Magnetic Resonance
^{1}H NMR	Proton Nuclear Magnetic Resonance
2D	Two-Dimensional
2-MHG	2-Mono(10,16-dihydroxy-Hexadecanoyl) Glycerol
^{31}P NMR	Phosphorus Nuclear Magnetic Resonance
ABA	Abscisic Acid
ABC	ATP Binding Cassette
ArE	Aromatic Ester
ATL2	Arabidopsis Toxicos en Levadura 2
ATP	Adenosine Triphosphate
ATR	Attenuated Total Reflection
ATT	ABERRANT INDUCTION OF TYPE THREE
BAHD	Benzyl alcohol O-acetyltransferase Anthocyanin O-hydroxycinnamoyltransferase N-Hydroxycinnamoyl/benzoyltransferase Deacetylvindoline 4-O-acetyltransferase
BAK1	BRASSINOSTEROID INSENSITIVE 1-ASSOCIATED RECEPTOR KINASE 1
BDG	BODYGUARD
BKK1	BAK1-LIKE 1
BMIM	1-Butyl-3-Methyl-Imidazolium
BSA	BOVINE SERUM ALBUMIN
CarbE	Carbohydrate Ester
CUD1	CUTIN DEFICIENT 1
CEP	Cutin Embedded Polysaccharide
CERK1	CHITIN ELICITOR RECEPTOR KINASE 1
COSY	^{1}H-^{1}H Correlation Spectroscopy
COM	Cutin Oligomeric Mixture
CUS1	CUTIN SYNTHASE 1

cv	Cultivar
CXT	CUTIN:XYLOGLUCAN TRANSACYLASE
CYP	CYTOCHROME P450
DAG	Diacylglycerol
DAMP	Damage-Associated Molecular Pattern
DCA	Dicarboxylic Acid
DCR	DEFECTIVE IN CUTICULAR RIDGES
DDO	Dodecan-1-Ol
DEG	Differentially Expressed Gene
DMSO	Dimethylsulfoxide
DSC	Differential Scanning Calorimetry
EE	Ethyl Ester
EH	EPOXIDE HYDROLASE
EMS	Ethyl Methanesulfonate
ETI	Effector-triggered Immunity
FTIR	Fourier Transform Infrared
GC-MS	Gas Chromatography – Mass Spectrometry
GDSL	Gly-Asp-Ser-Leu ESTERASES/ACYLHYDROLASES
GlyE	Glycerol Ester
GMC	GLUCOSE-METHANOL-CHOLINE OXIDASE
GO	Gene Ontology
GPAT	GLYCEROL-3-PHOSPHATE ACYLTRANSFERASE
GRP	GLYCINE-RICH PROTEIN
HPA	16-Hydroxypalmitic Acid
HRMAS	High Resolution Magic Angle Spinning
HSQC	Heteronuclear Single Quantum Coherence
HMBC	Heteronuclear Multiple Bond Correlation
HRP	HORSERADISH PEROXIDASE
HTH	HOTHEAD
IG	Induced Gene
LACS2	LONG-CHAIN ACYL-COA SYNTHETASE 2

LC-MS	Liquid Chromatography tandem Mass Spectrometry
LCR	LACERATA
LAE	Linear Aliphatic Esters
LRR	Leucine-Rich Repeat
LTP	LIPID TRANSFER PROTEIN
MAG	Monoacylglycerol
MALDI-TOF	Matrix-Assisted Laser Desorption Ionization Time-of-Flight
MAPK	MITOGEN-ACTIVATED PROTEIN KINASE
ME	Methyl Ester
MLG	Mixed-Linked β-1,3/1,4-Glucans
MS	Mass Spectrometry
MT	Micro-Tom
NBS	Nucleotide-Binding Site
NMR	Nuclear Magnetic Resonance
OE	Overexpression
OG	Oligogalacturonide
OH	Hydroxyl
OHFA	Hydroxy Fatty Acids
PAE	Primary aliphatic esters
PAMP	Pathogen-Associated Molecular Pattern
PBS	Phosphate-Buffered Saline
PCA	Principal Component Analysis
PDR	Pleiotropic Drug Resistance
PE	Propyl Ester
PEC	PERMEABLE CUTICLE
PER	PEROXIDASE
PI	Protease Inhibitors
PR	Pathogenesis Related
PRR	Pattern Recognition Receptor
PTI	Pattern-Triggered Immunity

PVDF	Polyvinylidene Difluoride
RK	RECEPTOR KINASE
RLCK	RECEPTOR-LIKE CYTOPLASMIC KINASE
RNA	Ribonucleic Acid
RNAi	RNA Interference
ROS	Reactive Oxygen Species
RST	Resurrection
SAE	Secondary Aliphatic Esters
SAXS	Small-Angle X-Ray Scattering
SDS-PAGE	Sodium Dodecyl Sulphate-Polyacrylamide Gel Electrophoresis
SEM	Scanning Electron Microscopy
SERK	SOMATIC EMBRYOGENESIS RECEPTOR KINASE
SHN	SHINE TRANSCRIPTION FACTOR
SM4	SYMPTOMS TO MULTIPLE *AVR* GENOTYPES 4
TAG	Triacylglycerol
TBS	Tris Buffered Saline
TBS-T	Tris Buffered Saline + Tween-20
TC	Tomato Compal
TFA	Trifluoroacetic Acid
TLC	Thin Layer Chromatography
TMS	Trimethylsilyl
UV	Ultraviolet
WAXS	Wide-Angle X-Ray Scattering
WIN	WAX INDUCER
WT	Wild Type

CHAPTER I

Chapter I contains the motivations and main objectives of the studies conducted on this project and a critical state-of-the-art review covering relevant aspects of the plant polyester cutin (chemistry, structure and functions), the contribution of the original work developed and future perspectives.

Accordingly, this chapter includes the following manuscript under preparation planned for submission as a review paper:

A Cutin Odyssey - Biosynthesis, Chemistry and Biological Roles - The Trident that Builds a Protective Barrier

Carlos J. S. Moreira, Artur Bento, Rita Escórcio, Vanessa G. Correia, Ricardo Barras, Cyril Zipfel, Cristina Silva Pereira

Author Contributions

C.J.S.M. prepared the initial draft of the manuscript; A.B., R.E. and R.B generated the figures and all authors participated in the writing, review and editing of the final version of this chapter.

Outline: This chapter presents the motivation behind the project, the experimental approach and main objectives. To contextualize the work developed, a critical state-of-the-art review is also presented, covering aspects of cutin's chemistry, structural arrangement and biological roles played by this important plant polyester.

Motivation and Objectives

Land plants have evolved a complex extracellular structural lipid polymer barrier to limit water loss, protect against UV radiation, strengthen their cell walls, and restrict microbial penetration – the cuticle. The polymeric matrix of this defensive shield – cutin, participates in the activation of defense responses during plant-pathogen interactions. Specific cutin monomers have the ability to activate plant immune responses, as observed by exogenous application of these monomers on *Arabidopsis thaliana* leaves. This treatment leads to higher resistance to necrotrophic fungi of *Arabidopsis* mutants expressing a fungal cutinase (*cute* plants), which present higher cuticle permeability.

A key question is whether, during the initial stages of its degradation by pathogens, cutin-derived oligomeric molecules with a certain degree of esterification are able to activate plant immunity, leading to hallmark responses such as apoplastic ROS burst and Ca^{2+} influx, further potentiating the activation of downstream signaling mechanisms.

I hypothesize that the cutin polymer (or oligomeric degradation products thereof) act as elicitors of the plant immune system, thereby conferring increased disease resistance to fungal pathogens. We are interested in unravelling the level of esterification of cutin-derived molecules that is needed to initiate a defensive response.

My major goal was to establish an *ex-situ* approach to characterize cutins with low degree of ester cleavage and oligomers obtained through their controlled chemical degradation in their ability to elicit pattern-triggered immunity. To guide discovery, an ionic liquid methodology to extract a highly esterified cutin (less than 5 % of ester cleavage) was established (Chapter II).

The characterization of the isolated cutins was performed through Scanning Electron Microscopy (SEM), solution-state Nuclear Magnetic Resonance (NMR), Gas Chromatography – Mass Spectrometry (GC-MS) and Differential Scanning Calorimetry (DSC). Apart from the establishment of a novel method for an uncomplicated recovery of cutin, the NMR acquired data of the cutin polymer reached unprecedent chemical resolution, improving current knowledge on its chemistry, *e.g.* identification of free end groups (Chapter II). Besides, collectively the acquired data opened new perspectives for its biotechnological exploitation, especially through the establishment of a quantitative correlation between the chemistry and the physical properties of plant polyesters (Chapter III). A library comprising the polymer, mixtures of oligomers obtained through its controlled hydrolysis (methanolysis) and monomers obtained through its complete alkaline hydrolysis or commercially available ones was built. Their capacity to act as immune elicitors was then tested in model plants using established chemiluminescence-based bioassays. These tests assessed the ability of each compound/mixture to trigger the production of apoplastic ROS and/or Ca^{2+} influx. Compounds/mixtures eliciting at least one of these defense responses, were evaluated for the capacity to activate mitogen-activated protein kinases. Finally, the best elicitor was characterized for its ability to trigger transcriptional reprogramming in the model plant *A. thaliana* (Chapter IV).

To contextualize the work developed, a comprehensive state-of-the-art review is presented in this chapter, containing already the contributions made so far by the studies developed within the scope of this PhD project.

A Cutin Odyssey - Biosynthesis, Chemistry and Biological Roles - The Trident That Builds a Protective Barrier

Carlos J. S. Moreira[1], Artur Bento[1], Rita Escórcio[1], Vanessa G. Correia[1], Ricardo Barras,[1] Cyril Zipfel[2,3], Cristina Silva Pereira[1]

[1] Instituto de Tecnologia Química e Biológica António Xavier – Universidade Nova de Lisboa (ITQB NOVA), Avenida da República 2780-157 Oeiras – Portugal

[2] Institute of Plant and Microbial Biology, Zurich-Basel Plant Science Center, University of Zurich, 8008 Zurich – Switzerland

[3] The Sainsbury Laboratory, University of East Anglia, Norwich Research Park, NR4 7UH, Norwich – UK

Introduction

One of the most impactful events in the evolution of life on earth was the colonization of land environments by plants approximately 470 million years ago[1]. This transition from an aquatic environment to land, often referred to as terrestrialization, led to the formation of terrestrial ecosystems as we know them today[2]. The importance of land plants is commonly associated with the increase in atmospheric oxygen that facilitated the bloom of animal life[3]. Nevertheless, other roles like providing shelter, food and even shaping the climate of our planet are still essential nowadays[4].

In order to survive an extremely desiccating environment, plants had to develop numerous adaptations to allow them to control water loss, to cope with constant UV radiation and to resist temperature stress[2]. One of the key adaptations was the development of a lipidic barrier called cuticle, which is deposited at the outermost surface of epidermal cells[5]. This barrier covers the aerial organs of most land plants and recently was also proposed to be present in the early stages of root cap formation[6]. The roles that are assigned to the cuticle include water loss control that is stomata-independent, protection

against UV radiation, prevention of organ fusion, mechanical reinforcement of the epidermal cell wall, and restriction of pathogen invasion[7].

The cuticle is composed of a polymeric matrix of the plant polyester cutin to which several lipids, usually referred as waxes, are associated. The cuticle is divided in two layers – the cuticular layer, which is enriched in cutin with embedded polysaccharides[8]; and the cuticle proper more enriched in waxes. These waxes can either occur within the polyester matrix (intra-cuticular waxes) or accumulate on top of the cutin layer (epicuticular waxes)[9].

Cutin is a polymer mainly composed by a network of long-chain fatty acids that provides the essential platform for the association of the other cuticle components. Additionally, cutin is extremely resistant to decay, even more than highly recalcitrant plant polymers such as lignin[10]. This characteristic allowed to trace this polyester back to fossil samples that date from approximately 400 million years ago in the *Devonian* period[11]. Altogether, these characteristics confirm cutin as central player in the roles assigned to the cuticle, thus of key relevance for the understanding of plant's evolution and adaptation.

With this review, we intend to give an overview of our current knowledge on cutin, covering aspects ranging from its biosynthesis to the chemistry and how the latter influences the biological roles of cutin within the cuticular matrix. While focusing mostly in two well-studied plant models – *Solanum lycopersicum* and *Arabidopsis thaliana* – relevant examples are also highlighted in different plant species to provide insights on the natural variability on the organization of this natural polyester.

Cutin

Cutin is a key component of the plant cuticle, a barrier that constitutes the interface between the plant and the external environment, covering the aerial organs of most land plants[7]. The exceptions are woody plants that present in their stem outer barks the polyester suberin, which is also present in the underground organs of plants[12]. Cutin can be found deposited on the outer surface of the epidermal cells and is assumed to have a role in first-line defense against both biotic and abiotic stresses[5]. However, very recently, it was demonstrated that a cutin-like polyester can be found during the early stages of *Arabidopsis* seedling establishment as part of a root cap cuticle, also showing defensive properties[6]. Although challenging the idea that cutin is only found in aboveground organs, this study points to a transient occurrence of cutin aiding root establishment previous to suberization of the endodermis of these tissues. This observation supports the idea defended by *Fich et al.* 2016, that, although cutin and suberin are always defined as distinct polymers, it is possible that this distinction is artificial and both polymers may exist as a single compositional continuum *in planta*.

Cutin is a plant polyester mainly based on C_{16} and C_{18} ω-hydroxy fatty acids with the presence of mid-chain hydroxyl groups, linked through ester bonds. Glycerol, aromatics and even dicarboxylic acids may also be present in residual amounts[13]. Although presenting this general composition, the chemistry of this polymer shows great variability between organs, developmental stage and plant species. In general, C_{16} ω-hydroxy acids are always present as key monomers, while the relative amount of the C_{18} monomers presents wide variation[14].

Taking *Arabidopsis thaliana* and *Solanum lycopersicum* as model plants, a comparison between their polymers reveals major compositional differences, highlighting the variability that cutin can display at a chemical level. The hydrolysate cutin' constituents identified in *Arabidopsis* leaves (obtained through extensive depolymerization reactions) demonstrated an enrichment in unsaturated C_{18} α, ω-dicarboxylic acids[15], similar to that found

in the epidermis of *Arabidopsis* stems[15]. Contrary to that reported for most plant species, cutin from *Arabidopsis* contains very reduced levels of mid-chain oxygenated compounds[16]. Due to this unusual chemical composition, these cutins are usually referred to as dicarboxylic acid (DCA)-rich cutins. Recent analyses, showed that glycerol, a monomer that is usually residual in most cutins, presents a molar ratio of 2:1 (glycerol: DCAs) in both leaf and stems of *Arabidopsis*[17]. Glycerol is a key cross-linking unit in plant polyesters and its abundance dramatically impacts the structural organization of these polymers[18]. Due to glycerol high abundance in cutin from *Arabidopsis*, the polymer structure differs from the usually reported cutin structural models. In the flowers of this model plant, the major cutin monomer is 10, 16-dihydroxyhexadecanoic acid, a common monomer in most species[13]. As referred above, a recent study performed on root cap formation led to the discovery of an atypical cutin polymer present in the early stages of root formation in *Arabidopsis* seedlings as part of a protective cuticle-*like* barrier. This polymer was enriched for C_{18} fatty acids together with a high contribution of C_{26} and C_{28} very long chain fatty acids that are uncommon monomers of plant cutins, as well as the unusual aromatic compound sinapic acid[6]. Altogether, the knowledge on the chemistry of *Arabidopsis* cutins is furthering the uniqueness of the cutin of this species that is however, as expected, also organ specific, opening questions about the localization-structure-function relationship.

Tomato is a well-established plant model for the study of cutin composition and structure[19]. Particularly, the peels of the fruit constitute a very appealing source of polymer due to its astomatous nature, which provides a continuous cuticular layer that can be easily recovered[20]. In general, tomato cutin consists of a mixture of C_{16} and C_{18} hydroxy fatty acids with small amounts of glycerol and aromatic compounds such as coumaric acid. Previous studies on the Ailsa Craig cultivar showed that during the maturation process of the fruit, C_{16} components can account for up to 88 % (*wt*) of the total cutin load, while C_{18} components accounted for up to 12 % (*wt*)[21]. The

monomer 9(10), 16-dihydroxyhexadecanoic acid is the most abundant at all developmental stages from immature green to red ripe. Although the precise amounts of some compounds may change, the abundance of the most representative monomers systematically increases along the maturation stages of the fruit, even the most residual ones such as coumaric acid[21]. A different study corroborated the classification of tomato cutins as C_{16} enriched cutins, further quantifying the presence of coumaric acid (< 0.5 %) and glycerol (up to 5 % *wt*) in the tomato fruit cutin[22]. In figure 1, an illustrative representation of the type of cutin isolated from different organs is presented for both *Arabidopsis* and tomato. Recently, it was also reported a higher presence of epoxide groups in cutin isolated from the peels of *Capsicum annum* (red pepper). Although being a C_{16} polyester[23], the presence of these chemical groups drastically influences its polymeric architecture[24].

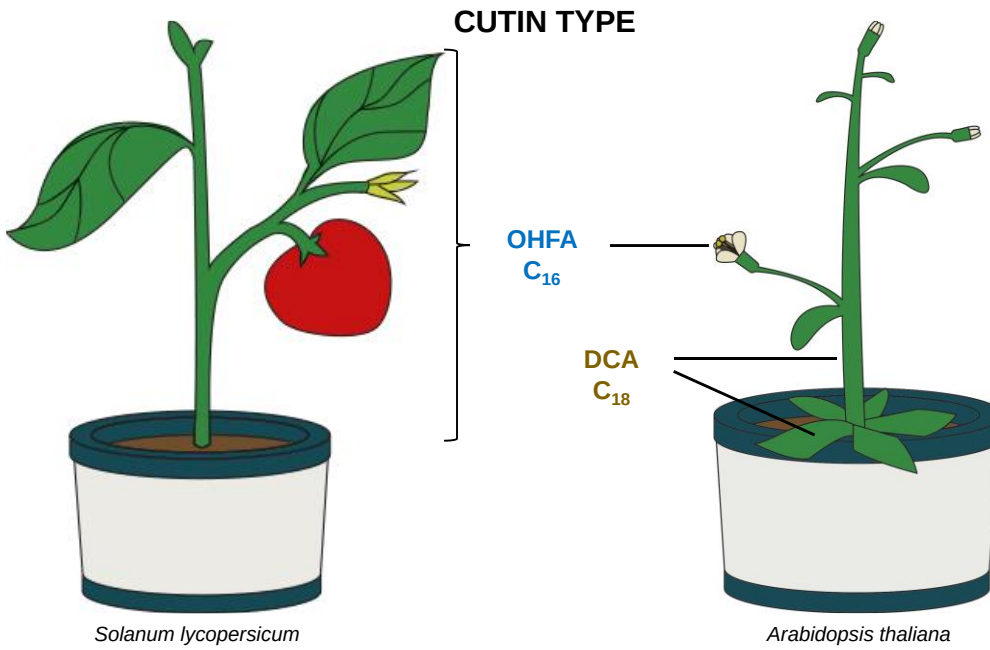

Figure 1. Schematic representation of the types of cutins found in different plant organs. Further details in figure 2.

Other plant species belonging to the same genus also show major differences in leaf cutin composition. This was highlighted through comparison of two species of eucalyptus that showed that both cutins were enriched for C_{18} monomers, but the ratio between C_{18} and C_{16} monomeric components was almost two-fold higher in *Eucalyptus camaldulensis* compared to *E. globulus*[25]. A similar trend was observed for the relative abundance of α, ω-dicarboxylic acids and glycerol. The observed differences on cutin composition inform that the structures of the polymer may differ significantly, even in closely related species[25].

Analytical tools used in cutin characterization

Despite our current knowledge on the composition and biosynthesis of the plant polyester cutin (and the continuously reported advances) unravelling its structural arrangement is still a major challenge. The main obstacles to acquire molecular-level structural information of cutin *in planta* – apart from those arising from limitations in the established techniques – result from cutin's insoluble nature, assembly with other cuticular components that hinders its purification, and inherent complexity due to a branched plus reticulated structure comprising variable monomer compositions[14]. To date, two main complementary strategies have been employed to study cutin: (1) the analysis of the whole polymer obtained through subtractive removal of the associated cuticular constituents or (2) the analysis of the hydrolysate obtained after its total or partial depolymerisation[14]. The most common approach to recover a near-native cutin (*i.e.* as found *in planta*) comprises the enzymatic removal of polysaccharides through the action of cellulases and pectinases, followed by a thorough dewaxing process using organic solvents with different polarities[26]. This approach has allowed for several structural characterization studies that involved Nuclear Magnetic Resonance (NMR)[27], Fourier Transform Infrared (FTIR) and/or Raman spectroscopic approaches[28]. Although promising, the best that these spectroscopic techniques can provide are parts of the puzzle (though significant) that reveal either a time-averaged

structure or a statistical distribution of possible structures. In particular, cutin spectral features through solid state NMR analysis show many overlapping signals[27]; an archetypal feature observed in other complex multifunctional polymers[29]. Better resolution can be attained using HRMAS that rely on the viscous phase promoted by the swelling of the polymer mediated by a deuterated solvent. HRMAS resolution can be further enhanced when using a 2D mode that increases the quality of the structural information that can be retrieved[14]. Spectroscopic approaches have played an important role on our current understanding of cutin by providing important information on the identity and conformation of specific functional groups[20]. Like solid state NMR, Raman and FTIR have the advantage of not destroying the samples; yet some limitations exist. For example, in Raman, the interference caused by the fluorescence effect may lead to signals overlap, and, in FTIR, the signal of water may mask other signals and the sample thickness and homogeneity influences the signal saturation[28].

To complement the information retrieved by the direct characterization of the polymer, diverse depolymerization techniques have been employed to obtain monomers and/or oligomers that help to elucidate how they are linked together. The most common approaches rely on the use of a strong base (*e.g.* NaOH) or a strong acid (*e.g.* HCl) to extensively hydrolyze the polymer. The resultant hydrolysate is usually analyzed by Gas Chromatography-Mass Spectrometry (GC-MS). This technique is very reliable not only for the identification but also for the quantification of cutin monomers/oligomers, allowing also to infer, to some extent, structural data[18,22]. Nevertheless, in some cutins, a part of the polymer might be recalcitrant to hydrolysis, and amongst the hydrolysate constituents some non-volatile high molecular weight oligomeric structures may be found. An alternative approach is to perform mild depolymerization reactions; usually using sodium methoxide ($NaOCH_3$) or calcium hydroxide ($Ca(OH)_2$) to obtain cutin oligomers that can be analyzed for example through solution-state NMR, increasing significantly the level of resolution and providing clues about the intramolecular linkages

between the polyester units[22]. The controlled depolymerization of cutin can also be attained through the action of cutin hydrolytic enzymes (cutinases), to obtain both monomers and oligomers. This strategy can be coupled to group specific labelling techniques such as dansylation or benzyl-O-alkylation, which allows for the determination of cutin oligomeric structure when combining several Mass Spectrometry (MS) methodologies[30]. Benzyl etherification of free OH groups of cutin is an experimental strategy used to probe cutin polymerization and when combined to GC-MS and Raman microspectrometric imaging allows to infer esterification and polymerization levels of this plant polyester[20]. The current reality points out for the need of multidisciplinary approaches that would involve the expertise of both polymer chemists and plant researchers, in a combined effort to improve the current methodologies to recover and analyze these complex polymers.

Very recently, we proposed an alternative methodology for the recovery of a near native cutin from the peels of fleshy tomato fruits[31]. This methodology uses as extraction solvent the ionic liquid cholinium hexanoate, which apparently dissolves most of the cuticular components except the polymer cutin that can be purified simply by filtration. Besides the inherent time efficiency of the extraction process, our data showed that different ionic liquids can selectively solubilize distinct cutin-associated polysaccharides, opening the possibility to resolve important questions in the mechanism of transport of cutin precursors. In our study, the ensuing polymer was submitted to extensive cryogenic milling to reduce its crystallinity and particle size yet eliminating possible oxidation side-reactions. This innovative strategy allowed for the first time to perform solution-state NMR analysis of cutin[31], constituting a decisive step forward to decipher its structural arrangement. Moreover, the possibility to obtain two-dimensional solution-state NMR spectra and perform quantifications either through ^{31}P NMR or by the use of an internal standard further enhanced the quality of the data. As such, the quantitative methods support/validate the assignments and the relative quantification of specific groups (free acids, aliphatic and aromatic hydroxyls and total esters) allowing

to establish direct comparisons between wild type and mutant plants impaired in key biosynthetic genes[24,31]. The combination of this strategy with the analysis of its monomeric/oligomeric constituents can provide means to overcome some of the major limitations inherent to the study of complex plant polymers, such as cutin. Additionally, it can push forward the understanding of cutin biosynthesis and its deposition *in planta*. This ionic liquid-based strategy to recover a highly esterified and preserved cutin polymer as well as its solution NMR characterization are further discussed in Chapter II.

Cutin structure

From all the efforts made over the years to try unraveling the structure of this polymer, several models on the architecture of cutin have been proposed. In a recent review, *Fich et al.* (2016) propose three possible molecular structures based in different monomeric compositions. The possibilities were: **a)** an elongating linear chain with single hydroxyl group fatty acids; **b)** a branched structure due to the presence of dihydroxy fatty acids; **c)** or the presence of dicarboxylic acids and glycerol that would allow for ester cross-link to occur. The truth is that the insoluble nature of cutin and its, still unclear, association with the epidermal cell wall, makes structure determination a huge challenge, but several contributions are here presented. A schematic representation of the most commonly found functional groups of cutin is depicted in figure 2.

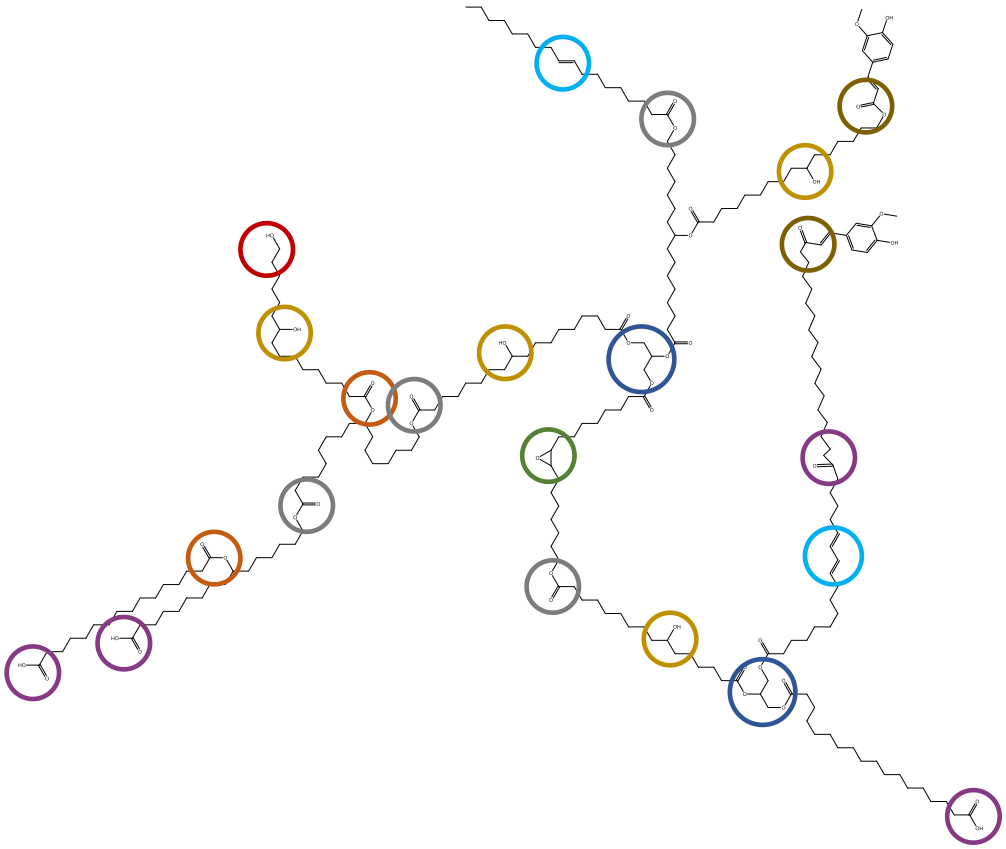

Figure 2 – Schematic representation of the most commonly found functional groups of plant cutin. Circle colors indicate the putative positions of each functional group (primary aliphatic ester, secondary aliphatic ester, acylglycerol ester, aromatic ester, primary hydroxyl groups, secondary hydroxyl groups, free acids, epoxide groups and alkene groups) in the structural arrangement of the plant polyester cutin.

As previously mentioned, in *A. thaliana*, one of the best characterized models, it was demonstrated that dicarboxylic acids account for more than 40 % of the total cutin monomer load, indicating that these are key structural components both in leaves and stems. One possibility is that these α- ω dicarboxylic acids could bridge hydroxyl groups from the aliphatic backbone of cutin to the ones present in cell wall components through ester bonds[16]. Additionally, the low mid-chain hydroxylation observed could lead to a less crosslinked arrangement and a parallel alignment of the aliphatic

chains. Both characteristics are in line with the observation that the cutin from *Arabidopsis* is much more similar to what is reported to suberin, a related polymer also DCA-rich, rather than with other cutins[16]. The presence of glycerol in this plant polyester was observed several years ago[18], but its structural role was just recently demonstrated. A molar ratio of 2:1 (glycerol: DCA) was observed in both leaves and stems of *Arabidopsis* plants. Moreover, loss of monomers in mutants depleted of key biosynthetic genes kept this proportion in the analyzed cutins, leading the authors to propose that Glycerol-DCA-Glycerol may constitute the major structural unit in *Arabidopsis* cutin[17]. Such an arrangement was seen in the past for suberin, although unusual, it is in line with the observations of *Franke et al. 2005*. One of the implications is related to the insolubility of cutin, which would require that at least one of the glycerol groups would be directly linked to the cell wall components. This way, cutin would be considered an heteropolymer instead of a polyester of exclusive lipidic nature[17]. As ω-hydroxy fatty acids (ω-OHFA) are considered keys monomers in most cutins it was important to understand how this structural organization would accommodate them. Three possibilities were proposed: 1 – cutin would be formed of Glycerol-DCA-(ω-OHFA)*n*-Glycerol units; 2 – (ω-OHFA)*n* would be esterified in different positions with glycerol; 3 – the DCA-rich domains of cutin would be spatially separated from the C_{16} ω-OHFA rich cutin[17].

A different study comparing distinct plant cutins provided clear evidence that a representative feature of the structure of this polymer is the interesterification of the ω-hydroxy acids[22]. After analyzing the products of the partial depolymerization, which were confirmed as representative of the polyester structure, the authors verified that almost all of the primary hydroxy groups are esterified and a large number of the secondary groups as well. A cutin rich in C_{16}-OHFAs like the one of the tomato fruits shows a high proportion of secondary esters which is indicative of a more branched structural arrangement leading to a less ordered and reticulated polyester. Recently these observations were further confirmed on a study with ionic liquid

isolated cutins from tomato, in which high levels of both esterification and reticulation were observed[31] (Chapter II). On the other hand, the C_{18}-rich cutins like the one of *Hedera helix* with low levels of secondary esters would give rise to a more linear and ordered polyester, with possible formation of secondary crystalline structures[22]. Curiously, using HRMAS NMR, it was possible to understand that in *Agave americana* a significant presence of epoxide groups in ester bonds turns this cutin very different from other well-studied cutins. Additionally, α-branched carboxylic acids were also present in the leaf cutin of this plant, which also presents an amorphous structure[32]. Recently, a similar trend to that observed for *A. americana* was also detected through solution-state NMR in *C. annum*, where the presence of epoxide groups, hinders the formation of crystalline regions, leading to a highly amorphous polyester[24]. Moreover, this cutin shows high levels of esterification which is characteristic of a very rigid and reticulated structural arrangement.

In fruit cuticles, the possibility of a covalent association of the cutin polyester with polysaccharides has also been recently proposed as a putative evolutionary marker important for land adaptation[33]. This feature was observed previously in studies involving the oligomeric structure of lime fruit, where it was detected, after controlled hydrolysis of the polyester, the presence of an oligomer that apart from the hydroxy fatty acid moiety also contained a sugar unit[34]. This may be indicative of a direct link between the polymer cutin and the cell wall, possibly strengthening the cell wall against biotic stress as observed for suberin[35]. This observation was further confirmed in a subsequent work in which a glucoside-linked hydroxy fatty acid tetramer was identified[36]. In fact, very recently, it was suggested that esterification between cutin monomers and cell wall derived polysaccharides can occur as a result of the action of a cutin: xyloglucan transacylase (CXT)[37], opening new questions about the true nature of the interaction between the constituents of the cuticle-cell wall continuum. Together, these observations strongly suggest the idea of alternative crosslinking possibilities that might influence the structure of cutin as well as the organization of the cuticular barrier.

In the tomato fruit, the removal of the polysaccharidic fraction from the cuticle decreases the stiffness of the barrier, strongly suggesting that polysaccharides might be somehow linked or incorporated into the cutin matrix, contributing directly to the elastic behavior of the cuticular membrane[38]. A very recent study also proposed that not only pectin, but also crystalline cellulose and hemicellulose are embedded into the matrix of cutin, being referred to as Cutin Embedded Polysaccharides (CEPs)[39]. Moreover, analysis of *CUS1*-silenced lines shows higher content of CEPs compared to WT purified cutins, demonstrating that there might be a correlation between the ratio of polyester/polysaccharides, cutin content and level of crosslinking. The presence of crystalline cellulose might influence the mechanical properties of the cuticular layer. Microcrystalline cellulose was detected in our recent study on cutin isolated from tomato peels using cholinium hexanoate; yet absent when imidazolium acetate was used instead[31]. More recently, we also performed a semi-quantitative immunoblot detection of microcrystalline cellulose, which made evident that a lower proportion is present in wild type cutins compared to the one from the *gpat6* and *cus1* mutants[24]. This dataset was complemented by the quantification of total hydrolysable carbohydrates present in ionic liquid isolated cutins, confirming their residual contribution (≤ 1 ng of carbohydrates per mg of cutin) for the polyester's physicochemical properties[24]. The strongest hypothesis proposed so far is that pectin might be covalently linked to cutin monomers through an ester bond. Additionally, esterified pectin might create a favorable environment to aid the diffusion of cutin precursors to the apoplast, which would occur in close association with the subsequent action of CUS1 in the polymerization steps[39].

Cutin is commonly presented as a polymer with high levels of branching, which was confirmed in the past with the observation that both primary and secondary hydroxy groups from the major cutin monomer in tomato can be esterified[20]. This is possible by the action of the CUS1 enzyme in a reaction that leads to the release of glycerol, also in accordance to the low levels of this monomeric constituent usually assigned to most cutins[20].

These features point to a highly esterified polymer with a highly reticulated arrangement. Moreover, the ratio of total esters *vs.* linear esters is significantly reduced in the *cus1* mutant when compared with the wild type, as confirmed by integration of the ^{1}H NMR signals (Chapter II). We broadened our analysis by introducing quantification strategies (use of benzene as internal standard and ^{31}P NMR) granting the possibility do discriminate and compare the specific contribution of primary and secondary esters in each sample, as well as the exact amount of free hydroxyl and acid groups[24]. This allowed establishing direct correlations between the esterification level and crystalline arrangement of distinct cutins, reinforcing the idea that lower degrees of esterification favor the formation of crystalline moieties and that secondary esters hinder the packing of aliphatic chains.

The occurrence of phenolics was proposed to correlate with the rigidity of the cutin matrix, as they influence chain mobility and may lead to a highly compact and rigid polymer. Their presence was suggested to result in a less elastic polyester during tomato fruit ripening[38]. Amorphous and highly crosslinked polymers like cutin also present some cavities that are possibly related to the diffusion of specific molecules across the polyester[40]. The storage and dissipation of energy are two properties assigned to cutin – already proposed as one of the most naturally occurring energy dense molecules. This was explained with the highly efficient chemical organization of this polyester, which could favor the efficient storage of carbon based energy[30]. Cutin is usually characterized by its amorphous nature, regardless that a few crystalline structures can also occur, as recently demonstrated by us using X-ray scattering and calorimetry analyses[24] (Chapter III). We analyzed the crystallinity and thermal properties of cutins isolated from two mutants impaired in key biosynthetic genes (*cus1* and *gpat6*) and the corresponding wild type. Both mutants present cutin with extremely organized crystalline regions resulting in enhanced resistance to temperature treatment compared to the wild type.

Cutin biosynthesis

Remarkable advances on the knowledge of cutin chemistry have been made along the years, especially by the identification of many of the composing monomeric constituents across a broad number of different plant species. However, our understanding of cutin functional relevance is still hindered by limited knowledge of the molecular and supra-molecular organization of the polymer. The biosynthetic pathway of cutin has been elucidated during the last years; it starts with the biosynthesis of the different monomers, which are then exported to the apoplast and subsequently polymerized on the external surface of the epidermal cell walls to form the polymer network[13] (Figure 3).

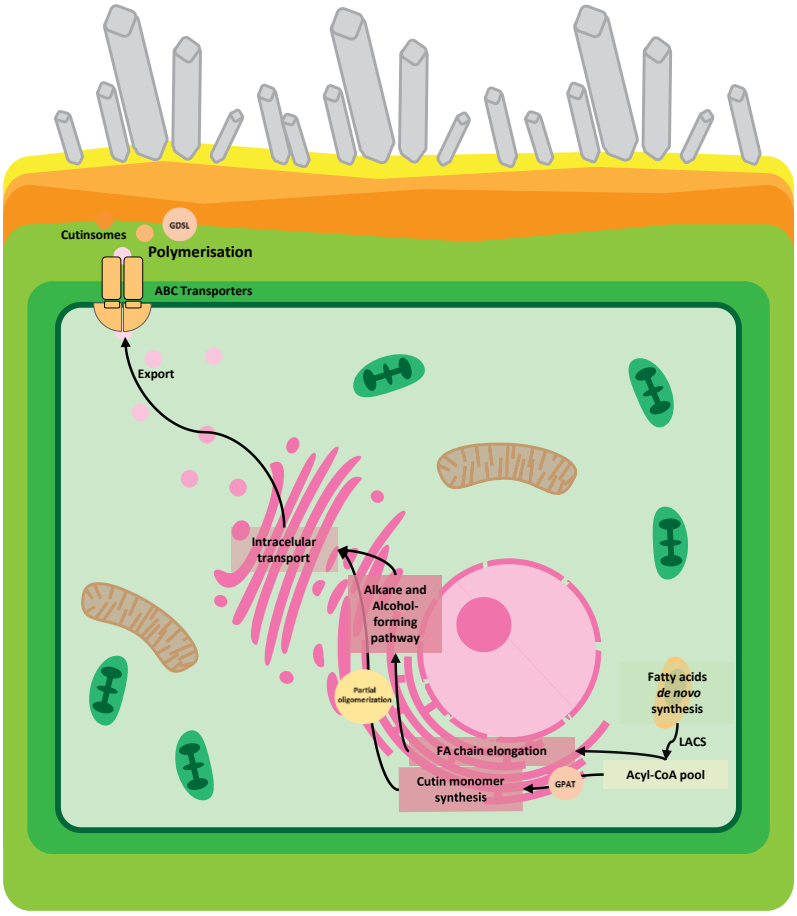

Figure 3. Schematic representation of cutin biosynthesis. Relevant protein families are highlighted.

The first step of the biosynthesis of cutin is the *de novo* fatty acid synthesis inside epidermal cells, followed by the ω- and mid-chain hydroxylation of the newly formed fatty acids, ultimately leading to the formation of a dihydroxyhexadecanoic acid-CoA ester[9,41]. In *Arabidopsis*, acyl-CoA precursors are synthesized by members of the long-chain acyl-CoA synthetases (LACS) family[42]. The coordinated action of two P450 cytochrome family enzymes is required to modify the initial precursor: a ω-hydroxylase (CYP86 subfamily) introduces a terminal hydroxyl group forming the intermediate ω-hydroxyhexadecanoic acid, which is then modified by a mid-chain hydroxylase (CYP77 subfamily) to form the 10,16-dihydroxyhexadecanoic acid[41] - the major cutin monomer in most plant species. Also in *Arabidopsis*, the LACERATA (LCR) gene was shown to encode for an additional cytochrome P450 monooxygenase responsible for the ω-hydroxylation of fatty acids during cutin biosynthesis.[43] In tomato, SlCYP86A69 which possesses NADPH-dependent ω-hydroxylation activity, is known to be under the control of the SlSHN3 transcription factor that regulates several genes related to cutin metabolism. This enzyme - SlCYP86A69 - can use both C_{18} and C_{16} fatty acids as substrates for ω-hydroxylation[44], and another one - SlCYP77A1 - catalyzes mid-chain hydroxylation of C_{16} fatty acids[45].

The formation of cutin precursors involves the action of members of the glycerol-3-phosphate acyl-CoA acyltransferase (GPAT), which are responsible for the synthesis of *sn*-2-monoacylglycerols from the biosynthesized oxygenated fatty acids[46]. The GPAT family has been analyzed in *Arabidopsis* and tomato plants. *Arabidopsis* has 8 members of the GPAT family, from which two - GPAT4 and GPAT8 - were previously reported to be expressed in the epidermal cells of the stem[47]. Using gain- and loss-of-function mutants it was demonstrated that GPAT4 is involved in the first steps of cutin synthesis and that its acyltransferase action is functionally redundant with that of GPAT8 in the DCA-rich cutins found on the stem and leaves of *Arabidopsis* plants[48]. More recently, it was demonstrated that

GPAT4 and GPAT6 present a bifunctional acyltransferase/phosphatase activity in C_{16}-enriched cutins. This observation, confirms their role in the formation of *sn*-2-monoacylglycerol, which constitute important intermediates in the process of cutin synthesis[49]. Not surprisingly, in tomato it was shown that the SlGPAT6 is able to produce monoacylglycerol (MAG), reinforcing the idea that this acyltransferase plays a relevant role in the synthesis of cutin during early stages of tomato fruit formation[50].

GPATs are just one part of an intricate machinery in the formation of cutin oligomers, since their formation also requires the action of the BAHD acyltransferase super family of enzymes[51]. In the surface of the flowers of *A. thaliana,* the *DEFECTIVE IN CUTICULAR RIDGES* (DCR) gene encodes for a putative acyltransferase that is essential for the incorporation of 9(10), 16-dihydroxyhexadecanoic acid in the polymer (*i.e.* oligomerization). Moreover, protein localization analysis suggested that the oligomerization occurs, at least partially, in the cytoplasm[51]. More recently, it was reported that the DCR encoded enzyme may also act as a diacylglycerol (DAG) acyltransferase, catalyzing the formation of triacylglycerol (TAG)[52]. These findings that support the important role of the DCR enzyme in cutin biosynthesis, led the authors to also propose that hydroxy fatty acids containing TAG may be precursors for cutin biosynthesis[52]. The role of this acyltransferase could be confirmed in tomato, as *SlDCR-RNAi* fruits presented significantly reduced levels of 9(10), 16-dihydroxyhexadecanoic acid, leading to cracking and subsequent suberization of the fruit surface[53].

The synthesis of additional cutin monomers relevant for cutin formation seems to involve a cytosolic epoxide hydrolase AtEH1 (EPOXIDE HYDROLASE 1), recently proposed as a key element in the synthesis process of poly-hydroxylated cutin monomers[54]. Moreover, the Hothead (HTH) gene, which encodes for a GMC oxidoreductase family member and is expressed in epidermal cells in *Arabidopsis*, catalyzes the oxidation of long-chain ω-hydroxy fatty acids to oxo-fatty acids, leading to the formation of α-,ω-dicarboxylic acids[55].

The sequence of biosynthetic reactions yielding cutin precursors occur intracellularly; however, the enzymes required for their polymerization localize extracellularly[56,57]. Consequently, these precursors need to be transported from the epidermal cell to the apoplastic space where the assembly of the polymer occurs[58]. The delivery of cutin building blocks (*i.e.* precursors) is thought to be mediated by vesicles that help delivering them to the plasma membrane, as previously demonstrated for wax precursors in *Arabidopsis*[59]. The final step of the export - delivery of cutin components to the apoplast is mediated by ABC transporters (ATP-binding cassette transporters)[58]. Several studies have been performed over the last years to identify members of this family of ABC transporters involved in this process. The ABCG11 transporter was the first to be reported has having a direct correlation with cutin monomer export. Consistently, the *abcg11* mutants showed features associated with cutin mis-polymerization, such as organ fusion, reduced cutin load and altered cuticular permeabilty[60]. However, these mutants displayed cutin monomers at the surface tissues of the plant, which is suggestive of the participation of other transporters. In fact, shortly after, the same authors reported that mutants of the ABCG13 transporter (closely related to ABCG11) show similar cuticular associated defects; yet, only in the floral organs of the plant, and a significantly reduced amount of cutin monomers[61]. Characterization of the *Permeable Cuticle1* (*pec1*) mutant in *Arabidopsis* led to the identification of a different transporter also involved in the cutin biosynthetic pathway. This mutant, which results from the knockout of the ABCG32 transporter of the PLEIOTROPIC DRUG RESISTANCE (PDR) family, shows enhanced cuticle permeability, high reduction of oxygenated fatty acids and structural alterations of the cuticular layer, thus indicating a role in cutin monomer export[62]. Very recently, a true ortholog of the AtABCG32 was reported in tomato (SlABCG42)[63]. Its expression under the control of the native promoter of the Arabidopsis transporter demonstrated the ability to complement the cutin defective deposition and permeability phenotypes in the *pec1/atabcg32* mutant.

As soon as the precursor cutin units reach the apoplastic space, their polymerization can happen through the action of specific enzymes that assemble the polymeric pieces into a structured lipidic layer. The main enzyme responsible for this step is a member of the Gly-Asp-Ser-Leu (GDSL) family of esterases/acylhydrolases, commonly called GDSL-lipases, which was recently named Cutin Synthase 1 (CUS1)[64]. The characterization of the *cutin deficient 1* (*cd1*) mutant in tomato guided the discovery that CD1 was an extracellular enzyme with cuticular localization required for cutin biosynthesis[57]. The mutant showed accumulation of 2-mono(10,16-dihydroxy-hexadecanoyl) glycerol (2-MHG), the 2-MAG configuration of the major monomer present in tomato cutin. In addition, a recombinant CD1 enzyme could perform *in vitro* the transesterification of 2-MHG, which ultimately lead to the formation of cutin oligomers[57]. Right after, a different group also characterized the *gdsl1* mutant in tomato confirming its cuticular localization, a hydrophobic environment that may favor the transesterification of ester precursors, consistent with the observations of the first study on the CD1 protein. Additionally, severe reduction in cutin monomer content (up to 95 %) and a significant decrease in polymerization were observed in this mutant, emphasizing that GDSL1 plays an essential role in cutin deposition and polymerisation[56]. A different enzyme from the α/β hydrolase family named BODYGUARD (BDG), was previously shown to be cell wall-localized and required for the formation of a proper cuticle structure[65]. More recently, it was demonstrated that the BDG enzyme is required for cutin biosynthesis in flowers and leaves of *Arabidopsis*, due to a great reduction in total cutin monomer load observed in *bdg* defective mutants[66]. Moreover, a up to 4-fold increase was observed when this gene was overexpressed, influencing preferentially the levels of C_{18} polyunsaturated ω-OH fatty acids and dicarboxylic acids. These observations reinforce the idea that BDG plays a specific function in the assembly of the cutin polymer, being required for the incorporation of specific monomers in different plant organs[66]. Importantly, the substrate-selectivity of

both BDG and CUS1, is indicative that additional enzymes may be required for the proper assembly of the cutin polyester; their discovery is critical for a comprehensive understanding of cutin biosynthesis.

Apart from the enzymatically driven polymerization of cutin, a complementary process involving specific nanoparticles that result from the self assembly of cutin precursors – cutinsomes – has been proposed[67]. This process relies on pure physicochemical interactions with no enzymatic involvement leading to the formation of globular nanostructures. These structures ranging from 40 to 200 nm are detected by immunolocalization, polymerized at the outer surface of epidermal cell walls[68], supporting the hypothesis of a polymerization step on the early stages of cuticle formation. These cutinsomes were already observed in *A. thaliana* and *S. lycopersicum*, and are considered as possible sources of branched and crosslinked oligomers, complementing the action of CUS1, which is able to generate both linear and branched cutin oligomers[67].

In fact, a great wealth of knowledge was generated in the last decades in cutin biosynthesis and polymerization. Nevertheless, how polymerization events complement each other and the actual sequence of events leading to the formation of the cuticular matrix of cutin still remains to be unraveled.

Biological roles of cutin

The structural arrangement of cutin, ultimately leads to specific properties that impact its biological functions as demonstrated by extant scientific literature.

Water control

It is well known that the cuticle is characterized as a barrier that helped plants to prevent water loss, when these organisms moved from aquatic to terrestrial ecosystems[7]. Intuitively, it would be assumed that a thick cuticle should provide a less permeable barrier, thus leading to plants that are more resistant to water loss[69]. Nevertheless, several studies have shown that no

correlation can be established between the thickness and the permeability of the cuticular barrier. The question that rises from these observations is whether the structural components of this barrier might have a direct role in water content control.

A study on three tomato cutin-deficient mutants (*cd1, cd2* and *cd3*) did not show any clear correlation between water loss and cutin content. All three mutants showed high reduction of cutin content (≥ 95 % *wt*) and the one that showed the lowest decrease *cd1* presented higher water permeability[70]. In *Arabidopsis*, the *pec1* mutant showed a decrease in aliphatic cutin monomers and also loss of barrier function, more specifically, increased non-stomatal water loss[62]. These studies did not demonstrate a direct effect of the cutin amount in the control of water transport, suggestive that its proper structural organization is needed to ensure the water barrier properties of the cuticle. In line with this idea, a positive correlation was observed between water loss and cutin monomer content in pepper, which was associated with an enrichment of the major cutin monomer (16-dihydroxy hexadecanoic acid) and an overall increase in the amount of C_{16} monomers[23]. Plants subjected to water deficit showed an increase in almost all classes of cutin monomers, implicating this polymer in the mechanisms of response against this abiotic stress in *Arabidopsis* leaves[71]. The proposed explanation was that such an enrichment, followed also by enrichment of wax monomers, would contribute to the formation of a less permeable cuticle, allowing the plant to cope with water deprivation. Also in *Arabidopsis*, the study of plants impaired in key cutin biosynthetic genes (*BDG, ATT1* and *LACS2*) led to the establishment of a correlation between cutin biosynthesis and the induction of ABA synthesis under osmotic stress conditions[72]. The results not only pointed out for a common defensive role, but also raised the possibility that a shared substrate acts as a signaling molecule for the activation of the ABA biosynthetic pathway and cutin biosynthesis. To summarize, although it is not clear the way cutin influences the water barrier properties of plant cuticles, it is plausible that a functional barrier needs cutin integrity and proper organization. Additionally,

cutin synthesis might also be intimately involved with other physiological response pathways to ensure water homeostasis in plant tissues.

Organ formation

A second biological role of this polyester is observed in the process of organogenesis. Several studies implicate cutin as having a direct impact in proper organ separation during plant development. Most of these studies analyzed plants impaired in key genes from the cutin biosynthetic pathway already mentioned in this review (*BDG, GPAT6, DCR*, *LCR*, *HTH* and *LACS*) and all showed phenotypes that include organ fusion and defective cuticle[41,43,51,65,73,74]. Moreover, at the level of the transcriptional regulation of these genes, we can also confirm the relevance of cutin for proper organ formation. Mutant plants impaired in the entire clade of *SHN* transcription factors, major regulators of the cutin biosynthetic pathway, also showed organ fusion in addition to early flower abcission[75]. To further support these observations, the expression of fungal or plant-derived cutin-degrading enzymes was shown not only to disrupt the cuticle barrier but also to result in organ fusion in the aerial organs of *Arabidopsis* plants[76,77]. Altogether, these observations clearly show that proper cutin assembly and organization is needed to ensure the integrity of the cuticular barrier, which is essential for the proper formation of plant organs.

Plant immunity

The epidermis is a tissue that has been identified as essential to perceive and transduce a plethora of environmental cues that thrive the proper plant developmental mechanisms. Apart from its primary role of providing physical protection, the shoot epidermis also constitutes an important platform for sensing external signals, which are crucial to orchestrate defensive responses[78]. The cuticle is the outermost defensive barrier of land plants and constitutes a barrier for the entrance of pathogens. Although bacteria and viruses usually infect by wounds or through stomata, fungi have been shown

to be able to penetrate the intact barrier[79]. This is possible due to the action of specific cutin-degrading enzymes produced by fungi. These extracellular enzymes usually referred to as cutinases are serine esterases that belong to the α/β hydrolase family[80]. These enzymes were first isolated in fungal organisms growing on cutin as the sole carbon source[81]. When secreted, fungal cutinases are able to hydrolyze the polymer, first into oligomers and, after longer incubations, these oligomers can be further hydrolyzed to monomers; although, it is still possible to observe the presence of dimers or larger oligomers after extensive cutinase treatment[79]. When the spore of a pathogenic fungus lands on the surface of a plant organ it secretes cutinases that lead to the release of cutin monomers. These cutin monomers trigger the expression of additional cutinase genes, which then targets the secretion of the enzymes to the infection structures[82].

Apart from the role of providing signals to aid fungal infection, cutin monomers were also proposed to constitute endogenous elicitors of plant defenses. The first indication was provided in a study with barley and rice in which, spray application of cutin monomers, resulted in acquired resistance against *Erysiphe graminis* and *Magnaporthe oryzae*, respectively[83]. A subsequent study from the same group focused on the action of free cutin monomers in suspension-cultured potato cells. The authors observed a rapid alkalinization of the cell suspension in response to cutin monomer treatment, as well as a stimulation of ethylene production and accumulation of plant defense-related genes[84]. These two studies constituted an initial step to the observation that cutin and the cuticular barrier may constitute a two-way interface in plant pathogen interactions.

Pointed out as potential immune elicitors in plants, cutin monomers were explored in the following years as damage-derived immune elicitors. Plants rely on their innate immune system to detect and respond to potential threats by pathogens. Accordingly, they have developed a two layer defensive system consisting of: a) pattern-triggered immunity (PTI) - a first line defense that relies on the action of surface localized pattern recognition receptors

(PRRs), which detect both pathogen-associated molecular patterns (PAMPs) and damage-associated molecular patterns (DAMPs), signatures derived from invading organisms or the host, respectively[85]; b) Effector-triggered Immunity (ETI) – a second layer of immunity that counts with the ability of intracellular receptors, most of which nucleotide-binding site leucine-rich repeat (NBS-LRR) proteins, to detect virulence effectors secreted to the intracellular space by the invading pathogens[85]. After the initial step of ligand perception by PRRs, the action of specific receptor-like cytoplasmic kinases (RLCKs) is required to link receptor activation with downstream intracellular signalling[86]. This process, ultimately leads to a defense response that frequently involves the production of reactive oxygen species (ROS), a rapid calcium influx, activation of mitogen-activated protein kinases (MAPKs) and the induction of immunity-related genes[87].

If plants are really able to perceive cutin constituents as DAMPs, in theory these should be among the first immune elicitors released during the early stages of infection[88]. Most of the studies focus on the specific action of cutin monomers due to the described action of the cutinase enzyme. When hypocotyls of cucumber with its epidermal surface abraded, mimicking a more permeable cuticle, were subjected to incubation with cutin hydrolysates from cucumber, tomato and apple, an accumulation of H_2O_2 was observed[89]. In addition to the direct eliciting activity, these cutin-derived components were also able to enhance the activity of a fungal elicitor of ROS. In a subsequent study from the same group it was observed that cucumber hypocotyls are able to generate H_2O_2 through a constitutive alternative pathway in response to a specific cucumber cutin monomer (DDO, dodecan-1-ol)[90]. A different cutin monomer - 16-hydroxypalmitic acid (HPA), was shown to induce the synthesis of H_2O_2 and to induce the expression of lipid transfer protein genes (*OsLTP1, OsLTP2* and *OsLTP5*), as well as a pathogenesis related gene (*PR-10*) in rice leaves[91]. In a subsequent study by the same group on the action of this cutin monomer in *Arabidopsis*, it was observed a similar induction of H_2O_2 and expression of pathogenesis related genes (*PR-1* and *PR-4*).

Moreover, the expression of two Glycine-rich Proteins genes (*AtGRP5* and *AtGRP23*), one of which is associated to cell reinforcement in response to mechanical tension, suggested a role of these proteins in pathogen defense in response to cutin derived signals[92].

To understand if changes in cutin monomer profile would lead to different patterns of disease susceptibility, several research projects with transformed plants were also conducted. The transformation of tomato with the yeast Δ-9 desaturase gene leads to an altered fatty acid profile, characterized by a specific increase in the cutin monomer 9-hexadecenoic acid. Monomers from this transformed polyester were able to inhibit spore germination of the powdery mildew agent *Erysiphe polygoni*, suggestive of the specific involvement of 9-hexadecenoic acid in this effect[93]. The study of the *Arabidopsis* mutant *lacs2* showed that when cutin biosynthesis is impaired a highly permeable cuticle is formed[94]. Nevertheless, contrarily to what would be intuitive, increased cuticle permeability enhanced the plant's resistance against major pathogens like *Botrytis cinerea* and *Scleotiorum sclerotinia*. The increased resistance could be explained by the secretion of a fungitoxic diffusate at the leaf surface once a more permeable barrier would allow for the diffusion of specific signals that would ultimately lead to the arrest of the infection[94]. Resistance to *Botrytis* was also observed in mutants of the *SM4* (*SYMPTOMS TO MULTIPLE AVR GENOTYPES 4*) gene, which encodes the LACS2 protein, that showed strong susceptibility to avirulent strains of *Pseudomonas syringae pv* tomato[95]. These observations strongly suggest the existence of specificity on the resistance mechanism to different pathogens associated with defects on cutin structure and composition. A different study compared the effects of the overexpression of a fungal cutinase in *Arabidopsis* (*cute* plants) with the *bdg* mutant, which is impaired in cutin biosynthesis. Both plants demonstrated similar cuticle-defective phenotypes, which resulted in full immunity against the major necrotroph *Botrytis cinerea*. Immunity was accompanied by the release of a diffusate with fungitoxic activity, possibly constituting a first line defense in plants with defective cuticles[96]. In addition,

a second line of defense included the specific induction of genes from the Lipid Transfer Proteins (LTP), members of the class III *PER* gene, and Proteinase Inhibitor (PI) families[96]. More recently, cuticle permeability was linked to higher ROS production upon infection with *Botrytis cinerea*, leading the authors to propose that the cuticle might act as a sensor for pathogen invasion that triggers ROS production upon cuticular disruption[97]. In contrast with the studies on *Arabidopsis*, the tomato mutant lines *cd1, cd2* and *cd3*, which display a dramatic reduction on cutin content (≥ 95 % *wt*), showed increased susceptibility to *Botrytis* infection compared to wild type fruits[70]. To increase the complexity of the potential action of cutin in plant resistance against pathogens, the *Arabidopsis Resurrection 1* (*rst1*) mutant showed elevated cutin monomer content and normal cuticular permeability. These features led to enhanced resistance against two major necrotrophs, *B. cinerea* and *A. brassicicola*, suggesting a different mechanism of resistance that is not directly related to cuticular permeability[98]. A strong correlation between defensive properties of cutin and its composition was established on a study of *gpat6* mutant lines in two *solanaceae* plants – *Nicotiana benthamiana* and *Solanum lycopersicum*. Overexpression of the *GPAT6* gene in *N*. *benthamiana* greatly increased the total leaf cutin content and enhanced resistance to *Phytophtora infestans*, while attenuation or knock out of its expression led to opposite effects, suggestive of cutin participation in resistance to *Phytophtora* infection[99]. Transcriptome analysis of the tomato *gpat6* mutant leaves upon infection with *P. infestans*, revealed a high induction of genes involved in immune responses. Among these, there were several leucine-rich repeat receptor kinases (RKs), with the most striking being *SERK3/BAK1* and a tomato homolog of *ERECTA*, which were correlated with a reduced number of stomata in the leaves of the mutant[99]. Being RKs important for PTI, this result represents strong evidence of the connection between cutin biosynthesis and plant immune signaling.

In the last decade, several groups also devoted their efforts to understand if the transcriptional regulation of cutin biosynthesis is linked to

plant defense. It was shown that a gain-of-function mutant (*shn1-1D*) of the transcription factor SHINE1/WAX INDUCER1 (SHN1/WIN1) that regulates plant's surface lipid metabolism - was characterized by altered cutin monomer content rendering a permeable cuticle. This mutant was more susceptible to *Botrytis cinerea* infection and, upon infection demonstrated increased ROS accumulation and strong activation of defense related genes, which resulted in the observed plant sensitivity and death[100]. In tomato, *slshn3-oe* leaves present higher cutin monomeric content associated with higher permeability and enhanced resistance to both *B. cinerea* and *X. campestris pv*. *vesicatoria*. Moreover, when cutin monomers of the *slshn3-oe* leaves where exogenously applied to wild type leaves, the activation of the expression of several pathogenesis-related genes upon infection was observed[101]. Very recently, it was shown that another *Arabidopsis* mutant called *eca2,* displaying constitutive expression of the ATL2 gene, which encodes a RING-H2 protein induced by PAMPs or DAMPs, also display a permeable cuticle associated to a reduced cutin content. In this case, the mutant plants were resistant to *P. syringae* and *B. cinerea*, which was explained by the fast ROS accumulation and transcriptional induction of both early and late defense-response genes[102].

Although cuticular deficiency may trigger the expression of specific defense-related genes, the mechanism through which this occurs is a mystery that remains unresolved. One of the strongest possibilities is that specific cutin monomers and/or oligomers play a signaling role because they seem to be perceived by plant cells, inducing immune responses[103].

To identify specific cutin-derived elicitors, the mechanisms involved in their perception and potential pathways triggered in response to pathogen invasion, we tested how different levels of cleavage of the polymer influence hallmark immune responses in the model plant *A. thaliana*. Our results show that cutin with low levels of ester cleavage and oligomers obtained by its controlled depolymerization are able to induce first line immune responses such as Ca^{2+} influx, MAPK activation and transcriptional reprogramming.

These results, which are presented on this thesis on Chapter IV, together with the observed defensive action of cutin monomers, seems to point out for a sequential activation of the immune system dependent on the level of esterification of the eliciting molecules, although additional tests are still needed to confirm this hypothesis. A schematic representation of the immune responses elicited by cutin-derived molecules is depicted in figure 4.

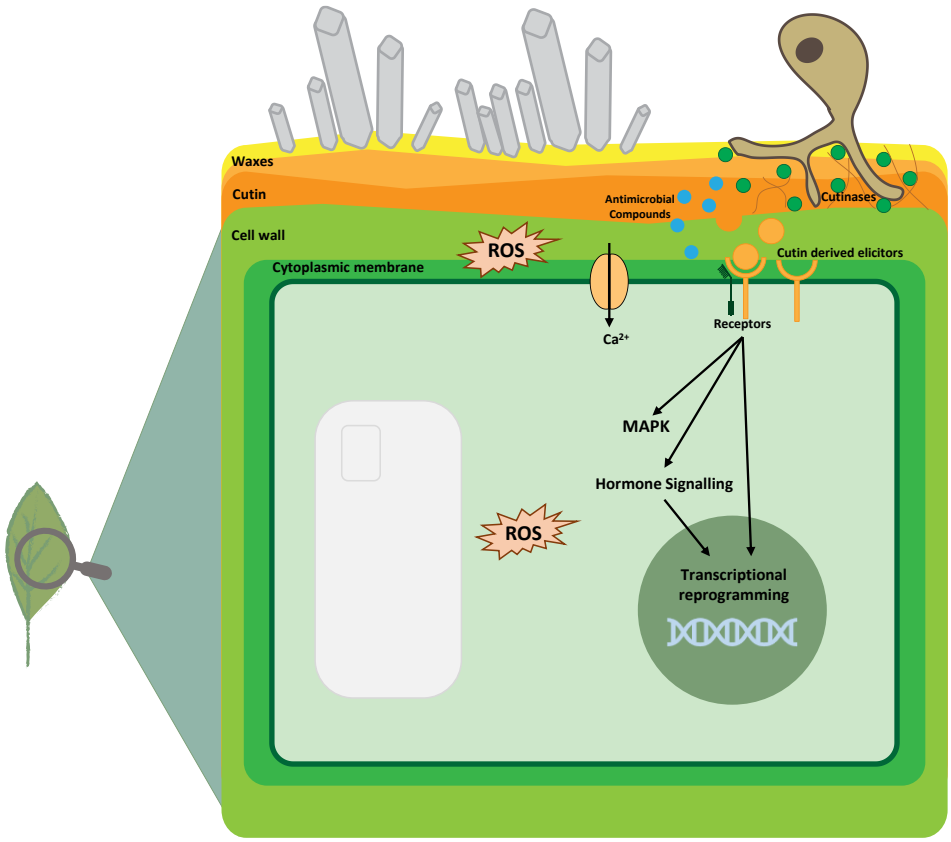

Figure 4. Schematic representation of the immune responses elicited by cutin derived molecules.

Contribution of this thesis and Future perspectives

The work developed in this thesis established an ionic liquid-based isolation method for cutin that renders high preservation of its polymeric backbone (Chapter II). Due to its simplicity, this methodology has the potential to be broadly adapted to different plant tissues and species. This constitutes an original contribution, suggesting an alternative cutin isolation strategy that, when coupled with cryogenic milling, allowed for the first time to obtain solution NMR spectra of this plant polyester (Chapter II). Moreover, when applied to different sources, the NMR-based characterization of cutins coupled with thermal and scattering analyses, setup a fine correlation between chemical and physicochemical properties, essential to exploit its biotechnological potential (Chapter III). The possibility to isolate a near-native cutin, allowed also to generate an *ex-situ* strategy to explore the effects on cutin degradation by pathogens in the activation of plant immunity (Chapter IV). Cutin degradation products are considered as DAMPs released during the early stages of infection. Although some monomers and hydrolysates have proven their ability to induce immune responses, the molecular mechanisms through which these products are sensed and how they trigger plant defenses remains unknown[104]. Moreover, the examples of oligogalacturonides (OGs), cellulose derived oligomers like cellobiose[105], Arabinoxylan-Oligosaccharides[106] and mixed-linked β-1,3/1,4-glucans (MLGs)[107], recently proposed as DAMPs together with the new data we present on this thesis for the action of cutin oligomers, strongly support the idea that oligomers may be the first elicitors perceived in cutin-mediated immunity. Our main goal was to demonstrate that upon hydrolysis, a certain degree of esterification was required for the initiation of the immune response. To complement the proposed hypothesis, future efforts should focus on the uniqueness of the eliciting activity demonstrated by cutin oligomeric mixtures at a transcriptional level (Chapter IV). Additionally, the effort to unravel the mechanism of perception of these signals will involve the generation of specific mutants, to identify the family of receptors able to sense these molecules. First observations based

on MAPK activation assays point to an undescribed pathway, as it was observed that common co-receptors are not involved in responsiveness to these oligomeric molecules (Chapter IV). We do not reject that monomers also act as elicitors, as it was already observed extensively in literature. Indeed, our results add complexity to the way cutin degradation works in plant defense pointing to the possibility of different levels of immune activation correlated with the degree of cleavage. Moreover, taking into consideration that several cell wall derived molecules also act as DAMPs, a synergistic effect from molecules deriving from different elements of the cuticle/cell wall continuum should also be considered in future studies.

Funding

This work was supported by the European Research Council (grant no. ERC 2014–CoG–647928), from Fundação para a Ciência e Tecnologia (FCT) by Project MOSTMICRO ITQB with refs UIDB/04612/2020 and UIDP/04612/2020, and Aralab (PhD contract no. 06/PlantsLife/2017 to C.J.S.M.).

References

1. Delwiche, C. F. & Cooper, E. D. The evolutionary origin of a terrestrial flora. *Current Biology* vol. 25 R899–R910 (2015).
2. Waters, E. R. Molecular adaptation and the origin of land plants. *Mol. Phylogenet. Evol.* **29**, 456–463 (2003).
3. Zhao, C. *et al.* Evolution of chloroplast retrograde signaling facilitates green plant adaptation to land. *Proc. Natl. Acad. Sci. U. S. A.* **116**, 5015–5020 (2019).
4. Beerling, D. J. *The emerald planet : how plants changed Earth's history*. (Oxford University Press, 2007).
5. Fich, E. A., Segerson, N. A. & Rose, J. K. C. The Plant Polyester Cutin: Biosynthesis, Structure, and Biological Roles. *Annu. Rev. Plant Biol.* **67**, 207–233 (2016).
6. Berhin, A. *et al.* The Root Cap Cuticle: A Cell Wall Structure for Seedling Establishment and Lateral Root Formation. *Cell* **176**, 1367-1378.e8 (2019).
7. Martin, L. B. B. & Rose, J. K. C. There's more than one way to skin a fruit: formation and functions of fruit cuticles. *J. Exp. Bot.* **65**, 4639–4651 (2014).
8. Philippe, G. *et al.* Plant cuticle embedded polysaccharides exhibit specific structural features. *New Phytol* (in press) (2020).
9. Yeats, T. H. & Rose, J. K. C. The formation and function of plant cuticles. *Plant Physiology* vol. 163 5–20 (2013).
10. Gupta, N. S. Molecular Decay of Plant Biopolymers. in 1–16 (Springer, Dordrecht, 2014). doi:10.1007/978-94-007-7936-5_1.
11. Taylor, E. L., Taylor, T. N. & Krings, M. *Paleobotany*. *Paleobotany* (Elsevier Inc., 2009). doi:10.1086/328501.
12. Li-Beisson, Y., Verdier, G., Xu, L. & Beisson, F. Cutin and Suberin Polyesters. in *eLS* 1–12 (John Wiley & Sons, Ltd, 2016). doi:10.1002/9780470015902.a0001920.pub3.

13. Mazurek, S. *et al.* Connecting the molecular structure of cutin to ultrastructure and physical properties of the cuticle in petals of arabidopsis. *Plant Physiol.* **173**, 1146–1163 (2017).
14. Fernández, V., Guzmán-Delgado, P., Graça, J., Santos, S. & Gil, L. Cuticle structure in relation to chemical composition: Re-assessing the prevailing model. *Frontiers in Plant Science* vol. 7 427 (2016).
15. Bonaventure, G., Beisson, F., Ohlrogge, J. & Pollard, M. Analysis of the aliphatic monomer composition of polyesters associated with Arabidopsis epidermis: Occurrence of octadeca-cis-6, cis-9-diene-1,18-dioate as the major component. *Plant J.* **40**, 920–930 (2004).
16. Franke, R. *et al.* Apoplastic polyesters in Arabidopsis surface tissues - A typical suberin and a particular cutin. *Phytochemistry* **66**, 2643–2658 (2005).
17. Yang, W., Pollard, M., Li-Beisson, Y. & Ohlrogge, J. Quantitative analysis of glycerol in dicarboxylic acid-rich cutins provides insights into Arabidopsis cutin structure. *Phytochemistry* **130**, 159–169 (2016).
18. Graça, J., Schreiber, L., Rodrigues, J. & Pereira, H. Glycerol and glyceryl esters of ω-hydroxyacids in cutins. *Phytochemistry* **61**, 205–215 (2002).
19. Petit, J., Bres, C., Mauxion, J. P., Bakan, B. & Rothan, C. Breeding for cuticle-associated traits in crop species: traits, targets, and strategies. *Journal of Experimental Botany* vol. 68 5369–5387 (2017).
20. Philippe, G. *et al.* Ester cross-link profiling of the cutin polymer of wild-type and cutin synthase tomato mutants highlights different mechanisms of polymerization. *Plant Physiol.* **170**, 807–820 (2016).
21. Kosma, D. K. *et al.* Fruit cuticle lipid composition during development in tomato ripening mutants. *Physiol. Plant.* **139**, 107–117 (2010).
22. Graça, J. & Lamosa, P. Linear and Branched Poly(ω-hydroxyacid) Esters in Plant Cutins. *J. Agric. Food Chem.* **58**, 9666–9674 (2010).

23. Parsons, E. P. *et al.* Fruit cuticle lipid composition and fruit post-harvest water loss in an advanced backcross generation of pepper (Capsicum sp.). *Physiol. Plant.* **146**, 15–25 (2012).
24. Bento, A. *et al.* Quantification of structure-property relationships for plant polyesters reveals suberin and cutin idiosyncrasies. *ACS Sustain. Chem. Sustain.* **Submitted**, (2021).
25. GuzmÃ¡n, P. *et al.* Chemical and structural analysis of Eucalyptus globulus and E. camaldulensis leaf cuticles: a lipidized cell wall region. *Front. Plant Sci.* **5**, 481 (2014).
26. Chatterjee, S. *et al.* Isolation and Biophysical Study of Fruit Cuticles. *J. Vis. Exp.* e3529 (2012) doi:10.3791/3529.
27. Serra, O., Chatterjee, S., Huang, W. & Stark, R. E. Mini-review: What nuclear magnetic resonance can tell us about protective tissues. *Plant Sci.* **195**, 120–124 (2012).
28. Heredia-Guerrero, J. A. *et al.* Infrared and Raman spectroscopic features of plant cuticles: A review. *Frontiers in Plant Science* vol. 5 305 (2014).
29. Emsley, J. W., Feeney, J. & Sutcliffe, L. H. *High Resolution Nuclear Magnetic Resonance Spectroscopy*. *Elsevier* vol. 2 (Elsevier, 1966).
30. Bhunia, R. K., Showman, L. J., Jose, A. & Nikolau, B. J. Combined use of cutinase and high-resolution mass-spectrometry to query the molecular architecture of cutin. *Plant Methods* **14**, 117 (2018).
31. Moreira, C. J. *et al.* An ionic liquid extraction that preserves the molecular structure of cutin shown by nuclear magnetic resonance. *Plant Physiol.* pp.01049.2020 (2020) doi:10.1104/pp.20.01049.
32. Deshmukh, A. P., Simpson, A. J., Hadad, C. M. & Hatcher, P. G. Insights into the structure of cutin and cutan from Agave americana leaf cuticle using HRMAS NMR spectroscopy. *Org. Geochem.* **36**, 1072–1085 (2005).
33. Bakan, B. & Marion, D. Assembly of the cutin polyester: From cells to extracellular cell walls. *Plants* **6**, 57 (2017).

34. Fang, X. *et al.* NMR studies of molecular structure in fruit cuticle polyesters. *Phytochemistry* **57**, 1035–1042 (2001).
35. Pollard, M., Beisson, F., Li, Y. & Ohlrogge, J. B. Building lipid barriers: biosynthesis of cutin and suberin. *Trends Plant Sci.* **13**, 236–246 (2008).
36. Tian, S. *et al.* Isolation and identification of oligomers from partial degradation of lime fruit cutin. *J. Agric. Food Chem.* **56**, 10318–10325 (2008).
37. Xin, A. & Fry, S. C. Cutin:xyloglucan transacylase (CXT) activity covalently links cutin to a plant cell-wall polysaccharide. *J. Plant Physiol.* **262**, 153446 (2021).
38. Ló pez-Casado, G., Matas, A. J., Domínguez, E., Cuartero, J. & Heredia, A. Biomechanics of isolated tomato (Solanum lycopersicum L.) fruit cuticles: the role of the cutin matrix and polysaccharides. *J. Exp. Bot.* **58**, 3875–3883 (2007).
39. Philippe, G. *et al.* Assembly of tomato fruit cuticles: a cross-talk between the cutin polyester and cell wall polysaccharides. *New Phytol.* **226**, 809–822 (2020).
40. Domínguez, E., Heredia-Guerrero, J. A. & Heredia, A. The biophysical design of plant cuticles: an overview. *New Phytol.* **189**, 938–949 (2011).
41. Li-Beisson, Y. *et al.* Nanoridges that characterize the surface morphology of flowers require the synthesis of cutin polyester. *Proc. Natl. Acad. Sci. U. S. A.* **106**, 22008–22013 (2009).
42. Lü, S. *et al.* Arabidopsis *CER8* encodes LONG-CHAIN ACYL-COA SYNTHETASE 1 (LACS1) that has overlapping functions with LACS2 in plant wax and cutin synthesis. *Plant J.* **59**, 553–564 (2009).
43. Wellesen, K. *et al.* Functional analysis of the LACERATA gene of Arabidopsis provides evidence for different roles of fatty acid ω-hydroxylation in development. *Proc. Natl. Acad. Sci. U. S. A.* **98**, 9694–9699 (2001).

44. Shi, J. X. *et al.* The tomato SlSHINE3 transcription factor regulates fruit cuticle formation and epidermal patterning. *New Phytol.* **197**, 468–480 (2013).
45. Lashbrooke, J. *et al.* The tomato MIXTA-like transcription factor coordinates fruit epidermis conical cell development and cuticular lipid biosynthesis and assembly. *Plant Physiol.* **169**, 2553–2571 (2015).
46. Beisson, F., Li-Beisson, Y. & Pollard, M. Solving the puzzles of cutin and suberin polymer biosynthesis. *Current Opinion in Plant Biology* vol. 15 329–337 (2012).
47. Suh, M. C. *et al.* Cuticular lipid composition, surface structure, and gene expression in Arabidopsis stem epidermis. *Plant Physiol.* **139**, 1649–1665 (2005).
48. Li, Y. *et al.* Identification of acyltransferases required for cutin biosynthesis and production of cutin with suberin-like monomers. *Proc. Natl. Acad. Sci. U. S. A.* **104**, 18339–18344 (2007).
49. Yang, W. *et al.* A distinct type of glycerol-3-phosphate acyltransferase with sn-2 preference and phosphatase activity producing 2-monoacylglycerol. *Proc. Natl. Acad. Sci. U. S. A.* **107**, 12040–12045 (2010).
50. Petit, J. *et al.* The glycerol-3-phosphate acyltransferase GPAT6 from tomato plays a central role in fruit cutin biosynthesis. *Plant Physiol.* **171**, 894–913 (2016).
51. Panikashvili, D., Shi, J. X., Schreiber, L. & Aharoni, A. The arabidopsis DCR encoding a soluble BAHD acyltransferase is required for cutin polyester formation and seed hydration properties. *Plant Physiol.* **151**, 1773–1789 (2009).
52. Rani, S. H., Krishna, T. H. A., Saha, S., Negi, A. S. & Rajasekharan, R. Defective in Cuticular Ridges (DCR) of Arabidopsis thaliana, a gene associated with surface cutin formation, encodes a soluble diacylglycerol acyltransferase. *J. Biol. Chem.* **285**, 38337–38347 (2010).

53. Lashbrooke, J. *et al.* MYB107 and MYB9 homologs regulate suberin deposition in angiosperms. *Plant Cell* **28**, 2097–2116 (2016).
54. E, P. *et al.* Arabidopsis thaliana EPOXIDE HYDROLASE1 (AtEH1) is a cytosolic epoxide hydrolase involved in the synthesis of poly-hydroxylated cutin monomers. *New Phytol.* **215**, 173–186 (2017).
55. Kurdyukov, S. *et al.* Genetic and biochemical evidence for involvement of HOTHEAD in the biosynthesis of long-chain α-,ω-dicarboxylic fatty acids and formation of extracellular matrix. *Planta* **224**, 315–329 (2006).
56. Girard, A. L. *et al.* Tomato GDSL1 is required for cutin deposition in the fruit cuticle. *Plant Cell* **24**, 3106–3121 (2012).
57. Yeats, T. H. *et al.* The identification of cutin synthase: Formation of the plant polyester cutin. *Nat. Chem. Biol.* **8**, 609–611 (2012).
58. Joubès, J. & Domergue, F. Biosynthesis of the Plant Cuticle. in *Hydrocarbons, Oils and Lipids: Diversity, Origin, Chemistry and Fate* 1–19 (Springer International Publishing, 2018). doi:10.1007/978-3-319-54529-5_8-1.
59. McFarlane, H. E. *et al.* Golgi- and trans-golgi network-mediated vesicle trafficking is required for wax secretion from epidermal cells. *Plant Physiol.* **164**, 1250–1260 (2014).
60. Panikashvili, D. *et al.* The arabidopsis DESPERADO/AtWBC11 transporter is required for cutin and wax secretion. *Plant Physiol.* **145**, 1345–1360 (2007).
61. Panikashvili, D., Shi, J. X., Schreiber, L. & Aharoni, A. The Arabidopsis ABCG13 transporter is required for flower cuticle secretion and patterning of the petal epidermis. *New Phytol.* **190**, 113–124 (2011).
62. Bessire, M. *et al.* A member of the PLEIOTROPIC DRUG RESISTANCE family of ATP binding cassette transporters is required for the formation of a functional cuticle in Arabidopsis. *Plant Cell* **23**, 1958–1970 (2011).

63. Elejalde-Palmett, C. *et al.* ABCG transporters export cutin precursors for the formation of the plant cuticle. *Curr. Biol.* **31**, 2111-2123.e9 (2021).
64. Yeats, T. H. *et al.* Tomato Cutin Deficient 1 (CD1) and putative orthologs comprise an ancient family of cutin synthase-like (CUS) proteins that are conserved among land plants. *Plant J.* **77**, 667–675 (2014).
65. Kurdyukov, S. *et al.* The epidermis-specific extracellular BODYGUARD controls cuticle development and morphogenesis in Arabidopsis. *Plant Cell* **18**, 321–339 (2006).
66. Jakobson, L. *et al.* BODYGUARD is required for the biosynthesis of cutin in Arabidopsis. *New Phytol.* **211**, 614–626 (2016).
67. Stępiński, D. *et al.* The Role of Cutinsomes in Plant Cuticle Formation. *Cells 2020, Vol. 9, Page 1778* **9**, 1778 (2020).
68. Heredia-Guerrero, J. A., Benítez, J. J. & Heredia, A. Self-assembled polyhydroxy fatty acids vesicles: a mechanism for plant cutin synthesis. *BioEssays* **30**, 273–277 (2008).
69. Riederer, M. & Schreiber, L. Protecting against water loss: analysis of the barrier properties of plant cuticles. *J. Exp. Bot.* **52**, 2023–2032 (2001).
70. Isaacson, T. *et al.* Cutin deficiency in the tomato fruit cuticle consistently affects resistance to microbial infection and biomechanical properties, but not transpirational water loss. *Plant J.* **60**, 363–377 (2009).
71. Kosma, D. K. *et al.* The impact of water deficiency on leaf cuticle lipids of Arabidopsis. *Plant Physiol.* **151**, 1918–1929 (2009).
72. Wang, Z. Y., Xiong, L., Li, W., Zhu, J. K. & Zhu, J. The plant cuticle is required for osmotic stress regulation of abscisic acid biosynthesis and osmotic stress tolerance in Arabidopsis. *Plant Cell* **23**, 1971–1984 (2011).

73. Weng, H., Molina, I., Shockey, J. & Browse, J. Organ fusion and defective cuticle function in a lacs1 lacs2 double mutant of Arabidopsis. *Planta* **231**, 1089–1100 (2010).
74. Krolikowski, K. A., Victor, J. L., Wagler, T. N., Lolle, S. J. & Pruitt, R. E. Isolation and characterization of the Arabidopsis organ fusion gene HOTHEAD. *Plant J.* **35**, 501–511 (2003).
75. Shi, J. X. *et al.* SHINE Transcription Factors Act Redundantly to Pattern the Archetypal Surface of Arabidopsis Flower Organs. *PLoS Genet.* **7**, e1001388 (2011).
76. Sieber, P. *et al.* Transgenic Arabidopsis plants expressing a fungal cutinase show alterations in the structure and properties of the cuticle and postgenital organ fusions. *Plant Cell* **12**, 721–737 (2000).
77. Takahashi, K. *et al.* Ectopic Expression of an Esterase, Which is a Candidate for the Unidentified Plant Cutinase, Causes Cuticular Defects in Arabidopsis thaliana. *Plant Cell Physiol.* **51**, 123–131 (2010).
78. Galletti, R., Verger, S., Hamant, O. & Ingram, G. C. Developing a 'thick skin': A paradoxical role for mechanical tension in maintaining epidermal integrity? *Development (Cambridge)* vol. 143 3249–3258 (2016).
79. Kolattukudy, P. E. Enzymatic Penetration of the Plant Cuticle by Fungal Pathogens. *Annu. Rev. Phytopathol.* **23**, 223–250 (1985).
80. Longhi, S. & Cambillau, C. Structure-activity of cutinase, a small lipolytic enzyme. *Biochimica et Biophysica Acta - Molecular and Cell Biology of Lipids* vol. 1441 185–196 (1999).
81. Kolattukudy, P. E., Crawford, M. S., Woloshuk, C. P., Ettinger, W. F. & Soliday, C. L. The Role of Cutin, the Plant Cuticular Hydroxy Fatty Acid Polymer, in the Fungal Interaction with Plants. in 152–175 (1987). doi:10.1021/bk-1987-0325.ch010.
82. Kolattukudy, P. E., Rogers, L. M., Li, D., Hwang, C. S. & Flaishman, M. A. Surface signaling in pathogenesis. *Proc. Natl. Acad. Sci. U. S. A.* **92**, 4080–4087 (1995).

83. Schweizer, P., Jeanguenat, A., Mösinger, E. & Métraux, J.-P. Plant Protection by Free Cutin Monomers in Two Cereal Pathosystems. in 371–374 (Springer, Dordrecht, 1994). doi:10.1007/978-94-011-0177-6_55.

84. Schweizer, P., Felix, G., Buchala, A., Muller, C. & Metraux, J.-P. Perception of free cutin monomers by plant cells. *Plant J.* **10**, 331–341 (1996).

85. Zipfel, C. Plant pattern-recognition receptors. *Trends in Immunology* vol. 35 345–351 (2014).

86. Macho, A. P. & Zipfel, C. Plant PRRs and the activation of innate immune signaling. *Molecular Cell* vol. 54 263–272 (2014).

87. Boller, T. & Felix, G. A Renaissance of Elicitors: Perception of Microbe-Associated Molecular Patterns and Danger Signals by Pattern-Recognition Receptors. *Annu. Rev. Plant Biol.* **60**, 379–406 (2009).

88. Chassot, C. & Métraux, J. P. The cuticle as source of signals for plant defense. in *Plant Biosystems* vol. 139 28–31 (Taylor & Francis Ltd , 2005).

89. Fauth, M. *et al.* Cutin monomers and surface wax constituents elicit H2O2 in conditioned cucumber hypocotyl segments and enhance the activity of other H2O2 elicitors. *Plant Physiol.* **117**, 1373–1380 (1998).

90. Kauss, H., Fauth, M., Merten, A. & Jeblick, W. Cucumber hypocotyls respond to cutin monomers via both an inducible and a constitutive H2O2-generating system. *Plant Physiol.* **120**, 1175–1182 (1999).

91. Kim, T. H., Park, J. H., Kim, M. C. & Cho, S. H. Cutin monomer induces expression of the rice OsLTP5 lipid transfer protein gene. *J. Plant Physiol.* **165**, 345–349 (2008).

92. Park, J. H., Suh, M. C., Kim, T. H., Kim, M. C. & Cho, S. H. Expression of glycine-rich protein genes, AtGRP5 and AtGRP23, induced by the cutin monomer 16-hydroxypalmitic acid in Arabidopsis thaliana. *Plant Physiol. Biochem.* **46**, 1015–1018 (2008).

93. Wang, C., Chin, C. K. & Gianfagna, T. Relationship between cutin monomers and tomato resistance to powdery mildew infection. *Physiol. Mol. Plant Pathol.* **57**, 55–61 (2000).
94. Bessire, M. *et al.* A permeable cuticle in Arabidopsis leads to a strong resistance to Botrytis cinerea. *EMBO J.* **26**, 2158–2168 (2007).
95. Tang, D., Simonich, M. T. & Innes, R. W. Mutations in LACS2, a long-chain acyl-coenzyme A synthetase, enhance susceptibility to avirulent Pseudomonas syringae but confer resistance to Botrytis cinerea in Arabidopsis. *Plant Physiol.* **144**, 1093–1103 (2007).
96. Chassot, C., Nawrath, C. & Métraux, J. P. Cuticular defects lead to full immunity to a major plant pathogen. *Plant J.* **49**, 972–980 (2007).
97. L'Haridon, F. *et al.* A Permeable Cuticle Is Associated with the Release of Reactive Oxygen Species and Induction of Innate Immunity. *PLoS Pathog.* **7**, e1002148 (2011).
98. Mang, H. G. *et al.* The Arabidopsis RESURRECTION1 gene regulates a novel antagonistic interaction in plant defense to biotrophs and necrotrophs. *Plant Physiol.* **151**, 290–305 (2009).
99. Fawke, S. *et al.* Glycerol-3-phosphate acyltransferase 6 controls filamentous pathogen interactions and cell wall properties of the tomato and *Nicotiana benthamiana* leaf epidermis. *New Phytol.* **223**, 1547–1559 (2019).
100. Sela, D. *et al.* Overexpression of AtSHN1/WIN1 Provokes Unique Defense Responses. *PLoS One* **8**, e70146 (2013).
101. Buxdorf, K. *et al.* The transcription factor SlSHINE3 modulates defense responses in tomato plants. *Plant Mol. Biol.* **84**, 37–47 (2014).
102. Blanc, C. *et al.* The cuticle mutant eca2 modifies plant defense responses to biotrophic and necrotrophic pathogens and herbivory insects. *Mol. Plant-Microbe Interact.* **31**, 344–355 (2018).
103. Reina-Pinto, J. J. & Yephremov, A. Surface lipids and plant defenses. *Plant Physiology and Biochemistry* vol. 47 540–549 (2009).

104. Aragón, W., Juan Reina-Pinto, J. & Serrano, M. The intimate talk between plants and microorganisms at the leaf surface. (2017) doi:10.1093/jxb/erx327.
105. de Azevedo Souza, C. *et al.* Cellulose-derived oligomers act as damage-associated molecular patterns and trigger defense-like responses. *Plant Physiol.* **173**, 2383–2398 (2017).
106. Mélida, H. *et al.* Arabinoxylan-Oligosaccharides Act as Damage Associated Molecular Patterns in Plants Regulating Disease Resistance. *Front. Plant Sci.* **0**, 1210 (2020).
107. Rebaque, D. *et al.* Cell wall-derived mixed-linked β-1,3/1,4-glucans trigger immune responses and disease resistance in plants. *Plant J.* **106**, 601–615 (2021).

CHAPTER II

Chapter II consists of the following published manuscript:

Carlos J.S. Moreira[#], Artur Bento[#], Joana Pais, Johann Petit, Rita Escórcio, Vanessa G. Correia, Ângela Pinheiro, Łukasz P. Haliński, Oleksandr O. Mykhaylyk, Christophe Rothan, and Cristina Silva Pereira. Plant Physiology, 2020, Volume 184, 592-606. (https://doi.org/10.1104/pp.20.01049) [#]equally contributing authors

Author contributions

C.S.P. supervised the project and the interpretation of data and prepared the final version of the manuscript; J.Pe. and C.R. contributed to plant material preparation; C.J.S.M., A.B., and R.E. performed ionic liquid synthesis, cutin extraction, and cryogenic milling; A.B. and V.G.C. analyzed the NMR data; J.Pa., A.P., J.Pe., and L.H. analyzed the gas chromatography-mass spectrometry data; O.O.M. and A.B. analyzed the wide-angle x-ray scattering data); A.B. and C.J.S.M. analyzed the differential scanning calorimetry data; C.J.S.M. and A.B. prepared the initial draft of the manuscript; and all authors read and approved the final version of the article.

Outline: The following chapter presents a published work in its original form. A novel ionic liquid-based methodology to isolate cutin is presented. When coupled with cryogenic milling, this approach allowed, for the first time to perform solution NMR characterization of cutin. The systematic characterization of cutin extracted from peels of the miniature tomato cultivar Micro-Tom in wild type and mutants of specific cutin biosynthetic genes is also presented in this chapter.

An Ionic Liquid Extraction That Preserves the Molecular Structure of Cutin Shown by Nuclear Magnetic Resonance

Carlos J. S. Moreira,[a,#] Artur Bento,[a,#] Joana Pais,[a] Johann Petit,[b] Rita Escórcio,[a] Vanessa G. Correia,[a] Ângela Pinheiro,[a] Łukasz P. Halinski,[c] Oleksandr O. Mykhaylyk,[d] Christophe Rothan,[b] and Cristina Silva Pereira,[a,*]

[a] Instituto de Tecnologia Química e Biológica António Xavier, Universidade Nova de Lisboa, 2780–157 Oeiras, Portugal

[b] Institut National de la Recherche Agronomique, University of Bordeaux, UMR 1332 Biologie du Fruit et Pathologie, F–33140 Villenave d'Ornon, France

[c] Department of Environmental Analysis, Faculty of Chemistry, University of Gdańsk, 80–308 Gdańsk, Poland

[d] Soft Matter Analytical Laboratory, Dainton Building, Department of Chemistry, The University of Sheffield, Sheffield S3 7HF, United Kingdom

[#]equally contributing authors;

**Corresponding author: Cristina Silva Pereira (spereira@itqb.unl.pt)*

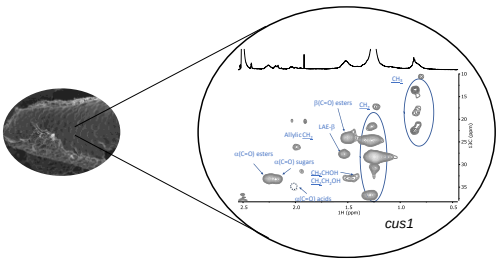

Novel ionic-liquid-based method for a fast and simple purification of a near native cutin, that combined with solution state NMR, can reveal important features in the molecular structure of cutin *in planta*.

Abstract

The biopolyester cutin is ubiquitous in land plants, building the polymeric matrix of the plant's outermost defensive barrier, the cuticle. Cutin influences many biological processes in planta; however, due to its complexity and highly branched nature, the native structure remains partially unresolved. Our aim was to define an original workflow for the purification and systematic characterization of the molecular structure of cutin. To purify cutin we tested the ionic liquids cholinium hexanoate and 1-butyl-3-methyl-imidazolium acetate. The ensuing polymeric materials are highly esterified, amorphous, and have a typical monomeric composition as demonstrated by solid-state NMR, complemented by spectroscopic, thermal, and x-ray scattering analyses. We performed a systematic study by solution-state NMR of cryogenically milled cutins extracted from tomatoes (*Solanum lycopersicum* 'Micro-Tom'; the wild type and the GLYCEROL-3-PHOSPHATE ACYLTRANSFERASE [GPAT6] and CUTIN SYNTHASE [CUS1] mutants). We resolved their molecular structures, relative distribution of ester aliphatics, free acid end-groups and free hydroxyl groups, differentiating between those derived from primary and secondary esters. Our data demonstrate the existence of free hydroxyl groups in cutin and provide insight into how the mutations affect the esterification arrangement of cutin. The usage of ionic liquids for studying plant polyesters has advantages over conventional approaches, since simple modifications can be applied to recover a biopolymer carrying distinct types/degrees of modifications (*e.g.* preservation of esters or cuticular polysaccharides), which in combination with the solution NMR methodologies developed here, constitutes essential tools to fingerprint the multifunctionality and the structure of cutin in planta.

Introduction

Plant polyesters, namely cutin and suberin, are the third most abundant plant polymers after cellulose/hemicellulose and lignin. Naturally, due to their high abundance in nature, plant polyesters are considered as promising substitutes for petroleum-based plastics[1]. In particular, cutin makes up the polymeric matrix of the cuticle that builds the protective layer of the aerial parts of land plants; an evolutionary feature acquired during the colonization of terrestrial environments[2]. The cuticle constituents (cutin and waxes) are deposited onto the polysaccharide layer of the walls of the epidermal cells[3]. Cutin is, in general, a highly branched polymer, mainly composed of C_{16} and C_{18} fatty acids, containing mostly terminal (ω-hydroxyl) and midchain hydroxyl groups, linked through ester bonds. Other functional groups, such as aromatics, dicarboxylic acids, and glycerol, can also be found in cutin in low amounts[4].

Over the years, many authors have contributed to elucidate the roles played by cutin in diverse biological processes of plant development, growth, and response to biotic and/or abiotic stresses[2]. However, current methods for the extraction and analysis of cutin polyesters have inherent limitations. The extraction of cutin from a plant source usually relies on time-consuming processes that include enzymatic digestion of polysaccharides followed by thorough organic solvent extraction of the soluble waxes present in the cuticle[5]. In addition, the chemical analyses of cutin used most frequently are based on total/partial hydrolysis of the polyesters and therefore disclose solely the monomeric constituents[6,7], although sometimes solid-state spectroscopic based analyses of the polymer are used[7,8]. The monomeric constituents can disclose a partial view of the basic composition of the biopolymer (*i.e.* the hydrolyzable constituents), providing insights into its biosynthesis[9], but they do not reveal the structural molecular organization, which remains largely unknown[2,9]. To advance our understanding of important cutin-related questions, such as interactions between cutin and the cell wall polymers or

the role of cutin in defense against pathogens[10], a better insight into the structure of cutin in its native state is required.

Ionic liquids, usually defined as salts in a liquid state below 100 °C, may facilitate the processing of plant polymers due to their capacity to induce swelling/solubilization and/or catalyze the cleavage of specific intermolecular bonds[11]. In particular, some imidazolium-based ionic liquids can efficiently disrupt the intermolecular hydrogen bonding between hydroxyl groups in cellulose[12], whereas some cholinium alkanoates can catalyze selectively the hydrolysis of intermolecular acylglycerol esters[13–15]. The latter ionic liquid was used by us to extract suberin from cork (*Quercus suber*), a plant polyester sharing chemical similarities with cutin, by catalyzing a selective and mild hydrolysis of acylglycerol esters yet preserving most extant linear aliphatic esters[15,16].

Our aim was to establish a novel cutin extraction method that allows the study of near-native cutin architecture and properties and is applicable to a wide range of plant species and tissues. To meet these criteria, the method should be rapid and easy to process, and should greatly preserve the chemical structure of cutin. To this end, we first established an ionic liquid approach for the extraction of cutin, with the solubilization of cutin from tomato (*Solanum lycopersicum*) peels as a proof of concept. We demonstrated that the cholinium hexanoate process renders a material that is enriched in cutin, as shown by scanning electronic microscopy (SEM), ^{13}C magic angle spinning NMR (^{13}C MAS NMR), and differential scanning calorimetry (DSC) analyses of cutin structure. These analyses were complemented by gas chromatography-mass spectrometry (GC-MS) analyses of the hydrolyzable constituents. In addition, we established the molecular structure of cutins in solution (solubilized with the aid of cryogenic milling) through high-resolution one- and two-dimensional (2D) solution state NMR analyses. Extension of our approach from a processing tomato cultivar to the miniature *cv* Micro-Tom, including two cutin biosynthesis and polymerization mutants, highlighted the consistency of our findings with published results but also revealed unknown

features of cutin. We therefore believe that our methodological approach will support discovery in the field of cutin biogenesis and biosynthesis.

Results

A Highly Esterified Cutin Was Purified Using Ionic Liquids That Mostly Mediate the Dissolution of Subcuticular Polysaccharides

Seeking to establish a method to extract cutin from tomato peels, we resorted to cholinium hexanoate and 1-butyl-3-methyl-imidazolium (BMIM) acetate. Cholinium hexanoate was chosen because of its ability to mediate the extraction of suberin from cork through mild and selective hydrolysis of acylglycerol ester bonds[15], and BMIM acetate was chosen for its proven ability to mediate the dissolution of cellulose[12]. First, we tested whether either ionic liquid (100 °C without stirring) hydrolyzes glyceryl trioctanoate and octyl octanoate, which contain an acylglycerol ester bond and a linear aliphatic ester bond, respectively. Glyceryl trioctanoate was hydrolyzed in the presence of both ionic liquids, yet the efficiency of the reaction was higher when cholinium hexanoate was used (Figure 1). Cholinium hexanoate did not catalyze the cleavage of octyl octanoate (Figure 1A), whereas BMIM acetate did catalyze this reaction albeit inefficiently (Figure 1B). As previously reported, cholinium hexanoate catalyzes specifically the hydrolysis of acylglycerol esters[15], although in this study the absence of agitation and the higher water content of the ionic liquid reduced the reaction efficiency.

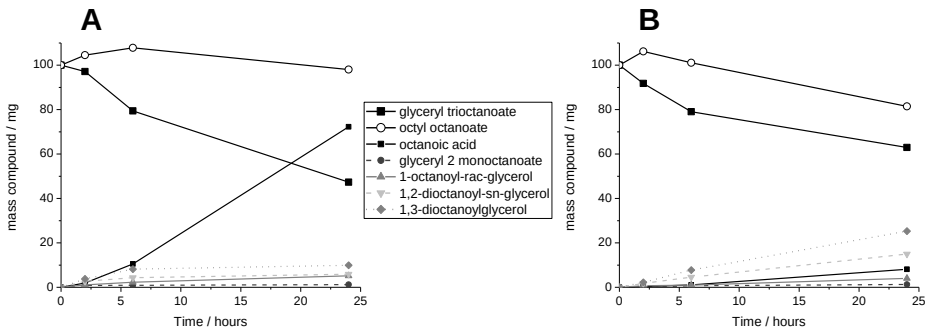

Figure 1. Quantitative analysis of the ionic liquid-mediated hydrolysis of ester bonds in model compounds. Compounds detected after the reaction of glyceryl trioctanoate and octyl octanoate with either cholinium hexanoate (A) or BMIM acetate (B) for 2, 6, and 24 h (the observed average SE values were negligible at < 4 %). All compounds were identified and quantified by GC-MS. At time zero, glyceryl trioctanoate and octyl octanoate were assumed to represent the only compounds present in the mixture.

We then tested the potential of these ionic liquids to isolate cutin from tomato peels after 2, 15, and 170 h compared to a conventional method (*i.e.* enzymatic removal of polysaccharides followed by organic solvent-mediated dewaxing). In the process of suberin extraction from cork using cholinium hexanoate, suberin in the filtrate is recovered by precipitation in an excess of water[14]. We preliminarily tested a 2-h reaction of tomato peel cutin in cholinium hexanoate and used attenuated total reflection-Fourier transform infrared spectroscopy (ATR-FTIR) to verify that the archetypal bands assigned to cutin, *i.e.* long-chain aliphatics (CH_2 and C=O), were detected in the insoluble fraction (not in the filtrate as observed for cork suberin) whereas the filtrate shows enrichment in bands usually assigned to polysaccharides (C-O-C; Figure S1). Accordingly, the insoluble fractions produced were characterized using SEM (Figure 2) and ^{13}C MAS NMR (Figure 3A). SEM imaging of the cutins extracted with either ionic liquid are virtually identical: a clean thick cutin-continuum showing the epidermal cell grooves (Figure 2, A–F). In the reference cutin, *i.e.* obtained through the conventional enzymatic-based process, the cutin continuum apparently overlaps with other

cellular components, and many intracellular spaces are not hollow (Figure 2G).

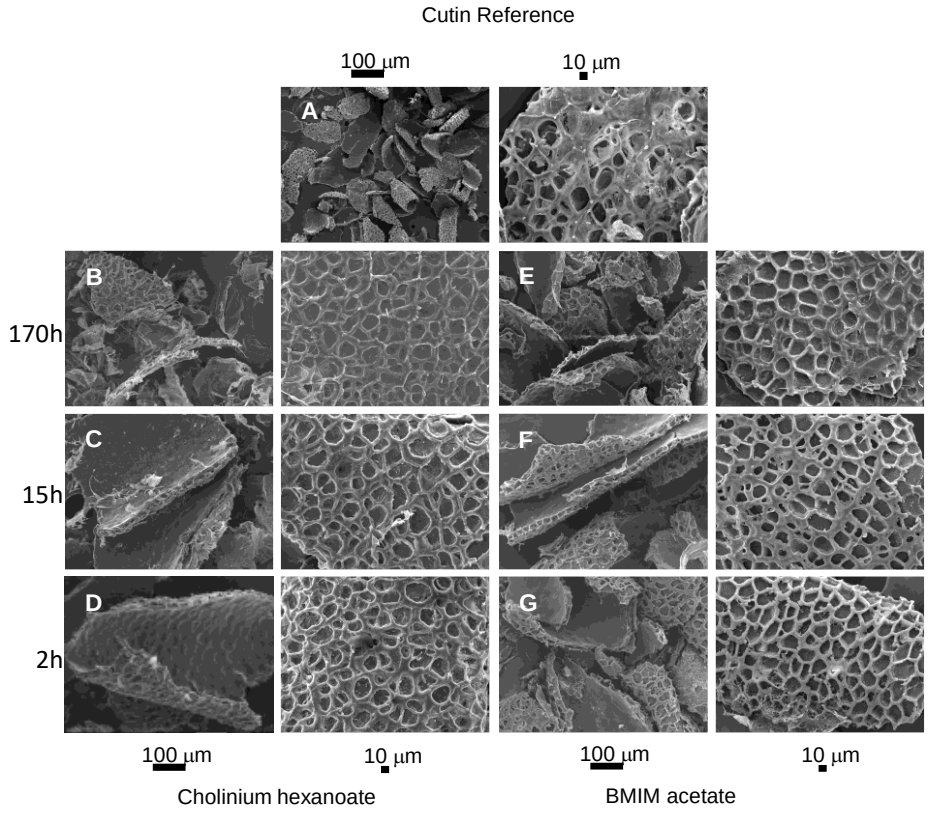

Figure 2. SEM analysis of cutin-enriched materials upon extraction. A, A representative cutin reference sample (*i.e.* obtained through the conventional enzymatic-based process) depicts many intracellular spaces that are not hollow. B to G, Imaging of cutin-enriched materials was obtained after treatment with cholinium hexanoate (B–D) or BMIM acetate (E–G) for 2, 15, and 170 h. All samples show a clean thick cutin continuum comprising the epidermal cell grooves.

In the ^{13}C MAS NMR spectrum of the reference cutin, the major structural classes assigned to cutin include the long methylene chains, $(CH_2)_n$, with major peaks at 26, 29, and 34 ppm; the oxygenated aliphatics, CH_2O (63 ppm) and CHO (73 ppm); and the carboxyl groups at 172 ppm, comprising the contribution of both esters and acids (Figure 3A)[10]. Only minor signals can be assigned to the aromatic region (105 and 130 ppm). The

spectral signatures of the remaining cutins are very similar, regardless of the ionic liquid used and the extraction time, and are also similar to the reference cutin spectrum (Figure 3; Table 1).

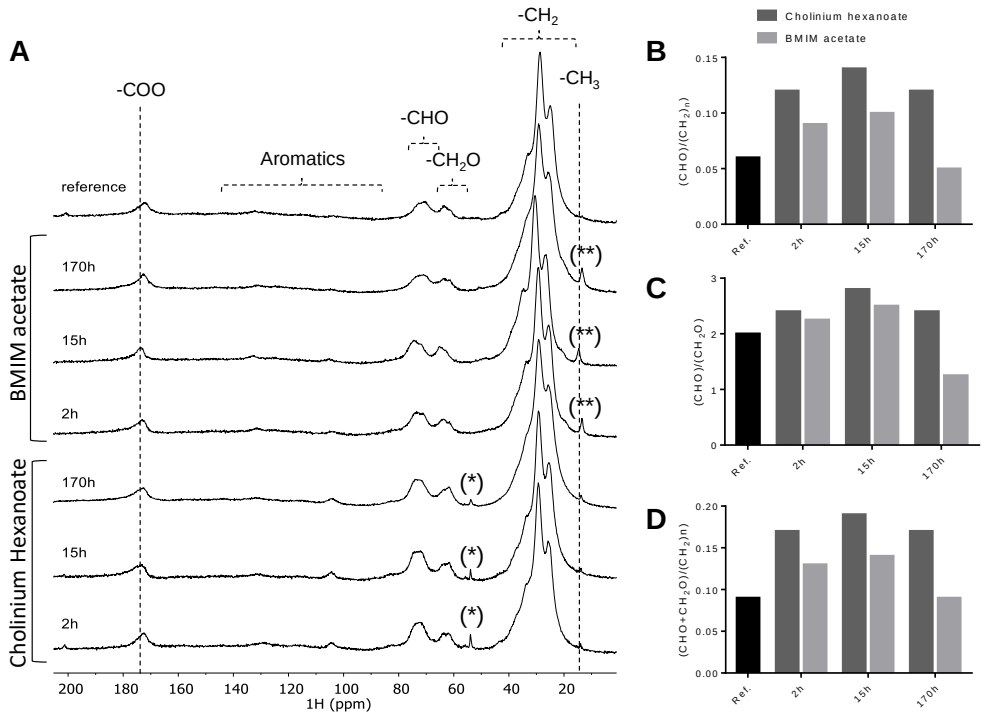

Figure 3. ^{13}C MAS NMR spectra obtained for the cutin-enriched materials upon extraction. Spectra of the reference cutin sample and cutin-enriched materials derived from reactions with cholinium hexanoate or BMIM acetate for 2, 15, and 170 h (A) and the corresponding calculated reticulation (B and C) and esterification (D) ratios. The regions assigned to the long methylene chains, oxygenated aliphatics, aromatics, and carboxyl groups are marked. The imidazolium-based cation contributes to the signal assigned to the CH_3 groups at 15 ppm (**), whereas the cholinium cation is seen in the signal at 54 ppm (*); both contaminants can be washed out.

Table 1. *Relative abundance of the contributions of the regions of aliphatics (10–50 ppm), oxygenated aliphatics (57–92 ppm), aromatics (92–165 ppm), and carboxyl groups (165–185 ppm) for each cutin ^{13}C MAS NMR spectrum*

Method	Cutin Major Structural Classes	Relative Abundance of the ^{13}C MAS NMR Assigned Regions				
		C=O	C=C	CHO	CH_2O	$(CH_2)_n$
		Carboxyls	Aromatics	Oxygenated Aliphatics		Aliphatics
				%		
Reference	—	5.1	1.7	5.1	2.6	85.5
Cholinium hexanoate	2 h	4.8	1.6	9.6	3.7	80.0
	2 h + TFA	3.9	3.1	10.2	4.7	78.1
	15 h	4.7	3.1	10.9	3.9	77.5
	170 h	4.7	3.1	9.1	3.9	65.0
BMIM acetate	2 h	5.6	4.0	7.2	3.2	80.0
	15 h	5.5	5.5	7.8	3.1	73.5
	170 h	5.6	6.5	4.0	3.2	80.6

The relative contributions of the signals assigned to aromatics for the cutins purified with either ionic liquid increased along the reaction time, possibly an artifact derived from phase corrections. The relative contributions of the oxygenated aliphatic region (57–92 ppm) are higher in ionic liquid-extracted cutins compared to the reference cutin (Figure 3A). This region might also comprise resonances derived from polysaccharides[10]. Most subcuticular polysaccharides can be removed from cutin using acidic hydrolysis mediated by trifluoroacetic acid (TFA)[17], although cellulose might not be totally removed[18]. In this study, the NMR spectra of cutins obtained using cholinium hexanoate (2-h reaction) before and after the acidic hydrolysis treatment are virtually identical (Table 1; Figure S2). The few observed alterations can be explained by the hydrolysis of esters during the acidic treatment[17]. Based on these results, the oxygenated aliphatics region can be mostly assigned to cutin. Consequently, the biopolymer reticulation level can be reasonably estimated through the ratio of the signal's integral in the CHO region of the oxygenated aliphatics (67–92 ppm) to that of the entire aliphatic region (8–50 ppm) or that of the CH_2O region (57–67 ppm)[10,19]. Based on the calculated reticulation ratios, cholinium hexanoate usage apparently rendered a biopolymer displaying higher reticulation compared to that attained with either BMIM acetate or the conventional approach (Figure 3, B and C). At this stage, one cannot exclude that the presence of cellulose embedded in the

biopolymer might increase the estimated reticulation levels. A similar trend was observed when estimating biopolymer esterification levels (Figure 3D), which can be inferred through the ratio of the integral of the total oxygenated aliphatic region (CHO and CH_2O) with that of the entire aliphatic region (8–50 ppm)[19]. Esterification of the cholinium cation with cutin's free acids was reported previously to be mechanistically very unlikely[15].

In order to further elucidate whether the ionic liquid-based extractions can indeed render a material enriched in cutin, we resorted to DSC (Figure 4A) and wide-angle x-ray scattering (WAXS; Figure 4B) measurement of the cutins extracted with the ionic liquids (2- and 170-h reactions) together with the reference cutin. The DSC thermograms are depicted in figure 4A. The cutins extracted using either ionic liquid for 2 h show higher enthalpy energies for melting the biopolymer and lower melting temperatures (ΔH = 129.6 J g^{-1} and T_m= 100.5 °C versus ΔH = 97.5 J g^{-1} and T_m = 100.6 °C, for cholinium hexanoate and BMIM acetate, respectively) compared to the reference cutin (ΔH = 70.5 J g^{-1} and T_m = 114.5 °C). All thermograms show a relatively broad melting curve (Figure 4A), which is typical for heterogeneous and amorphous materials[20], and similar glass transition temperatures (~ -20 °C). The peaks for the cutins that originated from the 2-h ionic liquid reactions are less broad compared to the reference cutin, suggestive of increased homogeneity. This feature was lost when extensive reaction times were used, consistent with the estimated reduction in biopolymer reticulation and esterification (Figure 3, B–D). The WAXS patterns of all cutin samples (Figure 4B) are mainly represented by a broad diffuse peak with maximum intensity at around q = 1.41 $Å^{-1}$, which most likely corresponds to an amorphous structure commonly formed by organic polymeric materials with an interchain distance of ~ 4.5 Å.

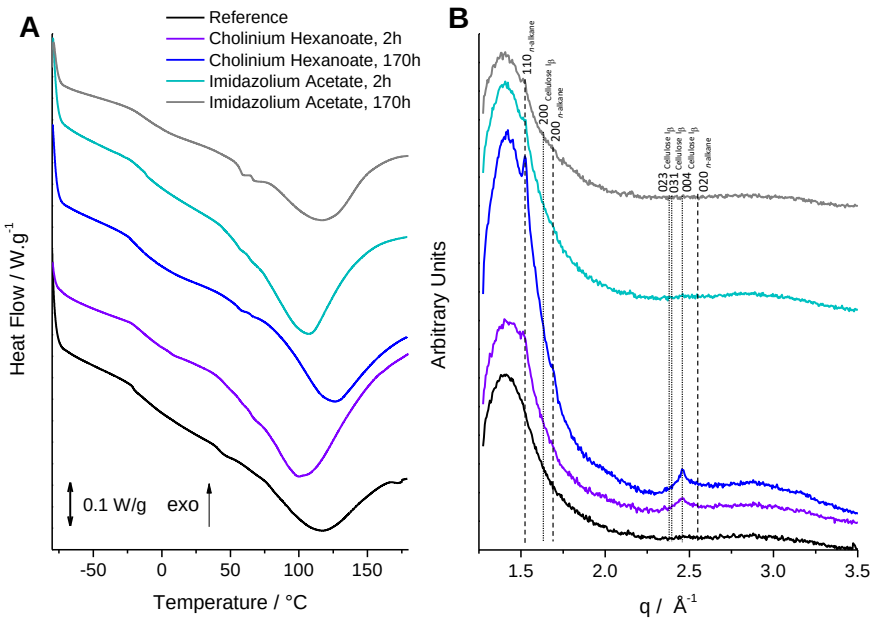

Figure 4. Analysis of the crystallinity properties of the cutin-enriched materials upon extraction. DSC thermograms (A) and WAXS patterns (B) collected for a reference enzymatically extracted cutin material (black curve) and cutin materials extracted from tomato peels using ionic liquids for various durations of treatment: cholinium hexanoate for 2 and 170 h (purple and blue curves, respectively) and imidazolium acetate for 2 and 170 h (gray and cyan curves, respectively). The vertical straight lines in WAXS patterns indicate the positions of diffraction peaks of cellulose (dotted lines) and crystallized n-alkane chains (dashed lines). Miller indexes assigned to the lines correspond to cellulose I_β (monoclinic space group $P12_11$) and *n*-alkane chain packing (orthorhombic space group Pnma).

Considering the composition of cutin, this amorphous structure should be related to randomly packed acyl chains. In contrast to the reference cutin, the scattering patterns of cutins extracted by either ionic liquid show diffraction peaks indicating the presence of a crystalline component. The first diffraction peak at q = 1.52 Å^{-1} and the second at q = 1.69 Å^{-1}, noticeable for cutin extracted by cholinium hexanoate for 170 h (Figure 4A, blue curve), can be

assigned to an orthorhombic crystal structure (space group Pnma; Miller indexes 110 and 200, respectively) commonly formed by compounds comprised of alkane-like chains such as triacylglycerols (b' phase)[21] or polyethylene[22,23]. This suggests that the extraction of cutin by the ionic liquids enriches this material with a crystalline component where some acyl chains tend to form crystals. A low level of branching of acyl chains in cutin may be favorable for the formation of an orthorhombic unit cell, which is thermodynamically more stable than the rotator phase formed by distorted alkane chains packed in a hexagonal array[24]. This observation is consistent with the DSC measurements (Figure 4A) indicating that the cutin extracted by cholinium hexanoate for 170 h, containing the highest fraction of the acyl crystalline component, has the highest peak melting point. The third diffraction peak, at q = 2.46 $Å^{-1}$, observed for cutin extracted by cholinium hexanoate (Figure 4B, purple and blue curves), cannot be related to the acyl chain crystalline structure. Its position is significantly shifted from a possible 020 peak at q = 2.55 $Å^{-1}$ generated by the orthorhombic structure (Figure 4B). The third peak is likely to be associated with a crystalline cellulose and can be assigned to 004 reflection of monoclinic cellulose I_β (space group $P12_11$)[25]. It must be noted that the most intense 200 diffraction peak of the cellulose I_β expected at q = 1.63 $Å^{-1}$ is not visible because of an overlap with the intense broad peak corresponding to the amorphous structure. Crystalline cellulose usually coexists with amorphous cellulose[25]. However, it would be difficult, if possible at all, to identify the amorphous cellulose component, with its expected peak maximum intensity at q = 1.52 $Å^{-1}$, from the broad diffuse peak observed by WAXS. Neither enzymatically extracted cutin (reference cutin) nor cutin extracted by BMIM acetate reveal the presence of crystalline cellulose in their scattering patterns (Figure 4B, black, cyan, and gray curves), indicating that both extraction methods led to its successful removal. This observation, together with the higher relative contribution of the oxygenated aliphatics region for cutin extracted with BMIM acetate compared with the

reference cutin (Table 1), suggests that some oxygenated aliphatics are lost during the enzymatic treatment.

Finally, the relative abundances of hydrolyzable cutin constituents were determined by GC-MS to disclose how ionic liquid extraction methods influence the composition of the biopolymer compared to the reference method (Table 2; Figure S3; Table S1). The reference cutin comprises ~ 13 % of nonhydrolyzable constituents, whereas cutin constituents attained using an ionic liquid display substantially higher recalcitrance (~ 20% to 30%), consistent with their estimated higher reticulation (Figure 3, B and C). In general, the monomeric compositions of the ionic liquid-extracted cutins are similar to that of the cutin reference (and also to the starting material; Table 2). Both the abundance and the diversity of fatty acids decreased as the reaction time in the ionic liquid increased (Table 2). This was more pronounced when BMIM acetate was used for 170 h, which rendered a cutin almost devoid of fatty acids and also containing nearly 2-fold less dicarboxylic acids. The fatty acids carry a methyl end-group that is esterified to the biopolymer through a single bond.

Table 2. *GC-MS quantitative analysis of the hydrolyzable constituents identified in cutin samples purified using either cholinium hexanoate or BMIM acetate in 2-, 15-, or 170-h reactions*

The reference cutin and the feedstock (i.e. untreated peels) were also analyzed for comparison. Results are given as wt % (n = 3). The identification yields (wt %) and the mass of the nonhydrolyzable fraction (recalcitrance [%]) are indicated.

Compound Name	Compound Abundances							
	Untreated Feedstock	Reference Cutin	Cholinium Hexanoate			BMIM Acetate		
			2 h	15 h	170 h	2 h	15 h	170 h
				wt %				
Fatty acids	2.60 ± 0.13	1.52 ± 0.24	1.27 ± 0.15	0.88 ± 0.13	0.67 ± 0.09	1.96 ± 0.2	0.74 ± 0.1	0.10 ± 0.06
Hexadecanoic acid	1.25 ± 0.04	0.74 ± 0.05	0.64 ± 0.04	0.41 ± 0.11	0.33 ± 0.03	0.63 ± 0.05	0.42 ± 0.03	0.10 ± 0.06
Octadeca-9,12-dienoic acid	0.43 ± 0.15	0.23 ± 0.05	0.20 ± 0.03	0.11 ± 0.01	–	0.74 ± 0.12	–	–
Octadec-9-enoic acid	–	0.24 ± 0.06	0.11 ± 0.02	0.09 ± 0.04	–	0.18 ± 0.03	–	–
Octadecanoic acid	0.91 ± 0.12	0.31 ± 0.10	0.09 ± 0.00	0.13 ± 0.05	0.12 ± 0.02	0.18 ± 0.04	0.13 ± 0.06	–
4-Oxocyclohexane-1-carboxylic acid	–	–	0.23 ± 0.08	0.14 ± 0.12	0.22 ± 0.06	0.23 ± 0.00	0.19 ± 0.02	–
Dicarboxylic acids	10.89 ± 1.08	18.38 ± 0.44	18.64 ± 0.49	19.2 ± 2.16	18.64 ± 0.58	18.45 ± 1.19	19.3 ± 0.21	9.99 ± 2.05
Nonanedioic acid[a]	–	0.43 ± 0.02	0.26 ± 0.02	0.26 ± 0.15	0.36 ± 0.01	0.27 ± 0.02	0.22 ± 0.04	–
Hexadecanedioic acid	0.56 ± 0.02	1.51 ± 0.07	1.30 ± 0.07	1.52 ± 0.10	1.22 ± 0.08	1.47 ± 0.07	1.42 ± 0.15	0.46 ± 0.07
8/9-Hydroxyhexadecanedioic acid[b]	10.33 ± 1.06	16.43 ± 0.38	17.08 ± 0.55	17.43 ± 2.01	17.06 ± 0.50	16.7 ± 1.14	17.66 ± 0.20	9.53 ± 0.23
ω-Hydroxy acids	11.13 ± 0.35	15.04 ± 0.31	18.42 ± 0.63	17.42 ± 2.22	17.69 ± 1.28	18.95 ± 0.4	18.49 ± 1.06	22.90 ± 1.68
16-Hydroxyhexadecanoic acid	5.38 ± 0.16	8.17 ± 0.21	8.20 ± 0.12	8.50 ± 0.65	8.32 ± 0.21	8.35 ± 0.23	8.48 ± 0.39	15.71 ± 0.68
16-Hydroxy-10-oxohexadecanoic acid	3.02 ± 0.28	2.29 ± 0.14	6.39 ± 0.52	6.21 ± 0.97	6.28 ± 0.61	6.81 ± 0.05	6.62 ± 0.39	1.80 ± 0.12
9, 10-Epoxy-18-hydroxyoctadecanoic acid	1.14 ± 0.24	1.93 ± 0.09	1.73 ± 0.07	1.63 ± 0.38	1.27 ± 0.32	1.67 ± 0.13	1.60 ± 0.14	2.38 ± 0.53
9, 10-Epoxy-18-hydroxyoctadecenoic acid	1.60 ± 0.15	2.65 ± 0.20	2.10 ± 0.25	1.62 ± 0.18	1.82 ± 0.55	2.11 ± 0.09	1.79 ± 0.18	3.01 ± 0.59
Polyhydroxy acids	55.05 ± 2.01	65.06 ± 0.65	61.67 ± 0.28	62.49 ± 4.06	63.01 ± 1.92	60.64 ± 1.69	61.47 ± 1.28	67.01 ± 1.44
10,16-Dihydroxyhexadecanoic acid[c]	53.22 ± 2.23	63.24 ± 0.98	58.83 ± 0.42	59.68 ± 5.03	61.20 ± 2.16	58.12 ± 1.89	58.97 ± 1.55	63.12 ± 2.42
9,10,18-Trihydroxyoctadecanoic acid	1.00 ± 0.11	0.94 ± 0.06	1.11 ± 0.32	1.19 ± 0.67	0.53 ± 0.00	0.85 ± 0.11	0.90 ± 0.13	1.51 ± 0.45
9,10,18-Trihydroxyoctadec-12-enoic acid	0.84 ± 0.39	0.89 ± 0.36	1.73 ± 0.07	1.63 ± 0.38	1.27 ± 0.32	1.67 ± 0.13	1.60 ± 0.14	2.38 ± 0.53
Sterols[d]	20.33 ± 1.07	–	–	–	–	–	–	–
Identification yield (%)	56.38 ± 2.46	50.7 ± 2.38	58.1 ± 0.88	59.34 ± 6.63	56.39 ± 1.20	58.02 ± 2.45	60.35 ± 3.46	82.15 ± 0.20
Recalcitrance (%)	22.14 ± 2.98	13.32 ± 1.39	28.3 ± 4.98	27.47 ± 0.58	33.07 ± 0.56	19.75 ± 0.36	20.21 ± 1.06	18.15 ± 2.48

[a]This compound was overestimated or overlapped with an unknown compound. [b]This compound was associated with the possible presence of unspecific isomers. [c]The major species of this compound was 10,16-diOH and minor species were 9,16- and 8,16-diOH. [d]Triterpenoids and sterols identified were β-amyrin (5.69 ± 0.44), α-amyrin (4.44 ± 0.20), δ-amyrin (7.53 ± 1.48), and stigmasterol (2.68 ± 0.49).

A Snapshot of the Molecular Structure of Cutin Purified by Cholinium Hexanoate Reveals Extant Free Hydroxyls and Free Acids

Our data made evident the potential of using short time reactions with either ionic liquid to recover from tomato peels a cutin continuum displaying esterification/reticulation levels and composition near that found in planta. In addition, cholinium hexanoate presents several advantages compared to BMIM acetate. It cleaves fewer ester bonds, rendering a more esterified biopolymer (Figure 3D), and unlike BMIM acetate, it is also biocompatible and biodegradable[26].

Recently, we used solution-state NMR to resolve the molecular structure of *in situ* suberin upon its solubilization in heated dimethylsulfoxide (DMSO) directly from cork after 4 h of cryogenic milling[16]. This inspired us to apply cryogenic milling for the solubilization of a cutin extracted with cholinium hexanoate after 2 h. Solving cutin's molecular structure would allow us to look "inside" its backbone, specifically at its esterification arrangement. The GC-MS analyses disclosed only the component hydrolyzable constituents (Table 2) and the solid-state analyses — ^{13}C MAS NMR, DSC, and WAXS (Figures 3 and 4) — revealed only the bulky chemical functionalities and properties of the purified cutin materials. Only after 10 h of cryogenic milling was the cutin solubilized in DMSO, reflecting cutin's much lower solubility compared to suberin. We analyzed the impact of the cryogenic milling process, especially the occurrence of oxidation reactions inside the grinding jar due to possible condensation of oxygen at low temperatures. Elemental analysis of cutin before and after the cryogenic milling process revealed that the relative percentages of the tested elements, including oxygen (Table S2), were unaltered after the treatment. Therefore, despite the solubility drawback, a solution-state ^{1}H NMR could be acquired with good resolution, showing the presence of many overlapping signals (Figure 5A), an archetypal feature observed in other complex multifunctional polymers[27].

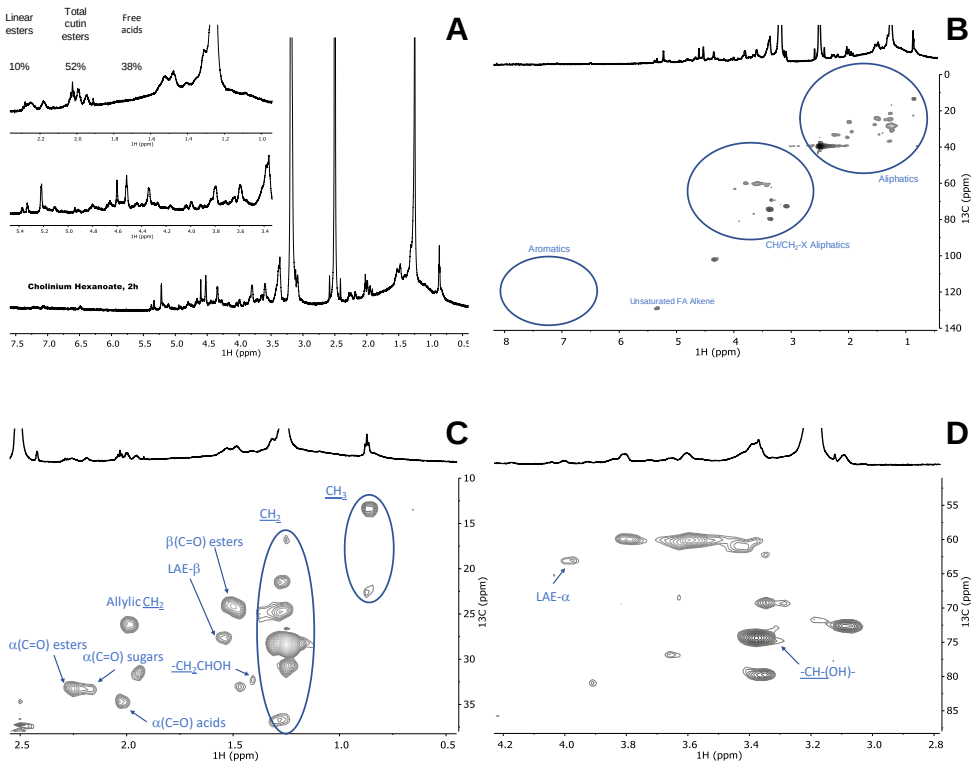

Figure 5. Wide-ranging NMR spectral characterization of cutin materials isolated with cholinium hexanoate (2 h). Shown are ^{1}H NMR spectra with inserts focusing on the aliphatic and oxygenated aliphatic regions (A) and the full HSQC spectrum (B) as well as regions corresponding to aliphatics (C) and CH/CH_2-X aliphatics (D) of the purified cutin. Some assignments (unlabeled) are uncertain or unidentified.

The relative abundances of aliphatics, CH/CH_2-X oxygenated aliphatics, and aromatics were estimated through integration of the ^{1}H spectrum as 70 %, 27 %, and 3 %, respectively. The assignment of ^{1}H chemical shifts for the constituent monomers was then achieved through a combination of ^{1}H-^{1}H correlation spectroscopy (COSY) and ^{1}H-^{13}C correlations, namely heteronuclear single-quantum correlation spectroscopy (HSQC) and heteronuclear multiple-bond correlation spectroscopy (HMBC; Figures S4–S6; Table S3). Previous NMR-based data for tomato cutin were attained through solution-state NMR analyses of oligomeric structures obtained by methanolysis of tomato peels[6] and high-

resolution MAS NMR analyses of tomato cutin swollen in DMSO[8]. These studies provided important baseline information for the assignment of the spectrum of cutin extracted with cholinium hexanoate for 2 h (Table S3).

The full range of the HSQC spectrum of cutin is depicted in Figure 5B, which highlights the regions corresponding to aliphatics and CH/CH_2-X aliphatics as well as aromatics. A detailed analysis of the HSQC spectrum of the two aliphatic regions with the assignment of CH_2 and CH_3 groups from the aliphatic chains, the ester bonds, and the free midchain hydroxyl groups is shown in Figure 5, C and D. Only secondary free hydroxyl groups were visible in the HSQC spectrum (CHOH midchain), consistent with their presence in cutin as suggested previously[28]. This observation is in agreement with the demonstration that cholinium hexanoate does not cleave primary ester bonds (Figure 1). Here, we assigned the β-(C=O) esters to a ^{1}H shift of 1.49 ppm and a ^{13}C shift of 24 ppm, but we could not detect the signal of β-(C=O) acids, even though they have been assigned before in tomato cutin using high-resolution MAS NMR[8]. *Deshmukh et al. (2003)* assigned the signals of aliphatic esters, primary and secondary alcohols, free acids, and α-branched carboxylic acids, yet the last two assignments could not be confirmed by HMBC. In this study, the signals of the β-(C=O) acids may overlap with that of the esters, and differentiating these signals from the small chemical shift differences observed in the acquired HSQC data is virtually impossible. The α-(C=O) signal displays two ^{1}H signals with a ^{13}C shift of 33 ppm, namely at 2.25 and 2.19 ppm, which can be assigned to esters and acids, respectively. The α-(C=O) signal with a ^{1}H shift of 2.17 ppm was previously assigned to xylan esters[29]. Based on the detection of vestigial amounts of microcrystalline cellulose in the cutin extracted with cholinium hexanoate for 2 h (Figure 4B), this signal may be associated with the presence of cellulose esters. Analysis of the cutin extracted with BMIM acetate (also cryogenically milled), which is apparently devoid of microcrystalline cellulose (Figure 4B), showed that the α-(C=O) signal displays a ^{13}C shift of 33 ppm and only a ^{1}H shift of 2.26 ppm (Figure S7). Finally, to precisely assign the free acids in the cutin extracted

with cholinium hexanoate for 2 h, we acquired the HMBC spectrum that confirmed their signal at a ^{13}C shift of 35 ppm and a ^{1}H shift of 2.02 ppm (Figure S6), consistent with the previously observed assignment in cork suberin, where the signal of the acids is at a ^{13}C shift of 36 ppm and a ^{1}H shift of 2.03 ppm and that of the esters displays a ^{13}C shift of 34 ppm and a ^{1}H broad shift from 2.33 to 2.27 ppm[16].

Based on the assignments defined above, we calculated the relative abundance of free acids, total esters (comprising primary and secondary aliphatic esters yet excluding sugar esters), and linear esters as 38 %, 52 %, and 10 %, respectively, through integration of the signals in the ^{1}H NMR (Figure 5A). No acylglycerol bonds were detected in the HSQC analyses of cutin (Figure 5B), consistent with the very low abundance of glycerol in tomato cutin[2]. We hypothesize that the free acids detected in the cutin spectra might mostly account for their natural occurrence, though one cannot exclude, at this stage, that some aliphatic esters might have undergone cleavage in the presence of cholinium hexanoate.

Ionic Liquid Extraction Followed by Solution NMR As a Tool to Scrutinize the Impact of Specific Mutations in the Molecular Structure of Cutin from cv Micro-Tom Tomatoes

Solving the molecular structure in solution of a near native cutin isolated from a processing tomato cultivar challenged us to test the suitability of the established cholinium hexanoate extraction for 2 h for purification and systematic characterization of cutins isolated from the tomato miniature 'Micro-Tom', which is particularly well suited for laboratory studies[30,31]. To introduce known diversity in cutin composition and structure, we further used both the wild type and mutants of *gpat6* and *cus1*, respectively[28,32,33], which show phenotypes with altered cutin composition and altered degrees of intrachain branching. In particular, in the *gpat6* mutant (formerly named the cutin deficient mutant, *cud1*)[28], synthesis of the major cutin precursor is

hampered so that a thinner cuticle enriched in fatty acids is produced with overall decreased levels of cutin[32]. In contrast, in the *cus1* tomato mutants, cutin polymerization is impaired[34,35] and the esterification of secondary OH groups of the dihydroxy acids is significantly reduced[28]. To minimize any possible effect of environmental conditions on the expression of the fruit cuticle phenotype, the *gpat6* and *cus1* mutants were grown side by side with wild-type plants. The relative abundance of the hydrolyzable constituents in the *cv* Micro-Tom cutins purified with cholinium hexanoate is depicted in table 3.

Table 3. *GC-MS quantitative analysis of the hydrolyzable constituents in cutin samples purified using cholinium hexanoate (2 h reaction) from wild-type and* cus1 *and* gpat6 *mutant 'Micro-Tom' tomato plants*

Results are given as % wt (n = 3). The identification yields (wt %) and the mass of the non-hydrolysable fraction (recalcitrance, %) are indicated below.

Compound Name	Compound Abundances		
	wt	*cus1*	*gpat6*
		wt %	
Fatty acids	0.50 ± 0.04	6.06 ± 0.81	5.60 ± 0.88
Hexadecanoic acid	0.27 ± 0.02	2.09 ± 0.26	1.59 ± 0.23
9,12-octadecadienoic	–	3.00 ± 0.59	2.22 ± 0.42
9-octadecenoic acid	0.24 ± 0.06	–	1.20 ± 0.16
Octadecanoic acid	–	0.96 ± 0.12	0.59 ± 0.11
Dicarboxylic acids	4.68 ± 0.32	7.23 ± 0.55	7.92 ± 0.5
Nonanedioic acid[a]	–	1.75 ± 0.37	0.88 ± 0.05
Hexadecandioic acid	0.60 ± 0.10	–	1.95 ± 0.23
8/9-hydroxyhexadecanedioic acid[b]	4.08 ± 0.23	5.48 ± 0.24	5.09 ± 0.25
ω-Hydroxy acids	5.47 ± 0.30	1.19 ± 0.02	1.56 ± 0.08
16-Hydroxyhexadecanoic acid	3.97 ± 0.23	1.19 ± 0.02	1.12 ± 0.09
16-Hydroxy-10-oxohexadecanoic acid	0.71 ± 0.04	–	0.44 ± 0.02
9, 10-Epoxy-18-hydroxyoctadecanoic acid	0.25 ± 0.05	–	–
9, 10-Epoxy-18-hydroxyoctadecenoic acid	0.54 ± 0.02	–	–
Polyhydroxy acids	89.35 ± 0.63	85.33 ± 1.32	84.86 ± 1.46
Dihydroxyhexadecanoic acid[c]	87.91 ± 0.48	83.87 ± 1.52	77.71 ± 2.50
9,10,18-Trihydroxyoctadecanoic acid	0.62 ± 0.06	0.91 ± 0.18	3.84 ± 0.76
9,10,18-Trihydroxyoctadec-12-enoic acid	0.82 ± 0.09	0.54 ± 0.04	3.31 ± 0.49
Sterols[d]	–	0.19 ± 0.04	–
Identification yield (%)	57.99 ± 1.26	37.49 ± 0.74	36.05 ± 1.75
Recalcitrance (%)	32.6 ± 3.68	44.26 ± 2.96	41.28 ± 0.97

[a]This compound was overestimated or overlapped with an unknown compound. [b]This compound was associated with the possible presence of unspecific isomers. [c]The major species of this compound was 10,16-diOH and minor species were 9,16- and 8,16-diOH. [d]The identified sterol was stigmasterol.

In general, the observed diversity/abundance of hydrolyzable constituents is similar to that previously reported[28,32], though there are some variations, possibly due to disparities in tomato growth conditions in the

greenhouse (season, light, temperature, and hygrometry). In addition, the cutins that originated from the mutants show an increase in the relative abundance of nonhydrolyzable constituents compared to the wild type (~ 10 % increase), and their identification yields decreased nearly 20 % due to higher diversity of unidentified monomers (Table 3). Cutin from both mutants displays a higher relative abundance of fatty acids and dicarboxylic acids (nearly 10- and 2-fold, respectively) and lower relative abundance of ω-hydroxyacids (five to three times) compared to wild-type cutin.

To confirm that free acids naturally occur in cutin (hence differentiating these from free acid groups formed during the ionic liquid extraction), we compared the spectra of cutin from the wild-type cultivar obtained through the ionic liquid process followed by cryogenic milling with that of the cuticle solubilized solely via cryogenic milling (Figure 6; Figures S8–S12).

The obtained ^{1}H NMR (Figure 6, A and B) and HSQC spectra (Figure 6, C–F) are very similar, although the presence of noncutin constituents in the cuticle contributes to the appearance of many signals that have yet to be assigned, *e.g.* in the CH_3 region (Figure 6D). Importantly, the signals previously assigned to free acids α-(C=O) acids are visible in both samples (Figure 6, C and D), as confirmed in the corresponding HMBC spectra (Figure S10). Accordingly, the free acids detected in the ionic liquid-purified cutins (Figs. 5, A–C, and 6, A and B) reflect their natural presence. The signal attributed to the terminal hydroxyls was only detected in the spectrum of the ionic liquid-extracted *cv* Micro-Tom cutin (Figure 6E). This observation suggests that the cholinium hexanoate treatment cleaved some primary esters in the *cv* Micro-Tom cutin, contrary to observations for cutin derived from the peels of processing tomatoes (Figure 5D). One possibility is that the cleavage of primary esters is greatly influenced by the native arrangement of the polymer.

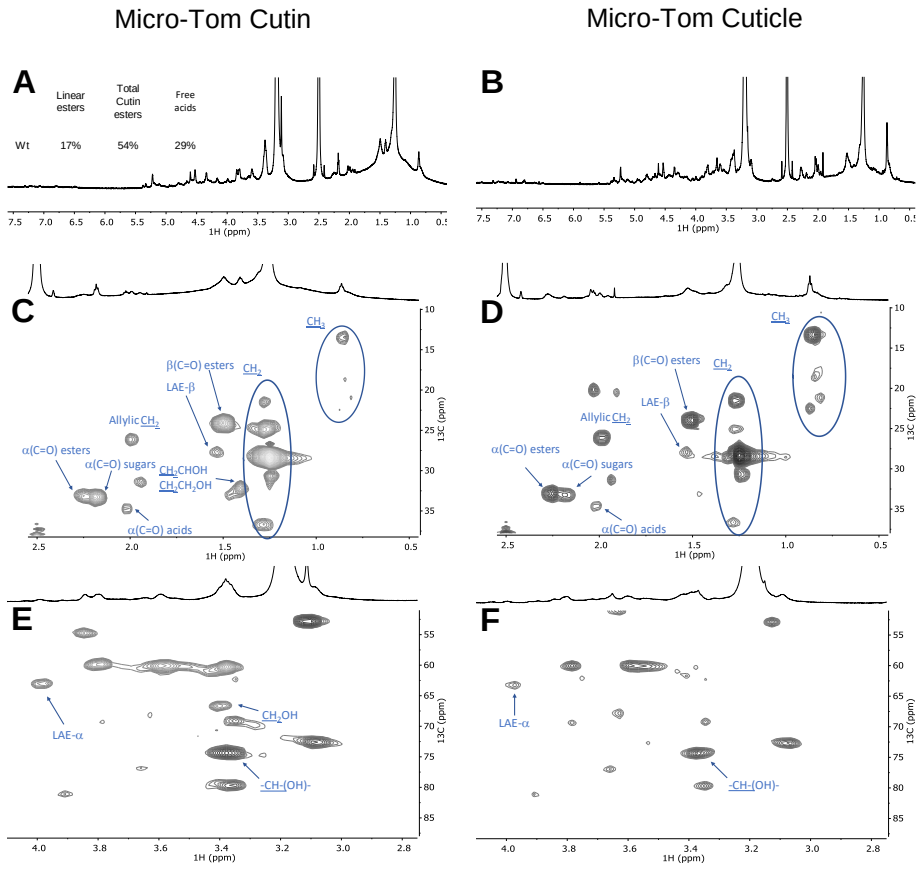

Figure 6. Wide-ranging NMR spectral characterization of Micro-Tom cutin isolated with cholinium hexanoate (2 h) and Micro-Tom untreated cuticle. The ^{1}H NMR spectra of cutin (A) and cuticle (B) samples, indicate the relative abundance (percent) of linear aliphatic esters (LAE-α), total esters [α(C=O) esters], and free acids [α(C=O) acids]; HSQC regions correspond to cutin (C) and cuticle (D) aliphatics and CH (E) and CH_2-X aliphatics (F). Some assignments (unlabeled) are uncertain or unidentified.

The impact of the mutations is seen by the relative abundances of aliphatics, CH/CH_2-X oxygenated aliphatics, and aromatics in the ^{1}H-spectra, which were estimated as 71 %, 29 %, and 0 % for the wild type (Figure 6A); 46 %, 50 %, and 4 % for the *gpat6* mutant (Figure 7A); and 39 %, 59 %, and 2 % for the *cus1* mutant (Figure 7B), respectively. In contrast to the wild type, the signal assigned to free acids could not be detected in either mutant (Figure 7). To confirm this observation, we compared the spectrum of cutin

from the *cus1* mutant purified by the ionic liquid followed by cryogenic milling with that of the *cus1* cuticle solubilized solely via cryogenic milling (Figure S13). The obtained HSQC spectra confirmed the absence of free acids in this mutant, further validating that the observed absence of this chemical group in the *cus1* and *gpat6* cutins is a consequence of the mutations and not of the sample processing (Figures S8–S19).

Based on the ^{1}H-spectral information, we also estimated the relative abundance of aliphatic esters (total percent) and primary aliphatic esters in the cutin of the mutants (Figure 7). Accordingly, the ratio of total esters *versus* linear esters is comparable in the wild type and the *gpat6* mutant but substantially lower in the *cus1* mutant. In other words, compared to the wild type, the *gpat6* mutant shows similar amounts of linear esters and secondary esters, in contrast to the *cus1* mutant, which shows a > 2-fold increase in linear esters but also the lowest esterification level (*i.e.* amount of secondary esters; Figure 7, A and B).

The magnification of the HSQC regions corresponding to aliphatics and CH/CH_2-X aliphatics for the cutins of the mutants is also shown (Figure 7, C–F; Figure S20). For both mutants, the signals assigned to terminal hydroxyls are visible (Figure 7, E and F), similar to that observed in the wild-type cutin (Figure 6E). The detected CH_3 groups are apparently enriched in both mutants compared to the wild type, consistent with the observed increase in relative abundance of hydrolyzable fatty acids for the mutants (Table 3) and with observations reported previously[28,32]. No acylglycerol was visible in the HSQC spectra of the cutin from the mutants, possibly because their abundance is below the detection limits of the analytical technique. The mutants show more non-assigned signals compared to wild-type cutin, consistent with the observed lower identification yields in the GC-MS data (Table 3). This might reflect also an altered diversity of cuticular polysaccharides in the mutants, a hypothesis that deserves further analysis in the near future and is sustained by recently published results for the *cus1* mutant[36].

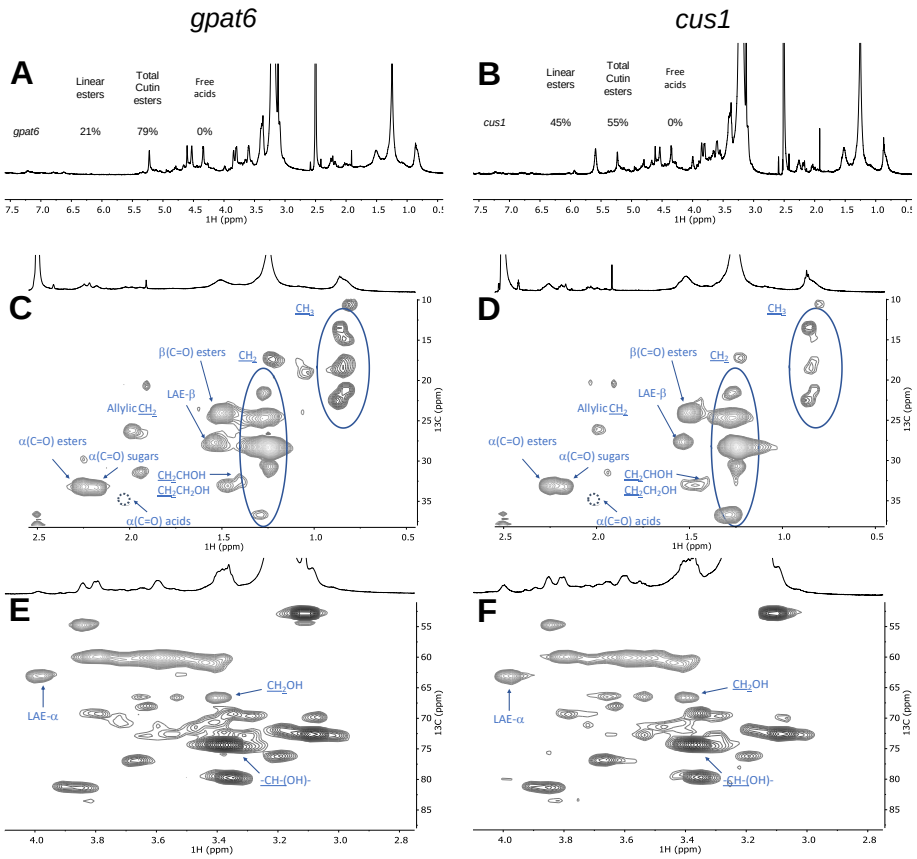

Figure 7. Wide-ranging NMR spectral characterization of *cv* Micro-Tom cutins isolated with cholinium hexanoate (2 h) from the *cus1* and *gpat6* mutants. A and B, ^{1}H NMR spectra of both samples (*gpat6* [A] and *cus1* [B]), showing the relative abundance (percent) of linear aliphatic esters (LAE-α), total esters [α(C=O) esters], and free acids [α(C=O) acids]. C to F, HSQC regions corresponding to aliphatics (C and D) and CH/CH_2-X aliphatics (E and F). Some assignments (unlabeled) are uncertain or unidentified. The absence of the signal assigned to α(C=O) acids is marked by a dashed circle. For simplicity, the wide-ranging NMR spectrum of the untreated cuticle from the *cus1* mutant is not shown (see Figure S13 for details).

Discussion

Considerable advances have been made in recent years on cuticle formation and properties[37]. However, while the successive steps of cutin biosynthesis, transport of precursors, and polymerization in the epidermal cell walls begin to be well untangled[2], the questions of the fine structure of the cutin layer and its association with polysaccharides are still largely unresolved[36]. An example of the intricate relationships between cutin, cell walls, and resistance to pathogens is provided by the tomato *gpat6* mutant analyzed herein, in which the mutation has a profound impact not only on cutin synthesis[32] but also on cell walls[36] and resistance to filamentous pathogens[38]. Insights into the structure and composition of native *gpat6* cutin would help considerably in deciphering the underlying mechanisms. More generally, the simple and rapid cutin extraction method described here, which preserves cutin in a near native state, will help our understanding of the role of cuticle in plant evolution and diversity[35,39], plant development[40], mechanical properties of the organ surface[4,41], resistance to pathogens[42], and fruit quality[33].

Advantages of Ionic Liquid Extraction with Respect to Conventional Cutin Extraction Methods

Our ionic liquid cutin extraction method performed on tomato peels, similar to the enzyme treatment method[5], demonstrates that subcuticular polysaccharides (which were found in the filtrate) are removed, but does so in a considerably shorter time (*i.e.* 2 h instead of days, and even weeks). Also, the ionic liquid extraction does not require any specific dewaxing step. When extracted with either ionic liquid, a cutin continuum is isolated, strengthening the suggestion that the ionic liquid does not substantially impact the cutin polyester. This contrasts with our previously reported results for suberin extraction from cork using cholinium hexanoate, where nanoparticles of the biopolymer are isolated[16] because the ionic liquid catalyzes the mild cleavage of acylglycerol ester bonds[15], which are not representative in tomato cutin.

Cholinium Hexanoate Extraction Preserves Features of Cuticular Polysaccharides

In this study, purification of the cutin continuum by ionic liquids is essentially due to the dissolution of the subcuticular polysaccharides and, to a minor extent, ester cleavage. Under the conditions of the extraction used here, both ionic liquids cleaved ester bonds very inefficiently; however, cholinium hexanoate apparently cleaves only the acylglycerol bonds, whereas BMIM acetate can also cleave linear ester bonds. Hence, the cholinium hexanoate presents the advantages of biocompatibility and milder cleavage of the polymer backbone. The most remarkable difference between the two is that only the cholinium hexanoate could preserve features of cuticular polysaccharides, which were specifically associated with the presence of microcrystalline cellulose. Cellulose with high levels of crystallinity was recently identified within the group of cutin-embedded polysaccharides[36], consistent with the ability of the ionic liquid process to speedily recover cutin with a near-native structure. This opens unexpected possibilities for exploiting both ionic liquids, alone or in combination, to study the association and function of cuticular polysaccharides.

Cholinium Hexanoate Extraction Confirms the Presence of Free Hydroxyls in Native Cutin and Highlights Differences in Free Fatty Acid Composition between the Wild Type and Mutants

Finally, the solution NMR spectra of cutins purified by cholinium hexanoate and the matching cuticles (both of which were solubilized in DMSO-*d6* with the aid of cryogenic milling) strengthened the observation that some free hydroxyls exist *in situ*, consistent with previous reports[28,32]. Results from a systematic NMR analysis of cutins purified by cholinium hexanoate, from both wild type and mutants of the same cultivar (*cv* Micro-Tom), show increased diversity of fatty acids in both mutants, yet only the *cus1* mutant

shows a substantially reduced esterification degree. These results are consistent with the functions of the enzymes inactivated in the mutants: CUS1 is a polymerizing enzyme[34,35], while GPAT6 catalyzes the synthesis of cutin precursors[32]. Remarkably, these results are also consistent with already published information on the mutants, obtained through a totally independent approach[28]. *In situ* analysis of cutin esterification levels by benzyl etherification of enzyme-treated cutin from tomato fruit peel showed that all/midchain hydroxylation of dihydroxy acids is increased strongly in the *cus1* mutant (linear polymers) but remains unaffected in the *gpat6* mutant, as in the wild type (normal inter-branching).

Remarkably, the NMR results of the ionic liquid extracted cutins strongly suggest that naturally occurring free acids exist in the wild-type tomatoes (detected also in the cuticle) but are lacking in the mutants (and in their cuticles, as observed for the *cus1* cuticle). This might be due to the thinner mutant cuticles, where total esterification of the cutin monomers could be more easily achieved. This deserves a detailed analysis in the near future, especially as (1) we could not yet detect the signal assigned to β(C=O) acid, only that of the α(C=O) acids that was assigned through the HMBC spectrum; and (2) the signal assigned to the α(C=O) esters partially overlaps with that of the α(C=O) sugars in the analyzed tomato cutins.

Conclusions

The proof of concept of the efficiency and reliability of the ionic liquid cutin extraction method described here was established using tomato peel as a model. Because of its simplicity, this method should be broadly applicable to other tissues and to other plant model and crop species, as confirmed by preliminary experiments. In the near future quantitative methods (and better spectral resolution for solving yet unknown signals) will require development to understand better how cutin molecular structure (and its association with cuticular polysaccharides) is impacted by mutations or along the development of the plant. In addition, our study emphasizes the suitability of exploiting ionic liquid extraction as an easy and scalable approach for exploiting plant lipid polymers as a bioresource for a range of applications. The ionic liquid processes tested here can be systematically tuned (*e.g.* time, temperature, and component ions) to ensure recovery of cutin with different degrees of structural preservation. Finally, the solution NMR methodologies developed here constitute essential tools to fingerprint the multifunctionality and structure of cutin *in planta*. Based on all the analyses done on the polymer morphology, thermal properties, and chemistry, we are confident that short-time reactions with cholinium hexanoate can ensure the isolation of cutin with minimal disruption of its polymeric network, yielding the biopolymer in a near-native configuration.

Materials and Methods

Plant Materials. Peels from the processing tomato (*Solanum lycopersicum* 'Roma') were manually removed, thoroughly washed, and then dried to a constant weight at 60 °C. After drying, the peels were milled using a Retsch ZM200 electric grinder (granulometry 0.5 mm; 10,000 rpm) and stored at room temperature for further processing. 'Micro-Tom' tomatoes from both wild-type plants and mutant plants generated by ethyl methanesulfonate mutagenesis[30] were cultivated as previously reported[43] and processed as described above. All tomato fruits used were in the red ripe developmental stage.

Chemicals. BMIM acetate (> 98%) was purchased from IoLiTec. Sodium hydroxide (> 98%) was from José Manuel Gomes dos Santos. Methanol (≥ 99.8%), DMSO (> 99.99%), hexane (> 95%), chloroform (> 99.98%), and dichloromethane (> 99.99%) were from Fisher Chemical. Cholinium hydrogen carbonate (~ 80% in water), hexanoic acid (> 99.5%), sodium azide (≥ 99.5%), sodium acetate (≥ 99%), cellulase (*Aspergillus niger*), and pectinase (Aspergillus aculeatus) were from Sigma Aldrich. Cholinium hexanoate was synthesized by dropwise addition of hexanoic acid to aqueous cholinium hydrogen carbonate in equimolar quantities, as previously described[26].

Ionic Liquid Hydrolysis of Standard Fatty Acids. Glyceryl trioctanoate and octyl octanoate (~ 50 mg) were mixed with either ionic liquid (1:10) at 100 °C, without stirring, for 2, 6, or 24 h. At the end of the reaction, the mixture was rapidly cooled to room temperature in ice, acidified to pH 3/3.5 with 1 M HCl solution, spiked with a known concentration of heptadecanoic acid (internal standard), and extracted three times using dichloromethane/water partition. The dried combined organic phases were derivatized with N,O-bis(trimethylsilyl)trifluorocetamide in pyridine (5:1) for 30 min at 90 °C. The TMS derivatives in the organic fractions were then analyzed by GC-MS as previously described[15], with minor modifications (ramp temperature 60 °C;

4 °C/min to 280 °C for 15 min, with source at 230 °C and electron impact ionization of 70 eV; see equipment in the “GC-MS Data” section). Triplicate independent reactions were performed.

Cutin Extractions

Enzymatic Process. Cutin was isolated from tomato as previously described[5]. In brief, tomato peels were immersed in an enzymatic cocktail containing 4 mL pectinase, 0.2 g cellulase, 13 mg NaN_3, and 196 mL of 50 mM sodium acetate buffer and incubated at 31 °C for 24 h with constant shaking. The isolated cuticles were successively dewaxed for 36 h by Soxhlet extraction with methanol, chloroform, and hexane (1:1:1), finally freeze dried, and stored at room temperature. This cutin enriched material was used as a reference material for the optimization phase of this study, *i.e.* selection of a suitable ionic liquid process.

Ionic Liquid Process. Cutin was extracted from tomato peels as previously described for suberin from cork[15], with slight modifications. In brief, 2 g of tomato peel powder were mixed in 20 g cholinium hexanoate or BMIM acetate and incubated for a defined period of time at 100 °C, without stirring. The reaction was stopped by the addition of 160 mL DMSO. The polymer was recovered by filtration using a nylon membrane filter (0.45 mm); then washed with an excess of deionized water with the aid of centrifugation (Eppendorf 5804 R centrifuge, 5,000 rpm at 4 °C for 30 min).

Treatment of Cutin Extracted Using Cholinium Hexanoate (2 h) with TFA. Six hundred milligrams of the cutin-enriched material obtained through extraction with cholinium hexanoate for 2 h was treated with 1 M of aqueous TFA solution for 60 min at 110 °C. The reaction mixture was filtered, and the insoluble material was washed with stirring using chloroform-methanol (1:1 [v/v]) for 2 h. The organic-insoluble material was separated by filtration, freeze-dried, and analyzed by ^{13}C MAS NMR.

Microscopic Analyses. Cutin samples were placed on an aluminum sample holder with double sided carbon tape and subsequently covered with a thin Au/Pd film on a Q150T ES Quorum Technologies sputter coater. SEM micrographs were acquired on a JEOL FEG-SEM model JSM-7001F.

Cryogenic Grinding Process. A RESTCH Cryomill equipped with a 25 mL grinding jar with six zirconium oxide grinding balls (10mm) was used. To optimize the solubilization level of the cutin-enriched materials needed to attain high NMR spectral resolution, cutin samples were cryogenically milled at -196 °C (liquid nitrogen) as follows: 3 min of precooling followed by 9 milling cycles, each comprising 3 min of milling at 30 Hz plus 0.5 min of intermediate cooling at 5 Hz. The ensuing samples were analyzed by ^{1}H NMR (3 mg dissolved in 400 mL of DMSO-d_6) and the 200 milling cycles were selected to systematically process cutin samples before 2D NMR analysis.

NMR Analysis. ^{13}C MAS NMR spectra were acquired on the cutin-enriched materials (± 250 mg), which were packed into 7 mm o.d. zirconia rotors (after grinding if needed), equipped with Kel-F caps. ^{13}C MAS with high-power continuous wave decoupling spectra were obtained at 75.49 MHz, on a Tecmag Redstone/Bruker 300 WB, with spinning rates of 3.1 to 3.3 kHz. In these experiments, 90° radio frequency pulses of ~ 4.5 ms and relaxation delays of 3 s were used. ^{13}C chemical shifts were referenced with respect to external Gly (^{13}CO observed at 176.03 ppm).

Solution-state NMR spectra of the cutin samples solubilized with the aid of cryogenic milling (see the "Cryogenic Grinding Process" section) were recorded using an Avance II + 800 MHz spectrometer (Bruker Biospin), with the exception of ^{1}H-^{13}C HMBC spectra, which were acquired using an Avance III 800 CRYO (Bruker Biospin). All NMR spectra (^{1}H, ^{1}H-^{1}H COSY, and ^{1}H-^{13}C HSQC) were acquired using 5-mm-diameter NMR tubes at 60 °C with 3 mg of cryomilled cutin in 400 mL DMSO-d_6.

MestReNova version 11.04-18998 (Mestrelab Research) was used to process the raw data acquired in the Bruker spectrometers.

DSC Data. Calorimetric analyses of the cutin-enriched materials were carried out in a TA Instruments Q200 calorimeter connected to a cooling system and calibrated with different standards (indium and empty cap). Sample weights ranged from 9 to 11 mg. A temperature interval from 280 °C to 220 °C was studied and the heating/cooling rate was 10 °C min^{-1}.

WAXS Data. WAXS data of the cutin-enriched materials were collected using a laboratory SAXS/WAXS beamline (Xeuss 2.0, Xenocs) equipped with a liquid gallium MetalJet x-ray source (Excillum; wavelength λ = 1.34 Å), FOX 3D Ga single reflection x-ray mirror and two sets of motorized scatterless slits for beam collimation, and a Pilatus 100k 2D pixel WAXS detector (Dectris). Loose cutin powder samples were enclosed between two flat kapton films and mounted on the beamline sample stage (the total sample thickness is ~ 1 mm). 2D WAXS patterns were recorded in a transmission mode over a q range of 1.3 $Å^{-1}$ to 3.5 $Å^{-1}$ [where $q = (4\pi\sin\theta)/\lambda = 2\pi/d$ is the length of the scattering vector, θ is one-half of the scattering angle, and d is the spacing in real space] using an exposure time of 1,200 s. The WAXS data were reduced (calibrated, integrated, and background-subtracted) using the Foxtrot software package supplied with the instrument.

GC-MS Data. A gas chromatograph (7820A, Agilent) equipped with a mass spectrometer (5977B, Agilent; quadrupole) was used. First, to release the hydrolyzable constituents, the cutin-enriched materials were treated with a solution of 0.5 M NaOH in methanol:water (1:1 [v/v]) at 95 °C for 4 h, cooled to room temperature, and acidified to pH 3/3.5 with 1 M HCl, then extracted by dichloromethane/ water partition (5x). The nonhydrolyzable fraction was recovered by filtration (0.2-mm nylon filters), washed, freeze-dried, and weighted (recalcitrance). The dried combined organic extracts were

sequentially derivatized (30 min at 90 °C): first, 2.0 M (trimethylsilyl)diazomethane in hexane, mixed in a methanol:toluene 2.5:1 solution (3:2); and second, N,O-bis(trimethylsilyl)trifluoroacetamide containing 1% (v/v) trimethylchlorosilane in pyridine (5:1). The derivatives were then analyzed by GC-MS (HP-5MS column) as follows: ramp temperature 80 °C, then 4 °C min^{-1} to 310 °C for 15 min. The MS scan mode, with source at 230 °C and electron impact ionization (EI+, 70 eV) was used for all samples. The GC-MS was first calibrated with pure reference compounds (representative monomers: heptadecanoic acid, hexadecanedioic acid, and ferulic acid) relative to hexadecane (internal standard). Each sample was analyzed in triplicate. Data acquisition was accomplished by MSD ChemStation (Agilent Technologies); compounds were identified based on the equipment spectral library (Wiley-National Institute of Standards and Technology) and references relying on diagnostic ions distinctive of each derivative and its spectrum profile (Table S1).

Accession Numbers

Sequence data from this article can be found in the GenBank/EMBL data libraries under accession numbers Solyc11g006250 (CUS1) and Solyc09g014350 (GPATt6).

Acknowledgements

The authors are grateful to Manolis Matzapetakis (Instituto de Tecnologia Química e Biológica António Xavier, Universidade Nova de Lisboa [ITQB NOVA]) and Maria João Ferreira (Instituto Superior Tecnico) for support in the solid-state NMR analyses and to Pedro Lamosa and Maria C. Leitão (ITQB NOVA) for support in the solution NMR and chromatographic analyses, respectively. The solution NMR data were acquired at the ITQB-NOVA with equipment funded by the Fundação para a Ciência e a Tecnologia. Finally, we are extremely grateful to Bénédicte Bakan and Didier Marion for fruitful scientific discussions during the manuscript preparation.

Funding

This work was supported by the European Research Council (grant no. ERC 2014–CoG–647928), the European Commission's Horizon 2020 research and innovation programme (project no. 713475–FLIPT–H2020–FETOPEN–2014-2015), the Fundação para a Ciência e Tecnologia (grant no. UID/Multi/04551/2019 [Research unit GREEN-it "Bioresources 4 Sustainability"] and project no. PTDC/AGR–TEC/1191/2014AAC), King's College London Medical Engineering Centre (Wellcome Trust EPSRC Centre of Excellence in Medical Engineering; capital equipment grant no. EP/M028437/1 to O.O.M.), and Aralab (PhD contract no. 06/PlantsLife/2017 to C.J.S.M.).

References

1. Heredia-Guerrero, J. A. *et al.* Cutin from agro-waste as a raw material for the production of bioplastics. *J. Exp. Bot.* **68**, 5401–5410 (2017).
2. Fich, E. A., Segerson, N. A. & Rose, J. K. C. The Plant Polyester Cutin: Biosynthesis, Structure, and Biological Roles. *Annu. Rev. Plant Biol.* **67**, 207–233 (2016).
3. Segado, P., Domínguez, E. & Heredia, A. Ultrastructure of the epidermal cell wall and cuticle of tomato fruit (Solanum lycopersicum L.) during development. *Plant Physiol.* **170**, 935–946 (2016).
4. Mazurek, S. *et al.* Connecting the molecular structure of cutin to ultrastructure and physical properties of the cuticle in petals of arabidopsis. *Plant Physiol.* **173**, 1146–1163 (2017).
5. Chatterjee, S. *et al.* Isolation and biophysical study of fruit cuticles. *J. Vis. Exp.* (2012) doi:10.3791/3529.
6. Graça, J. & Lamosa, P. Linear and Branched Poly(ω-hydroxyacid) Esters in Plant Cutins. *J. Agric. Food Chem.* **58**, 9666–9674 (2010).
7. Fernández, V., Guzmán-Delgado, P., Graça, J., Santos, S. & Gil, L. Cuticle structure in relation to chemical composition: Re-assessing the prevailing model. *Frontiers in Plant Science* vol. 7 427 (2016).
8. Deshmukh, A. P., Simpson, A. J. & Hatcher, P. G. Evidence for cross-linking in tomato cutin using HR-MAS NMR spectroscopy. *Phytochemistry* **64**, 1163–1170 (2003).
9. Bakan, B. & Marion, D. Assembly of the cutin polyester: From cells to extracellular cell walls. *Plants* **6**, 57 (2017).
10. Chatterjee, S. *et al.* Solid-State ^{13}C NMR Delineates the Architectural Design of Biopolymers in Native and Genetically Altered Tomato Fruit Cuticles. *Biomacromolecules* **17**, 215–224 (2016).
11. Rogers, R. D. & Seddon, K. R. Ionic Liquids - Solvents of the Future? *Science* vol. 302 792–793 (2003).

12. Li, Y., Wang, J., Liu, X. & Zhang, S. Towards a molecular understanding of cellulose dissolution in ionic liquids: Anion/cation effect, synergistic mechanism and physicochemical aspects. *Chem. Sci.* **9**, 4027–4043 (2018).
13. Garcia, H. *et al.* Dissolution of cork biopolymers in biocompatible ionic liquids. *Green Chem.* **12**, 367–369 (2010).
14. Ferreira, R. *et al.* Suberin isolation from cork using ionic liquids: Characterisation of ensuing products. *New J. Chem.* **36**, 2014–2024 (2012).
15. Ferreira, R. *et al.* Unveiling the dual role of the cholinium hexanoate ionic liquid as solvent and catalyst in suberin depolymerisation. *RSC Adv.* **4**, 2993–3002 (2014).
16. Correia, V. G. *et al.* The molecular structure and multifunctionality of the cryptic plant polymer suberin. *Mater. Today Bio* **5**, 100039 (2020).
17. Arrieta-Baez, D. & Stark, R. E. Using Trifluoroacetic Acid To Augment Studies of Potato Suberin Molecular Structure. *J. Agric. Food Chem.* **54**, 9636–9641 (2006).
18. Hernández Velasco, B. L. *et al.* Comparative studies of cutins from lime (Citrus aurantifolia) and grapefruit (Citrus paradisi) after TFA hydrolysis. *Phytochemistry* **144**, 78–86 (2017).
19. Matas, A. J. *et al.* Tissue- and cell-type specific transcriptome profiling of expanding tomato fruit provides insights into metabolic and regulatory specialization and cuticle formation. *Plant Cell* **23**, 3893–3910 (2011).
20. Benítez, J. J. *et al.* Valorization of tomato processing by-products: Fatty acid extraction and production of bio-based materials. *Materials (Basel).* **11**, 2211 (2018).
21. Mykhaylyk, O. O., Smith, K. W., Martin, C. M. & Ryan, A. J. Structural models of metastable phases occurring during the crystallization process of saturated/unsaturated triacylglycerols. in *Journal of Applied Crystallography* vol. 40 s297–s302 (2007).

22. Bunn, C. W. The Crystal Structure of Ethylene. *Trans. Faraday Soc.* **40**, 23–25 (1944).
23. Southern, J. H., Weeks, N., Porter, R. S. & Crystal, R. G. Unique polyethylene morphologies produced under extrusion conditions. *Macromol. Chem. Phys.* **162**, 19–30 (1972).
24. Small, D. M. Lateral chain packing in lipids and membranes. *J. Lipid Res.* **25**, 1490–1500 (1984).
25. Rongpipi, S., Ye, D., Gomez, E. D. & Gomez, E. W. Progress and opportunities in the characterization of cellulose – an important regulator of cell wall growth and mechanics. *Frontiers in Plant Science* vol. 9 1894 (2019).
26. Petkovic, M. *et al.* Novel biocompatible cholinium-based ionic liquids - Toxicity and biodegradability. *Green Chem.* **12**, 643–649 (2010).
27. Lyerla, J. R. High-resolution nuclear magnetic resonance spectroscopy. *Methods Exp. Phys.* **16**, 241–369 (1980).
28. Philippe, G. *et al.* Ester cross-link profiling of the cutin polymer of wild-type and cutin synthase tomato mutants highlights different mechanisms of polymerization. *Plant Physiol.* **170**, 807–820 (2016).
29. Zhang, X., Zhang, A., Liu, C. & Ren, J. Per-O-acylation of xylan at room temperature in dimethylsulfoxide/N-methylimidazole. *Cellulose* **23**, 2863–2876 (2016).
30. Just, D. *et al.* Micro-Tom mutants for functional analysis of target genes and discovery of new alleles in tomato. *Plant Biotechnology* vol. 30 225–231 (2013).
31. Garcia, V. *et al.* Rapid identification of causal mutations in tomato EMS populations via mapping-by-sequencing. *Nat. Protoc. 2016 1112* **11**, 2401–2418 (2016).
32. Petit, J. *et al.* The glycerol-3-phosphate acyltransferase GPAT6 from tomato plays a central role in fruit cutin biosynthesis. *Plant Physiol.* **171**, 894–913 (2016).

33. Petit, J., Bres, C., Mauxion, J. P., Bakan, B. & Rothan, C. Breeding for cuticle-associated traits in crop species: traits, targets, and strategies. *Journal of Experimental Botany* vol. 68 5369–5387 (2017).
34. Girard, A. L. *et al.* Tomato GDSL1 is required for cutin deposition in the fruit cuticle. *Plant Cell* **24**, 3106–3121 (2012).
35. Yeats, T. H. *et al.* The identification of cutin synthase: Formation of the plant polyester cutin. *Nat. Chem. Biol.* **8**, 609–611 (2012).
36. Philippe, G. *et al.* Assembly of tomato fruit cuticles: a cross-talk between the cutin polyester and cell wall polysaccharides. *New Phytol.* **226**, 809–822 (2020).
37. Nawrath, C. *et al.* Apoplastic Diffusion Barriers in Arabidopsis. *Arabidopsis Book* **11**, e0167 (2013).
38. Fawke, S. *et al.* Glycerol-3-phosphate acyltransferase 6 controls filamentous pathogen interactions and cell wall properties of the tomato and *Nicotiana benthamiana* leaf epidermis. *New Phytol.* **223**, 1547–1559 (2019).
39. Yeats, T. H. *et al.* Tomato Cutin Deficient 1 (CD1) and putative orthologs comprise an ancient family of cutin synthase-like (CUS) proteins that are conserved among land plants. *Plant J.* **77**, 667–675 (2014).
40. G, I. & C, N. The roles of the cuticle in plant development: organ adhesions and beyond. *J. Exp. Bot.* **68**, 5307–5321 (2017).
41. España, L. *et al.* Biomechanical properties of the tomato (Solanum lycopersicum) fruit cuticle during development are modulated by changes in the relative amounts of its components. *New Phytol.* **202**, 790–802 (2014).
42. Chassot, C., Nawrath, C. & Métraux, J. P. Cuticular defects lead to full immunity to a major plant pathogen. *Plant J.* **49**, 972–980 (2007).
43. Rothan, C. *et al.* Culture of the tomato Micro-Tom Cultivar in greenhouse. in *Methods in Molecular Biology* vol. 1363 57–64 (Humana Press Inc., 2016).

ANNEX

This annex contains the Supplementary Material published along the main body of the research paper which composes Chapter II. This intends to allow better and easier understanding of the methodologies and analyses performed.

Supplementary Data

The following supplementary materials are available.

Supplementary Tables and Figures (by order of appearance in the manuscript)

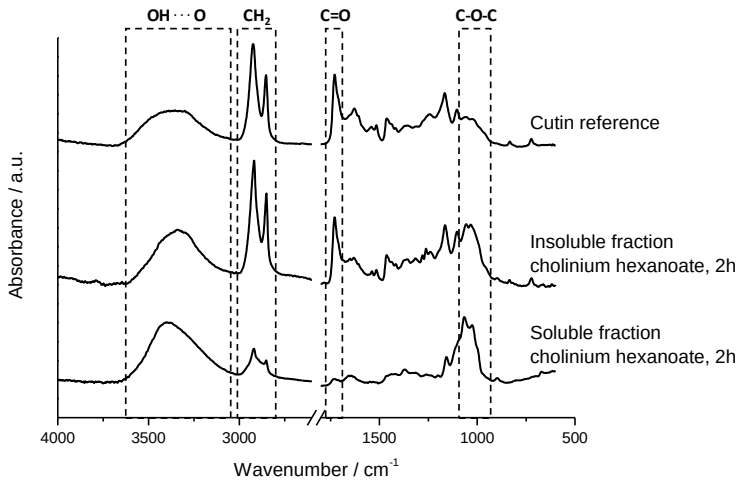

Figure S1 – Attenuated Total Reflectance – Fourier Transform Infrared (ATR-FTIR) of the soluble and insoluble fractions attained after the reaction of tomato peels with cholinium hexanoate (2 h, 100 °C) compared to a cutin reference isolated using the conventional enzymatic hydrolysis.

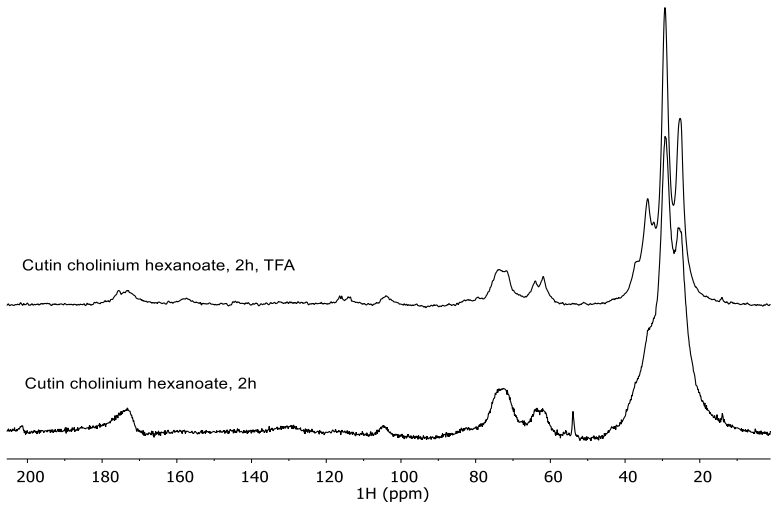

Figure S2 – ^{13}C MAS NMR spectrum of the cutin extracted with cholinium hexanoate followed or not by acidic hydrolysis with TFA. The signal previously assigned to the cholinium cation (54 ppm) was washed out.

Table S1 – Diagnostic ions used to identify the monomers extracted from tomato cutin and their retention times (Rt).

	Derivatization	Diagnostic Ions	Rt
FATTY ACIDS			
hexadecanoic acid	Methyl ester	270, 239, 227, 143, 129, 87, 24	26.79
octadecanoic acid	Methyl ester	298, 267, 255, 199, 143, 129,87,74	31.47
octadec-9-enoic acid	Methyl ester	296, 264, 222, 180, 125, 111, 97, 74, 85	30.89
octadeca-9,12-dienoic acid	Methyl ester	294, 263, 109, 95, 81, 67	30.71
4-oxocyclohexane-1-carboxylic acid	Methyl ester	166, 135, 107, 92, 77	11.90
DIACIDS			
nonanedioic acid [(a)]	di Methyl ester	185, 152, 111, 83, 74, 55	16.86
hexadecanedioic acid	di Methyl ester	283, 241, 209, 191, 168, 154, 135, 125, 112, 98, 84, 74, 69, 55	34.24
8/9-hydroxyhexadecanedioic acid [(b)]	di Methyl ester TMS ether	387, 273, 259, 245,231, 155, 129, 109, 95, 73, 55	38.34
HYDROXY ACIDS			
16-hydroxyhexadecanoic acid	Methyl ester TMS ether	343, 327, 311, 159, 146, 103, 89, 75, 73, 55	34.93
16-hydroxy-oxo-hexadecanoic acid	Methyl ester TMS ether	357, 341, 325, 214, 126, 111, 83, 75, 73, 55	37.60
9,10-epoxy-18-hydroxyoctadecanoic acid	Methyl ester TMS ether	489, 473, 457, 385, 303, 274, 259, 201, 155, 129, 121, 109, 103, 81, 75, 73, 55	43.86
9,10-epoxy-18-hydroxyoctadecenoic acid	Methyl ester TMS ether	471, 383, 303, 271, 259, 243, 213, 191, 155, 129, 121, 109, 103, 89, 75, 73, 55	43.31
POLYHYDROXYACIDS			
10,16-dihydroxyhexadecanoic acid [(c)]	Methyl ester TMS ether	431, 415, 399, 317, 303, 289, 275, 273, 259, 245, 159,146, 147, 129, 103, 95, 75, 73, 55	38.86
10,16-dihydroxyhexadecanoic acid [(c)]	TMS ester, TMS ether	489, 399, 383, 331, 317, 303, 289, 275, 217 and 204, 147, 129, 103, 95, 75, 73, 55	40.80
9,10,18- trihydroxyoctadecanoic acid	Methyl ester TMS ether	547, 332, 303, 259, 243, 212, 155, 147, 129, 109, 103, 81, 75, 73	44.421
9,10,18- trihydroxyoctadec-12-enoic acid	Methyl ester TMS ether	545, 361, 317, 271, 259, 155, 147, 129, 109, 103, 75, 73	43.960
STEROLS and TRITERPENOIDS			
stigmasterol	TMS ether	484, 394, 355, 255, 213, 159, 129, 83, 73	52.43
beta-amyrin	TMS ether	498, 394, 279, 257, 218, 203, 189, 147, 129, 95, 73	53.30
alpha-amyrin	TMS ether	498, 393, 279, 218, 203, 189, 175, 135, 73	53.84
delta-Amyrin	TMS ether	73, 109, 189, 190, 204, 205, 218, 257, 279, 498	53.14

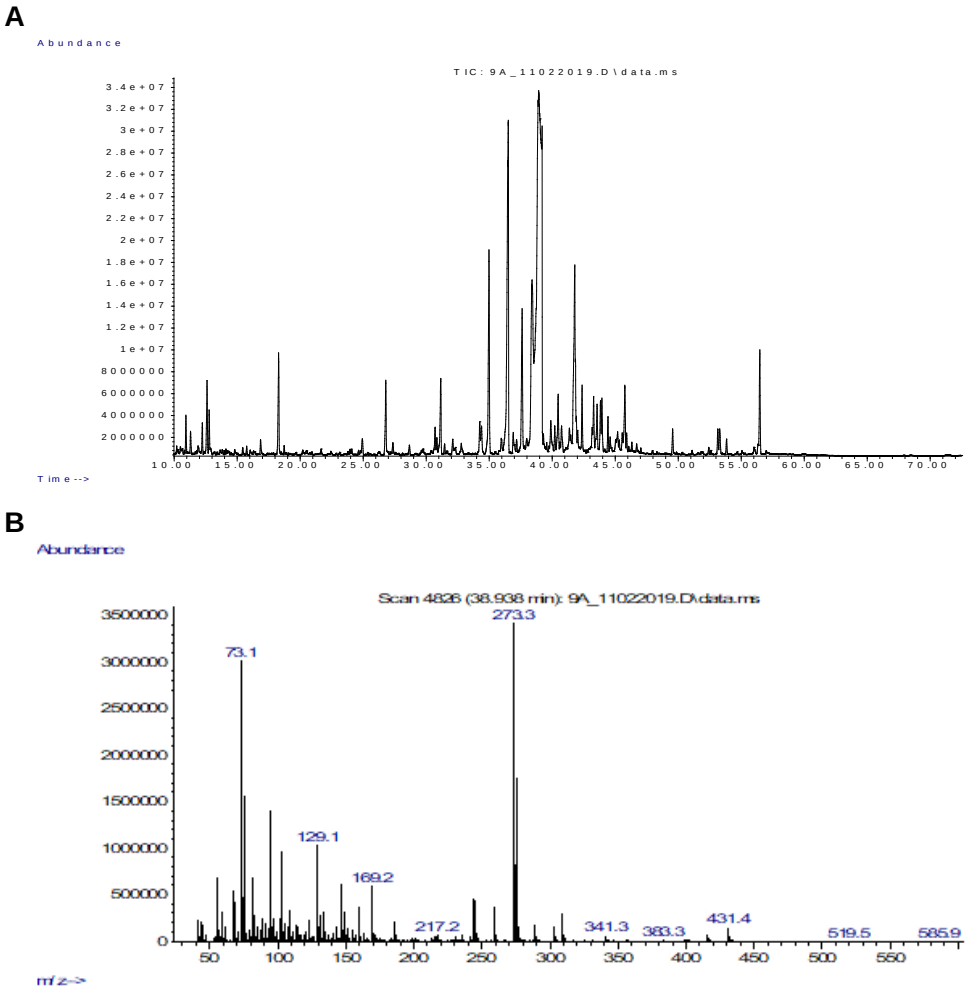

Figure S3 – Representative cutin GC-MS chromatogram. Compound identification was based on the equipment spectral library (NIST) and/or EI-MS fragmentation patterns. Taken as example, one representative full total ion current spectrum of cutin is depicted (A) as well as the EI-MS spectrum corresponding to the most abundant monomer (10, 16-dihydroxy hexadecenoic acid methyl ester TMS ether) (B).

Table S2 – Elemental analysis of cutin purified after treatment with cholinium hexanoate 2 h before and after cryogenic milling.

Sample	Cutin	Cutin after cryogenic milling
Nitrogen (N)	< 1*	< 1*
Carbon (C)	63.98 ± 0.16	62.62 ± 0.19
Hydrogen (H)	9.08 ± 0.12	9.05 ± 0.04
Oxygen (O)	26.96 ± 0.27	28.33 ± 0.23

*corresponding peak areas were outside the calibration curve, the value may be subject to error yet shown since the monomer 4-(2-aminoethyl)phenol contains N. Deviation from theoretical percentage (should be <0.4%). n.d., element not detected in the sample.

Table S3 – Monomeric composition of cutin extracted using cholinium hexanoate (2 h), identified by NMR. Chemical structures and ^{1}H and ^{13}C chemical shifts (ppm) of the cutin monomers. Signals not resolved in the NMR spectra due to overlapping signals or not yet assigned are not shown in this table.

Chemical structure	Chemical shifts (ppm)
Fatty acids (n= 1-2)	
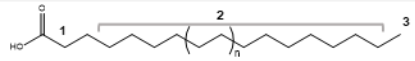	^{1}H NMR (800.33 MHz, DMSO-*d6*) δ 0.86 (m, 3H, H-3), 1.25 (m, 2H, H-2), 2.02 (m, 2H, H-1). ^{13}C NMR (201.42 MHz, DMSO-*d6*) δ 13.39 (C-3), 28.34 (C-2), 34.67 (C-1).
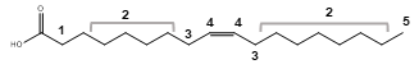	^{1}H NMR (800.33 MHz, DMSO-*d6*) δ 0.86 (m, 3H, H-5), 1.25 (m, 2H, H-2), 1.99 (m, 2H, H-3), 2.02 (m, 2H, H-1), 5.34 (m, 2H, H-4). ^{13}C NMR (201.42 MHz, DMSO-*d6*) δ 13.39 (C-5), 26.13 (C-3), 28.34 (C-2), 34.67 (C-1), 129.07 (C-4).
Dicarboxylic Acids	
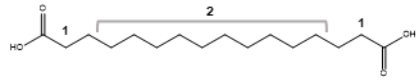	^{1}H NMR (800.33 MHz, DMSO-*d6*) δ 1.25 (m, 2H, H-2), 2.02 (m, 2H, H-1). ^{13}C NMR (201.42 MHz, DMSO-*d6*) δ 28.34 (C-2), 34.67 (C-1).
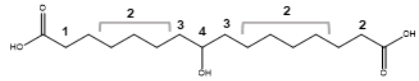	^{1}H NMR (800.33 MHz, DMSO-*d6*) δ 1.25 (m, 2H, H-2), 1.41 (m, 2H, H-3), 2.02 (m, 2H, H-1), 3.38 (m, 2H, H-4). ^{13}C NMR (201.42 MHz, DMSO-*d6*) δ 28.34 (C-2), 32.26 (C-3), 34.67 (C-1), 74.31 (C-4).
ω-hydroxyacids	
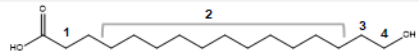	^{1}H NMR (800.33 MHz, DMSO-*d6*) δ 1.25 (m, 2H, H-2), 1.42 (m, 2H, H-3), 2.02 (m, 2H, H-1), 3.41 (m, 2H, H-4). ^{13}C NMR (201.42 MHz, DMSO-*d6*) δ 28.34 (C-2), 33.08 (C-3), 34.67 (C-1), 67.64 (C-4).
Polyhydroxyacids	
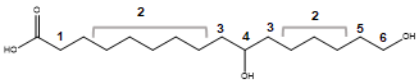	^{1}H NMR (800.33 MHz, DMSO-*d6*) δ 1.25 (m, 2H, H-2), 1.41 (m, 2H, H-3), 1.42 (m, 2H, H-5), 2.02 (m, 2H, H-1), 3.38 (m, 2H, H-4), 3.41 (m, 2H, H-6). ^{13}C NMR (201.42 MHz, DMSO-*d6*) δ 28.34 (C-2), 32.26 (C-3), 33.08 (C-5), 34.67 (C-1), 67.64 (C-6), 74.31 (C-4).
LINEAR ALIPHATIC ESTERS	
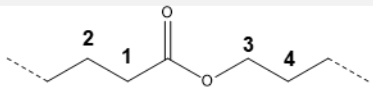	^{1}H NMR (800.33 MHz, DMSO-*d6*) δ 1.49 (m, 2H, H-4), 1.54 (m, 2H, H-2), 2.25 (m, 2H, H-1), 3.98 (m, 2H, H-3). ^{13}C NMR (201.42 MHz, DMSO-*d6*) δ 24.02 (C-4), 27.60 (C-2), 33.27 (C-1), 63.05 (C-3).

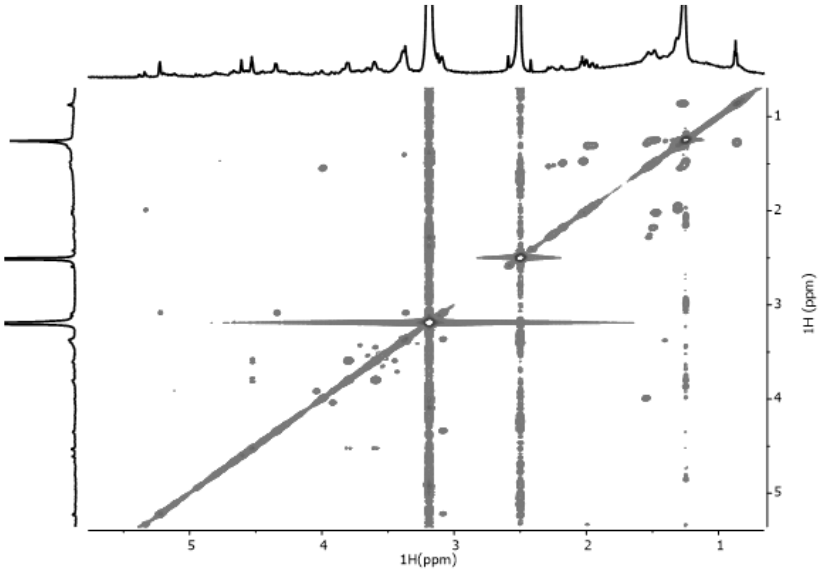

Figure S4 – 2D-^{1}H-^{1}H COSY-NMR spectrum (COrrelated SpectroscopY) of cutin extracted using cholinium hexanoate (2 h) in DMSO- d_6 at 60 ºC.

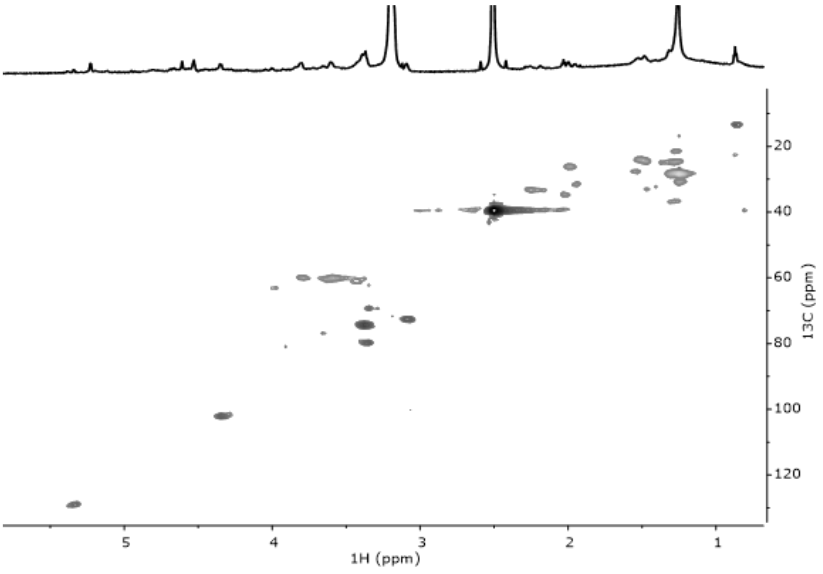

Figure S5 – 2D-^{1}H-^{13}C HSQC-NMR spectrum (Heteronuclear Single Quantum Coherence) of cutin extracted using cholinium hexanoate (2 h) in DMSO- d_6 at 60 ºC.

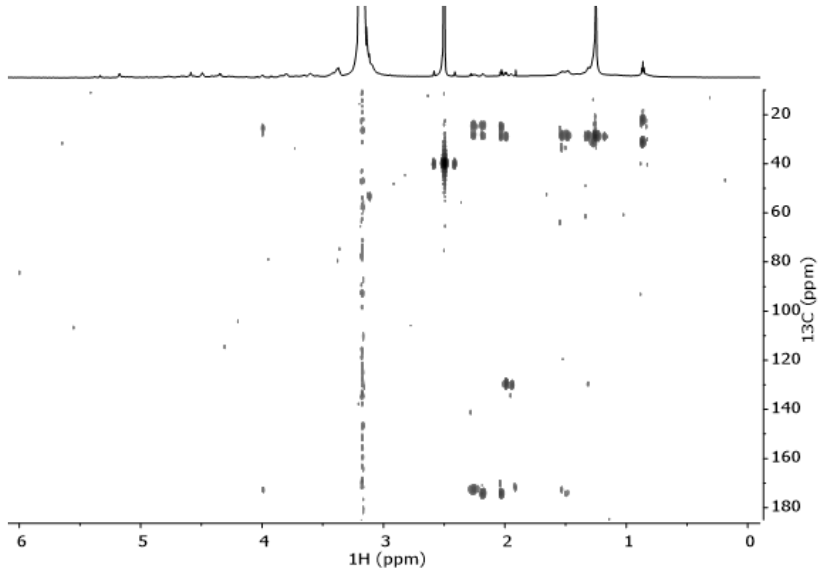

Figure S6 – 2D-^{1}H-^{13}C HMBC-NMR spectrum (Heteronuclear Multiple Bond Correlation) of cutin extracted using cholinium hexanoate (2 h) in DMSO-d_6 at 60 ºC.

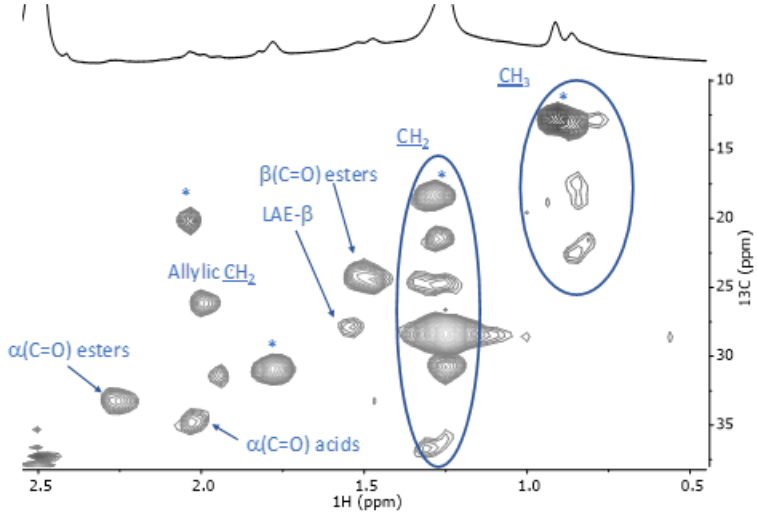

Figure S7 – 2D-^{1}H-^{13}C HSQC-NMR spectrum (Heteronuclear Single Quantum Coherence) of cutin extracted using 1-butyl-3-methylimidazolium acetate (2 h) in DMSO-d_6 at 60 ºC. Magnification of the HSQC region corresponding to aliphatics. Some correlations (unlabelled) are uncertain or unidentified. * corresponds to signals assigned to the 1-butyl-3-methylimidazolium cation.

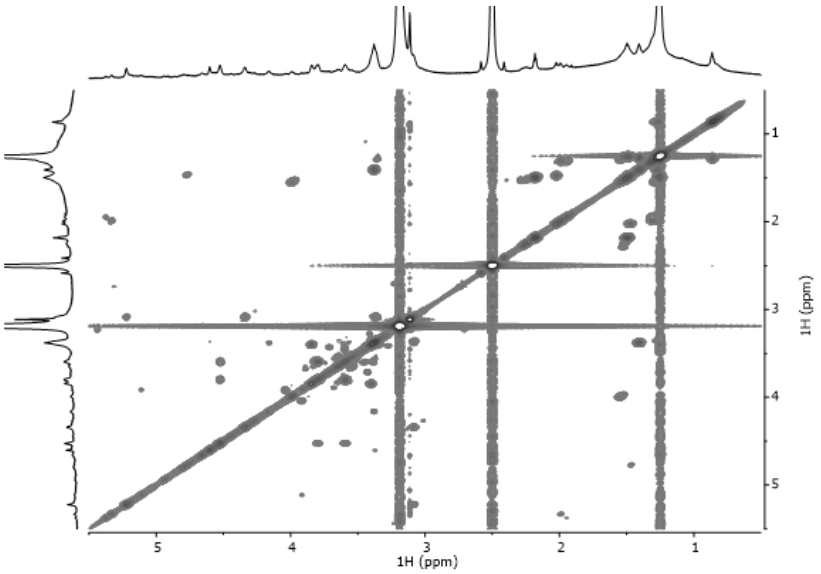

Figure S8 – 2D-^{1}H-^{1}H COSY-NMR spectrum (COrrelated SpectroscopY) of Micro-Tom cutin isolated with cholinium hexanoate (2 h) in DMSO-d_6 at 60 ºC.

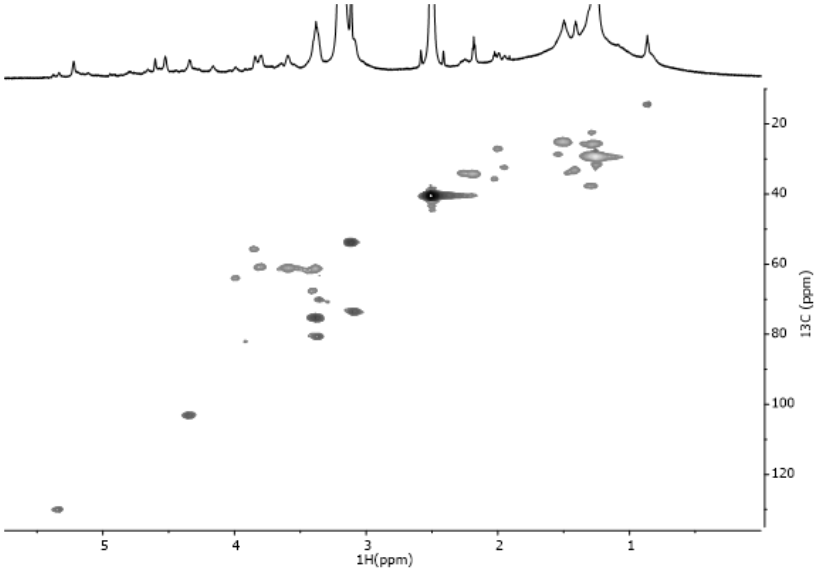

Figure S9 – 2D-^{1}H-^{13}C HSQC-NMR spectrum (Heteronuclear Single Quantum Coherence) of Micro-Tom cutin isolated with cholinium hexanoate (2 h) in DMSO-d_6 at 60 ºC.

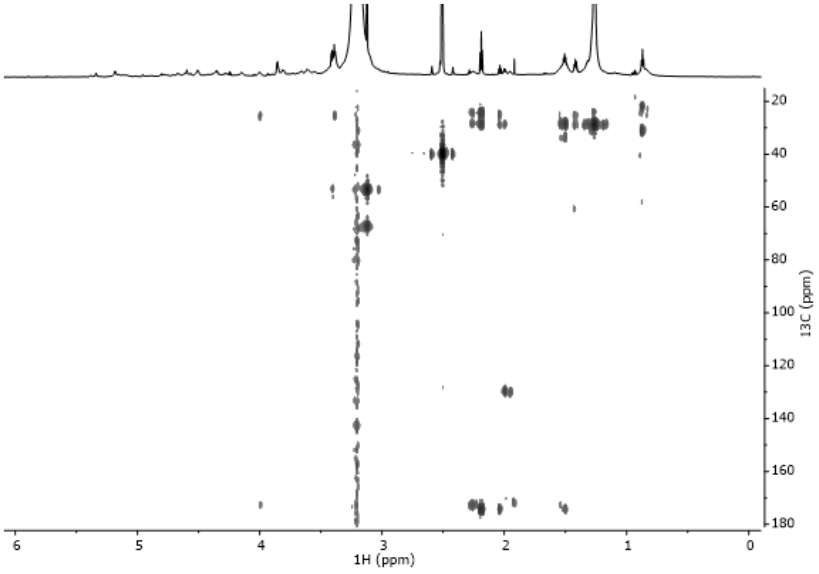

Figure S10 – 2D-^{1}H-^{13}C HMBC-NMR spectrum (Heteronuclear Multiple Bond Correlation) of Micro-Tom cutin isolated with cholinium hexanoate (2 h) in DMSO-d_6 at 60 ºC**.**

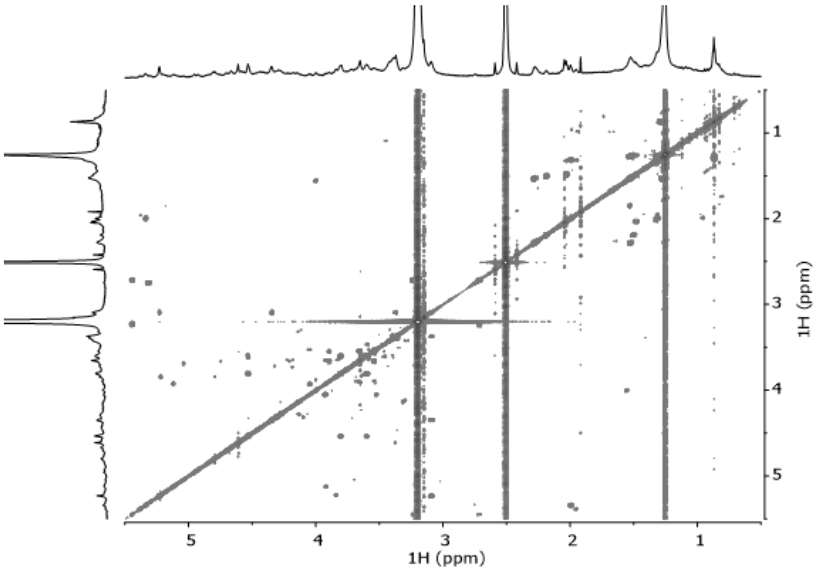

Figure S11 – 2D-^{1}H-^{1}H COSY-NMR spectrum (COrrelated SpectroscopY) of Micro-tom cuticle in DMSO-d_6 at 60 ºC.

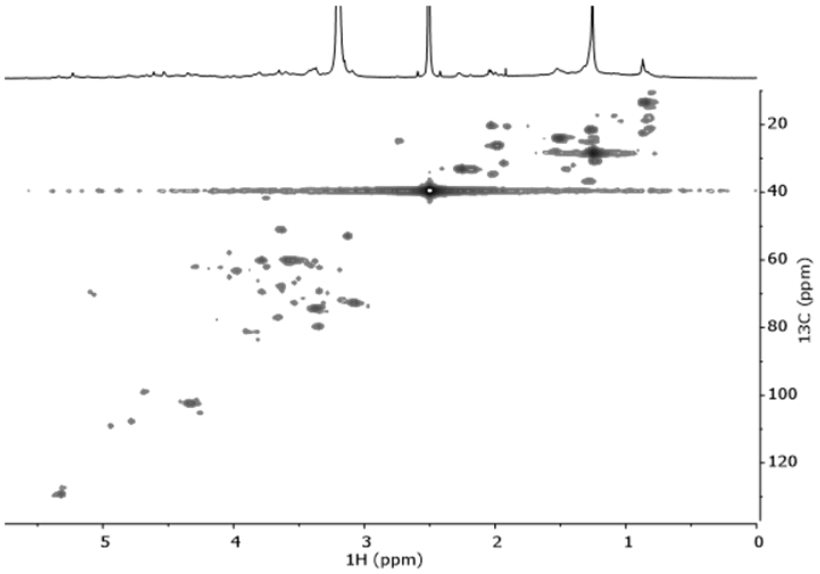

Figure S12 – 2D-^{1}H-^{13}C HSQC-NMR spectrum (Heteronuclear Single Quantum Coherence) of Micro-Tom cuticle in DMSO-d_6 at 60 ºC.

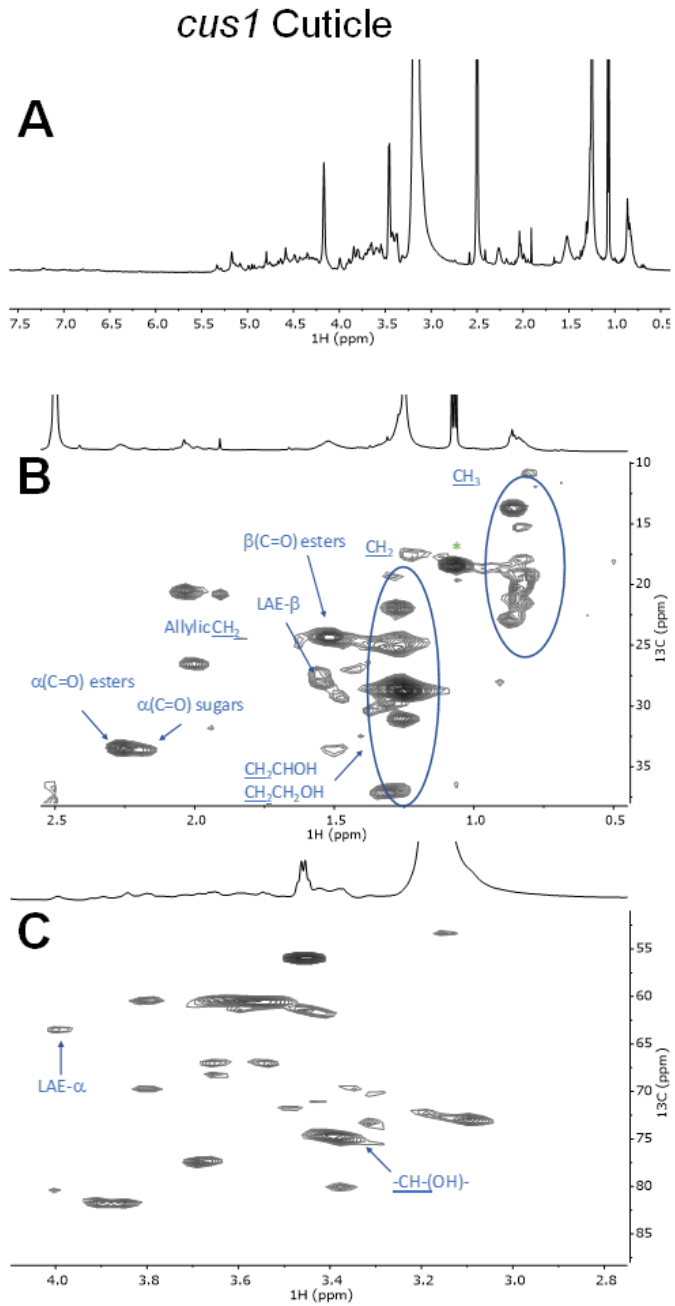

Figure S13 – Wide-ranging NMR spectral characterization of Micro-Tom from *cus1* untreated cuticle. The ^{1}H NMR spectra of both samples (A), HSQC regions corresponding to aliphatics (B) and CH/CH_2-X aliphatics (C). Some correlations (unlabeled) are uncertain or unidentified.

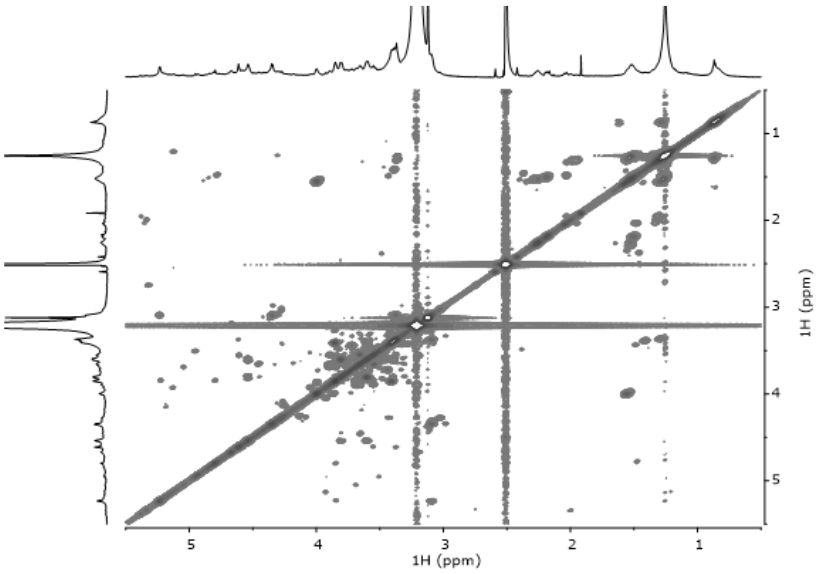

Figure S14 – 2D-^{1}H-^{1}H COSY-NMR spectrum (COrrelated SpectroscopY) of Micro-Tom cutin isolated with cholinium hexanoate (2 h) from the *cus1* mutant in DMSO-d_6 at 60 ºC.

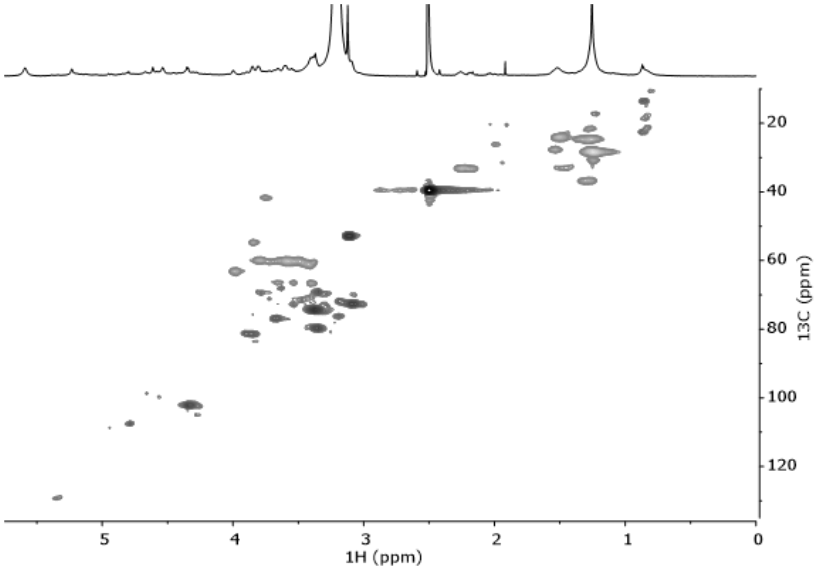

Figure S15 – 2D-^{1}H-^{13}C HSQC-NMR spectrum (Heteronuclear Single Quantum Coherence) of Micro-Tom cutin isolated with cholinium hexanoate (2 h) from the *cus1* mutant in DMSO-d_6 at 60 ºC.

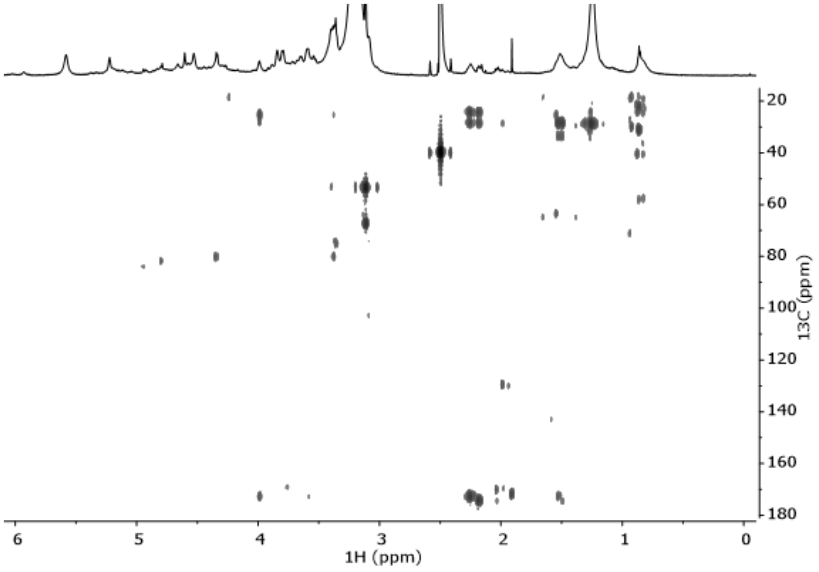

Figure S16 – 2D-^{1}H-^{13}C HMBC-NMR spectrum (Heteronuclear Multiple Bond Correlation) of Micro-Tom cutin isolated with cholinium hexanoate (2 h) from the *cus1* mutant in DMSO-d_6 at 60 ºC.

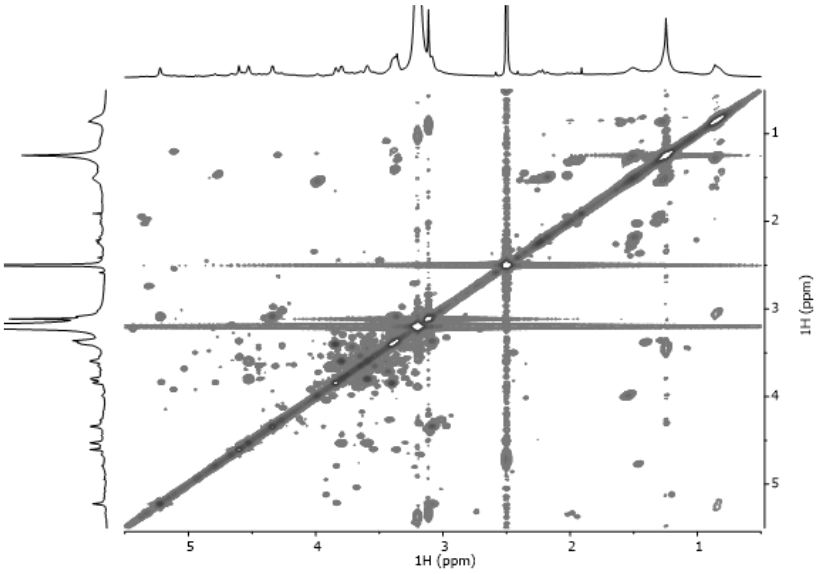

Figure S17 – 2D-^{1}H-^{1}H COSY-NMR spectrum (COrrelated SpectroscopY) of Micro-Tom cutin isolated with cholinium hexanoate (2 h) from the *gpat6* mutant in DMSO-d_6 at 60 ºC.

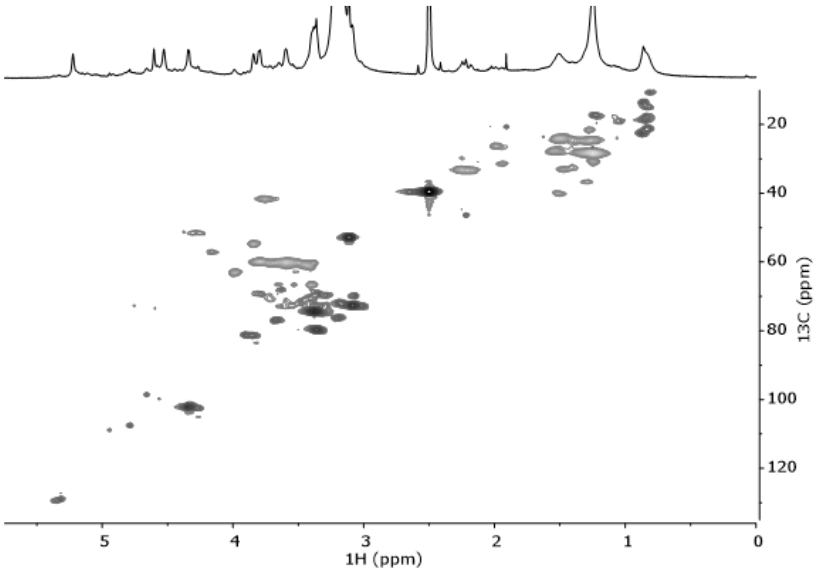

Figure S18 – 2D-^{1}H-^{13}C HSQC-NMR spectrum (Heteronuclear Single Quantum Coherence) of Micro-Tom cutin isolated with cholinium hexanoate (2 h) from the *gpat6* mutant in DMSO-d_6 at 60 ºC.

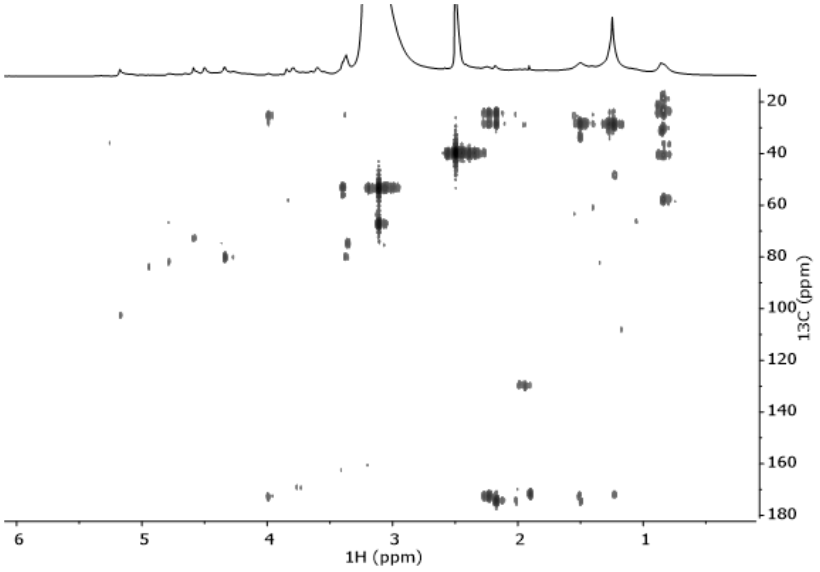

Figure S19 – 2D-^{1}H-^{13}C HMBC-NMR spectrum (Heteronuclear Multiple Bond Correlation) of Micro-Tom cutin isolated with cholinium hexanoate (2 h) from the *gpat6* mutant in DMSO-d_6 at 60 ºC.

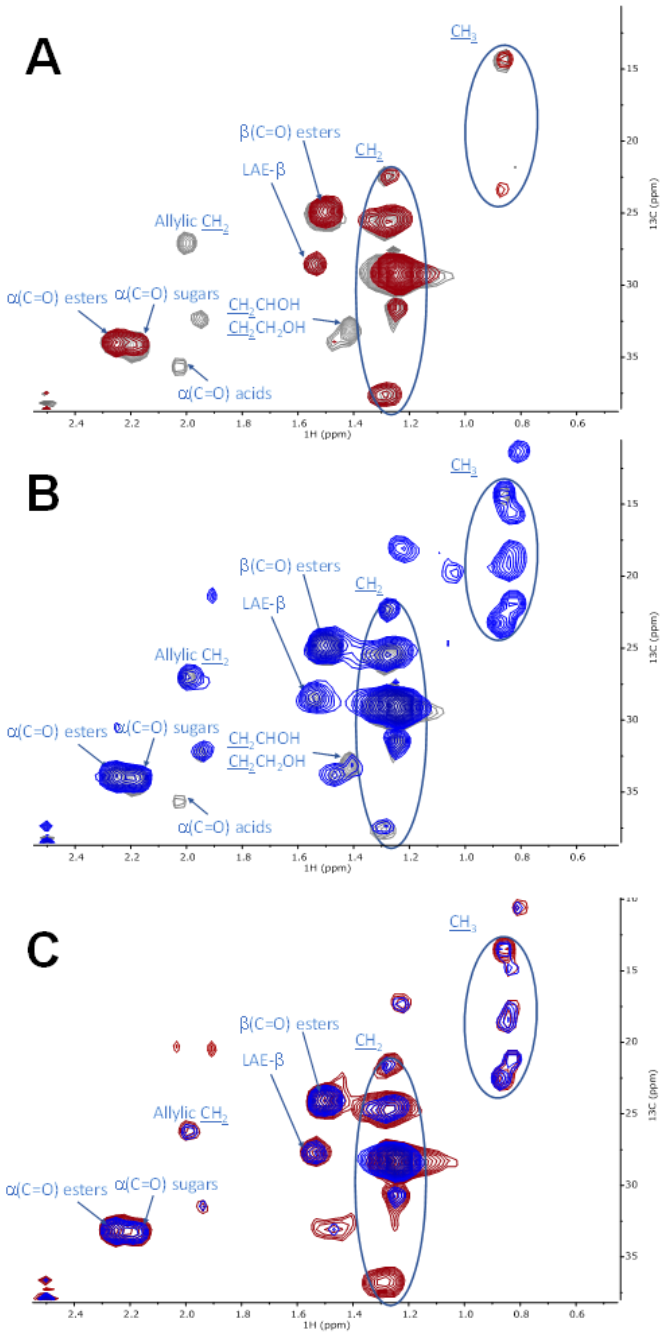

Figure S20 – Overlaps of the 2D-^{1}H-^{13}C HSQC-NMR spectra (Heteronuclear Single Quantum Coherence) of Micro-Tom cutins isolated with cholinium hexanoate (2 h) from the wild type (grey) and each of the mutants, *cus1* (red) and *gpat6* (blue) in DMSO- d_6 at 60 ºC.

CHAPTER III

Chapter III consists of the following published manuscript:

Artur Bento, **Carlos J. S. Moreira,[±]** Vanessa G. Correia,[±] Rita Escórcio, Rúben Rodrigues, Ana S. Tomé, Nathalie Geneix, Johann Petit, Bénédicte Bakan, Christophe Rothan, Oleksandr O. Mykhaylyk and Cristina Silva Pereira. ACS Sustainable Chemistry & Engineering, 2021. (https://doi.org/10.1021/acssuschemeng.1c04733) [±]equally contributing authors.

Author Contributions

C.S.P and O.O.M designed the project and acquired the funding. C.S.P., O.O.M., B.B. and C.R. provided the resources. C.J.S.M. and A.B. performed experiments related to cutin isolation from tomato and pepper peels; A.B., V.G.C. and R.R. performed experiments related to suberin extraction from cork and potato. C.J.S.M. and A.B. prepared samples for NMR and DSC characterization of cutin and suberin samples. A.B. and C.J.S.M. ran DCS experiments and analyzed the data. A.B. ran NMR experiments and A.B. and V.G.C. analyzed the data; A.B. and O.O.M performed WAXS analyses of all samples and corresponding data analysis; A.B., C.J.S.M, V.G.C and N.G. performed total carbohydrate and cellulose quantification and analysis the results; A.B., C.J.S.M and V.G.C wrote the initial draft of the manuscript. All authors participated in the writing of the final version of the manuscript, including review and editing.

Outline: The following chapter presents a submitted manuscript in its original form. In this chapter the systematic characterization of cutin and suberin from two different sources each is presented. A correlation between chemical structure and its impact on crystallinity and thermal resistance are presented for both plant polyesters. Five rules are proposed to demonstrate how the quantification of structure-property relationships can help to guide the development of novel bio-based materials.

Quantification of Structure-Property Relationships for Plant Polyesters Reveals Suberin and Cutin Idiosyncrasies

Artur Bento,[a] Carlos J. S. Moreira,[a,±] Vanessa G. Correia,[a,±] Rita Escórcio,[a] Rúben Rodrigues,[a] Ana S. Tomé,[a] Nathalie Geneix,[b] Johann Petit,[c] B. Bakan,[b] Christophe Rothan,[c] Oleksandr O. Mykhaylyk,[d] and Cristina Silva Pereira[a,*]

[a] Instituto de Tecnologia Química e Biológica António Xavier, Universidade Nova de Lisboa (ITQB NOVA), Av. da República, 2780-157, Oeiras, Portugal

[b] INRAE, UR BIA 1268, 44316, Nantes, France

[c] UMR 1332 BFP, INRAE, Univ. Bordeaux, F-33140 Villenave d'Ornon, France

[d] Soft Matter Analytical Laboratory, Dainton Building, Department of Chemistry, The University of Sheffield, Sheffield, S3 7HF, UK

± equally contributing authors;

*corresponding author: Cristina Silva Pereira (spereira@itqb.unl.pt)

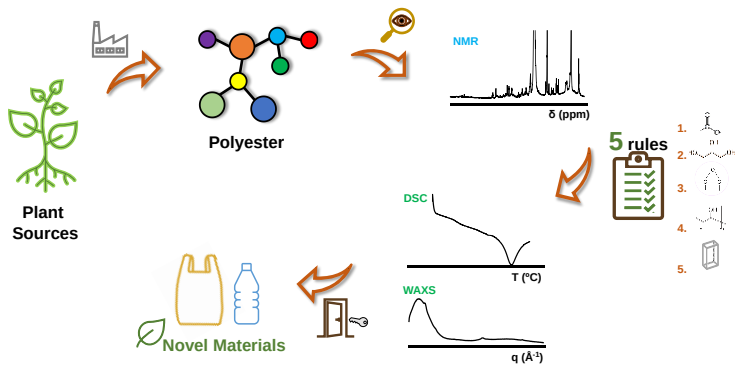

A detailed look into the chemical structure of native plant polyesters for the identification of crucial physical properties: 5 rules towards the development of novel green materials.

Abstract

Polyesters, as they exist *in planta*, are promising materials with which to begin the development of “green” replacements. Cutin and suberin, polyesters found ubiquitously in plants, are prime candidates. Samples enriched for plant polyesters, and in which their native backbones were largely preserved, were studied to identify “natural” structural features; features that influence critical physical properties. Quantitative NMR, DSC and X-ray scattering methods were used to quantify structure-property relationships in these polymeric materials. The degree of esterification, namely the presence of acylglycerol linkages in suberin and of secondary esters in cutin, and the existence of mid-chain epoxide groups defining the packing of the aliphatic chains were observed. This packing determines polymer crystallinity, the resulting crystal structure and the melting temperature. To evaluate the strength of this rule, tomato cutin from the same genotype; studying wild-type plants and two well-characterized mutants, was analyzed. The results show that cutin’s material properties are influenced by the amount of unbound aliphatic hydroxyl groups and by the length of the aliphatic chain. Collectively the acquired data can be used as a tool to guide the selection of plant polyesters with precise structural features, and hence physicochemical properties.

Introduction

The use of synthetic plastics became widespread in the first half of the last century. This increased usage reflects their matchless durability, mechanical resistance, non-permeability, versatility, as well as their low production costs[1]. Plastics include a diverse range of materials, *e.g.* polyethylene, polyethylene terephthalate, polyvinyl chloride and polystyrene[2], that are generated through harmful petroleum-based syntheses. These materials are employed in a vast range of products, many of which are single-use. At the end of the product life-cycle the limited degradability of these materials contributes to a massive pollution problem and to the destruction of habitats around the world. The plague of plastic pollution, especially that of microplastics in marine ecosystems, has a staggering impact on wildlife[3]. An increased awareness of this situation is driving the development of novel, sustainable alternatives as can be seen, for example, in the European Strategy for Plastics in a Circular Economy[4].

During land colonization by plants, *ca*. 450 million years ago, plants acquired the capacity to synthesize cutin and, a related biopolymer, suberin[5]. These cell-wall heteropolymers exhibit barrier properties and contribute to controlling water loss, provide insulation against climatic variability, and protection against both abiotic and biotic pressures[5]. They are ubiquitously present in land plants as a major component of the cell walls of the epidermis (cutin) and of periderms (suberin; *e.g.* tree bark and tuber periderms) where they build defensive hydrophobic barriers[5]. Naturally, they can be regarded as evolutionarily optimized, multifunctional biopolymers that control many aspects of plant biology. Changes to cutin and/or suberin result in many divergent phenotypes. Examples include alterations to: susceptibility to abiotic/biotic pressures; morphology; permeability and others[6,7]. These polymers (*i.e.* polyesters) constitute the third most abundant class of plant polymers, after cellulose/hemicellulose and lignin. Thus, these materials should be considered as frontrunners in the development of bioplastics as alternatives to their synthetic counterparts.

Cutin and suberin are composed of an extremely complex heterogeneous mixture of monomeric units that contain both linear alkyl and aromatic moieties of monomers linked through aliphatic esters[8]. Amongst the major differences, are the presence of C_{16}/C_{18} ω-hydroxyacids in cutin, and the presence of both C_{16}-C_{28} ω hydroxyacids and C_{16}-C_{26} α,ω-diacids in suberin[9]. Suberin extraction from plant periderms implies ester cleavage, which is typically achieved using nonspecific, hydrolysis-based processes that release the monomeric constituents[10]. Recovery of cutin usually involves time-consuming enzymatic-based hydrolyses[11], whereas subsequent chemical analyses often resort to extensive hydrolyses similar to those applied to suberin extraction[12]. To date, extraction of suberin while preserving its esterified polymer network, has only been achieved through the use of mild ionic liquid-catalysts that promote the selective and limited hydrolysis of acylglycerol esters[13]. Recently, it was demonstrated the suitability of this method for the isolation of suberin from cork[14] and potato peels[15]. This methodology allowed to extract suberin while largely maintaining its native backbone, *i.e.* containing glycerol at levels close to its natural abundance. Additionally, a similar method could be used for the uncomplicated isolation of a highly esterified cutin matrix from tomato peels. This is due to the ability of the ionic liquid to solubilize the non-cuticular polysaccharides and waxes[16]. As a result, these ionic liquid-based processes represent a unique approach with which to obtain materials enriched in plant polyesters that maintain a highly esterified polymeric backbone. The extracted materials should closely mimic the physicochemical properties of the polyester barriers found in planta. This strategy clearly differs from the design of polymer materials that require extensive depolymerization followed by subsequent re-polymerization[10,17,18], yet we believe that these approaches should be seen as two complementary.

With the aim of supporting knowledge-based development of materials derived from plant polyesters, the structures of distinct plant polyesters at both macro- and nano-scales were systematically characterized. Specifically, cork and potato peel were used as suberin sources, and peel from tomato and red

pepper as cutin sources. The chosen raw materials are readily available as agro-industrial residues and are generated in thousands of tons per year just in Europe[19]. The plant polyesters were purified using established ionic liquid-based extraction methods[14,16]. Structural and chemical characterization of the materials was performed by combining analyses using Nuclear Magnetic Resonance (NMR) and Wide-Angle X-ray Scattering (WAXS complemented by thermal (Differential Scanning Calorimetry, DSC) and morphological (Scanning Electron Microscopy, SEM) analyses. To refine the understanding of how the chemical structure impacts the crystallinity and thermal resistance of the ensuing materials, cutin materials extracted from a defined tomato genotype (Micro-Tom) were also analyzed. Cutin was extracted from wild-type plants and also from two mutants defective in cutin biosynthesis. How each polymeric backbone, carrying distinct levels of esterification and mid-chain functionalities, assembles at both nano- and macro- levels, to form materials with diverse physicochemical properties is discussed in great detail.

Results and discussion

Morphological characterization reveals different levels of structural organization

Cutin and suberin were purified from the corresponding plant sources using cholinium hexanoate (2 h) as previously established[14,16]. Importantly, although these processes rely on the same catalyst - cholinium hexanoate, cutin is isolated from the cuticle as an insoluble component (following solubilization of polysaccharides and waxes in the ionic liquid), whereas suberin is recovered from the supernatant, which contains the ionic liquid as a soluble component, by precipitation in an excess of water (Figure S1). Naturally, the cutin and suberin samples exhibited very different morphological features, as observed by SEM (Figure 1).

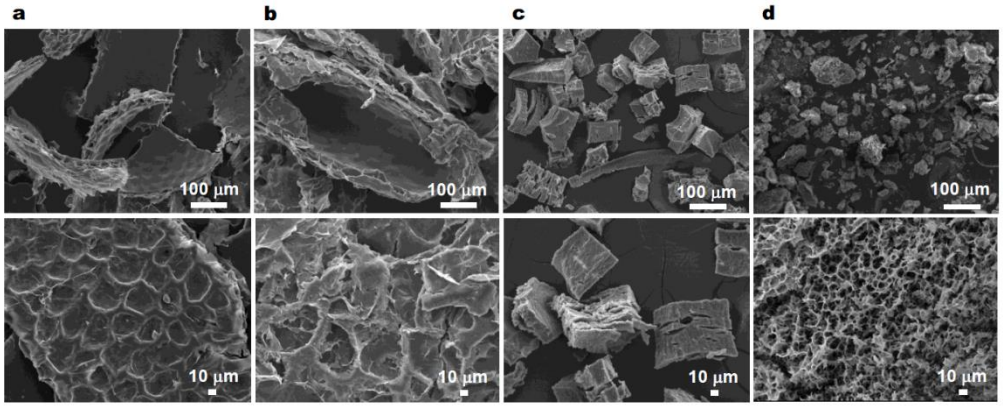

Figure 1. Morphological characterization of plant polyesters. SEM micrographs of cutin recovered from tomato peel (a), pepper peel (b), and of suberin from cork (c) and potato peel (d), following cholinium hexanoate extraction for 2 hours.

The integrity of the cellular structure was largely preserved following the ionic liquid-based extraction of cutin from either tomato or pepper peels. A clean, thick cutin-continuum that showed the epidermal cell grooves was revealed (Figure 1a-b). The purified cork and potato suberin samples consist of ordered and elongated polygon structures (Figure 1c) and of porous and irregular

particles (Figure 1d), respectively. As such, the observed morphology of each type of polyester, upon extraction with cholinium hexanoate, is consistent with that previously reported for comparable samples[14,16], highlighting the reproducibility of the extraction method.

Ionic liquid-mediated hydrolysis is ester-type specific

The capacity of an ionic liquid to hydrolyze octan-4-yl octanoate (secondary aliphatic ester), sucrose monolaurate (ester link between a fatty acid and a sugar), ethyl 4-hydroxy-3-methoxy-cinnamate (ester link between an alcohol and an aromatic acid) and poly(1,4-butylene adipate) (synthetic linear polyester) was evaluated. This dataset aims to complement data obtained previously with octyl-octanoate (primary aliphatic ester) and glyceryl-trioctanoate (acylglycerol ester) that showed virtually no ester cleavage and mild, yet progressive ester cleavage, respectively[13,16]. All the compounds tested here were largely resistant to the ionic liquid-mediated hydrolysis achieving only *ca.* 5 % of ester cleavage after 2 h (Figures S2 and S3). Analyses of longer reaction times (until 24 h) demonstrated that the hydrolysis is ester-type specific as follows: acylglycerol ester > sugar ester ≅ aromatic ester > secondary aliphatic ester ≅ primary aliphatic ester. The hydrolysis of the poly(1,4-butylene adipate) (Figure S4) did not occur, similar to that observed before with octyl-octanoate[16]. Collectively the data showed that after 2 h the ionic liquid mediated mild cleavage of distinct ester types, except of primary aliphatic esters that remain intact, consistent with the recovery of highly preserved esterified plant polyesters.

Nuclear magnetic resonance unveils quantitative chemical fingerprints for each plant polyester

The elemental composition of either plant polyester under study is similar to what has been previously reported (Table S1)[13,20–24]. Note that small differences between the two polyester types, cutin and suberin, were observed. Small differences were also observed for same polyester type originating from different plant sources. In planta, the polyester backbone is linked to cell wall polysaccharides; a hypothesis supported by experimental data[25–27]. To test for the presence of polysaccharide moieties, the amount of hydrolysable carbohydrates present in each polyester type was analyzed (Table S2). The amounts of carbohydrates present in the polyester samples were below 0.1 %, with potato suberin reporting the highest value (1.16 ng/mg) and pepper cutin the lowest (0.12 ng/mg).

In recent studies, following successful solubilization of tomato cutin and cork suberin in DMSO, high-resolution, solution-state NMR spectra were acquired[14,16]. These previous studies enabled more details of the chemistry of the two polymers (*e.g.* for tomato cutin, the esterification level, assignment of esters, free acids and alcohols[16]; for suberin, the ratio of linear aliphatic/acylglycerol esters and the relative abundance of acylglycerol configurations[14]). In the present study, this methodological approach was used by resorting to a cryoprobe to further enhance the sensitivity of the NMR analyses. Thus, it was possible to expand the list of assigned signals and to quantify specific molecular features. The ^{1}H NMR spectra for all samples was obtained at high resolution and, in agreement with previous reports, exhibited many overlapping signals (Figure 2aI-dI)[14,16]. The assignment of signals was achieved through a combination of 2D spectra (^{1}H-^{1}H COSY, ^{1}H-^{13}C HSQC and ^{1}H-^{13}C HMBC, Figures S5-S16, full list of assignments in Tables S3-S4), guided by previous NMR data for tomato cutin[16] and cork suberin[14], as well as NMR data from oligomeric structures obtained through methanolysis of tomato peels[12].

The analysis of the HSQC spectra for, both cutin samples shows the presence of two aliphatic regions with the assignment of CH_2 and CH_3 groups from the aliphatic chains, the ester bonds and the free mid-chain hydroxyl groups (Figure 2aII, 2bII).

It was possible to assign two new signals related to secondary aliphatic ester bonds (SAE) and epoxide rings (Figure 2aIII, 2bIII). The secondary ester bonds were assigned to a ^{13}C shift of 72.61 ppm and ^{1}H shift of 4.77 ppm, while the signal assigned to the epoxide rings (only detected in pepper cutin) have a ^{13}C shift of 55.43 ppm and ^{1}H shift of 2.82 ppm. Moreover, in the HSQC spectrum of tomato cutin it was only possible to detect secondary free hydroxyl groups (CHOH mid-chain), which contrasts with the detection of signals related to both primary (CH_2OH) and secondary hydroxyl (CH-(OH)-) groups in pepper cutin.

In the HSQC spectra of both cutin samples, two signals were detected for the α-(C=O) with a ^{13}C shift of 33 ppm associated with a ^{1}H shift of 2.25 ppm and of 2.19 ppm, which can be assigned to esters (Figure 2aII, 2bII). Vestigial amounts of microcrystalline cellulose were previously detected in tomato cutin samples purified by cholinium hexanoate[16]. Accordingly, the ^{1}H shift at 2.19 ppm may be associated with the presence of cellulose esters. The ^{13}C shift at 34.66 ppm and ^{1}H shift of 2.03 ppm was assigned to the free acids, a signal only present in tomato cutin, and absent in pepper cutin (Figure 2aII, 2bII). In the HMBC spectrum of these biopolyesters (Figures S7, S10), the $^{3}J_{CH}$ (three bond distance C···H) couplings detected, involving the ester carbonyl quaternary carbons, provided additional support for the presence of signals derived from esters and acids. Two different quaternary carbonyl carbons were present, with small differences in their chemical shifts: the carbon in the primary aliphatic ester (PAE), at 172.34 ppm; and the carbon in the free acid, at 173.96 ppm. These assignments were confirmed by their $^{3}J_{CH}$ connectivity: the primary ester carbon was coupled with the methylene protons, and the free acid was not coupled with any proton group with a $^{3}J_{CH}$ coupling.

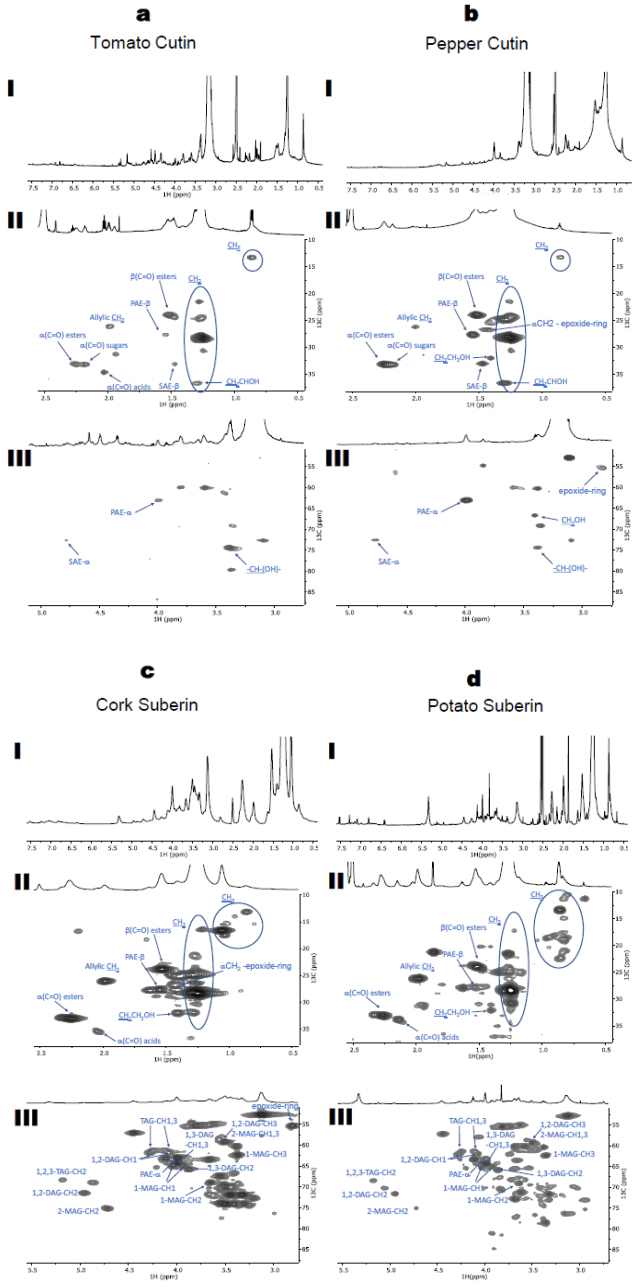

Figure 2. Wide-ranging NMR spectral characterization of tomato cutin (a); pepper cutin (b); cork suberin (c); and potato suberin (d) upon isolation using cholinium hexanoate extraction for 2 hours. ^{1}H NMR spectra of all samples (I); and the HSQC regions corresponding to aliphatics (II) and CH/CH_2-X aliphatics (III). Some correlations (unlabeled) are uncertain or unidentified.

For both suberin samples, the HSQC spectra show the presence of two aliphatic regions with the assignment of CH_2 and CH_3 groups from the aliphatic chains, the ester bonds and the free primary hydroxyl groups (Figure 2cII, 2dII). In these two polymers, signals that could be assigned to all five glycerol configurations (1,2,3-triacylglycerol (TAG), 1,2-diacylglycerol (1,2-DAG), 1,3,-dyacylglycerol (1,3-DAG), 2-monoacylglycerol (2-MAG) and 1-monoacylglycerol (1-MAG)) were detected, as previously reported for cork suberin[14], and potato suberin[15]. Moreover, the presence of the signal assigned to the epoxide groups was only observed in cork suberin at ^{13}C shift of 55.41 ppm and ^{1}H shift of 2.80 ppm, consistent with a previous report[14].

In both suberin samples, the signals related to the presence of α-(C=O) esters with a ^{13}C shift of 33.05 ppm and ^{1}H shift of 2.26 ppm, and presence of free acids at ^{13}C shift of 35.43 ppm and ^{1}H shift of 2.03 ppm were detected (Figure 2cII, 2dII). These assignments were confirmed by HMBC (Figures S13, S16). Two different quaternary carbonyl carbons were observed: in the primary aliphatic ester, at 173.01 ppm; and in the free acid, at 175.63 ppm.

The ionic liquid-based approach extracts plant polyesters that retain high levels of esterification; this can be shown quantitatively through NMR. To infer the degree of esterification, the relative abundances of total aliphatic esters was estimated, through the integration of the corresponding NMR signals. This approach allowed to discriminate the contributions of primary and secondary aliphatic esters in cutin; as well as primary and acylglycerol aliphatic esters in suberin (Table 1).

The ratio between primary and secondary esters provides meaningful information on the polymeric arrangement of cutin. Specifically, tomato cutin is enriched in secondary esters, whereas pepper cutin shows higher levels of primary esters. The amount of total esters in pepper cutin is threefold higher than is found in tomato cutin. This is consistent with the presence of a much more esterified cutin in pepper. Additionally, tomato cutin exhibits higher levels

of free hydroxyl groups, which also supports the idea of a lower degree of esterification[28].

Table 1. Chemical characterization of cutin and suberin samples. NMR quantification of the main functional groups in both plant polyesters from each source; and HPLC quantification of glycerol present in the recovered polymeric materials.

			Purified plant polyesters			
			Cutin		Suberin	
			Tomato	Pepper	Cork	Potato
NMR	Primary esters (%)		20[i] [0.2]	59[i] [1.77]	30[iii]	17[iii]
	Secondary esters (%)		80[i] [0.8]	41[i] [1.23]	-	-
	Total esters		1[ii]	3[ii]	-	-
	Acylglycerol esters (%)		-	-	70[iii]	83[iii]
	Free acids[iv] (%)		0.04	n.d.	0.47	0.66
	Glycerol configuration[v] (%)	1,2,3-TAG	n.d.	n.d.	6	12
		1,2-DAG			19	18
		1,3-DAG			25	38
		1-MAG			23	28
		2-MAG			27	4
	^{31}P NMR quantification (mmol/g)	Free acids	0.07	0.05	0.30	0.43
		OH aliphatics	4.17	0.34	2.39	5.89
		OH aromatics	n.d.	0.01	0.44	0.49
HPLC	Glycerol (%, w/w)		n.d.	n.d.	3.86 ± 0.31	2.16 ± 0.20

[i]Relative abundances of primary and secondary esters present in cutin calculated through the integration of signals in the ^{1}H NMR spectra. Values in brackets correspond to the normalized values using the amount of the total esters in each sample.
[ii]Integration of the total ester signal was normalized to benzene for comparison between samples.
[iii]Relative abundances of linear and acylglycerol esters present in suberin calculated by the integration of each signal's volume contour in the ^{1}H ^{13}C HSQC spectra.
[iv]Content of free acids relative to the total area of ^{1}H spectrum.
[v]Relative abundances of glycerol configurations calculated through volume contour in the ^{1}H-^{13}C HSQC spectra. n.d. refers to not detected, TAG, DAG, and MAG stand for triacylglycerol, diacylglycerol, and monoacylglycerol, respectively.

The presence of free acids was observed in the ^{1}H and HSQC spectra from tomato cutin (0.04 %, Table 1 and as reported previously[16]), but were undetected in the pepper cutin spectra. Glycerol was not detected in the HSQC analyses of either cutin sample (Figure 2aIII, 2bIII), nor could it be quantified by liquid chromatography (*i.e.* below the quantification limit of the method), which is consistent with a very low abundance of this monomer[29].

In contrast with cutin, glycerol is known to be a structural monomer in the polymeric arrangement of suberin[30]. Resorting to liquid chromatography, the glycerol content found in cork and potato suberin was quantified, consisting of 3.86 % and 2.16 % (w/w), respectively. This difference suggests that cork suberin is more esterified than potato suberin. Bearing in mind the mode of action of cholinium hexanoate, a selective catalyst that mildly hydrolyses the acylglycerol esters in suberin, the relative abundance of each acylglycerol configuration was inferred through their contour volume integrals in the HSQC spectra[14,15]. Both biopolymers contained all five possible configurations, similar to what was reported previously[14,15]. Overall, the data show that cork suberin has longer polyester chains, due to a greater degree of esterification (*viz.* higher glycerol content, and more acylglycerol and primary esters), compared to potato suberin (Table 1).

Since the esterification level of each polyester-type was distinctively evaluated, *i.e.* levels of secondary esters in cutin and acylglycerol esters in suberin, ^{31}P NMR was performed to systematically quantify specific free chemical groups in all samples. This methodology was initially proposed for the quantitative analysis of lignocellulosic polymers and involves the selective labeling of free OH groups[31]. The presence of free acids and OH aliphatics could be detected in all samples. This confirms the presence of free acids in pepper cutin, despite the lack of a corresponding signal in both the ^{1}H and HSQC NMR spectra for this sample. Cutin samples have 5-10 times lower amounts of free acids compared to suberin samples. While tomato cutin and both suberin samples have similar OH aliphatic content, pepper cutin has a striking 7-17 fold lower amount of this component. Both suberin exhibit similar high levels of OH aromatics; functionalities also found in pepper cutin, but at very low amounts (Table 1).

Through the use of high-resolution NMR-based methods, the esterification level in cutin and suberin was quantified. The identification and quantification of mid-chain and end-chain chemical groups in these materials was achieved, reflecting their astonishing chemical variability: each material

reflects a particular polyester chemistry. A schematic representation of these findings, along with the relative abundance of selected components for each polyester, is depicted in figure 3.

Functional Groups	Cutin		Suberin	
	Tomato	Pepper	Cork	Potato
Primary Aliphatic Esters	+	++	++	+
Secondary Aliphatic Esters	++	+++	-	-
Acylglycerol Esters	-	-	+++	+++
Free Acids	+	+	+++	+++
Primary & Secondary OH groups	+++	+	+++	+++
Epoxide groups	-	+	+++	+

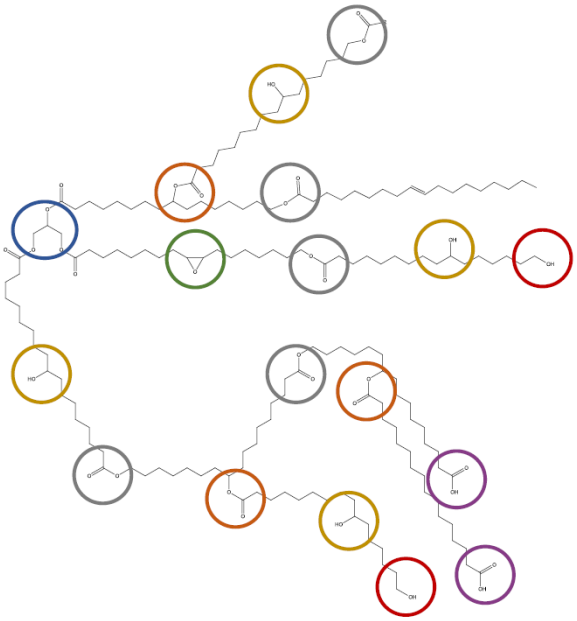

Figure 3. Schematic representation of the main mid-chain and end-chain functionalities (highlighted in different colors) of the plant polyesters cutin and suberin. Their relative abundance (– absent; + present) in different polyester types and from different sources is depicted to ease the understanding of the primary polymeric structure.

Cutin and suberin polymeric arrangement significantly impacts their physicochemical properties

The composition of a plant polyester dictates its structural organization and thus is responsible for its physicochemical properties. It is important to identify critical structural features of plant polyesters, including those at the molecular level, as these greatly influence the macro-structural arrangement and thus the physicochemical properties of these polymeric materials. To this end, DSC and X-ray scattering techniques, which provide information about

the thermal profile and fundamental structural features of materials respectively (Figure 4), have been employed in a combination with NMR results (Table 1 and Figure 2) to establish relationships between chemical composition and structural properties.

The DSC thermograms acquired for both cutin and suberin samples demonstrate pronounced melting peak(s) that indicate the presence of crystalline component(s) in these materials. Tomato cutin shows a higher enthalpy (ΔH = 98.1 J.g^{-1}) compared to pepper cutin (ΔH = 49.7 J.g^{-1}; Figure 4a) suggesting that the former has a higher degree of crystallinity. This is also consistent with the WAXS results (Figure 4b).

The WAXS pattern obtained for the tomato cutin matches that reported previously for a similar material[16]: a broad peak at q ~ 1.41 Å^{-1} and two weak diffraction peaks at q ~ 1.52 Å^{-1} and 1.69 Å^{-1} (Figure 4b, black curve) corresponding to d-spacings of 4.45 Å, and 4.13 Å and 3.72 Å, respectively. Such a WAXS pattern is characteristic of a semicrystalline polymer with small crystalline domains. The broad peak (d ~ 4.45 Å) can be assigned to the inter-chain distance between acyl chains forming either an amorphous polymer structure[32] or a hexagonal packing similar to rotator phases[33]. The two weak diffraction peaks can be attributed to domains of acyl chains ordered in an orthorhombic crystal structure (space group Pnma, Miller indexes 110 and 200, respectively) usually formed by molecules that consist of alkane-like chains such as triacylglycerols (β' phase)[34] or polyethylene[35,36]. None of these diffraction peaks (that indicate the formation of well-ordered crystalline moieties in tomato cutin) could be observed in the WAXS patterns for pepper cutin (Figure 4b, red curve). The more amorphous nature of pepper cutin is possibly due to the abundance of secondary esters and epoxide groups. In tomato cutin, secondary esters are present at a lower amount and epoxide groups are entirely absent (Table 1).

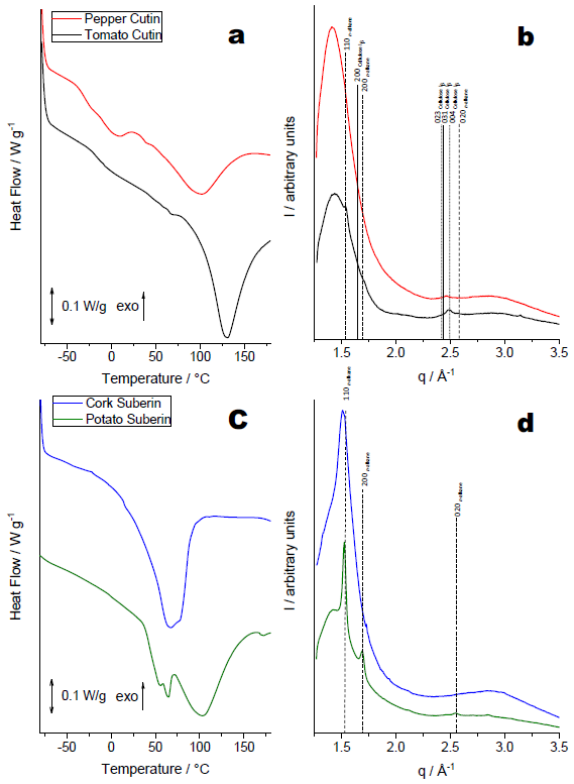

Figure 4. DSC thermograms (a, c) and WAXS patterns (b, d) collected for cutin and suberin samples isolated using cholinium hexanoate extraction for 2 hours. The vertical straight lines in the WAXS patterns indicate the position of diffraction peaks of cellulose (dotted lines) and crystallized n-alkane chains (dashed lines). Miller indexes assigned to the lines correspond to I_β cellulose (monoclinic space group $P12_11$) and n-alkane chain packing (orthorhombic space group Pnma).

The orthorhombic crystal structure observed in tomato cutin is consistent with its higher melting temperature (123 ºC) compared with that of pepper cutin (100 ºC) (Figure 4a). The lower esterification level of the acyl chains in tomato cutin, compared with pepper cutin, possibly facilitates the formation of an orthorhombic unit cell. Such a unit cell is thermodynamically more stable than a rotator phase that is likely to be formed by distorted (esterified) alkane chains packed in a hexagonal array[33]. Collectively, the acquired data strongly suggest that both the esterification level (mainly related

to the presence of secondary esters in cutin) and the presence of mid-chain epoxide groups are the key features that control packing of the aliphatic chains; increasing the esterification level and abundance of mid-chain epoxides reduces cutin's crystallinity and melting temperature.

Finally, the diffraction peak at q ~ 2.46 $Å^{-1}$, observed for both cutin samples (Figure 4b), cannot be related to the acyl chain crystalline structure. Its position is significantly shifted from a possible 020 peak of the orthorhombic structure expected at q = 2.55 $Å^{-1}$ (Figure 4b). This peak is likely to be associated with crystalline cellulose and can be assigned to a 004 reflection of monoclinic I_β cellulose (space group $P12_11$)[37]. Notably, the most intense 200 diffraction peak of the I_β cellulose expected at q = 1.63 $Å^{-1}$ is not visible because of an overlap with an intense broad peak that corresponds to the amorphous polymer structure. Crystalline cellulose usually coexists with amorphous cellulose[37], but it would be difficult to identify the amorphous cellulose component, with its expected maximum peak intensity at q = 1.52 $Å^{-1}$, from the broad diffuse peak observed in cutin's WAXS patterns. Using specific antibodies for crystalline cellulose, comparable semi-quantitative levels were estimated for both samples (Figure S17). The amount of hydrolysable carbohydrates (< 0.05 %) is higher in tomato cutin than pepper cutin (Table S2).

The thermal characterization of suberin samples revealed that much higher enthalpy was needed to melt the crystals in potato suberin (ΔH = 117.6 $J.g^{-1}$) compared to cork suberin (ΔH = 81 $J.g^{-1}$) (Figure 4c). These values are in good agreement with the corresponding WAXS patterns (Figure 4d). The cork suberin pattern shows a broad peak between q = 1.35 $Å^{-1}$ and 1.6 $Å^{-1}$, similar to cutin (Figure 4b), overlapping with a relatively sharp diffraction peak at q ~ 1.5 $Å^{-1}$ (Figure 4d, blue curve). This pattern is characteristic of an amorphous polymer with a significant amount of crystalline component indicated by the diffraction peak at q ~ 1.5 $Å^{-1}$ (d ~ 4.2 Å), which could correspond to a 100 reflection of a hexagonal rotator phase structure formed by acyl-chain packing. The potato

suberin WAXS pattern shows a broad peak similar to that observed for the cork suberin and also exhibits three additional pronounced peaks at q = 1.52 Å^{-1}, 1.69 Å^{-1} and 2.55 Å^{-1} that are characteristic of crystalline moieties corresponding to an orthorhombic structure (Figure 4d, green curve). In contrast to cutin, WAXS patterns for suberin showed no signs of crystalline cellulose. Very low amounts of hydrolysable carbohydrates could be detected in these samples (Table S2).

The calorimetric analysis of both suberin samples revealed a thermal profile that is strikingly distinct from cutin, specifically the presence of more than one melting point. In particular, potato suberin has three melting temperatures (56, 65 and 103 ºC), while cork suberin exhibits two melting temperatures (67 and 78 ºC; Figure 4c). The more organized crystalline structure of potato suberin naturally results in both higher enthalpy and melting temperature compared to cork suberin. As concluded for cutin, the formation of crystalline structures is influenced by the esterification level, which in suberin is mainly dictated by the presence of both acylglycerol esters and epoxide groups. Hence, in cork suberin the presence of epoxide groups hinders the packing of the aliphatic chains rendering a less organized polymeric structure. Notably, the orthorhombic structure observed in the potato suberin WAXS pattern matches that observed in the tomato cutin (Figure 4b, black curve), showing an unexpected similarity between these two distinct types of plant polyesters at the nanoscale. Both potato suberin and tomato cutin have lower esterification levels than their counterparts, but the former has more orthorhombic crystalline moieties. This shows that the packing of the aliphatic chains is eased by the presence of the acylglycerol linkages that are present in suberin but not by the secondary esters present in cutin. This finding is also consistent with previous studies[34].

Overall, the acquired data show that the exploitation of different plant sources, containing plant polyesters with distinct chemistries, can be used to tune the physical properties of extracted materials. Considering the range of physicochemical properties exhibited by different plant polyesters, or by

polyesters from different sources, it would be desirable to continue to use tomato cutin as a model with which to further analyze how specific structural alterations influence physicochemical properties.

Genetic modifications allow the fine-tuning of cutin physicochemical properties

The physicochemical properties of polyesters from a defined genotype, Micro-Tom cultivar, and from two of its well-characterized mutants were analyzed. The selected mutants were *gpat6* (*GLYCEROL-3-PHOSPHATE ACYLTRANSFERASE* gene) and *cus1* (*CUTIN SYNTHASE* gene)[28,38,39], that exhibit altered cutin composition and altered degrees of intra-chain branching. In the *gpat6* mutant (formerly named cutin-deficient mutant *cud1*)[28], the synthesis of the major cutin precursor is hindered, resulting in a thinner cuticle with decreased levels of cutin but enriched in fatty acids[38]. In the *cus1* mutant, cutin polymerization is impaired[40,41] and the presence of secondary esters is greatly reduced[28]. The cutin samples were purified from tomato peels using the established ionic liquid method[16] and analyzed using the same procedures used for other samples in this study. SEM revealed that all cutin samples extracted from Micro-Tom tomato peels (Figure S18) showed similar morphologies to those of both tomato and pepper cutin (Figure 1), as well as to those previously reported by us for cutin from the same genotype[16]. Our main goal was to analyze if specific alterations in cutin biosynthesis would lead to predictable alterations in the physicochemical properties of the resulting polymers. This constitutes an unmatched approach to confirm the importance of cutin esterification levels and how they relate to its thermal resistance and crystallinity.

The assignment of the NMR signals was attained through a combination of 2D spectra (^{1}H-^{1}H COSY, ^{1}H-^{13}C HSQC and ^{1}H-^{13}C HMBC, Figures S19-S27); and is in good agreement with previous reports[16]. The magnification of the HSQC regions corresponding to aliphatics and CH/CH_2-X aliphatics for all cutin samples (Figure S28) revealed that both

cutins extracted from the mutant strains are enriched in CH_3 groups when compared to cutin from the wild-type strain. This is consistent with previous studies[16,28,38]. All of the crucial quantifications required for the analysis of the polymeric structural organization are summarized in Table 2.

Table 2. Chemical characterization of cutin samples from Micro-Tom cultivars. NMR quantification of the main functional groups in the cutin samples derived from Micro-Tom tomato peel - wild-type, *cus1* and *gpat6* - isolated using cholinium hexanoate extraction for 2 hours.

			Purified cutin from Micro-Tom tomatoes peels		
			Wild-type	***cus1***	***gpat6***
NMR	Primary esters[i)]		66 [6.6]	78 [6.24]	25 [0.75]
	Secondary esters [i)]		34 [3.4]	22 [1.76]	75 [2.25]
	Total esters[ii)]		10	8	3
	Free acids[iii)]		0.14	n.d.	n.d.
	^{31}P quantification (mmol/g)	Free acids	0.065	0.067	0.029
		OH aliphatics	2.467	7.82	7.609
		OH aromatics	0.168	n.d.	n.d.

[i)]Relative abundances of primary and secondary esters present in cutin calculated through integration of signals in the ^{1}H NMR spectra. Values in parentheses show the normalized values using the amount of total esters in each sample.
[ii)]Integration of the total ester signal was normalized with benzene for comparison between samples.
[iii)]Content of free acids relative to the total area of ^{1}H spectrum.

As anticipated, the analyzed cutin samples exhibit great differences in the degree of esterification and in the content of OH aliphatics. The cutin extracted from the wild type Micro-Tom cultivar is more esterified than that of both mutants; cutin from the *gpat6* mutant is the least esterified. The trend observed for the amount of secondary esters (normalized values) is wild-type > *gpat6* > *cus1*. The trend for the amount of OH aliphatics, calculated by ^{31}P NMR, is *cus1* > *gpat6* > wild-type. The observed increase in the content of free OH aliphatics correlates with a decrease in the secondary ester content. This observation is also in general agreement with previously published data on these mutants that was obtained using an independent approach (detection of benzyl etherified OH groups in cutin hydrolysates)[28]. The amount of free OH groups detected by ^{31}P NMR may include some free OH groups from cuticular polysaccharides (regardless of their very low

abundance; Table S2). Additionally, free acids are less abundant in the *gpat6* cutin, and OH aromatics are only detected in the wild-type cutin. Here, the structural features (total, primary and secondary esters; Table 2) were precisely assigned and constitute absolute values. This differs from a previous study on similar cutin materials where their relative abundances were qualitatively inferred[16]. The ability to systematically compare the absolute quantities of structural features associated with mutations that affect cutin biosynthesis is a powerful methodology, one that deserves a more focused analysis in the near future.

The DSC thermograms of all Micro-Tom cutin samples (Figure 5a) show considerably higher melting temperatures for cutin from both mutants (*cus1* 169 ºC, and *gpat6* 175 ºC) compared to the wild type (131 ºC). The thermal resistance of the wild-type cutin is close to that observed for tomato cutin purified from commercial tomatoes (123 °C, Figure 4a), reflecting the impact of the plant raw material.

The enthalpy required to melt the crystalline moieties present in the polymeric materials shows a similar trend: *cus1* and *gpat6* cutin samples display much higher enthalpy (*cus1* 159 $J.g^{-1}$, and *gpat6* 124 $J.g^{-1}$) compared to the wild-type (82 $J.g^{-1}$). The WAXS patterns of the Micro-Tom tomato cutin samples (Figure 5b) are similar to those obtained for the commercial tomato cutin (Figure 4b): a broad band near q = 1.44 $Å^{-1}$ and three weak diffraction peaks at q ~ 1.52 $Å^{-1}$, 1.69 $Å^{-1}$ and q ~ 2.46 $Å^{-1}$ (Figure 5b). The peaks related to the orthorhombic structure of the crystals are, however, more pronounced in the cutin extracted from both mutants compared to that of the wild type. This reflects the higher degree of crystallinity found in the cutin extracted from the mutants. The third diffraction peak at q ~ 2.46 $Å^{-1}$ observed for all Micro-Tom cutin samples should be related to the 004 reflection of monoclinic I_β cellulose (space group $P12_11$) (Figure 5b), in analogy to both commercial tomato and pepper cutin (Figure 4b). The presence of crystalline cellulose could be confirmed through immunoblotting (Figure S17). The estimated, semi-quantitative values make it evident that a lower proportion of

microcrystalline cellulose is present in cutin from wild-type plants compared to either mutant. The results obtained are consistent with WAXS results showing that the crystalline cellulose diffraction peak of the wild type cutin is significantly less intense in comparison with that from the mutant cutins (Figure 5b). Interestingly, the cutin samples extracted from the peel of wild-type cultivars, the commercial cultivar and the miniaturized Micro-Tom tomatoes, showed almost identical levels of microcrystalline cellulose (Figure S17) and of total hydrolysable carbohydrates (Table S2). The last are also comparable in either cutin extracted from the mutants. These results suggest that the higher thermal resistance of the cutin extracted from either mutant may include the contribution from cuticular polysaccharides (regardless of their very low abundance; Table S2). The presence of cuticular polysaccharides in either cutin sample is consistent with data recently reported for tomato cutin extracted using the conventional enzymatic-based approach[26]. This result adds support to previous data that suggested the existence of crosstalk between lipid and polysaccharide deposition in these mutants plant cuticles[26,38]; either mutation would affect both the cutin polymer and the cuticular polysaccharides.

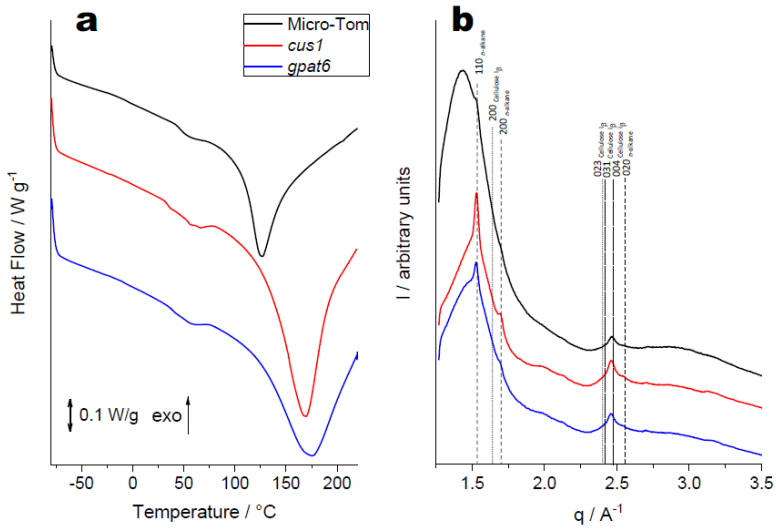

Figure 5. DSC thermograms (a) and WAXS patterns (b) collected for cutin samples extracted from Micro-Tom tomato peel - wild-type, *cus1* and *gpat6* - isolated using cholinium hexanoate extraction for 2 hours. The vertical straight lines in WAXS patterns indicate the position of diffraction peaks of cellulose (dotted lines) and crystallized *n*-alkane chains (dashed lines). Miller indexes assigned to the lines correspond to I_β cellulose (monoclinic space group $P12_11$) and *n*-alkane chain packing (orthorhombic space group Pnma).

Finally, the low crystallinity of the wild-type cutin is likely related to its high degree of esterification along with the high amount of secondary esters. The *cus1* mutant has a more crystalline cutin due to the low abundance of secondary esters (normalized values) and high OH aliphatics content. These modifications permit the polymeric chains to pack into an orthorhombic structure. Although the amount of secondary esters in cutin extracted from the *gpat6* mutant has an intermediate value (*i.e.* higher than *cus1* cutin but lower than the wild-type) it is more crystalline than the wild-type cutin. We hypothesize that the high content of unbound OH aliphatics in conjunction with the shorter polymeric chain lengths (inferred by the low amount of primary esters) facilitates the organization of the polymeric chains into a more crystalline material. Additionally, the enrichment of fatty acids in either mutant cutin may also play a crucial role in the crystallization of the polymeric chains.

Conclusions

Plant polyesters constitute multifunctional polymers that can be isolated preserving high esterification levels. Through a systematic analysis of the chemistry, structure, thermal resistance and crystallinity of distinctive plant polyesters, we have identified the most critical “natural” structural features that influence their material properties. Specifically, quantitative NMR methods, DSC and X-ray scattering data were collected and their integration defines the Rules Of Thumb For The Quantification Of The Structure-Property Relationships Of Plant Polyesters. These rules are outlined below:

1. Despite the amorphous nature of the polymeric materials analyzed here, the degree of esterification dictates the packing of the aliphatic chains (also influenced by their length) and hence polymer crystallinity (and the resultant crystal structure) and melting temperature.
2. A low degree of esterification favors the formation of crystalline regions, yet the packing of the aliphatic chains is easier to accomplish in the presence of acylglycerol bonds when compared to secondary esters.
3. The packing of the aliphatic chains is greatly influenced by the presence of mid-chain epoxide groups.
4. Increased amounts of unbound OH aliphatic groups and smaller chain lengths (inferred from the amount of primary esters) facilitate the organization of the polymeric chains.
5. A low degree of esterification of the acyl chains in the polyester favors the formation of alkane microcrystals with an orthorhombic structure.

How the molecular weight of the polymer correlates with the physicochemical properties remains unanswered because their broad insolubility in organic solvents hinders the development of a method with which to analyze both polyester types. Further characterization of their mechanical properties (in addition to their molecular weight) will be essential

to refine these proposed rules, with the eventual aim of developing a user-friendly computing toolbox.

Finally, it is worth reinforcing the broad applicability of the quantitative NMR workflow developed here for the collection of thorough quantitative molecular structure data on diverse plant polyesters. This can be applied in materials sciences, specifically for the design of polyester-materials, supporting the selection of suitable plant sources and/or downstream-processes (*e.g.* control of esterification level/type). The workflow also constitutes an essential tool for the structural characterization of polyesters from model plant genotypes and may support the identification of cultivars carrying features that may be correlated with higher resistance to abiotic pressures (*e.g.* climate change).

To conclude, we have deduced the Rules Of Thumb For The Quantification Of The Structure-Property Relationships Of Plant Polyesters following a systematic characterization of the structure, chemistry, thermal resistance and crystallinity of two polyesters types, in both cases greatly preserving the natural polymeric backbone. Unexpectedly, similar crystal structures were observed in distinct polyester types (potato suberin and tomato cutin) and highly thermally resistant cutin was found in both Micro-Tom mutants. The future holds promise; we have started to learn how to tune specific properties of plant polyesters through genetic manipulation or through the selection of different source materials; supporting the development of materials for specific applications in the future.

Materials and Methods

Plant Material. Peels from commercially available tomato (*Solanum lycopersicum*) and red pepper (*Capsicum annum*) were manually removed, thoroughly washed and then dried until constant weight at 60 °C. After drying, the peels were milled using a Retsch ZM200 electric grinder (granulometry 0.5 mm; 10000 rpm) and stored at room temperature until further processing. Micro-Tom cultivar tomatoes were provided by Institut National de la Recherche Agronomique (INRA) in Bordeaux; both mutants (*gpat6* and *cus1*) were generated in the miniature cultivar Micro-Tom by an ethyl methanesulfonate (EMS) mutagenesis[42]. All fruits used were in the red ripe developmental stage.

Granulated cork (bark from *Quercus suber* L.) was obtained from Amorim & Irmãos SA (Santa Maria de Lamas, Portugal) and white potatoes (*Solanum tuberosum* L., *cv.* Monalisa) from Batatas Mirense, Lda. (Mira, Portugal). Raw potato tubers were peeled; the peels were scraped in boiled water to ensure minimum pulp content and dried at 50 ºC until constant weight. Both plant sources were first milled (Retsch ZM200 electric grinder; granulometry 0.5 mm; 10000 rpm), then extractives removed by sequential Soxhlet extraction with solvents of increasing polarity (dichloromethane, ethanol and water) as previously described[13]. The extractive-free preparations were washed in an excess of deionized water for complete removal of low molecular weight compounds and dried until constant weight at 60 °C before use.

Chemicals. Sodium hydroxide (> 98 %) was purchased from José Manuel Gomes dos Santos; methanol (≥ 99.8 %), ethanol (99.8 %), dimethyl sulfoxide (DMSO, > 99.99 %), hexane (> 95 %), chloroform (> 99.98 %), dichloromethane (> 99.99 %) from Fisher Chemical; cholinium hydrogen carbonate (~ 80% in water), hexanoic acid (> 99.5%), sucrose monolaurate (> 97 %), 4-octanol (> 97 %), octanoic acid (≥ 98 %), *p*-toluene-sulfonic acid

monohydrate (> 98 %), sulfuric acid (95-97 %), deuterated chloroform (CDCl3, 99.8%), poly(1,4-Butylene Adipate) (Mw ~ 12.000 g/mol), from Sigma-Aldrich; deuterated dimethyl sulfoxide (DMSO-*d6*, > 99.99%) from Merck; and ethyl 4-hydroxy-3-methoxy-cinnamate (99 %) from Alfaesar. Cholinium hexanoate was synthesized by dropwise addition of hexanoic acid to aqueous cholinium hydrogen carbonate in equimolar quantities, as previously described[43].

Isolation of plant polyester enriched materials. Suberin[13] and cutin[16] were extracted from cork/potato peel and tomato/pepper peels, respectively as previously described. In brief, 2 g of the plant source (previously ground to a fine powder) were mixed in 20 g of ionic liquid (cholinium hexanoate) and incubated for 2 hours at 100 °C without stirring. The reaction was stopped by the addition of 160 mL of DMSO. The insoluble residue was separated by filtration using a nylon membrane filter (0.45 µm). Suberin materials were recovered from the filtrate through precipitation in an excess of water, whereas cutin materials were recovered from the insoluble fraction retained on the filter. The ensuing materials, *i.e.* purified plant polyesters, were washed with an excess of deionized water with the aid of centrifugation (Beckman J2-MC centrifuge, 11655 *g* at 4 °C for 30 minutes) and subsequently freeze-dried. The ensuing polyester powders were kept at room temperature until further analysis.

Synthesis of octan-4-yl octanoate. A mixture of 4-octanol (1 mL) with octanoic acid (0.5 mL) in the presence of a catalytic amount of H_2SO_4 and *p*-toluene-sulfonic acid monohydrate was prepared. The mixture was allowed to react at 60 ºC under continuous stirring, for one week. The end product was recovered by adding a saturated solution of NaCl to remove the 4-octanol in excess (washing step). Yellow oil (74.5 %); ^{1}H NMR (400 MHz, $CDCl_3$): 4.88 (quintet, J=5.4Hz, 1H); 2.28 (t, J=7.5Hz, 2H); 1.59 (m, 3H); 1.49 (m, 3H);

1.30 (m, 19H); 0.87 (m, 14H); ^{13}C NMR (100 MHz, $CDCl_3$): 73.76; 36.34; 34.68; 33.85; 31.87; 29.21; 27.64; 25.32; 22.76; 18.70; 14.14.

Testing the ability of an ionic liquid to hydrolyze ester bonds linking distinct monomers. Standard compounds carrying distinct types of esters bonds were tested, namely octan-4-yl octanoate, sucrose monolaurate, ethyl 4-hydroxy-3-methoxy-cinnamate and poly(1,4-butylene adipate). Either standard compound (~ 50 mg) was mixed with cholinium hexanoate (1:10, w/w) at 100 °C, with stirring, for 2, 6, or 24 h. To stop the poly(1,4-butylene adipate) reaction, an excess of water was added, then the reaction products were recovered by centrifugation (15557 *g*, 4 °C, 30 minutes), lyophilized and analyzed by NMR (*see below*). For the remaining standards, the reaction was stopped by placing the reaction mix on ice. The mixture was then acidified to pH 3/3.5 with 1 M HCl solution, spiked with a known concentration of hexadecane (internal standard), and extracted three times using a dichloromethane/water partition. The dried combined organic phases were derivatized with N,O-bis(trimethylsilyl)trifluorocetamide in pyridine (5:1) for 30 min at 90 °C. The TMS derivatives in the organic fractions were then analyzed by GC-MS (Agilent: 7820A GC and 5977B quadrupole MS; HP-5MS column) as follows: ramp temperature 80 °C, then 4 °C/min to 310 °C for 15 min. The MS scan mode, with source at 230 °C and electron impact ionization (EI^+, 70 eV) was used for all samples. Each sample was analyzed in technical duplicates. Data acquisition was carried out using MSD ChemStation (Agilent Technologies); compounds were identified based on the equipment's spectral library (Wiley-National Institute of Standards and Technology).

Microscopic analyses. Plant polyester samples were placed on an aluminum sample holder with double sided carbon tape and subsequently covered with a thin Au/Pd film on a Q150T ES Quorum Technologies sputter coater. SEM micrographs were acquired on a JEOL FEG-SEM model JSM-7001F.

Cryogenic grinding process. A RESTCH Cryomill equipped with a 25 mL grinding jar with 4 zirconium oxide grinding balls (10 mm) was used. All samples of purified cutin were cryogenically milled at -196 ºC (liquid nitrogen) using 200 milling cycles as follows: 3 min of pre-cooling followed by 9 milling cycles, each cycle consisting of 3 min of milling at 30 Hz followed by 0.5 min of intermediate cooling at 5 Hz.

Nuclear Magnetic Resonance (NMR). NMR spectra of polyesters (either plant polyesters or the synthetic polyester) were recorded using an Avance III 800 CRYO (Bruker Biospin, Rheinstetten, Germany), except for the HSQC spectra of purified suberin where an Avance II+ 800 was used instead (Bruker Biospin, Rheinstetten, Germany). All NMR spectra (^{1}H, ^{1}H-^{1}H COSY, ^{1}H-^{13}C HSQC, ^{1}H-^{13}C HMBC) were acquired in DMSO-d_6 using 5 mm diameter NMR tubes, at 60 °C as follows: 3 mg of cryomilled cutin, or 20 mg of suberin in 400 µL of DMSO-d_6. Quantitative ^{31}P NMR of suberin and cutin was also performed using an Avance III 500 (Bruker Biospin, Rheinstetten, Germany)[31]. NMR spectra of octan-4-yl octanoate were recorded using an Avance III 400 (Bruker Biospin, Rheinstetten, Germany). All NMR spectra (^{1}H, ^{1}H-^{1}H COSY, ^{1}H-^{13}C HSQC, ^{1}H-^{13}C HMBC) were acquired in $CDCl_3$ using 5 mm diameter NMR tubes, at 25 ºC. MestReNova, Version 11.04-18998 (Mestrelab Research, S.L.) was used to process the raw data acquired in the Bruker spectrometers.

Differential scanning calorimetry (DSC). The DSC analyses were carried out in a TA Instruments Q200 calorimeter connected to a cooling system and calibrated with different standards (indium, empty cap). The polyester sample weights ranged from 9 to 11 mg. A temperature interval from -80 ºC to 220 ºC has been studied and the used heating/cooling rate was 10 ºC·min^{-1}. In order to compare DSC and X-ray scattering results, enthalpy and melting points were measured using the first heating curve.

Wide-Angle X-ray Scattering (WAXS). WAXS data were collected using a laboratory SAXS/WAXS beamline (Xeuss 2.0, Xenocs, France) equipped with a liquid gallium MetalJet X-ray source (Excillum, Sweden) (wavelength λ = 1.34 Å), two sets of motorized scatterless slits for beam collimation and a Pilatus 100k two-dimensional (2D) pixel WAXS detector (Dectris, Switzerland). Loose cutin and suberin powder samples were enclosed between two flat kapton films and mounted on the beamline sample stage (the total sample thickness is about 1 mm). 2D WAXS patterns were recorded in a transmission mode over a q range of 1.3 $Å^{-1}$ to 3.5 $Å^{-1}$ [where $q = (4\pi\sin\theta)/\lambda = 2\pi/d$ is the length of the scattering vector, θ is one-half of the scattering angle and d is spacing in real space] using an exposure time of 1200 seconds. The WAXS data were reduced (calibrated, integrated and background-subtracted) using the Foxtrot software package supplied with the instrument.

Glycerol quantification by high-performance liquid chromatography (HPLC). The purified polyester samples were submitted to alkaline hydrolysis to release the hydrolysable monomeric constituents. Briefly, samples were treated with a solution of 0.5 M NaOH in methanol/water (1:1, v/v) at 95 ºC, for 4 hours. The mixture was cooled to room temperature, acidified to pH 3–3.5 with 1 M HCl, and extracted five times using a dichloromethane/water partition. The aqueous phases were analyzed by HPLC, using a Waters chromatographer Alliance 2695, connected to an LKB 2142 Differential Refractometer detector (Bromma, Sweden). Data acquisition was accomplished using the Empower 2 software (Waters). Chromatographic separation was undertaken at 60 ºC using an Aminex HPX-87H column (300 x 7.8 mm) with 9 µm particle size (Bio-Rad, Hercules, California). Elution was carried out isocratically, at a flow rate of 0.5 $mL \cdot min^{-1}$, with 0.005 N of H_2SO_4, and the sample volume injected was 20 µL. Glycerol quantification was carried out using an external calibration curve within the

quantification limits of 0.1 – 1 mM. The samples were analyzed in triplicate in three independent experiments.

Semi-quantitative analyses of crystalline cellulose by Dot-blot immunoassay. The cryogenically milled cutin samples (4 mg) were suspended in 1 mL of 3 M NaOH. The suspension was vortexed for 1 hour, sonicated twice for 1 min each using a microtip (Q-Sonica, USA) followed by 24 hours under magnetic stirring. Standard crystalline cellulose (Avicel*PH-101, Sigma France) was used for the quantification of crystalline cellulose content in cutin samples. Dilution of both samples and standards were spotted in triplicate onto PVDF blotting membrane (Amersham Hybond P 0.45µ, GE Healthcare, France) with 2 µL volume per dot. For the calibration curve, standards were spotted in decreasing concentrations: 0.8, 0.6, 0.4, 0.2, 0.1, 0.08, 0.06, 0.04, 0.02, 0.01 $mg \cdot mL^{-1}$. The membrane was immersed in a 3% bovine serum albumin (BSA, Sigma, France) solution in Phosphate Buffer Saline (PBS = 137 $mmol \cdot L^{-1}$ NaCl, 2.7 $mmol \cdot L^{-1}$ KCl, 10 $mmol \cdot L^{-1}$ Na_2HPO_4, and 1.8 $mmol \cdot L^{-1}$ KH_2PO_4, pH 7.4) for 30 min and was washed three times with PBS-Tween (PBS with 0.05 % Tween 20). The membrane was immersed in 1/1300 diluted CMB3a recombinant protein[44] in PBS-BSA-Tween (0.3 % BSA in PBS-Tween), followed by 120 min incubation and finally washed with PBS-tween as described above. The histidine tag of CMB3a was detected using an IgG anti-histidine mouse antibody (Sigma, France) diluted 1/2000 in PBS-BSA-Tween and revealed by a peroxidase assay (Sigma, France) with the chemiluminescent substrate (Western Bright™ Quantum chemiluminescence HRP substrate, ADVANSTA-K12042-D20, Menlo Park, USA), and a Fuji Las3000 (Fujifilm, France) camera for detection. Image analysis was conducted with ImageJ (imagej.nih.gov/ij/download.html). Each sample was analyzed in three independent assays; the obtained values reveal, semi-quantitatively, the abundance of crystalline cellulose in the different samples.

Quantitative analyses of total carbohydrate content. To evaluate the sugar moiety content of the plant polyesters purified using the ionic liquid-based processes, the samples were subjected to acid hydrolysis (1 M H_2SO_4 in methanol) for 4 h at 90 ºC. The hydrolysable sugars were recovered in the supernatant through centrifugation (18514 *g*, 4 °C, 20 min) and the pH was neutralized using 5 M NaOH in water. All samples were dried under a flux of nitrogen at room temperature. Quantification of carbohydrates in the dried hydrolysates was performed using the total carbohydrate assay kit from Sigma-Aldrich according to the manufacturer's instructions. The samples were analyzed in triplicates in two independent experiments.

Accession Numbers

Sequence data from this article can be found in the GenBank/EMBL data libraries under accession numbers Solyc11g006250 (CUS1) and Solyc09g014350 (GPATt6).

Acknowledgements

The authors are thankful to Pedro Lamosa and Maria C. Leitão (ITQB NOVA) for support with the NMR and chromatographic analyses, respectively, and to James Yates (ITQB NOVA) for proofreading the manuscript.

Funding

We acknowledge funding from the European Research Council through grant ERC 2014-CoG-647928, from the European Union's Horizon 2020 research and innovation program within the project 713475 – FLIPT – H2020-FETOPEN-2014-2015, and from Fundação para a Ciência e Tecnologia (FCT) by Project MOSTMICRO ITQB with refs UIDB/04612/2020 and UIDP/04612/2020. The NMR data were acquired at CERMAX, ITQB-NOVA, Oeiras, Portugal with equipment funded by FCT. C.J.S.M. is grateful to Aralab, Portugal, for the PhD contract 06/PlantsLife/2017. O.O.M. thanks EPSRC for a capital equipment grant to purchase the Xenocs/Excillum SAXS/WAXS laboratory beamline (EP/M028437/1).

References

1. Heredia-Guerrero, J. A. & Athanassiou, A. Editorial: Non-polysaccharide Plant Polymeric Materials. *Front. Mater.* **3**, (2016).
2. Siddique, R., Khatib, J. & Kaur, I. Use of recycled plastic in concrete: A review. *Waste Manag.* **28**, 1835–1852 (2008).
3. Galloway, T. S., Cole, M. & Lewis, C. Interactions of microplastic debris throughout the marine ecosystem. *Nature Ecology and Evolution* vol. 1 1–8 (2017).
4. Matthews, C., Moran, F. & Jaiswal, A. K. A review on European Union's strategy for plastics in a circular economy and its impact on food safety. *J. Clean. Prod.* **283**, 125263 (2021).
5. Philippe, G. *et al.* Cutin and suberin: assembly and origins of specialized lipidic cell wall scaffolds. *Current Opinion in Plant Biology* vol. 55 11–20 (2020).
6. Vishwanath, S. J., Delude, C., Domergue, F. & Rowland, O. Suberin: biosynthesis, regulation, and polymer assembly of a protective extracellular barrier. *Plant Cell Rep.* **34**, 573–586 (2015).
7. Martin, L. B. B. & Rose, J. K. C. There's more than one way to skin a fruit: formation and functions of fruit cuticles. *J. Exp. Bot.* **65**, 4639–4651 (2014).
8. Schreiber, L. *et al.* Transport barriers made of cutin, suberin and associated waxes. *Trends Plant Sci.* **15**, 546–53 (2010).
9. Nawrath, C. The Biopolymers Cutin and Suberin. *Arab. B.* **1**, e0021 (2002).
10. Sousa, A. F., Gandini, A., Silvestre, A. J. D. & Pascoal Neto, C. Synthesis and Characterization of Novel Biopolyesters from Suberin and Model Comonomers. *ChemSusChem* **1**, 1020–1025 (2008).
11. Chatterjee, S. *et al.* Isolation and Biophysical Study of Fruit Cuticles. *J. Vis. Exp.* e3529 (2012) doi:10.3791/3529.
12. Graça, J. & Lamosa, P. Linear and Branched Poly(ω-hydroxyacid) Esters in Plant Cutins. *J. Agric. Food Chem.* **58**, 9666–9674 (2010).

13. Ferreira, R. *et al.* Unveiling the dual role of the cholinium hexanoate ionic liquid as solvent and catalyst in suberin depolymerisation. *RSC Adv.* **4**, 2993–3002 (2014).
14. Correia, V. G. *et al.* The molecular structure and multifunctionality of the cryptic plant polymer suberin. *Mater. Today Bio* **5**, 100039 (2020).
15. Rodrigues, R. *et al.* Sustainable plant polyesters as substrates for optical gas sensors. *Mater. Today Bio* **8**, 100083 (2020).
16. Moreira, C. J. S. *et al.* An ionic liquid extraction that preserves the molecular structure of cutin shown by nuclear magnetic resonance. *Plant Physiol.* **184**, (2020).
17. Benítez, J. J. *et al.* Valorization of tomato processing by-products: Fatty acid extraction and production of bio-based materials. *Materials (Basel).* **11**, 2211 (2018).
18. Marc, M. *et al.* Bioinspired co-polyesters of hydroxy-fatty acids extracted from tomato peel agro-wastes and glycerol with tunable mechanical, thermal and barrier properties. *Ind. Crops Prod.* **170**, 113718 (2021).
19. Bedoić, R., Ćosić, B. & Duić, N. Technical potential and geographic distribution of agricultural residues, co-products and by-products in the European Union. *Sci. Total Environ.* **686**, 568–579 (2019).
20. Mattinen, M. L. *et al.* Structure of the polyphenolic component of suberin isolated from potato (Solanum tuberosum war. Nikola). *J. Agric. Food Chem.* **57**, 9747–9753 (2009).
21. Liang, S. & McDonald, A. G. Chemical and thermal characterization of potato peel waste and its fermentation residue as potential resources for biofuel and bioproducts production. *J. Agric. Food Chem.* **62**, 8421–8429 (2014).
22. Johnson, E. J., Dorot, O., Liu, J., Chefetz, B. & Xing, B. Spectroscopic Characterization of Aliphatic Moieties in Four Plant Cuticles. *Commun. Soil Sci. Plant Anal.* **38**, 2461–2478 (2007).

23. CHEN, B. liang & LI, Y. gui. Sorption of 1-naphthol by plant cuticular fractions. *J. Environ. Sci.* **19**, 1214–1220 (2007).
24. Hartman, B. E. & Hatcher, P. G. Hydrothermal liquefaction of isolated cuticle of Agave americana and Capsicum annuum: Chemical characterization of petroleum-like products. *Fuel* **156**, 225–233 (2015).
25. Xin, A. & Fry, S. C. Cutin:xyloglucan transacylase (CXT) activity covalently links cutin to a plant cell-wall polysaccharide. *J. Plant Physiol.* **262**, 153446 (2021).
26. Philippe, G. *et al.* Assembly of tomato fruit cuticles: a cross-talk between the cutin polyester and cell wall polysaccharides. *New Phytol.* **226**, 809–822 (2020).
27. Deshmukh, A. P., Simpson, A. J. & Hatcher, P. G. Evidence for cross-linking in tomato cutin using HR-MAS NMR spectroscopy. *Phytochemistry* **64**, 1163–1170 (2003).
28. Philippe, G. *et al.* Ester cross-link profiling of the cutin polymer of wild-type and cutin synthase tomato mutants highlights different mechanisms of polymerization. *Plant Physiol.* **170**, 807–820 (2016).
29. Fich, E. A., Segerson, N. A. & Rose, J. K. C. The Plant Polyester Cutin: Biosynthesis, Structure, and Biological Roles. *Annu. Rev. Plant Biol.* **67**, 207–233 (2016).
30. Graça, J. & Santos, S. Glycerol-derived ester oligomers from cork suberin. *Chem. Phys. Lipids* **144**, 96–107 (2006).
31. Meng, X. *et al.* Determination of hydroxyl groups in biorefinery resources via quantitative 31P NMR spectroscopy. *Nat. Protoc. 2019 149* **14**, 2627–2647 (2019).
32. Heredia-Guerrero, J. A., Domínguez, E., Luna, M., Benítez, J. J. & Heredia, A. Structural characterization of polyhydroxy fatty acid nanoparticles related to plant lipid biopolyesters. *Chem. Phys. Lipids* **163**, 329–333 (2010).
33. Small, D. M. Lateral chain packing in lipids and membranes. *J. Lipid Res.* **25**, 1490–1500 (1984).

34. Mykhaylyk, O. O., Smith, K. W., Martin, C. M. & Ryan, A. J. Structural models of metastable phases occurring during the crystallization process of saturated/unsaturated triacylglycerols. in *Journal of Applied Crystallography* vol. 40 s297–s302 (2007).
35. Southern, J. H., Weeks, N., Porter, R. S. & Crystal, R. G. Unique polyethylene morphologies produced under extrusion conditions. *Macromol. Chem. Phys.* **162**, 19–30 (1972).
36. Bunn, C. W. The Crystal Structure of Ethylene. *Trans. Faraday Soc.* **40**, 23–25 (1944).
37. Rongpipi, S., Ye, D., Gomez, E. D. & Gomez, E. W. Progress and opportunities in the characterization of cellulose – an important regulator of cell wall growth and mechanics. *Frontiers in Plant Science* vol. 9 1894 (2019).
38. Petit, J. *et al.* The glycerol-3-phosphate acyltransferase GPAT6 from tomato plays a central role in fruit cutin biosynthesis. *Plant Physiol.* **171**, 894–913 (2016).
39. Petit, J., Bres, C., Mauxion, J. P., Bakan, B. & Rothan, C. Breeding for cuticle-associated traits in crop species: traits, targets, and strategies. *Journal of Experimental Botany* vol. 68 5369–5387 (2017).
40. Girard, A.-L. *et al.* Tomato GDSL1 Is Required for Cutin Deposition in the Fruit Cuticle. *Plant Cell* **24**, 3119–3134 (2012).
41. Yeats, T. H. *et al.* The identification of cutin synthase: Formation of the plant polyester cutin. *Nat. Chem. Biol.* **8**, 609–611 (2012).
42. Just, D. *et al.* Micro-Tom mutants for functional analysis of target genes and discovery of new alleles in tomato. *Plant Biotechnology* vol. 30 225–231 (2013).
43. Petkovic, M. *et al.* Novel biocompatible cholinium-based ionic liquids - Toxicity and biodegradability. *Green Chem.* **12**, 643–649 (2010).
44. Blake, A. W. *et al.* Understanding the Biological Rationale for the Diversity of Cellulose-directed Carbohydrate-binding Modules in Prokaryotic Enzymes. *J. Biol. Chem.* **281**, 29321–29329 (2006).

ANNEX

This annex contains the Supplementary Material published along the main body of the research paper which composes Chapter III. This intends to allow better and easier understanding of the methodologies and analyses performed.

Supplementary Data

The following supplementary materials are available.

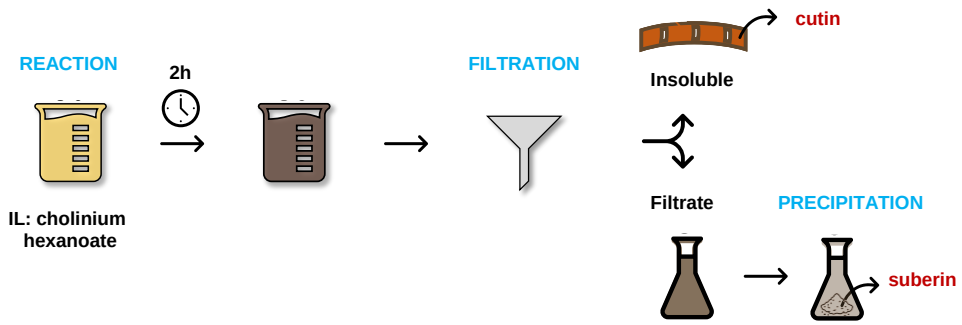

Figure S1 – Schematics of the extraction process

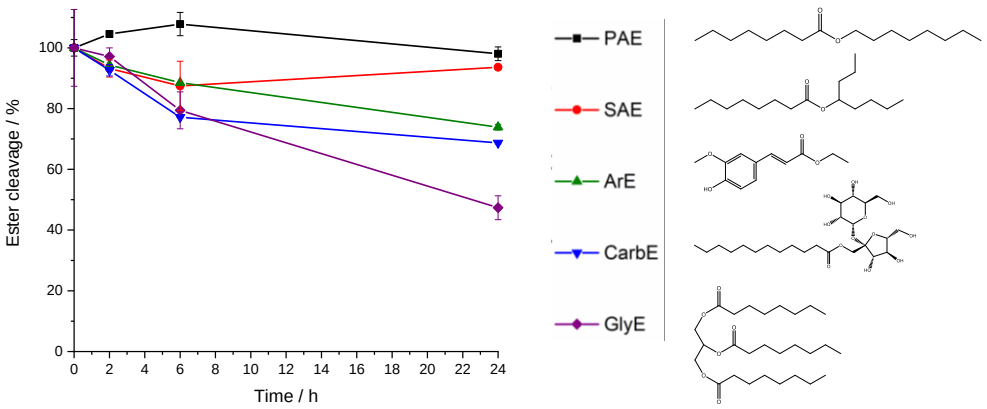

Figure S2 –The capacity of the cholinium hexanoate to mediate the hydrolysis of distinct ester-type bonds, up to 24h at 100 ºC with stirring, was analyzed by GC-MS. Standard compounds representative of five ester-types were used: a primary aliphatic ester (PAE, octyl octanoate), a secondary aliphatic ester (SAE, octan-4-yl octanoate), an aromatic ester (ArE, ethyl 4-hydroxy-3-methoxy-cinnamate), a carbohydrate ester (CarbE, sucrose monolaurate) and a glycerol ester (GlyE, glyceryl trioctanoate). PAE and GlyE kinetic curves were adapted from a dataset published before by us[1].

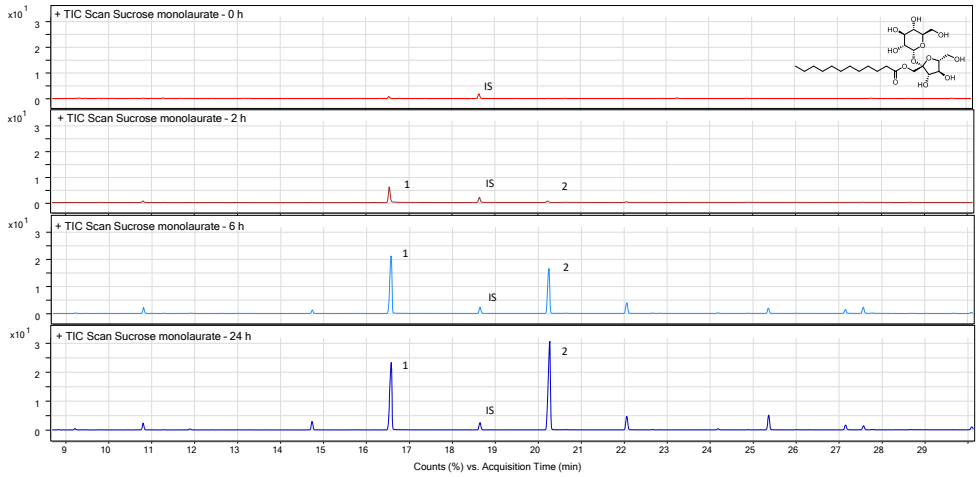

Figure S3 - Representative GC-MS chromatograms of the model compound sucrose monolaurate after reaction with cholinium hexanoate at increasing time points. Over time the peak assigned to dodecanoic acid - hydrolysis product of sucrose monolaurate, increased. IS – internal standard (hexadecane); 1 – dodecanoic acid, methyl ester; 2 – dodecanoic acid, trimethylsilyl ester.

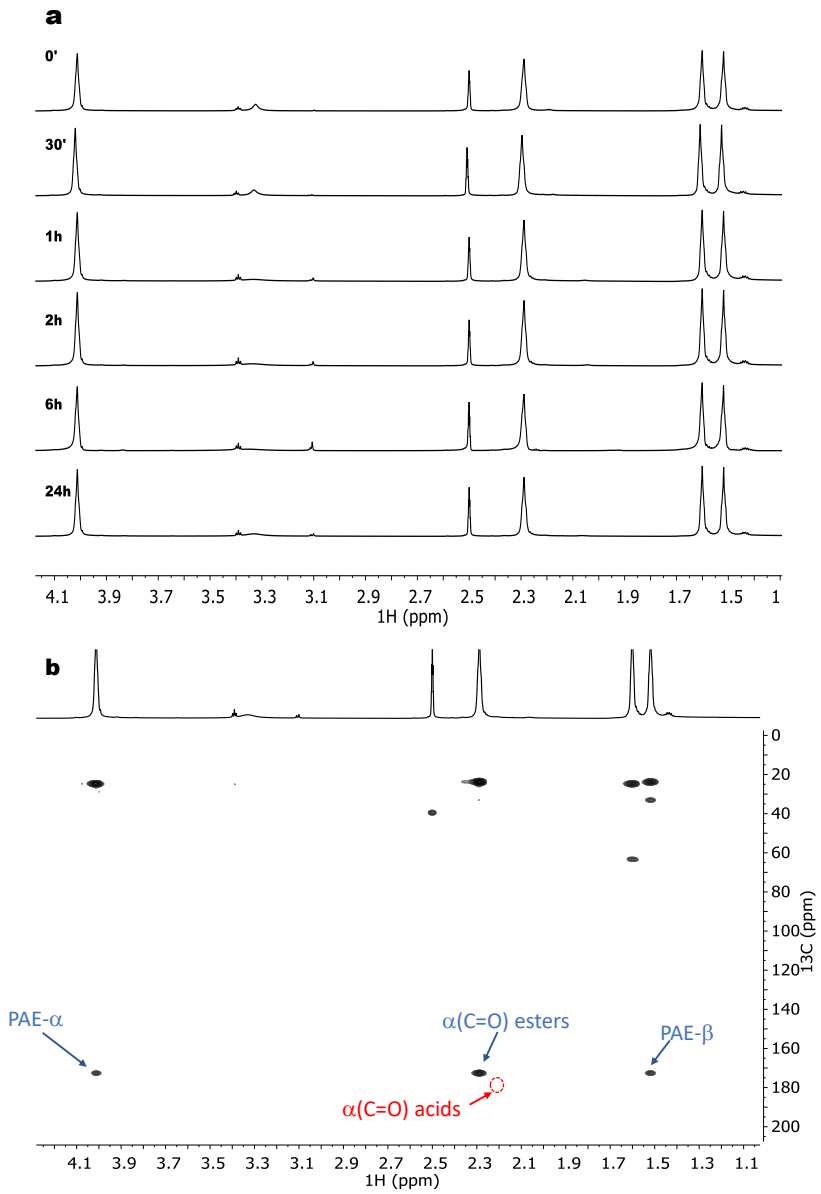

Figure S4 - The capacity of the cholinium hexanoate to mediate the hydrolysis of primary aliphatic esters bonds in a synthetic polymer, poly(1,4-butyl adipate), up to 24 h at 100 ºC with stirring, was analyzed by NMR: a) ^{1}H NMR in DMSO-d_6 in different time points, b) representative of ^{1}H-^{13}C HMBC NMR after 24 h of reaction. The dashed circle marks the region of the spectrum where the signal assigned to the acid resulting from the hydrolysis would be noticed.

Table S1 – Elemental analysis of tomato cutin, pepper cutin, cork suberin and potato suberin. Relative percentage of Nitrogen (N), Carbon (C), Hydrogen (H) and Oxygen (O) in the different samples

	Sample	Tomato Cutin	Pepper Cutin	Cork Suberin	Potato suberin
Elemental Analysis	Nitrogen (N)[a] (%)	< 1	< 1	1.60 ± 0.08	2.33 ± 0.07
	Carbon (C) (%)	63.98 ± 0.16	67.63 ± 0.02	64.07 ± 0.02	60.65 ± 0.11
	Hydrogen (H) (%)	9.08 ± 0.12	9.79 ± 0.03	8.86 ± 0.06	8.54 ± 0.07
	Oxygen (O) (%)	26.96 ± 0.27	22.60 ± 0.04	26.08 ± 0.04	28.50 ± 0.11

a) corresponding peak areas were outside the calibration curve, the suberin values may be subject to error yet shown since the monomer 4-(2-aminoethyl)phenol contains N. Deviation from theoretical percentage (should be < 0.4 %);

Table S2 – Total carbohydrate quantification of cutin and suberin samples.

Samples	ng (carbohydrate)/mg (plant polyester)
Tomato cutin	0.489 ± 0.127
Pepper cutin	0.124 ± 0.016
Cork suberin	0.21 ± 0.033
Potato suberin	1.16 ± 0.31
Micro-Tom *wt*	0.387 ± 0.072
Micro-Tom *cus1*	1.022 ± 0.496
Micro-Tom *gpat6*	0.541 ± 0.175

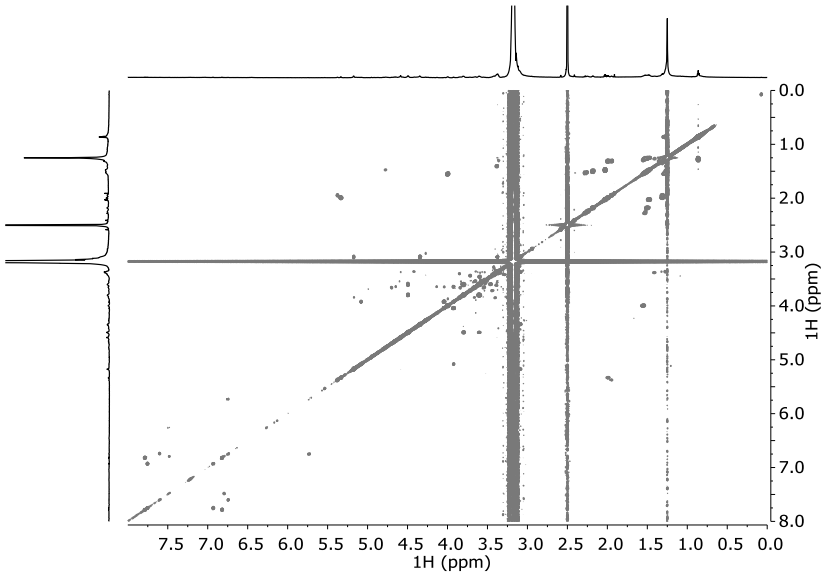

Figure S5 – 2D-^{1}H-^{1}H COSY-NMR spectrum (COrrelated SpectroscopY) of tomato cutin extracted using cholinium hexanoate (2 h) in DMSO-d_6 at 60 ºC.

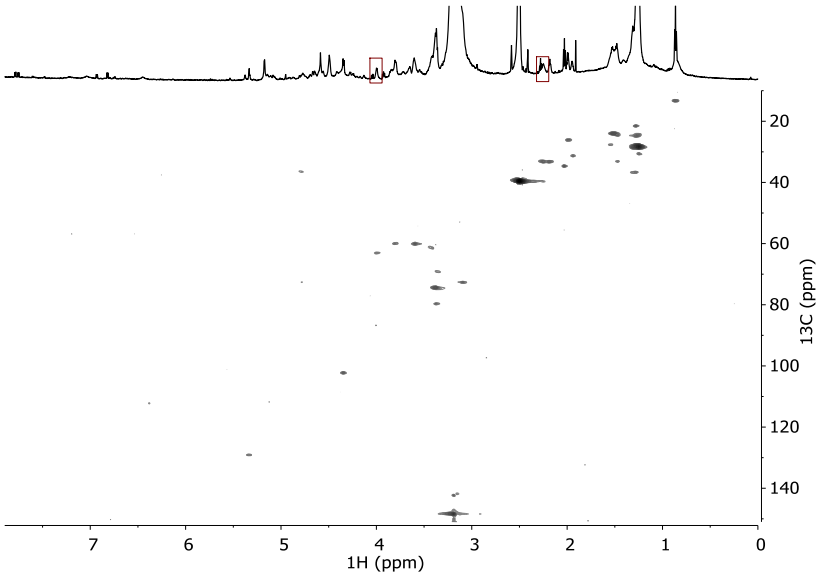

Figure S6 – 2D-^{1}H-^{13}C HSQC-NMR spectrum (Heteronuclear Single Quantum Coherence) of tomato cutin extracted using cholinium hexanoate (2 h) in DMSO-d_6 at 60 ºC. The red rectangles mark signals used for the integration of specific functional groups, all of which showed no overlap of resonances with other chemical groups as shown by the bi-dimensional NMR correlations done.

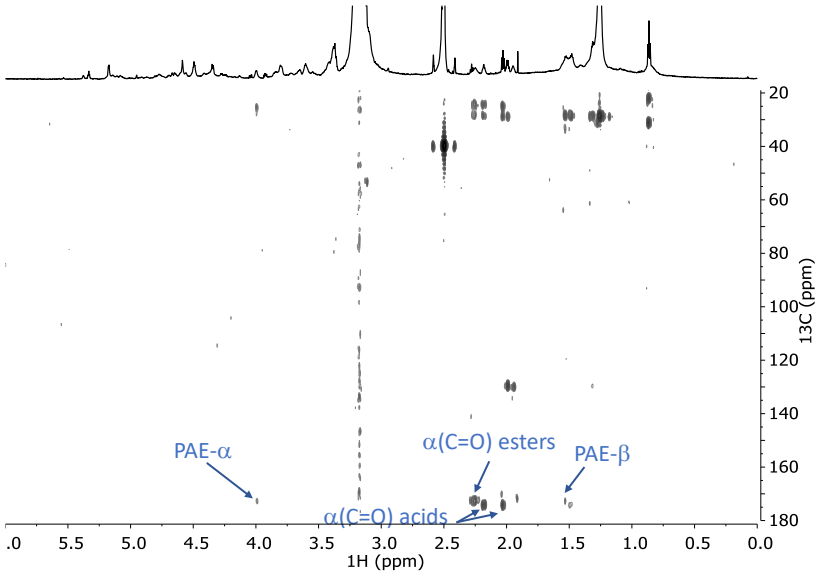

Figure S7 – 2D-^{1}H-^{13}C HMBC-NMR spectrum (Heteronuclear Multiple Bond Correlation) of tomato cutin extracted using cholinium hexanoate (2 h) in DMSO- d_6 at 60 ºC.

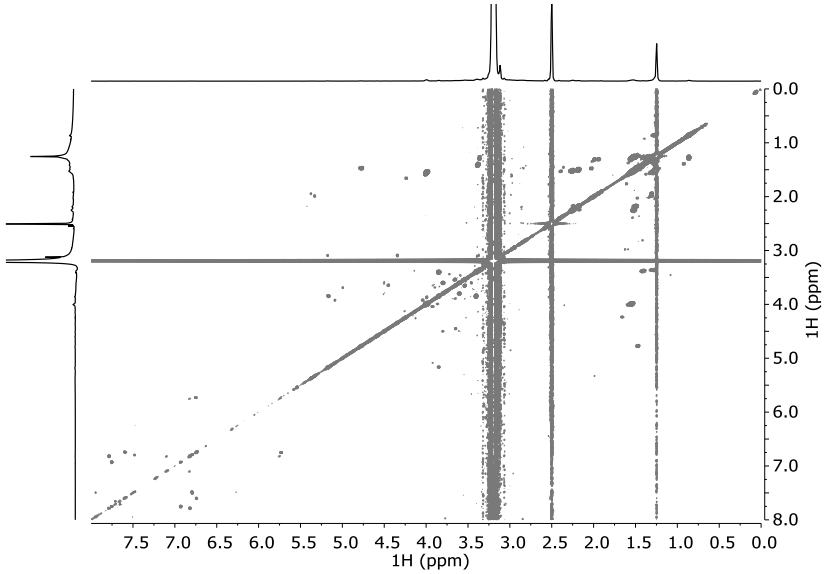

Figure S8 – 2D-^{1}H-^{1}H COSY-NMR spectrum (COrrelated SpectroscopY) of pepper cutin isolated with cholinium hexanoate (2 h) in DMSO- d_6 at 60 ºC.

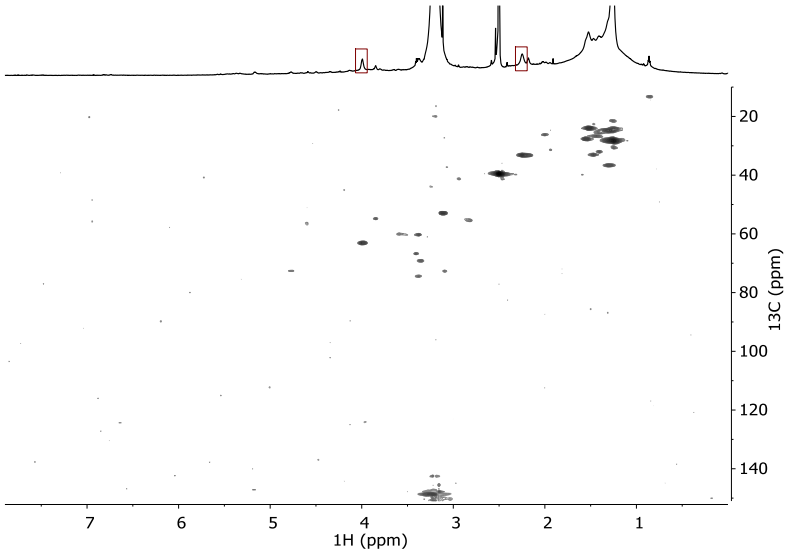

Figure S9 – 2D-^{1}H-^{13}C HSQC-NMR spectrum (Heteronuclear Single Quantum Coherence) of pepper cutin isolated with cholinium hexanoate (2 h) in DMSO- d_6 at 60 ºC. The red rectangles mark signals used for the integration of specific functional groups, all of which showed no overlap of resonances with other chemical groups as shown by the bi-dimensional NMR correlations done.

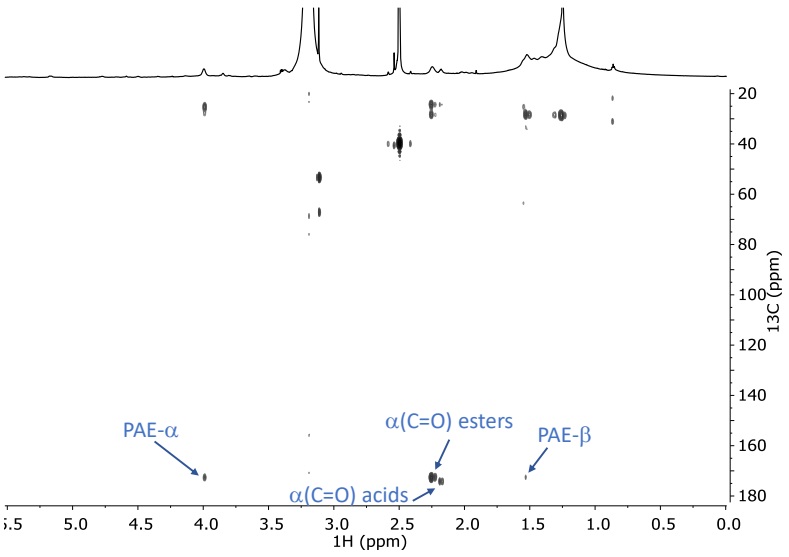

Figure S10 – 2D-^{1}H-^{13}C HMBC-NMR spectrum (Heteronuclear Multiple Bond Correlation) of pepper cutin isolated with cholinium hexanoate (2 h) in DMSO- d_6 at 60 ºC.

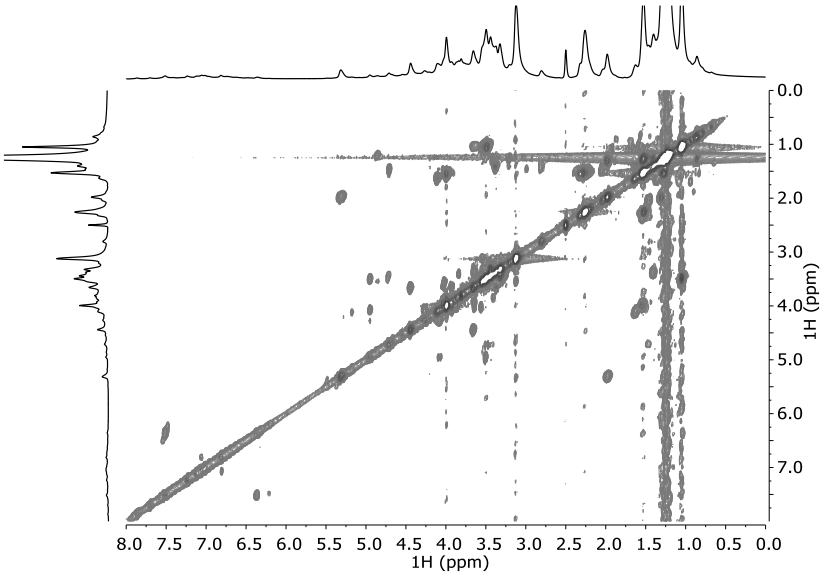

Figure S11 – 2D-^{1}H-^{1}H COSY-NMR spectrum (COrrelated SpectroscopY) of cork suberin in DMSO-d_6 at 60 ºC.

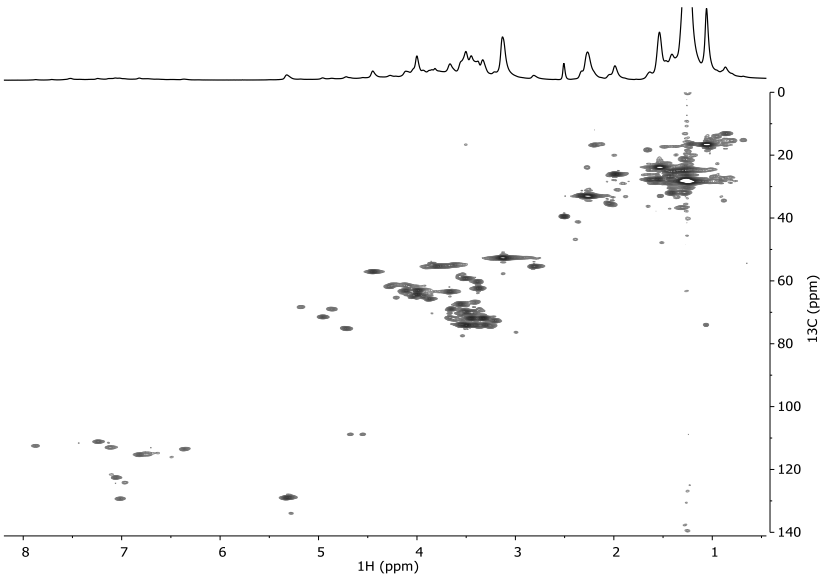

Figure S12 – 2D-^{1}H-^{13}C HSQC-NMR spectrum (Heteronuclear Single Quantum Coherence) of cork suberin in DMSO- d_6 at 60 ºC.

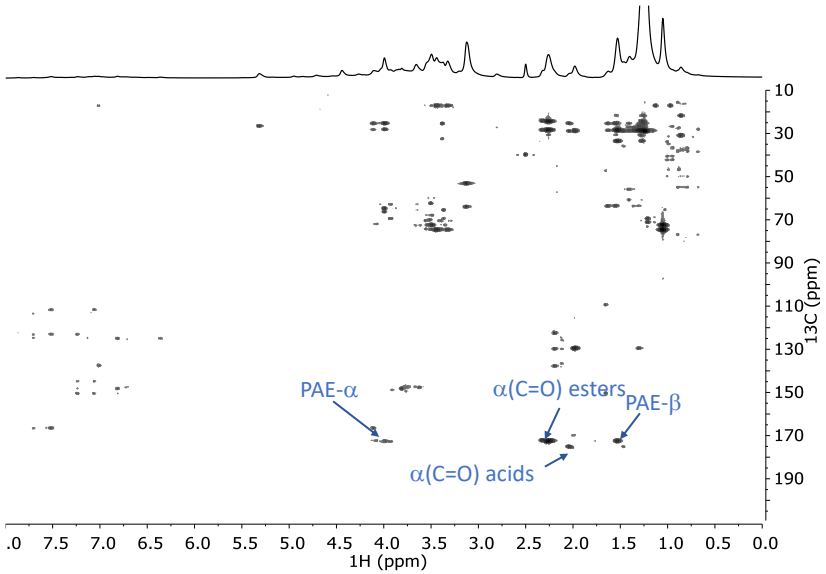

Figure S13 – 2D-^{1}H-^{13}C HMBC-NMR spectrum (Heteronuclear Multiple Bond Correlation) of cork suberin isolated with cholinium hexanoate (2 h) in DMSO- d_6 at 60 ºC.

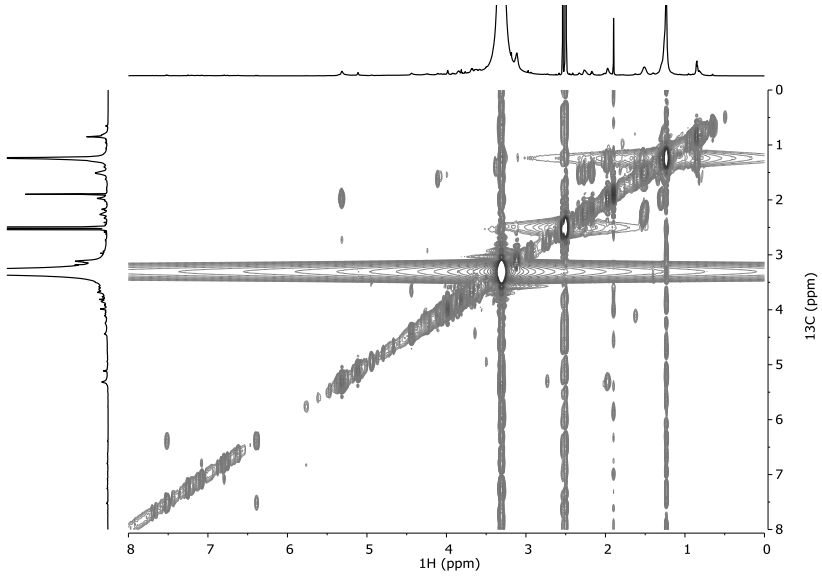

Figure S14 – 2D-^{1}H-^{1}H COSY-NMR spectrum (COrrelated SpectroscopY) of potato suberin in DMSO-d_6 at 60 ºC.

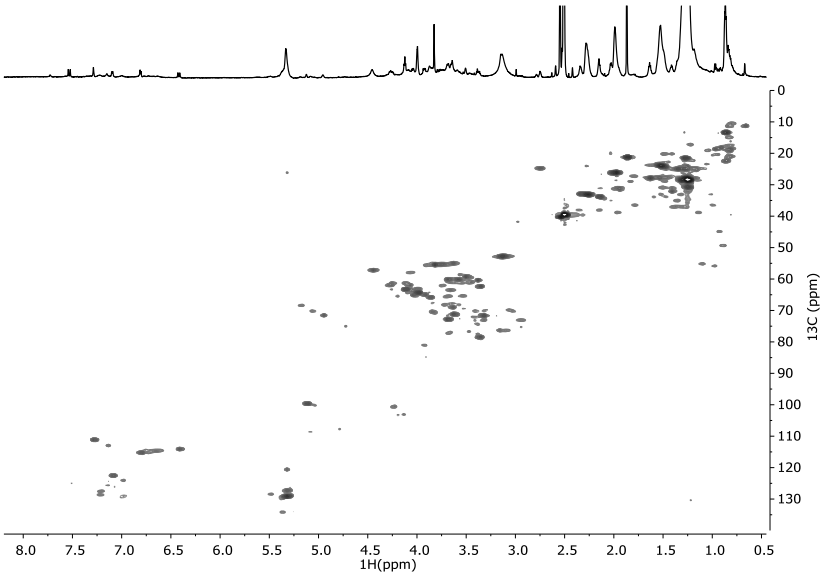

Figure S15 – 2D-^{1}H-^{13}C HSQC-NMR spectrum (Heteronuclear Single Quantum Coherence) of potato suberin in DMSO- d_6 at 60 ºC.

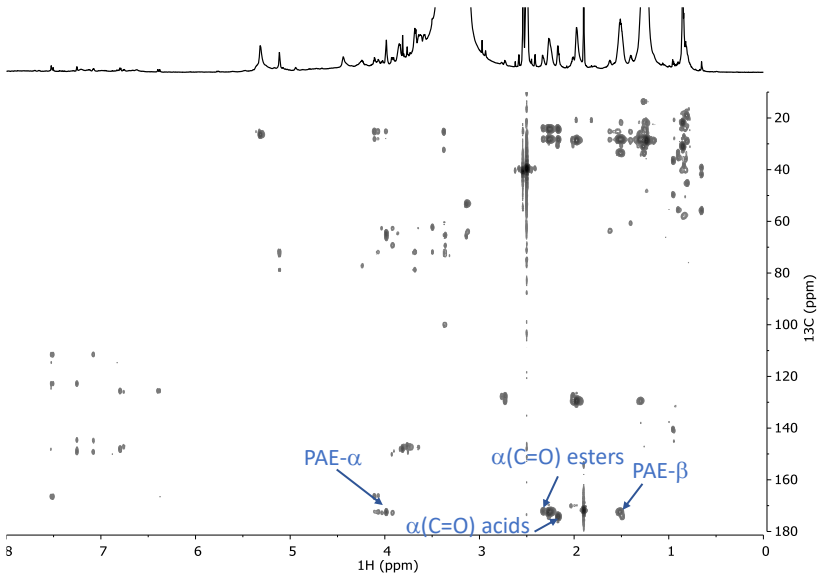

Figure S16 – 2D-^{1}H-^{13}C HMBC-NMR spectrum (Heteronuclear Multiple Bond Correlation) of potato suberin isolated with cholinium hexanoate (2 h) in DMSO- d_6 at 60 ºC.

Table S3 – Monomeric composition of cutin purified from tomato or pepper using cholinium hexanoate (2 h), identified by NMR. Chemical structures and ^{1}H and ^{13}C chemical shifts (ppm) of the cutin monomers. Signals not resolved in the NMR spectra due to overlapping signals or not yet assigned are not shown in this table. Most of the signals have been assigned before by us[1].

CHEMICAL STRUCTURE	CHEMICAL SHIFTS (PPM)
FATTY ACIDS (N= 1-2)	
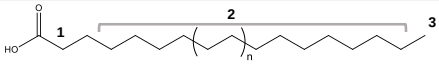	^{1}H NMR (800.33 MHz, DMSO-d_6) δ 0.86 (m, 3H, H-3), 1.25 (m, 2H, H-2), 2.02 (m, 2H, H-1). ^{13}C NMR (201.42 MHz, DMSO-*d*6) δ 13.39 (C-3), 28.34 (C-2), 34.67 (C-1).
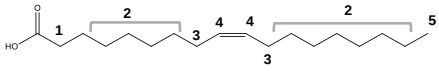	^{1}H NMR (800.33 MHz, DMSO-*d*6) δ 0.86 (m, 3H, H-5), 1.25 (m, 2H, H-2), 1.99 (m, 2H, H-3), 2.02 (m, 2H, H-1), 5.34 (m, 2H, H-4). ^{13}C NMR (201.42 MHz, DMSO-*d*6) δ 13.39 (C-5), 26.13 (C-3), 28.34 (C-2), 34.67 (C-1), 129.07 (C-4).
DICARBOXYLIC ACIDS	
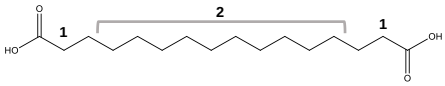	^{1}H NMR (800.33 MHz, DMSO-*d*6) δ 1.25 (m, 2H, H-2), 2.02 (m, 2H, H-1). ^{13}C NMR (201.42 MHz, DMSO-*d*6) δ 28.34 (C-2), 34.67 (C-1).
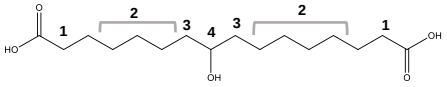	^{1}H NMR (800.33 MHz, DMSO-*d*6) δ 1.25 (m, 2H, H-2), 1.30 (m, 2H, H-3), 2.02 (m, 2H, H-1), 3.38 (m, 2H, H-4). ^{13}C NMR (201.42 MHz, DMSO-*d*6) δ 28.34 (C-2), 34.67 (C-1), 36.64 (C-3), 74.31 (C-4).
Ω-HYDROXYACIDS	
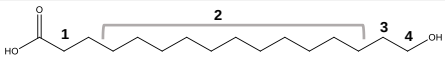	^{1}H NMR (800.33 MHz, DMSO-*d*6) δ 1.25 (m, 2H, H-2), 1.41 (m, 2H, H-3), 2.02 (m, 2H, H-1), 3.41 (m, 2H, H-4). ^{13}C NMR (201.42 MHz, DMSO-*d*6) δ 28.34 (C-2), 32.03 (C-3), 34.67 (C-1), 67.64 (C-4).

Table S4 – Monomeric composition of suberin extracted from cork or potato using cholinium hexanoate (2 h), identified by NMR. Chemical structures and ^{1}H and ^{13}C chemical shifts (ppm) of the cutin monomers. Signals not resolved in the NMR spectra due to overlapping signals or not yet assigned are not shown in this table. Most of the signals have been assigned before by us[2].

CHEMICAL STRUCTURE	CHEMICAL SHIFTS (PPM)
C18 MID-CHAIN MODIFIED	
Ω-HYDROXYACIDS	
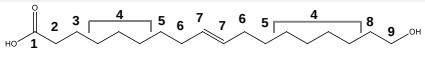	^{1}H NMR (800.33 MHz, DMSO-*d*6) δ 1.24 (m, 2H, H-4), 1.41 (m, 2H, H-5), 1.41 (m, 2H, H-8), 1.46 (m, 2H, H-3), 1.98 (m, 2H, H-6) 2.03 (m, 2H, H-2), 3.39 (m, 2H, H-9), 5.31 (m, 2H, H-7) ^{13}C NMR (201.42 MHz, DMSO-*d*6) δ 26.13 (C-3), 27.07 (C-6), 29.86 (C-5), 29.35 (C-4), 32.95 (C-8), 36.40 (C-2), 61.32 (C-9), 129.98 (C-7), 172.20 (C-1)
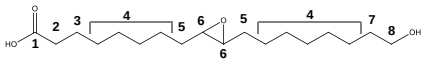	^{1}H NMR (800.33 MHz, DMSO-*d*6) δ 1.24 (m, 2H, H-4), 1.41 (m, 2H, H-7), 1.43 (m, 2H, H-5), 1.46 (m, 2H, H-3), 2.03 (m, 2H, H-2), 2.80 (m, 2H, H-6), 3.39 (m, 2H, H-8) ^{13}C NMR (201.42 MHz, DMSO-*d*6) δ 26.13 (C-3), 29.35 (C-4), 27.83 (C-5), 32.95 (C-7), 36.40 (C-2), 56.38 (C-6), 61.32 (C-8), 172.20 (C-1)
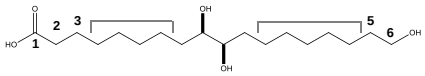	^{1}H NMR (800.33 MHz, DMSO-*d*6) δ 1.24 (m, 2H, H-4), 1.41 (m, 2H, H-5), 1.46 (m, 2H, H-3), 2.03 (m, 2H, H-2), 3.39 (m, 2H, H-6) ^{13}C NMR (201.42 MHz, DMSO-*d*6) δ 26.13 (C-3), 29.35 (C-4), 32.95 (C-5), 36.40 (C-2), 61.32 (C-6), 172.20 (C-1)

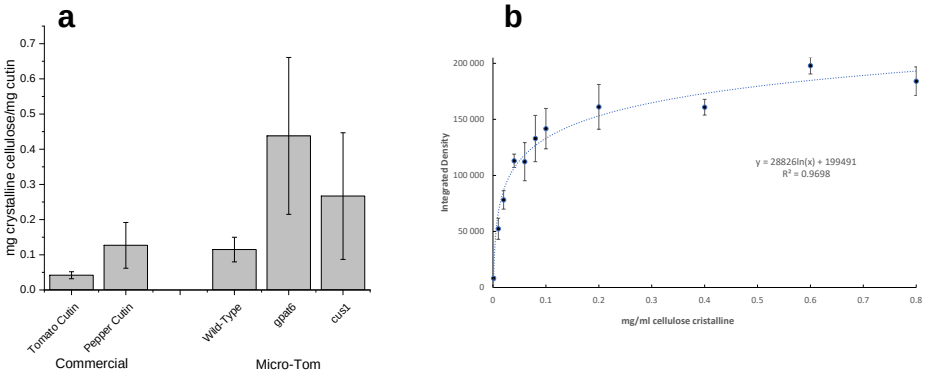

Figure S17 – Quantification of crystalline cellulose concentration with ImageJ software of cutin from tomato, pepper and Micro-tom (wild type and mutants) purified with cholinium hexanoate. The result was expressed in mg of crystalline cellulose per mg of cutin in sample (a). The error bars represent the standard deviations of three independent measurements. Standard calibration curve for quantitative detection of crystalline cellulose based on direct dot-blot immunoassay using Image J software (b). The error bars represent the standard deviations of three independent measurements.

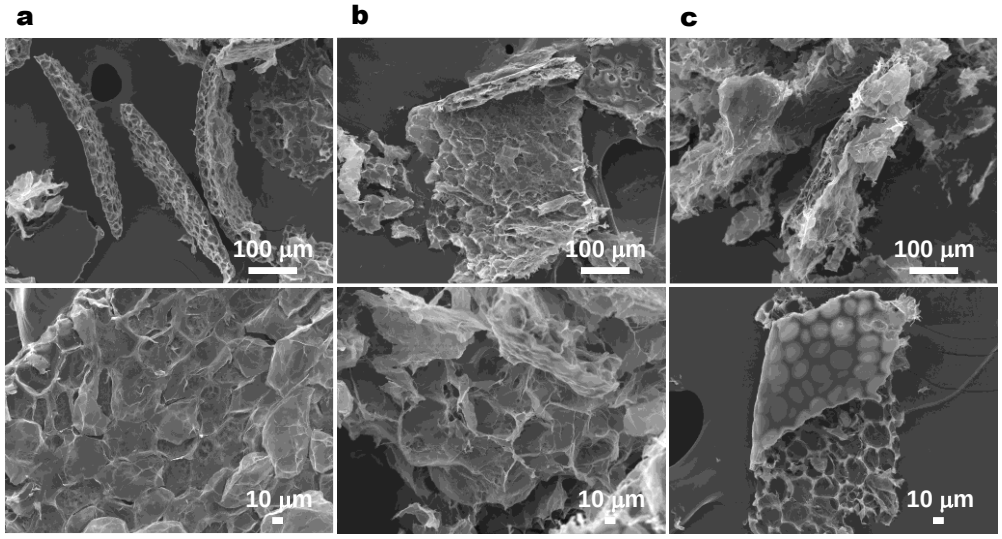

Figure S18 - SEM micrographs of cutin samples extracted from Micro-Tom tomatoes, wild type (a) and the mutants *cus1* (b) and *gpat6* (c), using cholinium hexanoate extraction for 2h.

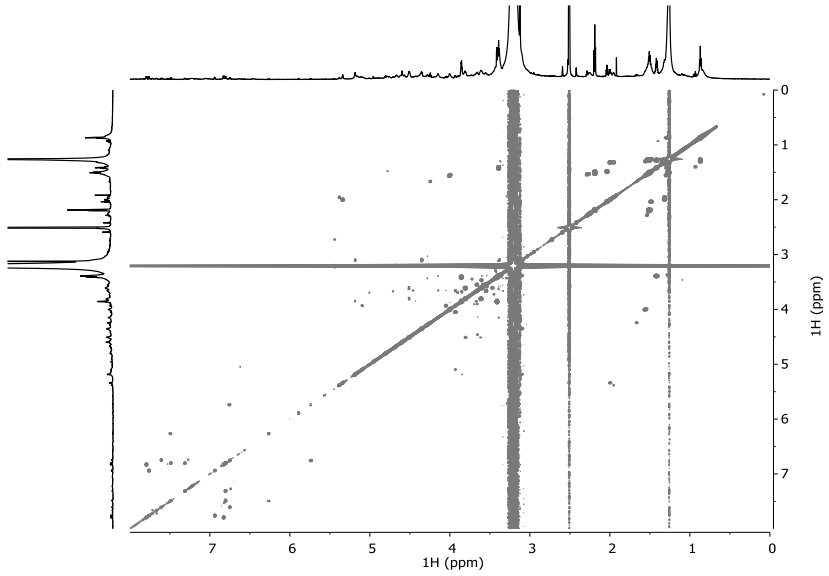

Figure S19 – 2D-^{1}H-^{1}H COSY-NMR spectrum (COrrelated SpectroscopY) of Micro-Tom cutin isolated with cholinium hexanoate (2 h) in DMSO-d_6 at 60 ºC.

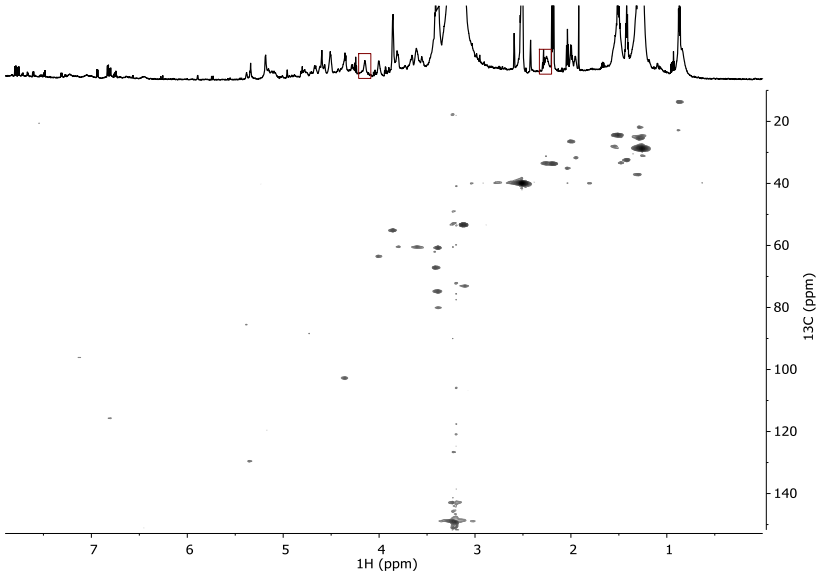

Figure S20 – 2D-^{1}H-^{13}C HSQC-NMR spectrum (Heteronuclear Single Quantum Coherence) of Micro-Tom cutin isolated with cholinium hexanoate (2 h) in DMSO-d_6 at 60 ºC. The red rectangles mark signals used for the integration of specific functional groups, all of which showed no overlap of resonances with other chemical groups as shown by the bi-dimensional NMR correlations done.

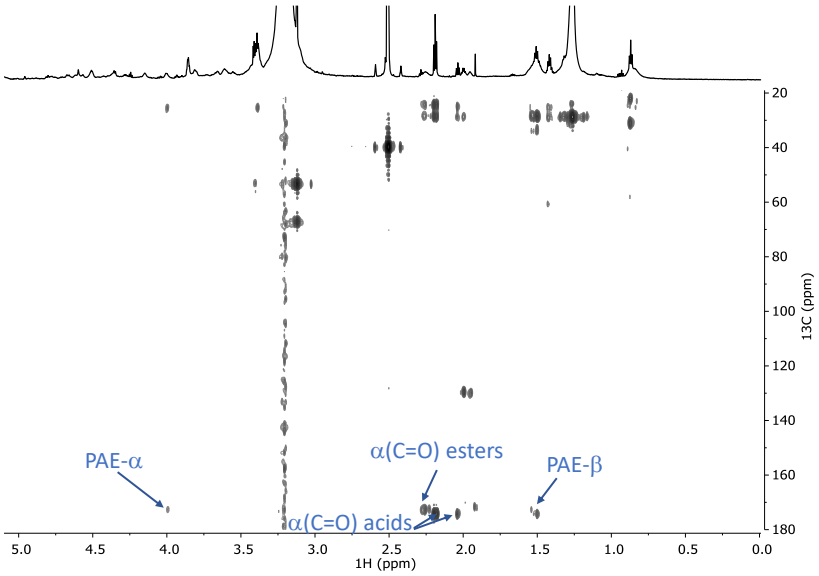

Figure S21 – 2D-^{1}H-^{13}C HMBC-NMR spectrum (Heteronuclear Multiple Bond Correlation) of Micro-Tom cutin isolated with cholinium hexanoate (2 h) in DMSO-d_6 at 60 ºC.

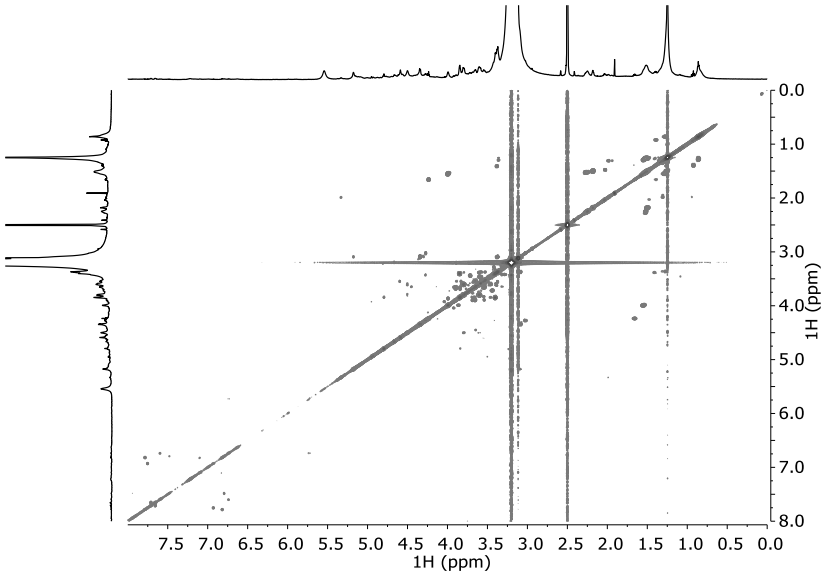

Figure S22 – 2D-^{1}H-^{1}H COSY-NMR spectrum (COrrelated SpectroscopY) of Micro-Tom cutin isolated with cholinium hexanoate (2 h) from the *cus1* mutant in DMSO- d_6 at 60 ºC.

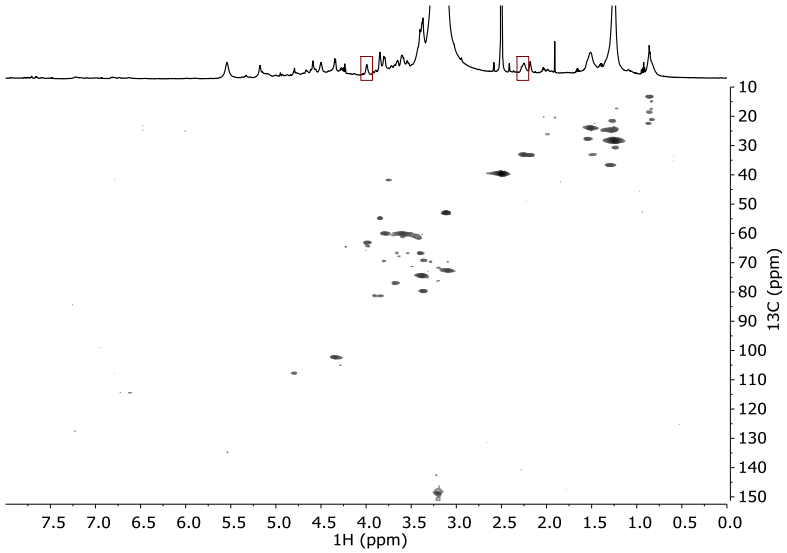

Figure S23 – 2D-^{1}H-^{13}C HSQC-NMR spectrum (Heteronuclear Single Quantum Coherence) of Micro-Tom cutin isolated with cholinium hexanoate (2 h) from the *cus1* mutant in DMSO- d_6 at 60 ºC. The red rectangles mark signals used for the integration of specific functional groups, all of which showed no overlap of resonances with other chemical groups as shown by the bi-dimensional NMR correlations done.

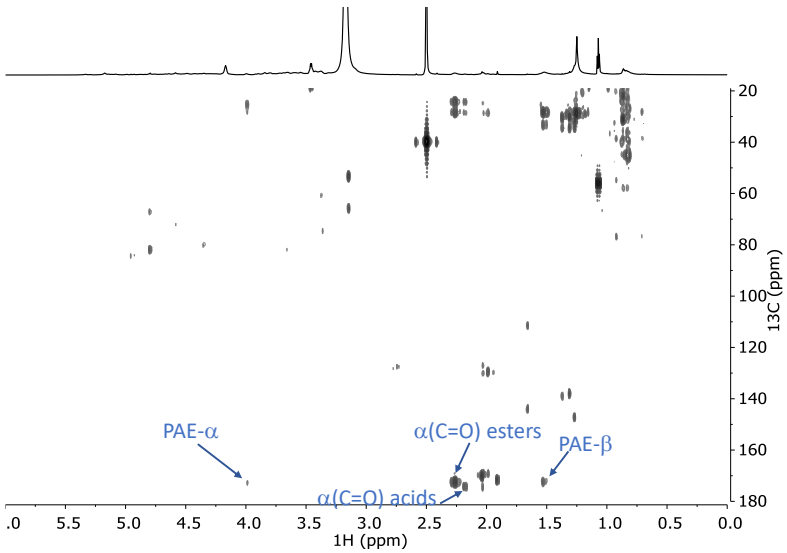

Figure S24 – 2D-^{1}H-^{13}C HMBC-NMR spectrum (Heteronuclear Multiple Bond Correlation) of Micro-Tom cutin isolated with cholinium hexanoate (2 h) from the *cus1* mutant in DMSO- d_6 at 60 ºC.

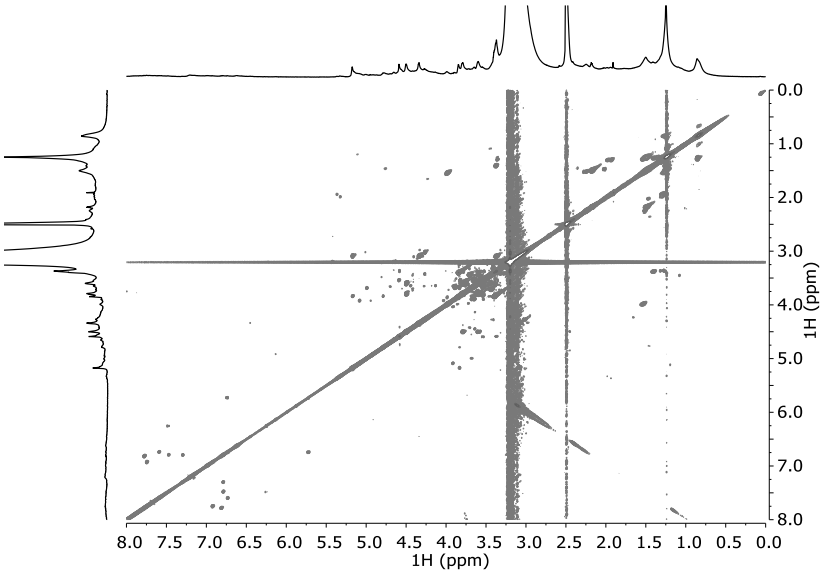

Figure S25 – 2D-^{1}H-^{1}H COSY-NMR spectrum (COrrelated SpectroscopY) of Micro-Tom cutin isolated with cholinium hexanoate (2 h) from the *gpat6* mutant in DMSO-d_6 at 60 ºC.

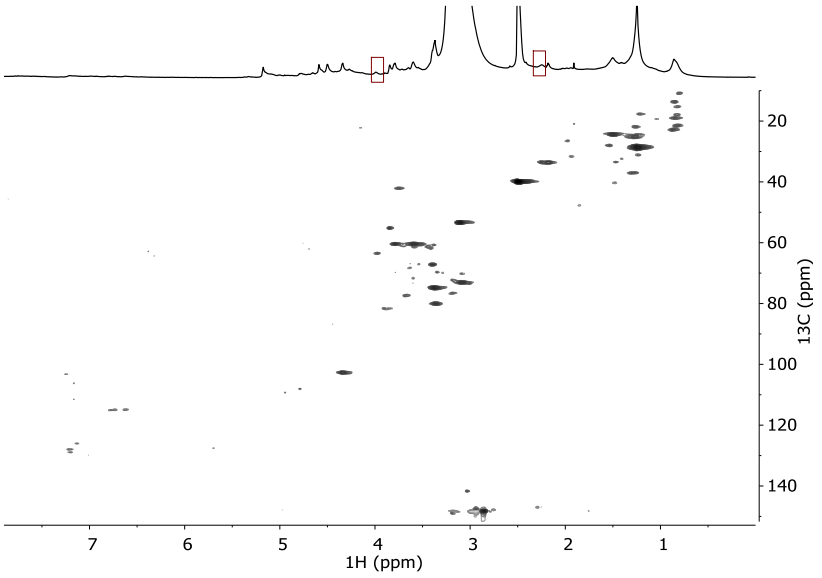

Figure S26 – 2D-^{1}H-^{13}C HSQC-NMR spectrum (Heteronuclear Single Quantum Coherence) of Micro-Tom cutin isolated with cholinium hexanoate (2 h) from the *gpat6* mutant in DMSO- d_6 at 60 ºC. The red rectangles mark signals used for the integration of specific functional groups, all of which showed no overlap of resonances with other chemical groups as shown by the bi-dimensional NMR correlations done.

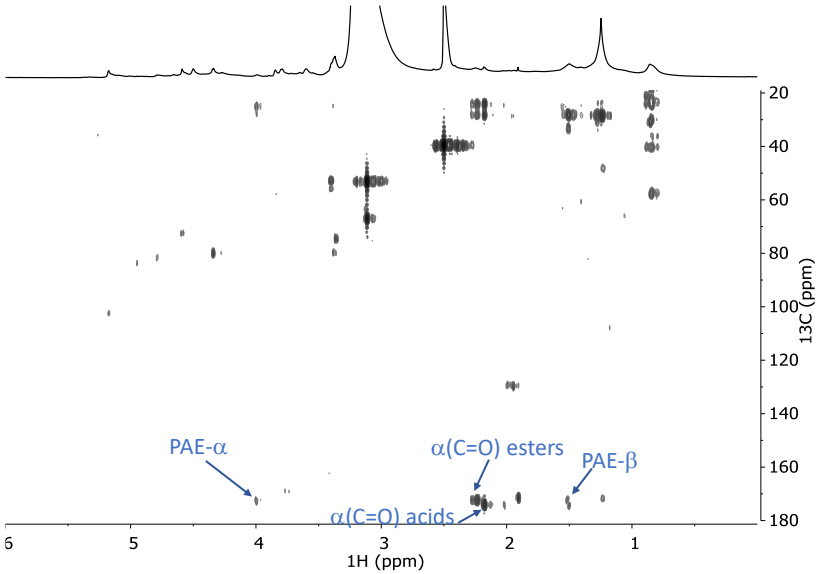

Figure S27 – 2D-^{1}H-^{13}C HMBC-NMR spectrum (Heteronuclear Multiple Bond Correlation) of Micro-Tom cutin isolated with cholinium hexanoate (2 h) from the *gpat6* mutant in DMSO-d_6 at 60 ºC.

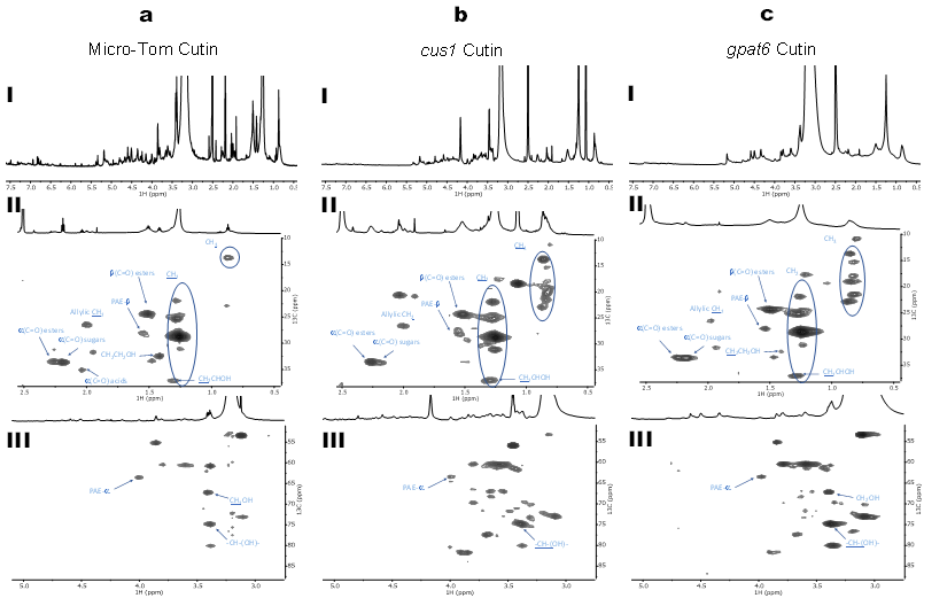

Figure S28 - Wide-ranging NMR spectral characterisation of Micro-tom cutins: wild-type (a), *cus1* (b) and *gpat6* (c) mutants; upon isolation with cholinium hexanoate (2 h). The ^{1}H NMR spectra of all samples (I); HSQC regions corresponding to aliphatics (II) and CH/CH2-X aliphatics (III). Some correlations (unlabelled) are uncertain or unidentified.

References

(1) Moreira, C. J. S.; Bento, A.; Pais, J.; Petit, J.; Escórcio, R.; Correia, V. G.; Pinheiro, Â.; Haliński, Ł. P.; Mykhaylyk, O. O.; Rothan, C.; et al. An Ionic Liquid Extraction That Preserves the Molecular Structure of Cutin Shown by Nuclear Magnetic Resonance. *Plant Physiol.* **2020**, *184* (2), 592–606. https://doi.org/10.1104/pp.20.01049.

(2) Correia, V. G.; Bento, A.; Pais, J.; Rodrigues, R.; Haliński, P.; Frydrych, M.; Greenhalgh, A.; Stepnowski, P.; Vollrath, F.; King, A. W. T.; et al. The Molecular Structure and Multifunctionality of the Cryptic Plant Polymer Suberin. *Mater. Today Bio* **2020**, *5*, 100039. https://doi.org/10.1016/j.mtbio.2019.100039.

CHAPTER IV

Chapter IV consists of the manuscript under preparation:

Carlos J.S. Moreira, Rita Escórcio, Marta Bjornson, Celso Martins, Ana S. Tomé, Artur Bento, Cristina Silva Pereira and Cyril Zipfel

Author Contributions

C.S.P. and C.Z. designed the project and acquired the funding. C.S.P. and C.Z. provided the resources. C.J.S.M. and R.E. performed isolation of cutin from tomato pomace, partial and extensive depolymerization reactions, and extraction generated mixtures of cutin oligomers and monomers. C.J.S.M. performed all the immune assays presented in this chapter and analyzed the data. C.M. built the script for RNA sequencing data analysis and gave training to use it to C.J.S.M. C.M and C.J.S.M. analyzed the RNA sequencing data. M.B. performed the comparative analysis of RNA sequencing generated for this chapter with previously reported datasets of alternative elicitors of plant immunity and abiotic stress conditions. R.E. and A.B. ran NMR experiments and analyzed the data. R.E. performed TLC characterization of COMs and analyzed the data. A.S.T. performed GC-MS characterization of cutin and COMs. C.J.S.M. wrote the initial draft of this chapter. All authors
to the final version of the chapter, including review and editing.

Outline: The following chapter presents a manuscript under preparation. This chapter introduces cutin oligomers as DAMPs able to induce hallmark immune responses in the model plant *A. thaliana* such as Ca^{2+} influx, MAPK activation, and transcriptional reprogramming with common and unique signatures.

Cutin-Derived Oligomers Act as Damage-Associated Molecular Patterns (DAMPs) in *Arabidopsis thaliana*

Carlos J.S. Moreira[a], Rita Escórcio[a], Marta Bjornson[b], Celso Martins[a], Ana S. Tomé[a], Artur Bento[a], Cristina Silva Pereira[a,*] and Cyril Zipfel[b,c*]

[a]Instituto de Tecnologia Química e Biológica António Xavier, Universidade Nova de Lisboa, Oeiras, Portugal.
[b]Institute of Plant and Microbial Biology, Zurich-Basel Plant Science Center, University of Zurich, Zurich, Switzerland.
[c]The Sainsbury Laboratory, University of East Anglia, Norwich Research Park, Norwich, United Kingdom.

[*]Corresponding authors: Cyril Zipfel (cyril.zipfel@botinst.uzh.ch) and Cristina Silva Pereira (spereira@itqb.unl.pt)

Abstract

The cuticle constitutes the outermost defensive barrier of most land plants. It comprises a polymeric matrix - the plant polyester cutin and associated organic solvent soluble waxes. This lipid shield constitutes the first line of defense against pathogen invasion, besides protecting the plant from many abiotic stresses. Data suggestive of the capacity of monomers derived from cutin to act as immune elicitors in plants have been produced during the last decades. However, how the plant perceives these eliciting monomers is not fully understood. Similarly, it has never been analyzed if cutin oligomeric structures, carrying distinct levels of esterification, can potentiate a comparable or superior elicitor effect. In this study, we explored the ability of cutin oligomers to act as DAMPs able to activate PTI in model plants. The collected data demonstrated that cutin oligomeric mixtures (COM) are able to induce Ca^{2+} influx and MAPK activation in the model plant *Arabidopsis thaliana*. Additionally, a unique transcriptional reprogramming profile could be detected after treatment of this plant with COMs. The initial chemical characterization of the mixtures tested allowed to confirm the oligomeric and lipidic nature of the elicitor, pointing to a low molecular weight molecule.

Introduction

Plants started colonizing land environments approximately 450 million years ago[1]. This transition was accompanied by a series of challenges imposed by an extremely desiccating environment[2]. In order to control water loss, protect themselves against UV radiation, reinforce the epidermal cell layer, and protect against pathogens, plants developed a hydrophobic barrier – the cuticle[3,4]. The cuticle is composed by a polymeric matrix of the plant polyester cutin, to which organic solvent soluble lipids (waxes) associate[5]. Additionally, a direct interaction with polysaccharides that build up the epidermal cell walls, on which it is deposited, has been proposed for long[6,7], but the true nature of this interaction remains uncertain.

During infection of the aerial organs of plants, fungal spores release cutin-degrading enzymes, usually known as cutinases that present esterase activity[8] and release cutin-derived molecules. These molecules are then perceived by the fungus as a signal to increase the production of cutinases leading to the formation of a breach[9]. The spore will then germinate, allowing the fungus to invade the plant organ through the opening of the cuticular barrier.

To avoid pathogen invasion, plants have developed a highly specialized mechanism to sense and circumvent biotic threats by using cell surface pattern recognition receptors (PRRs)[10]. These receptors perceive two types of molecular signatures: pathogen-associated molecular patterns (PAMPs) and damage-associated molecular patterns (DAMPs), derived from the invading pathogens or released from plant tissues, respectively[10]. Cutin-derived molecules are regarded as DAMPs due to their ability to induce defense responses such as accumulation of reactive oxygen species (ROS) and upregulation of defense related genes[11–13]. Moreover, mixtures of monomers extracted from plants with higher levels of cuticular permeability, when exogenously applied, can confer enhanced resistance against major necrotrophs[14]. To date, several studies have demonstrated that cutin monomers are able to induce defense responses that include ROS

production, upregulation of defense related genes and production of antimicrobial compounds[15]. As such, cutin monomers are generally regarded as DAMPs; although common hallmark early immune responses, such as increase in intracellular calcium and activation of mitogen-activated protein kinases (MAPKs) were never observed for these molecules[15,16] Nevertheless, evidence for the possibility of the induction of a calcium burst was observed after wounding of *Arabidopsis thaliana* plants, where calcium channel inhibitors impair ROS production[17]. During polyester degradation, it is expected that the first events of ester cleavage result in a mildly cleaved backbone, followed by the release of oligomers that will ultimately be broken down into monomeric units.

Recently, our team was able to develop an ionic liquid-based methodology to recover cutin from tomato[18]. This approach allowed to recover a polyester demonstrating high preservation of its polymeric backbone[19]. To try to understand the role played by cutin-derived molecules released during early stages of pathogen infection, we employed a controlled chemical depolymerization reaction to generate an oligomeric mixture. This cutin oligomeric mixture (COM) showed the ability to induce changes in intracellular Ca^{2+} concentrations and MAPK activation in the model plant *Arabidopsis thaliana* Col-0. Moreover, a unique transcriptional reprogramming was triggered by our COM in these plants. With this study we propose that cutin derived oligomers act as DAMPs able to activate pattern-triggered immunity (PTI) in plants and that they are perceived by yet uncharacterized PRR(s). Moreover, chemical characterization through chromatographic or spectroscopic methodologies allowed to confirm that a certain degree of esterification is needed to allow the observed eliciting activity.

Results and discussion

Eliciting potential of cutin and cutin oligomeric mixtures

With the aim of understanding how degradation of cutin might influence hallmark early immune responses, we performed a screening on a set of cutin derived compounds. This library included cutin isolated from the peels of two types of tomato and pepper, commercially available model compounds and soups of monomers resulting from the total hydrolysis of all cutins. This library was complemented with suberin extracted from cork and the corresponding soup of monomers for comparison with a different plant polyester (Table S1).

The strategy was to test the eliciting potential of all compounds for two early immune responses – ROS burst and Ca^{2+} influx. To test in parallel if specificity was observed in the response, three model plants were used on the study – *Solanum lycopersicum* 'Moneymaker', *Nicotiana benthamiana* and *Arabidopsis thaliana* Col-0. ROS was tested via the activity of HRP, which acts on its substrate luminol in the presence of H_2O_2 to produce luminescence[20]. After testing all compounds, a clear ROS response could only be observed for cutin isolated from the pomace of tomato Compal (TC) and only in tomato plants (Figure 1A). All the remaining compounds were unable to induce any response different from the mock treatment (data not shown), including soups of monomers (Figure 1B). In *A. thaliana*, the DAMP Pep1[21] was used as positive control, confirming that plants were able to respond to elicitor treatment, just were not responding to cutin monomers treatment.

For the calcium response, only *Nicotiana benthamiana* and *Arabidopsis thaliana* plants were tested, both expressing aequorin, a widely used calcium activated reporter of immune responses in plants[22]. In both *A. thaliana* and *N. benthamiana*, the only reproducible response observed was when cutin oligomeric mixtures (COMs) obtained through a controlled depolymerization reaction performed with sodium methoxide and methanol anhydrous (Figure S1) were tested.

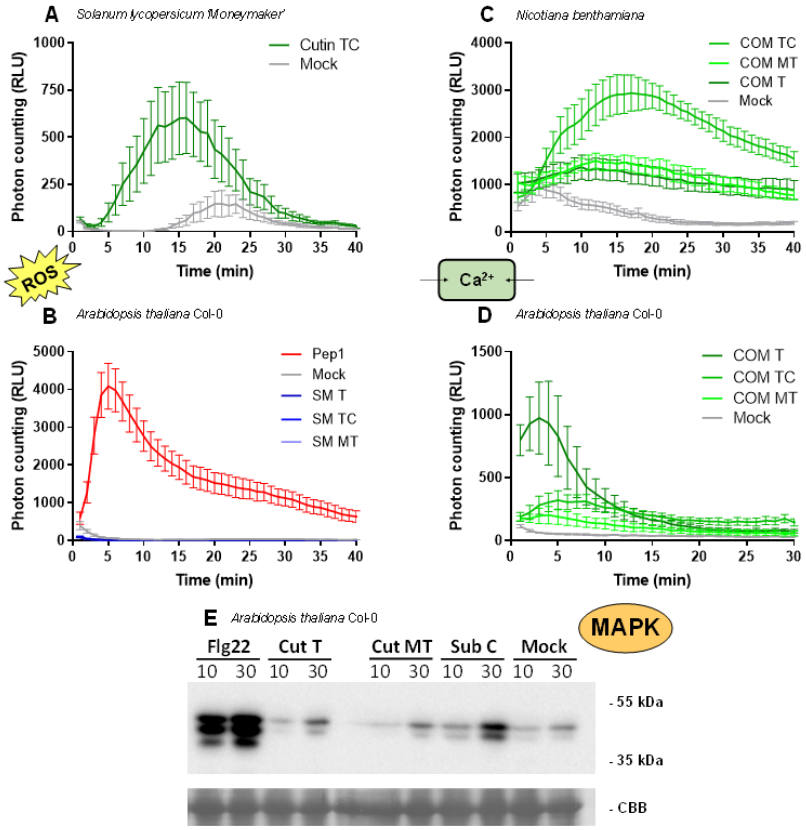

Figure 1 – Main results obtained from the initial screening on cutin and cutin-derived molecules with potential to elicit plant immunity. Luminescence-based detection of apoplastic ROS: (A) in *Solanum lycopersicum* 'Moneymaker' plants upon treatment with 2 mg/mL of cutin extracted from tomato pomace from Compal (TC) in water, against the mock control; and (B) in *Arabidopsis thaliana* Col-0 plants upon treatment with 2 mg/mL of soup of monomers (SM) obtained from commercial tomato (T), tomato pomace from Compal (TC) and the miniature tomato cultivar Micro-Tom (MT), against the corresponding mock control. Luminescence-based detection of calcium influx: (C) in *Nicotiana benthamiana* and (D) *Arabidopsis thaliana* plants, both expressing the calcium reporter aequorin, upon treatment with 1 mg/mL of COM TC, 800 µg/mL of COM T and 200 µg/mL of COM MT against the corresponding mock control. Western blot evaluation of MAPK activation in 14-day-old *Arabidopsis thaliana* Col-0 seedlings upon treatment with 3 mg/mL cutin from commercial tomato (Cut T) and from the miniature tomato cultivar Micro-Tom (Cut MT) or suberin from cork (Sub C) against the corresponding mock control.

These mixtures obtained from the cutin extracted from a commercial tomato (COM T), tomato pomace (COM TC) and the miniature cultivar Micro-Tom (COM MT) were all active (Figure 1C and 1D). To complete our screening, the potential of our library to activate MAP kinases was evaluated through western blot using an antibody that recognizes the phosphorylated – active – forms of MPKs, and thus enable observation of the activation of MPK 3, 4, 6 and 11 during PTI signaling[23]. As seen in figure 1E, both polyesters – cutin and suberin – seem to induce MAPK activation, while the other compounds did not demonstrate the ability to activate MAP kinases compared to mock treatment (data not shown).

The screening demonstrated that cutin is able to induce a ROS burst and activate MAP kinases in plants – which together with recently reported findings that ionic liquid isolated cutins present a low degree of ester cleavage[18,19] – could be indicative of a response induced by early stages of cutin degradation by pathogens during infection. Moreover, the observation that oligomers derived from these cutins are able to induce a strong Ca^{2+} response seems to reinforce the idea that not only monomers but also oligomers released earlier during infection may act as elicitors of plant immunity. The eliciting activity demonstrated by both the polymer and oligomers derived from its hydrolysis in all plants tested, strongly suggests that the responses triggered are not specific and that the chemical nature of the eliciting molecules should be common and similarly recognized by all plants tested (Table S2).

Cutin is able to induce a ROS burst in Arabidopsis thaliana Col-0

In order to confirm the initial results obtained in the screening, we decided to focus on the activity of the polymer cutin, the oligomeric mixtures obtained through its controlled methanolysis, and the soups of monomers resulting from its complete hydrolysis. Additionally, a monomer described in literature to have eliciting effect, namely in the activation of ROS production,

hydroxy palmitic acid (HPA)[12,13] was also tested. *Arabidopsis thaliana* was chosen as the model plant, because both Ca^{2+} and MAPK responses had been observed during the screening and due to the higher amount of genetic material available for further characterizations.

Cutin showed the ability to induce a strong ROS burst compared to the mock treatment. The effect was not only reproducible, as it was also extended in time and the response was not depleted even after 45 min after the treatment (Figure 2A and 2B). When cutin oligomeric mixtures were tested this response was not observed. To try to understand if some chemical interference with the reporter of luminescence was happening a co-treatment with a strong inducer of immunity, flg22[24], was performed. Flg22 treatment induced a strong ROS burst as expected; nevertheless, when plants were co-treated with flg22 and COM the signal were almost completely abolished to levels similar to mock treatment, while COM treatment itself remained with a signal much lower than the mock control (Figure 2C and 2D). These observations strongly suggest that some chemical reaction might be occurring, hindering the activity of the HRP enzyme and/or the luminol, not allowing to detect any luminescence signal.

In agreement with these results, a ROS burst was not observed after treatment with either a soup of monomers or the HPA cutin monomer (Figure S2A and S2B). Together, these results suggest that the experimental difficulty with measuring ROS with HRP/luminol is indeed based on the chemical nature of cutin oligomer/monomers themselves. Future efforts should focus on finding a new experimental approach, to confirm if both COMs and monomers might induce a ROS burst under the conditions tested. Despite these limitations, cutin polymer cleavage products have the potential to induce a ROS burst as demonstrated by the effect of cutin, which is representative of a polymer with low degree of cleavage mimicking the result of a very mild hydrolysis (less than 5 % ester cleavage), as previously demonstrated[19].

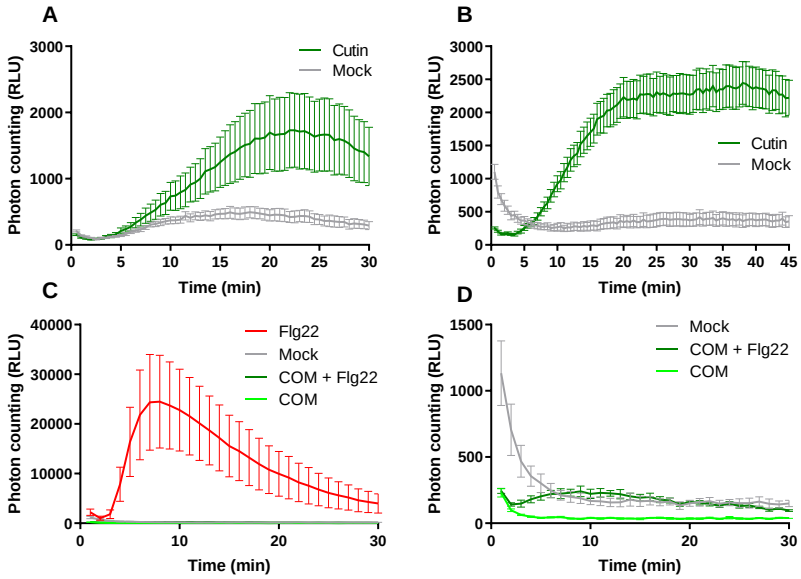

Figure 2 – Luminescence-based detection of apoplastic ROS: in *Arabidopsis thaliana* Col-0 seedlings upon treatment with 1 mg/mL of cutin isolated from tomato pomace against the corresponding mock control (A – B); and upon co-treatment with 2 mg/mL COM and 100 nM flg22 against individual treatments with COM and flg22 at the same concentrations and the corresponding mock control (C – D).

Cutin oligomeric mixtures induce calcium influx in Arabidopsis thaliana

To confirm the results obtained in the screening, the cutin oligomeric mixture (COM) ability to induce calcium influx was tested in *Arabidopsis thaliana* seedlings expressing aequorin. Results show a clear and reproducible induction of this immune output (Figure 3A and 3B). To understand how cutin would behave in terms of calcium response activation we also tested the cutin polyester from which the oligomeric mixture was obtained. Interestingly, it was possible to observe that cutin is not only able to induce this hallmark immune output, but also that it induces a different pattern of response (Figure 3C). Indeed, at different time points two maximum response peaks at 3 and 12 min respectively were observed. This result suggests that more than one eliciting molecule might be present in cutin,

inducing responses with different timings. Moreover, the fact that COM induces a calcium response that has its maximum usually between 3 and 5 min, might also indicate that the type of hydrolysis used to obtain this oligomeric mixture is favoring the occurrence of one type of these potential elicitor molecules. During infection, several pathogens secrete enzymes able to perform ester cleavage on this polymer[15]. This degradation will be continuous until monomers are released, and a breach is open to allow pathogen invasion of the host. To try to mimic this scenario, we recovered the non-hydrolyzed fraction resulting from the reaction that gave rise to our COM and re-hydrolyzed it using the same conditions, obtaining a second oligomeric mixture (COM II) that was also tested for calcium influx induction. Not only this mixture was able to induce calcium influx, but also it did so with higher intensity. COM II induced a response with more than two-fold the intensity of the response elicited by COM (Figure 3D) at the same overall mixture concentration.

To complement the study, both the soup of monomers resulting from the total depolymerization of cutin and the HPA monomer were tested. In both cases, we could not observe any response consistent with activation of this hallmark output, even testing increasing concentrations (Figure S3). Overall, the data point out that mild cleavage of the esters and release of oligomeric components are able to induce calcium influx in *Arabidopsis thaliana*, but extensive cleavage reduces the ability to induce this hallmark response in the conditions tested.

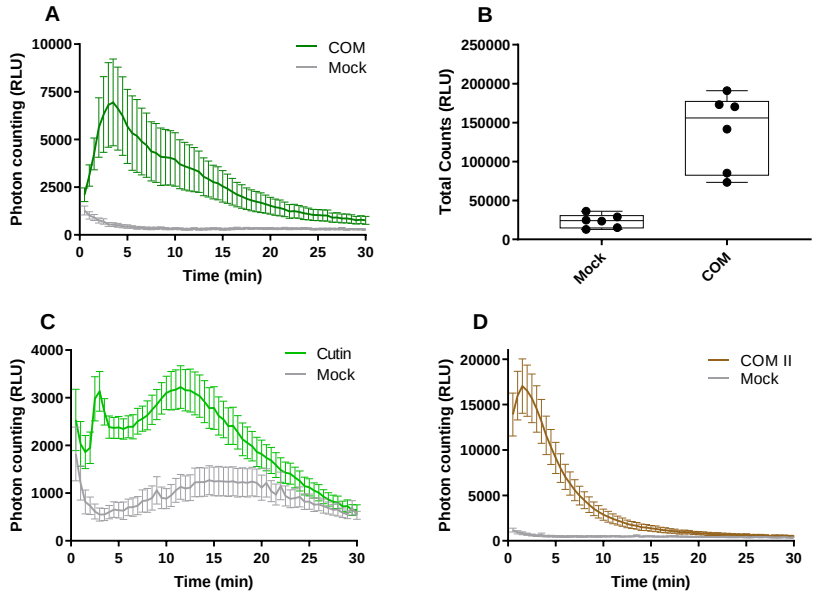

Figure 3 – Luminescence-based detection of calcium influx in *Arabidopsis thaliana* seedlings expressing the calcium reporter aequorin, upon treatment with 2 mg/mL of COM (A) and corresponding plot of the total photon counts for the six biological replicates tested (B), 1 mg/mL of cutin (C) and 2 mg/mL of COM II against the corresponding mock control.

Cutin oligomeric mixtures (COM) induce MAPK activation

To test whether oligomers derived from cutin degradation are able to induce later signaling events occurring downstream to their perception by the plant, the ability to induce MAP kinases was evaluated through western blotting. Apart from the wild type plants, the double mutant *bak1-5 bkk1* belonging to the Somatic Embryogenesis Receptor Kinase (SERK) family of common PRR coreceptors[25], the single mutant *cerk1-2* from the Chitin Elicitor Receptor Kinase 1 (CERK1), another major coreceptor of PRRs[25], and the triple mutant *bak1-5 bbk1 cerk1* (*bbc*) were tested. SERKs commonly interact with leucine-rich repeat-type PRRs, while CERK interacts with LysM-motif-type PRRs[26]. Thus, differences in response in these co-receptor mutants would provide a hint as to the family of PRR(s) that recognize active

COMs. The goal was to test if the inactivation of common PRR co-receptors could give us an initial insight on the potential perception mechanism of cutin-derived oligomeric elicitors.

After 10 min of treatment, COM was able to induce a clear activation of MAP kinases in wild-type plants and all the mutants tested (Figure 4). Moreover, treatment with COM II and cutin also showed that these compounds are also able to activate MAP kinases (Figure S4). These results point to the ability of mildly cleaved cutin, and oligomers derived from its depolymerization, to trigger signaling cascades that may lead to transcriptional reprogramming of the plant to cope with the attack. Moreover, all the tested co-receptor mutants were responsive to the treatments. This result suggests that the mechanism by which such molecules are perceived is not dependent on the families of PRRs known to associate with these co-receptors nor on already described PRRs that form complexes with them.

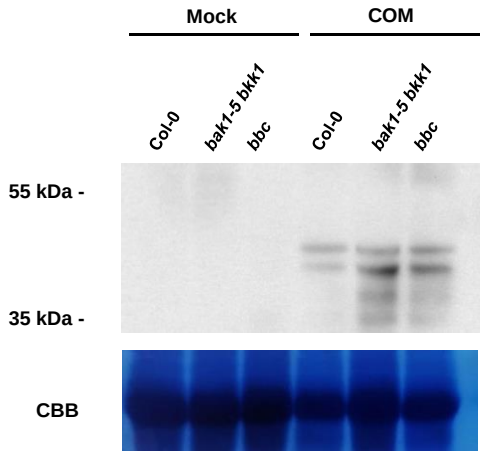

Figure 4 – Western blot evaluation of MAPK activation in 14-day-old *Arabidopsis thaliana* seedlings from wild type Col-0 and the *bak1-5 bkk1 and bbc* mutants, upon treatment with 3 mg/mL of COM against the corresponding mock control.

COM treatment triggers a unique transcriptional reprogramming in Arabidopsis thaliana

Inspired by our results we decided to explore the ability of the COM to trigger transcriptional reprogramming in *Arabidopsis thaliana*. Seedlings were treated with COM or the mock control for 30 min, and the transcriptional response of the plant to COM compared to the mock treatment was evaluated by RNA-seq.

First, a principal components analysis (PCA) clearly demonstrated that both treatments have distinct transcriptomic profiles clearly separating from each other (Figure S5).

A total of 528 differentially expressed genes (DEGs) resulted from the COM treatment, of which 479 genes were upregulated, while only 49 were downregulated compared to the mock treatment (Figure S6).

Enriched gene ontology (GO) categories were only obtained for the subset of upregulated genes due to the small size of the downregulated subset. This analysis clearly showed enrichment for terms related to activation of plant immunity, particularly ‘response to wounding’ and ‘response to other organism’ (Figure S7).

Together with the previous observation of calcium influx and MAPK activation, these results strongly suggest that cutin-derived oligomeric mixtures may act as elicitors of plant immunity being perceived as DAMPs.

To deepen the analysis, a comparison between the transcriptional reprogramming induced by COM treatment and that of seven other elicitors, published by Bjornson et al. (2021) was performed. The comparison revealed that COM treatment presents similarity with the effect of other elicitors, sharing 140 induced genes, further confirming its potential as elicitor of plant immunity. Moreover, a high degree of uniqueness in the transcriptional reprogramming generated could be observed due to the large fraction of genes uniquely induced by COM compared to all the other tested elicitors (Figure 5). In fact, such level of specificity in transcriptional reprogramming was previously only

observed for flg22[27] (Figure 5), despite the lower number of genes induced by COM treatment.

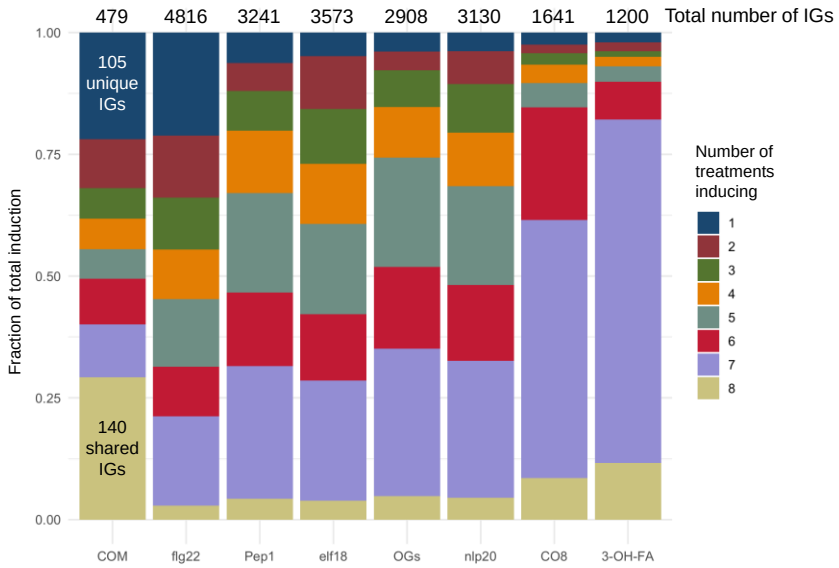

Figure 5 – Comparison of genes induced by treatment of COM with those induced by seven other elicitors of plant immunity. The total number of induced genes (IGs) for each elicitor (over all time points in Bjornson, et al 2021) is presented and the number of genes induced by all treatments or solely by COM are highlighted.

A correlation between COM treatment and the other seven elicitor treatment also depicted low correlation, further reinforcing that the kind of response that is being triggered by COM is clearly distinct from the type of physiological defense responses triggered by the other elicitors (Figure S8).

To further evaluate the uniqueness on the effect triggered by COM treatment, a direct comparison with the effect of seven different types of abiotic stresses was performed. Results highlight that 32 genes were induced solely by COM and not by any of the other elicitors and abiotic stresses studied (Table 1). This set of genes could be regarded as the eliciting signature of the COM and constitutes strong evidence, supporting its role as elicitor of PTI. The remaining genes that were unique against all the other seven elicitors but

showed to also be induced by certain abiotic stresses are presented in Table S3.

Table 1 – List of genes uniquely induced by the COM treatment after comparison with seven different elicitors of plant immunity and seven different types of abiotic stress conditions. Genes for which there was no attributed name on the TAIR database were labelled as NA.

Gene	Log_2 FC	padj	ASI	Name	Short Description
AT3G19700	4.752	9.67E-03	0	IKU2	Leucine rich repeat (LRR) kinase
AT1G27080	3.582	2.03E-02	0	AtNPF2.12	Protein with low-affinity nitrate transporter activity
AT5G07880	3.419	6.19E-10	0	ATSNAP29	Member of mammalian SNAP25 Gene Family
AT3G46070	3.407	1.37E-04	0	NA	C2H2-type zinc finger family protein
AT3G56980	2.815	6.64E-05	0	BHLH039	Basic helix-loop-helix transcription factor protein
AT1G64940	2.637	2.91E-03	0	CYP89A6	Member of the CYP89A family
AT4G36040	2.290	1.14E-37	0	DJC23	Chaperone DnaJ-domain superfamily protein
AT5G22890	1.967	7.40E-19	0	STOP2	Sensitive to proton rhizotoxicity 2.
AT5G42600	1.940	3.45E-02	0	MRN1	Oxidosqualene synthase that produces monocyclic triterpenes
AT3G04530	1.651	5.10E-04	0	ATPPCK2	Arabidopsis phosphoenolpyruvate carboxylase kinase
AT3G21260	1.646	2.60E-06	0	GLTP3	Glycolipid transfer protein (GLTP) family protein
AT3G21270	1.560	5.18E-15	0	ADOF2	Dof zinc finger protein
AT5G54630	1.534	3.48E-09	0	NA	Zinc finger protein-like protein
AT4G19865	1.474	1.34E-04	0	NA	Galactose oxidase/kelch repeat superfamily protein
AT5G66690	1.434	2.82E-09	0	UGT72E2	UDPG:coniferyl alcohol glucosyltransferase
AT5G51500	1.397	3.88E-02	0	NA	Plant invertase/pectin methylesterase inhibitor superfamily
AT2G36090	1.394	6.92E-04	0	NA	F-box family protein
AT1G66800	1.385	2.90E-02	0	NA	NAD(P)-binding Rossmann-fold superfamily protein
AT1G28470	1.382	5.47E-04	0	ANAC010	NAC domain containing protein 10
AT1G35260	1.355	3.01E-11	0	MLP165	MLP-like protein 165
AT2G28690	1.257	6.11E-06	0	NA	TOX high mobility group box protein
AT1G64780	1.225	1.78E-02	0	AMT1	Ammonium transporter protein
AT3G25290	1.194	1.29E-05	0	NA	Auxin-responsive family protein
AT3G09270	1.090	1.38E-04	0	ATGSTU8	Glutathione transferase belonging to the tau class of GSTs.
AT5G03670	1.082	5.70E-04	0	TRM28	Histone-lysine N-methyltransferase SETD1B-like protein
AT3G18400	1.071	3.32E-03	0	ANAC058	NAC domain containing protein 58
AT5G03240	1.063	4.55E-04	0	UBQ3	Ubiquitin that is attached to proteins destined for degradation
AT1G05530	1.055	3.40E-02	0	UGT2	Protein with glucosyltransferase activity
AT3G52360	1.027	1.80E-04	0	NA	Transmembrane protein
AT3G14680	1.008	7.13E-03	0	CYP72A14	Putative cytochrome P450
AT3G61410	1.008	3.84E-02	0	NA	U-box kinase family protein
AT1G68795	1.005	1.07E-02	0	CLE12	Putative ligand homologous to the Clavata3 gene

NMR-based characterization of COMs confirms their oligomeric nature

Polysaccharides are commonly found as contaminants in cutins isolated using ionic liquids; nevertheless, the amounts at which they are present are residual[19]. Nonetheless, many molecules derived from cell wall polysaccharides acting as immune elicitors were identified in the last years, like oligogalacturonides (OGs)[28], cellobiose[29], arabinoxylan oligosaccharides[30] and mixed-linked β-1,3/1,4-glucans (MLGs)[31]. To further confirm that the true nature of the elicitor molecules is lipidic, we decided to

measure the total amount of polysaccharides present in our oligomeric mixtures COM and COM II (Table 2). Results clearly show that, although present, polysaccharides exist in residual amounts in our samples, at the level of picograms per mg of either COM, which is below the µg-mg/mL usually used to test such elicitor compounds[29]. This clearly confirms the lipidic nature of our mixtures and that the eliciting effect should come from cutin derived molecules.

Table 2 – Quantification of the total carbohydrate content in cutin oligomeric mixtures (COMs).

Samples	pg (carbohydrate)/mg (oligomeric mixture)	carbohydrate content (%)
COM	41.05 ± 7.25	$4.11 \times 10^{-7} \pm 7.25 \times 10^{-8}$
COM II	43.83 ± 25.05	$4.38 \times 10^{-7} \pm 2.51 \times 10^{-7}$

To further confirm that oligomers are present in our mixtures, NMR-based characterizations of both COMs and cutin from which they were derived was performed (Figure 6). The analysis of the HSQC spectra for cutin and both cutin oligomeric mixtures obtained from its methanolysis showed the presence of all the signals previously assigned in recent studies published by our group[18,19].

From the analysis of the magnifications of the HSQC spectra, new signals were detected in tomato pomace cutin that were not previously detected in tomato peels cutin. These signals confirm the presence of acylglycerol esters in two signals assigned to different glycerol configurations, the first with a ^{13}C shift of 69.34 ppm and ^{1}H shift of 5.18 ppm corresponding to the 1, 2, 3-TAG-CH2 configuration and the second with a ^{13}C shift of 62.26 ppm and ^{1}H shifts of 4.13 ppm and 4.26 ppm, corresponding to the 1, 2, 3-TAG-CH1,3 configuration. This signal is not detected in any spectra of COM and COM II, thus indicating that it should not have a particular effect in the eliciting activity observed for both cutin oligomeric mixtures. However, one cannot discard the hypothesis that they may be associated to the occurrence

of the second peak observed in calcium response induced by cutin. The analysis of the HSQC spectra of the two oligomeric mixtures also shows the presence of signals that were not previously assigned to cutin in past studies. In both COMs, we could observe a signal with a ^{13}C shift of 50.83 ppm and ^{1}H shift of 3.56 ppm corresponding to methyl esters that are formed as result of the action of methanol during the partial depolymerization methanolysis reaction[32]. Although present in both cutin oligomeric mixtures, the fact that they are absent in cutin, which also shows eliciting activity, reduces the possibility that these molecules are responsible for the observed activation of plant immunity. Specific signals could be observed in the NMR spectrum of each mixture, namely that of propyl esters (^{13}C shift of 63.73 ppm and ^{1}H shift of 4.09 ppm) and that of ethyl esters (^{13}C shift of 59.31 ppm and a ^{1}H shift of 4.03 ppm), present in COM and COM II spectra, respectively. The reaction that might have led to these esters is still uncertain; nevertheless, the fact that they do not occur in both mixtures and that both have an eliciting effect also makes difficult to correlate these esters with the observed eliciting activity. The analysis of the HSQC spectra for all three samples clearly shows a strong presence of oligomers in our COMs, confirmed by the detection of the signals assigned to primary aliphatic esters (PAE) and secondary aliphatic esters (SAE) in both cutin and COMs obtained from its partial depolymerization.

Additionally, to infer the degree of esterification of each sample, we estimated, through the integration of the corresponding NMR signals, detected in the ^{1}H spectra (Figure S9) the relative abundances of all the esters present. This was possible due to the use of an internal standard, further allowing to clearly discriminate the contributions of primary and secondary aliphatic esters in all samples (Table 3).

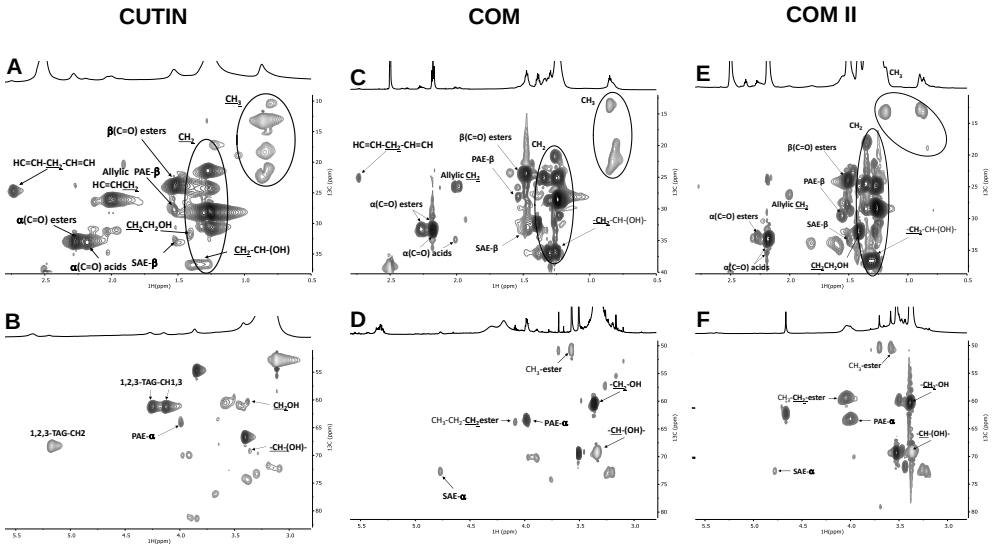

Figure 6 – NMR characterization of cutin and cutin oligomeric mixtures obtained from its methanolysis. Magnification of the HSQC spectral regions corresponding to aliphatics (A, C and E) and CH/CH2-X aliphatics (B, D and F) for each sample. Some correlations (unlabeled) are uncertain or unidentified.

Table 3 – Chemical characterization of cutin and cutin oligomeric mixtures. NMR quantification of the relative abundances of all esters present in cutin calculated through the integration of signals in the corresponding ^{1}H NMR spectra. Ester types detected on this analysis include TAG (Triacylglycerol esters), PAE (Primary aliphatic esters), SAE (Secondary aliphatic esters), ME (Methyl esters), PE (Propyl esters) and EE (Ethyl esters). Esters that were not detected on a sample are labelled as *n.d.*

Ester / Sample	TAG (%)	PAE (%)	SAE (%)	ME (%)	PE (%)	EE (%)
CUTIN	51.4	25.1	23.5	*n.d.*	*n.d.*	*n.d.*
COM	*n.d.*	28.5	32.7	28.4	10.5	*n.d.*
COM II	*n.d.*	20.5	11.1	17.6	*n.d.*	50.8

Overall, our data confirmed the oligomeric nature of the active COMs, further revealing novel aspects of their composition that may aid future efforts to unveil the chemical identity of the active molecules present in such mixtures.

Chromatographic characterization of both COMs points to selection of specific chemical groups that may explain their immune elicitor activity

Trying to reach the chemical identity of the active molecules within our oligomeric mixtures, we started by performing thin layer chromatography (TLC) of our cutin oligomeric mixtures. After the initial elution of each sample, two different staining solutions were used to try to understand which compounds were separating in the plate. The corresponding retardation factor (rf) was calculated for each fraction separating in the TLC plate (Table S4). As expected, the cutin sample did not elute in the used solution, due to its insoluble nature. This result suggests that no free molecules, soluble in the eluent, were retained in cutin. The comparison between both COMs clearly showed, after staining with both solutions, that the complexity of the mixture seems to reduce from the first methanolysis to the second. This observation suggests that the first depolymerization reaction “cleans” cutin from several non-active molecules, generating a mixture most likely with reduced amount of the active ones. This could explain why COM II seems to have more activity in calcium influx induction. Nevertheless, to address this, future efforts will need to focus on subsequent depolymerization reactions of the recalcitrant fraction, further mimicking the degradation imposed by pathogens during infection. An intriguing observation was that UV exposure that usually is used to detect the presence of aromatic compounds, revealed very intense bands, which is indicative of their association with other compounds present in the mixture, raising the possibility of their relevance for the eliciting activity of the oligomeric mixtures.

The GC-MS based analysis of the hydrolysable monomeric constituents of each sample (chromatograms presented in Figure S10) shows that COM mostly consist of the major cutin monomer 10, 16-dihydroxyhexadecanoic acid (~ 40 %) with an enrichment for alkanoic and α, ω-Alkanedioic acids in terms of relative abundance compared to the cutin (Table 4). COM II monomeric composition is of lower complexity than

that of COM and the relative abundance of 10, 16-dihydroxyhexadecanoic acid increase more than twofold. These results suggest that this monomer is most likely one of the constituents of the active molecule. Although still inconclusive, the monomeric composition of each cutin oligomeric mixture will help to guide the discovery of the chemical identity of the elicitor present in these mixtures.

Table 4 – GC-MS characterization of cutin and cutin oligomeric mixtures. List of the monomeric hydrolysable constituents of each sample after total depolymerization and derivatization. Monomers that were not detected in a specific sample are labelled as *n.d.*

	Relative percentage (%)		
Compound	**Cutin**	**COM**	**COM II**
Alkanoic acids	**14.73 ± 0.79**	**40.21 ± 1.13**	**3.74 ± 1.09**
tetradecanoic acid	*n.d.*	0.45 ± 0.22	*n.d.*
hexadecanoic acid	3.22 ± 0.74	7.34 ± 0.16	1.14 ± 0.32
9,12-octadecadienoic acid	5.68 ± 0.35	18.44 ± 0.59	1.36 ± 0.40
9-octadecenoic acid	4.35 ± 0.23	9.13 ± 0.36	1.24 ± 0.37
octadecanoic acid	1.48 ± 0.14	3.16 ± 0.17	n.d.
ω-Hydroxyalkanoic acids	**84.61 ± 0.36**	**45.96 ± 0.84**	**94.75 ± 1.12**
16-hydroxyhexadecanoic acid	1.49 ± 0.47	2.99 ± 0.07	1.46 ± 0.49
10,16-Dihydroxyhexadecanoic acid	83.25 ± 1.01	39.91 ± 0.77	92.40 ± 0.98
9,10-epoxy-18-hydroxyoctadecanoic acid	*n.d.*	1.11 ± 0.15	1.18 ± 0.42
α, ω-Alkanedioic acids	**1.03 ± 0.46**	**13.83 ± 0.55**	**1.51 ± 0.29**
octanedioic acid	*n.d.*	1.15 ± 0.06	*n.d.*
nonanedioic acid	0.71 ± 0.44	7.15 ± 0.32	1.08 ± 0.31
hexadecanedioic acid	0.63 ± 0.25	4.94 ± 0.20	0.57 ± 0.20
Identification yield (%)	61.19 ± 10.28	49.68 ± 7.32	68.29 ± 12.13
Recalcitrance (%)	26.33 ± 1.53	8.75 ± 3.46	6.00 ± 1.82

Conclusions

The cuticle is the plant's outermost defensive barrier being the first shield counteracting the invasion by several pathogens. Some of these pathogens are able to secrete enzymes that degrade the polymeric matrix of the cuticle – cutin. This makes of extreme relevance the study on how the degradation of this plant polyester influences activation of plant immune defenses. Past efforts mostly focused on the action of monomers that are released after extensive depolymerization of cutin, in stages of infection closer to the opening of a breach and subsequent pathogen invasion of the tissues[15]. Our goal was to study if during the initial stages of degradation, oligomeric signals are released that might also activate plant immunity. To guide discovery, we established an *ex-situ* approach using ionic liquid extracted cutins, that show high preservation of its polymeric backbone as our matrix. The controlled depolymerization by methanolysis allowed obtaining cutin oligomeric fractions to be tested as potential elicitors of immunity. These fractions induced calcium influx, MAP kinase activation and transcriptional reprograming in the model plant *Arabidopsis thaliana*. Moreover, the alterations in the transcriptome show a degree of uniqueness that allows to select some marker genes to be tested in future studies. The fact that we are working with a mixture and not a pure compound makes our findings even more relevant, since one or more oligomeric molecules might be responsible by the observed activity, but their relative amount in the mixture might be low. This could also explain why we observed a much lower number of genes induced by this treatment compared to other described elicitors of immunity; nevertheless, future efforts will focus on achieving the pure elicitor molecules to study their full potential as activators of immunity in plants. The initial chemical characterization allowed to confirm the oligomeric nature of the active molecules, which is in line with all the other tests performed on this study, where activity of monomers was never observed. Future efforts will focus on identifying the active molecules through MS-based methodologies. The purification of the active molecules might allow to overcome technical

limitations that hinder, for instance, the ability to test if apoplastic ROS might be another immune output of COM treatment. Future work should also focus on the identification of the PRR(s) involved in COM perception.

Materials and Methods

Plant Material and Growth Conditions. Tomato pomace was obtained by Sumol + Compal, SA., and dried at 60 °C for one week until constant weight. Dry pomace was then milled using a Retsch ZM200 electric grinder (granulometry 0.5 mm; 10000 rpm) and stored at room temperature until further use.

For the initial screening tests (ROS burst and Ca^{2+} influx), adult plants (4-week-old) of *Arabidopsis thaliana* Col-0, *Solanum lycopersicum* 'Moneymaker' and *Nicotiana benthamiana* were used.

Arabidopsis thaliana Col-0 seeds were germinated on soil and plants were grown on an Aralab Fitoclima climate chamber with 150 $\mu mol \cdot s^{-1} \cdot m^{-2}$ light intensity, following a 10 h/14 h day/night cycle, under constant temperature of 20 °C and 60 % humidity. Plants were watered automatically for 10 min three times per week. *Solanum lycopersicum* 'Moneymaker' seeds were germinated on soil and plants were grown on a Conviron climate chamber with 120 $\mu mol \cdot s^{-1} \cdot m^{-2}$ light intensity, following a 12 h/12 h day/night cycle, under temperatures of 21 ºC during the day and 19 ºC at night and constant humidity of 60 %. Plants were watered manually three times per week. *Nicotiana benthamiana* plants seeds were germinated on soil and plants grown on a greenhouse room with 150 $\mu mol \cdot s^{-1} \cdot m^{-2}$ light intensity, following 16 h/8 h day/night cycle, under constant temperature of 24 ºC. These plants were watered automatically daily for 20 min.

For the experiments aiming to evaluate the eliciting effect of cutin oligomeric mixtures, seedlings of *Arabidopsis thaliana* Col-0 and the mutants *bak1-5 bkk1*, *cerk1-2*^{AEQ} and *bbc* [33–35], all in the Col-0 background, were used. Seeds were germinated on plates with 0.5 x Murashige and Skoog (MS) basal

salt mixture supplemented with 1 % (w/v) sucrose and 0.9 % (w/v) phytoagar. After four days, seedlings were transferred to 24-well sterile culture plates containing liquid 0.5x MS supplemented with 1 % (w/v) sucrose and allowed to grow until 8-day-old (Ca^{2+}), 11-day-old (ROS) and 14-day.old (MAPK and RNA-seq). These seedlings were grown in sterile conditions in a Aralab Fitoclima climate chamber with 120 $\mu mol \cdot s^{-1} \cdot m^{-2}$ light intensity, following a 16 h/8 h day/night cycle, under temperatures of 20 ºC during the day and 18 ºC at night.

Cutin Extraction. Cutin was extracted from tomato pomace as previously described for cutin peels[18]. In brief, tomato pomace and cholinium hexanoate were mixed (1:10) and incubated for 2 h at 100 °C. The reaction was stopped by the addition of 80 mL of DMSO per gram of tomato pomace. The polyester was recovered by filtration using a nylon membrane filter (0.45 µm). Purification was obtained by washing with an excess of deionized water to remove all traces of DMSO. Purified cutins were then freeze dried and stored at room temperature for further use.

Cutin Hydrolysis. To obtain a cutin oligomeric mixture (COM), a sodium methoxide-catalyzed methanolysis was performed. The controlled hydrolysis was achieved by mixing 20 mL of anhydrous methanol with 0.1 M sodium methoxide. This mixture was added to 0.5 g of cutin and further incubated at 40 ºC for 2 h without stirring. The resulting mixture was then cooled to room temperature and centrifuged (4 ºC, 30 min, 4000 *g*) to recover the non-hydrolyzed cutin fraction. The supernatant (hydrolyzed fraction) was acidified to pH 3–3.5 by addition of HCl 37 % and subsequently centrifuged (4 °C, 30 min, 4000 *g*). The resulting precipitate was recovered, and the supernatant extracted three times by dichloromethane/water partition to release the hydrolysates; and sodium sulphate anhydrous was added to remove water. The solution was concentrated under a constant nitrogen flux at 40 ºC.

To obtain a soup of monomers (SM), a sodium hydroxide alkaline hydrolysis was performed. The extensive hydrolysis was achieved by mixing a solution of 0.5 M NaOH in methanol/water (1:1, v/v) at 95 ºC with the cutin powder, for 4 h; subsequently cooled to room temperature and acidified to pH 3/3.5 with 1 M HCl, then extracted by dichloromethane/water partition to release the hydrolysable constituents. The solution was concentrated under a constant nitrogen flux at 40 ºC.

Immune assays. *ROS burst and Ca^{2+} influx* – To test elicitor-induced oxidative burst, either leaf discs collected using a 4 mm biopsy punch or seedlings were transferred to white 96-well plates (one leaf disc or seedling per well) and equilibrated overnight in sterile ultrapure water (ROS) or coelenterazine solution (Ca^{2+}) . In the following day, the equilibration solution was removed and replaced with a solution containing 100 µg/mL - 2 mg/mL of COM, COM II, HPA or SM in 0.5 % (v/v) DMSO in MiliQ water; cutin in MiliQ water; or 100 nM (flg22 and Pep1) in MiliQ water, each mixed with 1 mM luminol, and 10 µg/mL HRP.

Luminescence was detected and measured for 30 - 45 min using a Photek system equipped with a photon counting camera (leaf discs) or a Tecan Spark microplate reader (seedlings).

MAPK activation – For MAPK activation assays 14-day-old seedlings were used. The growth media was removed by inverting the plate on clean paper towels. Seedlings were then treated for 10 min with 1 mL of 3 mg/mL of COM and COM II in 0.5 % DMSO in MiliQ water, 2 mg/mL cutin or suberin in MiliQ water, 100 nM flg22 and corresponding mock solutions. Two seedlings per treatment were dried on clean paper towels, subsequently transferred to 1.5 mL tubes and instantly frozen in liquid nitrogen. All treated seedlings were stored at -80 °C until further use.

Frozen seedlings were then pulverized using a nitrogen-cooled plastic micropestle. To the pulverized tissue, 150 µL of extraction buffer containing

50 mM Tris-HCl pH 7.5, 150 mM NaCl, 2 mM EDTA, 10 %(v/v) glycerol, 2 mM DTT, 1 %(v/v) Igepal, and supplemented with protease and phosphatase inhibitors (equivalent to Sigma-Aldrich plant protease inhibitor cocktail and phosphatase inhibitor cocktails #2 and #3) was added. The tissue was then ground at 1800 rpm using an automatic stirrer fitted with a plastic micropestle. The tubes were centrifuged at 15,000 *g* for 20 min at 4 °C in a refrigerated microcentrifuge. After centrifugation, 50 µL of extract were transferred to a fresh 1.5 mL eppendorf tube. Samples were prepared for SDS-PAGE by heating at 80 °C for 10 min in the presence of 6x SDS loading buffer and 100 mM DTT.

Proteins were loaded to a 12 % (v/v) polyacrylamide gels, separated at 120 V for ≅ 120 min and subsequently transferred to a PVDF membrane at 100 V for 90 min at 4 °C. Membranes were then blocked for 2 h at room temperature or overnight at 4 °C in 5 %(w/v) milk in Tris buffered saline (50 mM Tris-HCl pH 7.4, 150 mM NaCl; TBS) containing 0.1 %(v/v) Tween-20 (TBS-T). Blots were probed in a 1:4000 dilution of the NEB anti-p42/p44-erk primary antibody in 5 % BSA in TBS-T for 2 h, followed by washing 4 times for 10 min each in TBS-T. Blots were then probed with a 1:10000 dilution of anti-rabbit secondary antibody in 5 % milk in TBS-T for 1 h, followed by washing 3 times for 5 min each in TBS-T. Finally, blots were washed for 5 min in TBS and treated with either standard ECL substrate or SuperSignal West Femto high sensitivity substrate (ThermoFisher Scientific). Blots were imaged using a Bio-Rad ChemiDoc Imaging System (Bio-Rad Laboratories).

RNA Extraction and Sequencing. For RNA-seq experiments, 14-day-old seedlings were grown as described above. After nine days of growth in liquid MS medium supplemented with 1 % sucrose, the medium was removed from the wells and replaced with 600 µL of fresh liquid MS per well. The following day, 400 µl of 3 mg/mL of COM in 0.5 % DMSO in MiliQ water or the corresponding mock solution were added to each well. Seedlings were treated

for 10 min and then two wells, for a total of four seedlings were collected and instantly frozen in liquid nitrogen. In total, four biological replicates were generated for each treatment (COM and mock) and stored at -80 ºC for further processing.

Frozen seedlings were pulverized while frozen using a Spex SamplePrep Geno Grinder 2010 at 1500 rpm for 90 s. Total RNA was extracted at 4 ºC from two ground seedlings as previously described[36] by addition of 900 µL of TRI reagent (Ambion) and 200 µL of chloroform, recovery of 400 µL from the aqueous phase, precipitation with 500 µL of isopropanol and washing with 70 % ethanol. All samples were then solubilized in 30 µL of RNase-free water. Samples were subsequently subjected to DNase treatment using a TURBO DNA-free Kit (Ambion) according to manufacturer's instructions. The reaction mix was incubated at 37 ºC for 30 min, after which the inactivation reagent was added and incubated for 5 min at room temperature. After centrifugation the supernatant was transferred to a new tube. Quantification and quality assessment of all RNA samples were evaluated on a TapeStation (Agilent) and RNA sequencing performed by the Beijing Genomics Institute (BGI).

RNA-seq data processing. For paired-end RNA sequencing (RNA-seq), libraries were generated at BGI according to the DNBSEQ stranded mRNA library system. Eight samples were indexed and sequenced using the DNBseq™ sequencing platform (20 million reads per sample). Generated FastQ files were analyzed with FastQC, and any low-quality reads were trimmed with Trimmomatic[37].

All libraries were aligned to the *A. thaliana* genome assembly TAIR10 with gene annotations from Ensembl Plants v.49 using the HISAT2 v.2.1.0 pipeline[38] followed by read counts with HTSeq v. 0.13.5[39]. All RNA-seq experiments were carried out with four biological replicates. Differential expression analysis, and quality control principal-component analysis (PCA) and MA plots were generated using the DESeq2 v.1.30.0 R package[40]. The

genes that showed |log2| > 1-fold changes in expression with an adjusted P value below 0.05 are defined as significantly differentially expressed genes (DEGs) in this analysis. Transcript abundance was defined as transcripts per kilobase million (TPM). Gene Ontology enrichment of the differentially expressed genes was performed with the topGO v.2.42.0 R package, using the Fisher exact test to attain significantly enriched categories.

Comparative analysis of transcriptome modification upon elicitor treatment. Differentially expressed gene lists in response to seven elicitors (3-OH-FA, CO8, elf18, flg22, nlp20, OGs, Pep1) upon treatment under similar conditions as COM were obtained from Bjornson, *et al*. (2021)[27]. This study followed a time course from 5 min to 3 h post-elicitation: a gene list was obtained for each elicitor with genes significantly induced at any time. Abiotic stress treatment analysis for seven abiotic stresses (heat, cold, drought, salt, high osmolarity, UV-B light, wounding) was also obtained from Bjornson, *et al.* (2021), based on ATH1 microarray experiments presented in Killian, *et al*. 2007[41]. This study followed a time course from 5 min to 12 h post-elicitation: a gene list was obtained for each elicitor with genes significantly induced at any time up to 3 h. Comparisons and visualizations among differentially expressed genes were performed in R using the tools of the tidyverse v.1.3.1 package[42]. Spearman correlation among log_2 (fold changes) for treatments was calculated using the Hmisc package in R v.4.5-0) and visualized using the corrplot package v.0.89. Annotation data for genes induced specifically by COM was obtained from the *Arabidopsis* information resource (TAIR) via Bioconductor package org.At.tair.db v.3.10.0.

Quantitative analyses of total carbohydrate content. To evaluate the sugar moiety content of cutin purified using ionic liquids and oligomeric mixtures derived from its controlled depolymerization, all samples were subjected to an acid hydrolysis (1 M H_2SO_4 in methanol) for 4h at 90 ºC. The hydrolysable sugars were recovered in the supernatant through centrifugation

(18514 *g*, 4 °C, 20 minutes) and the pH was neutralized using 5 M NaOH in water. All samples were dried under a flux of nitrogen at room temperature. Quantification of carbohydrates in the dried hydrolysates was performed using the total carbohydrate assay kit from Sigma-Aldrich according to the manufacturer's instructions. The samples were analyzed in triplicates.

NMR characterization of cutin and cutin oligomeric mixtures. NMR spectra of cutin and cutin oligomeric mixtures (COMs) resulting from its hydrolysis were recorded using an Avance III 800 CRYO (Bruker Biospin, Rheinstetten, Germany). All NMR spectra (^{1}H, ^{1}H-^{1}H COSY, ^{1}H-^{13}C HSQC, ^{1}H-^{13}C HMBC) were acquired in DMSO-d_6 using 5 mm-diameter NMR tubes, at 60 °C as follows: 20 mg of cryomilled cutin or 15 mg of COMs in 400 µL of DMSO-d_6. For quantification purposes, 1.25 mg of benzene (internal standard) was added to each sample. MestReNova, Version 11.04-18998 (Mestrelab Research, S.L.) was used to process the raw data acquired in the Bruker spectrometers.

GC-MS characterization of cutin and cutin oligomeric mixtures. To release the hydrolysable constituents, all cutin derived samples were treated with a solution of 0.5 M NaOH in methanol:water (1:1 [v/v]) at 95 °C for 4 h. The mixture was cooled to room temperature and acidified to pH 3–3.5 with HCl 1 M, spiked with a known concentration of hexadecane (internal standard), and extracted three times with dichloromethane. Sodium sulphate anhydrous was added to the organic phase to remove water and concentrated under a nitrogen flow. The non-hydrolysable fraction was recovered by filtration (cellulose nitrate filter) and subsequently washed, dried, and weighted (recalcitrance). The dried combined organic extracts were sequentially derivatized: firstly, 2.0 M (trimethylsilyl)diazomethane in hexane, mixed in a methanol:toluene 2.5:1 solution (3:2); and secondly, N,O-bis(trimethylsilyl)trifluoroacetamide containing 1 % (v/v) of trimethylchlorosilane in pyridine (5:1), both steps performed for 30 min at

90 °C. The derivatives were then analyzed by GC-MS (Agilent: 7820A GC and 5977B quadrupole MS; HP-5MS column) as follows: ramp temperature 80 °C, then 2 °C·min^{-1} to 310 °C for 15 min. The MS scan mode, with source at 230 °C and electron impact ionization (EI+, 70 eV) was used for all samples. Data acquisition was accomplished by MSD ChemStation (Agilent Technologies); compounds were identified based on the equipment spectral library (Wiley-National Institute of Standards and Technology) and quantified using external standards of the major classes of the aliphatic monomers (heptadecanoic acid, hexadecanedioic acid and pentadecanol). All samples were analyzed in triplicates, each with technical duplicates.

Thin Layer Chromatography (TLC)-based characterization of cutin oligomeric mixtures. Both cutin oligomeric mixtures (COMs) and the cutin from which they resulted were characterized by TLC on plates coated with Merck Silica gel 60 F_{254} and the retardation factor (rf) for each obtained fraction calculated. Samples were eluted on benzene/ethyl ether (1:1 v/v) solution. Alcohols, phenols, alkenes and carbonyl groups were detected with a phosphomolybdic acid universal stain solution, revealing on heating, blue-black spots on yellow green. Organic acids (*e.g.* carboxylic acids) were revealed with a solution of bromocresol green, with a few drops of 0.1 M sodium hydroxide, as yellow spots on a green background. UV detection at two different wavelengths (254 and 365 nm) was used to evaluate the presence of aromatic compounds.

Acknowledgements

The authors are thankful to Pedro Lamosa (ITQB NOVA) for support with the NMR analyses.

Funding

We acknowledge funding from the European Research Council through grant ERC 2014-CoG-647928 and from Fundação para a Ciência e Tecnologia (FCT) by Project MOSTMICRO ITQB with refs UIDB/04612/2020 and UIDP/04612/2020 to Silva Pereira's lab and from the University of Zurich to the Zipfel's lab. The NMR data were acquired at CERMAX, ITQB-NOVA, Oeiras, Portugal with equipment funded by FCT. C.J.S.M. is grateful to Aralab, Portugal, for the PhD contract 06/PlantsLife/2017; to EMBO through the short-term fellowship 8003 and contract financed by the University of Zurich.

References

1. Delwiche, C. F. & Cooper, E. D. The evolutionary origin of a terrestrial flora. *Current Biology* vol. 25 R899–R910 (2015).
2. Waters, E. R. Molecular adaptation and the origin of land plants. *Mol. Phylogenet. Evol.* **29**, 456–463 (2003).
3. Fich, E. A., Segerson, N. A. & Rose, J. K. C. The Plant Polyester Cutin: Biosynthesis, Structure, and Biological Roles. *Annu. Rev. Plant Biol.* **67**, 207–233 (2016).
4. Martin, L. B. B. & Rose, J. K. C. There's more than one way to skin a fruit: formation and functions of fruit cuticles. *J. Exp. Bot.* **65**, 4639–4651 (2014).
5. Yeats, T. H. & Rose, J. K. C. The formation and function of plant cuticles. *Plant Physiology* vol. 163 5–20 (2013).
6. Philippe, G. *et al.* Plant cuticle embedded polysaccharides exhibit specific structural features. *New Phytol* (in press) (2020).
7. Xin, A. & Fry, S. C. Cutin:xyloglucan transacylase (CXT) activity covalently links cutin to a plant cell-wall polysaccharide. *J. Plant Physiol.* **262**, 153446 (2021).
8. Longhi, S. & Cambillau, C. Structure-activity of cutinase, a small lipolytic enzyme. *Biochimica et Biophysica Acta - Molecular and Cell Biology of Lipids* vol. 1441 185–196 (1999).
9. Kolattukudy, P. E., Rogers, L. M., Li, D., Hwang, C. S. & Flaishman, M. A. Surface signaling in pathogenesis. *Proc. Natl. Acad. Sci. U. S. A.* **92**, 4080–4087 (1995).
10. Zipfel, C. Plant pattern-recognition receptors. *Trends in Immunology* vol. 35 345–351 (2014).
11. Kauss, H., Fauth, M., Merten, A. & Jeblick, W. Cucumber hypocotyls respond to cutin monomers via both an inducible and a constitutive H2O2-generating system. *Plant Physiol.* **120**, 1175–1182 (1999).

12. Kim, T. H., Park, J. H., Kim, M. C. & Cho, S. H. Cutin monomer induces expression of the rice OsLTP5 lipid transfer protein gene. *J. Plant Physiol.* **165**, 345–349 (2008).
13. Park, J. H., Suh, M. C., Kim, T. H., Kim, M. C. & Cho, S. H. Expression of glycine-rich protein genes, AtGRP5 and AtGRP23, induced by the cutin monomer 16-hydroxypalmitic acid in Arabidopsis thaliana. *Plant Physiol. Biochem.* **46**, 1015–1018 (2008).
14. Buxdorf, K. *et al.* The transcription factor SlSHINE3 modulates defense responses in tomato plants. *Plant Mol. Biol.* **84**, 37–47 (2014).
15. Serrano, M., Coluccia, F., Torres, M., L'Haridon, F. & Métraux, J.-P. The cuticle and plant defense to pathogens. *Front. Plant Sci.* **0**, 274 (2014).
16. Hou, S., Liu, Z., Shen, H. & Wu, D. Damage-Associated Molecular Pattern-Triggered Immunity in Plants. *Front. Plant Sci.* **10**, (2019).
17. Beneloujaephajri, E., Costa, A., L'Haridon, F., Métraux, J.-P. & Binda, M. Production of reactive oxygen species and wound-induced resistance in Arabidopsis thaliana against Botrytis cinereaare preceded and depend on a burst of calcium. *BMC Plant Biol. 2013 131* **13**, 1–10 (2013).
18. Moreira, C. J. S. *et al.* An ionic liquid extraction that preserves the molecular structure of cutin shown by nuclear magnetic resonance. *Plant Physiol.* **184**, (2020).
19. Bento, A. *et al.* Quantification of structure-property relationships for plant polyesters reveals suberin and cutin idiosyncrasies. *ACS Sustain. Chem. Sustain.* **Submitted**, (2021).
20. Zhu, H., Jia, Z., Trush, M. A. & Li, Y. R. A Highly Sensitive Chemiluminometric Assay for Real-Time Detection of Biological Hydrogen Peroxide Formation. *React. Oxyg. species (Apex, N.C.)* **1**, 216 (2016).

21. Huffaker, A., Pearce, G. & Ryan, C. A. An endogenous peptide signal in Arabidopsis activates components of the innate immune response. *Proc. Natl. Acad. Sci. U. S. A.* **103**, 10098–10103 (2006).
22. Mithöfer, A. & Mazars, C. Aequorin-based measurements of intracellular Ca 2+-signatures in plant cells. *Biol. Proced. Online* • **4**, 105–118 (2002).
23. Willmann, R., Haischer, D. J. & Gust, A. A. Analysis of MAPK Activities Using MAPK-Specific Antibodies. *Methods Mol. Biol.* **1171**, 27–37 (2014).
24. Felix, G., Duran, J. D., Volko, S. & Boller, T. Plants have a sensitive perception system for the most conserved domain of bacterial flagellin. *Plant J.* **18**, 265–276 (1999).
25. Tang, D., Wang, G. & Zhou, J.-M. Receptor Kinases in Plant-Pathogen Interactions: More Than Pattern Recognition. *Plant Cell* **29**, 618–637 (2017).
26. Macho, A. P. & Zipfel, C. Plant PRRs and the activation of innate immune signaling. *Molecular Cell* vol. 54 263–272 (2014).
27. M, B., P, P., T, N. & C, Z. The transcriptional landscape of Arabidopsis thaliana pattern-triggered immunity. *Nat. plants* **7**, 579–586 (2021).
28. Ferrari, S. *et al.* Oligogalacturonides: plant damage-associated molecular patterns and regulators of growth and development. *Front. Plant Sci.* **0**, 49 (2013).
29. de Azevedo Souza, C. *et al.* Cellulose-derived oligomers act as damage-associated molecular patterns and trigger defense-like responses. *Plant Physiol.* **173**, 2383–2398 (2017).
30. Mélida, H. *et al.* Arabinoxylan-Oligosaccharides Act as Damage Associated Molecular Patterns in Plants Regulating Disease Resistance. *Front. Plant Sci.* **0**, 1210 (2020).
31. Rebaque, D. *et al.* Cell wall-derived mixed-linked β-1,3/1,4-glucans trigger immune responses and disease resistance in plants. *Plant J.* **106**, 601–615 (2021).

32. Graça, J. & Lamosa, P. Linear and Branched Poly(ω-hydroxyacid) Esters in Plant Cutins. *J. Agric. Food Chem.* **58**, 9666–9674 (2010).
33. Roux, M. *et al.* The Arabidopsis Leucine-Rich Repeat Receptor–Like Kinases BAK1/SERK3 and BKK1/SERK4 Are Required for Innate Immunity to Hemibiotrophic and Biotrophic Pathogens. *Plant Cell* **23**, 2440 (2011).
34. Ranf, S., Eschen-Lippold, L., Pecher, P., Lee, J. & Scheel, D. Interplay between calcium signalling and early signalling elements during defence responses to microbe- or damage-associated molecular patterns. *Plant J.* **68**, 100–113 (2011).
35. Xin, X.-F. *et al.* Bacteria establish an aqueous living space in plants crucial for virulence. *Nature* **539**, 524 (2016).
36. Shi, H. & Bressan, R. RNA Extraction. *Methods Mol. Biol.* **323**, 345–348 (2006).
37. Bolger, A. M., Lohse, M. & Usadel, B. Trimmomatic: a flexible trimmer for Illumina sequence data. *Bioinformatics* **30**, 2114–2120 (2014).
38. Kim, D., Langmead, B. & Salzberg, S. L. HISAT: a fast spliced aligner with low memory requirements. *Nat. Methods 2015 124* **12**, 357–360 (2015).
39. Anders, S., Pyl, P. T. & Huber, W. HTSeq—a Python framework to work with high-throughput sequencing data. *Bioinformatics* **31**, 166–169 (2015).
40. Love, M. I., Huber, W. & Anders, S. Moderated estimation of fold change and dispersion for RNA-seq data with DESeq2. *Genome Biol. 2014 1512* **15**, 1–21 (2014).
41. Kilian, J. *et al.* The AtGenExpress global stress expression data set: protocols, evaluation and model data analysis of UV-B light, drought and cold stress responses. *Plant J.* **50**, 347–363 (2007).
42. Wickham, H. *et al.* Welcome to the Tidyverse. *J. Open Source Softw.* **4**, 1686 (2019).

ANNEX

This annex contains the Supplementary Material published along the main body of the research paper which composes Chapter IV. This intends to allow better and easier understanding of the methodologies and analyses performed.

Supplementary Data

The following supplementary materials are available.

Table S1 – List of compounds tested in the initial screening for immune eliciting potential of cutin derived molecules. The library was composed by commercially available model compounds (CMCs), the polyesters cutin and suberin extracted from different plant sources, cutin oligomeric mixtures (COMs) generated by partial depolymerization of the polymer, and soups of monomers (SMs) resulting from extensive depolymerization of cutin and suberin.

Code	**Compound**	**Observations**
CMC1	Glycerol	Alcohol
CMC2	16-Hydroxypalmitic acid	C_{16}
CMC3	Hexadecanedioic acid	C_{16}
CMC4	Linoleic acid	C_{16}
CMC5	Oleic acid	C_{16}
CMC6	Palmitic acid	C_{16}
CMC7	Aleuritic acid	C_{16}
CMC8	Glyceryl stearate	C_{18}
CMC9	Glyceryl tristearate	C_{18}
CMC10	12-hydroxystearic acid	C_{18}
CMC11	Stearic acid	C_{18}
CMC12	Octanedioic acid	C_{18}
Cutin T	Cutin Tomato ‘Roma’	Ionic liquid isolated cutin
Cutin TC	Cutin Tomato Pomace (Compal)	Ionic liquid isolated cutin
Cutin MT	Cutin Tomato Micro-Tom	Ionic liquid isolated cutin
COM T	Cutin Oligomeric Mixture Tomato ‘Roma’	Methanolysis
COM TC	Cutin Oligomeric Mixture Tomato Pomace (Compal)	Methanolysis
COM MT	Cutin Oligomeric Mixture Tomato Micro-Tom	Methanolysis
SM T	Cutin Monomeric Mixture Tomato ‘Roma’	Total alkaline hydrolysis
SM TC	Cutin Monomeric Mixture Tomato Pomace (Compal)	Total alkaline hydrolysis
SM MT	Cutin Monomeric Mixture Tomato Micro-Tom	Total alkaline hydrolysis
Sub C	Suberin Cork Oak	Ionic liquid isolated suberin
SM Sub C	Suberin Monomeric Mixture Cork Oak	Total alkaline hydrolysis

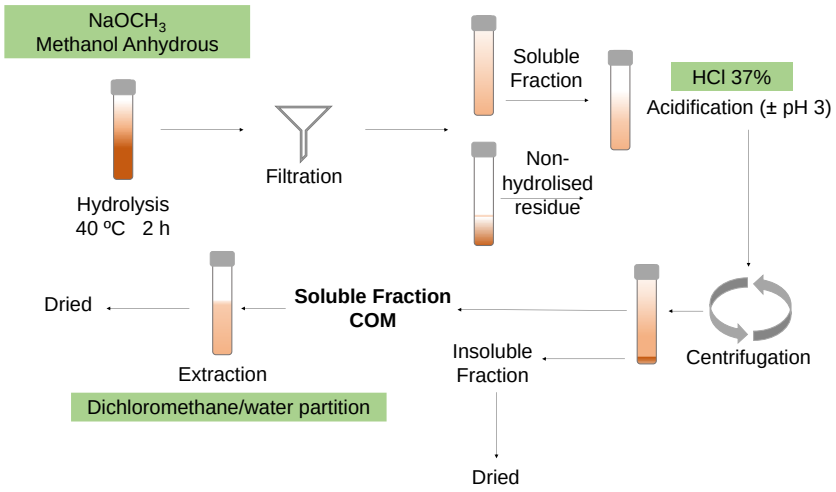

Figure S1 – Schematic representation of the hydrolysis reaction performed to cutins extracted from different types of tomato to obtain cutin oligomeric mixtures (COM).

Table S2 – Major results obtained from all the tests performed during the initial screening of the library of potential elicitors of immunity on the three model plants *Solanum lycopersicum*, *Nicotiana benthamiana* and *Arabidopsis thaliana*. Plants not tested are labelled as *n.t.* and responses not detected after treatment are labelled as *n.d.*.

Model Plant / **Test**	*Solanum lycopersicum*	*Nicotiana benthamiana*	*Arabidopsis thaliana*
ROS burst	**CUTIN**	*n. d.*	*n. d.*
Ca^{2+} influx	*n. t.*	**COM**	**COM**
MAPK activation	*n. t.*	*n. t.*	**CUTIN / SUBERIN**

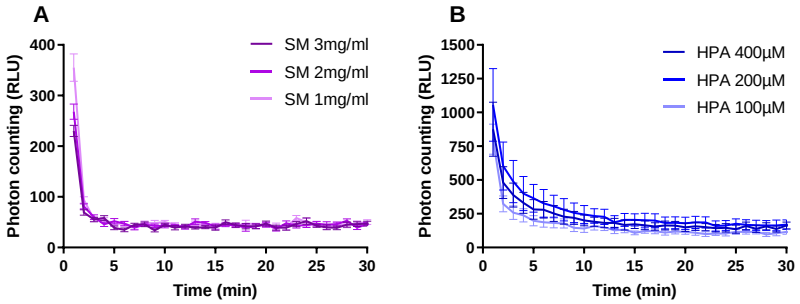

Figure S2 – Luminescence-based detection of apoplastic ROS: in *Arabidopsis thaliana* Col-0 seedlings upon treatment with 1-3 mg/mL of soup of monomers resulting from the hydrolysis of tomato pomace cutin (A); and upon treatment with 100-400 µM of the cutin monomer HPA (B).

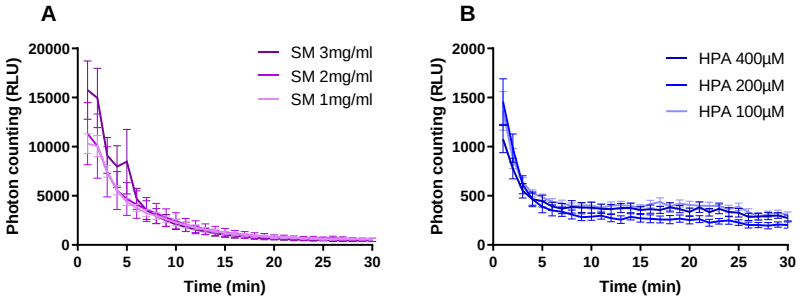

Figure S3 – Luminescence-based detection of calcium influx in *Arabidopsis thaliana* seedlings expressing the calcium reporter aequorin, upon treatment with 1-3 mg/mL of cutin derived soup of monomers (A) and 100-400 µM of the cutin monomer HPA (B).

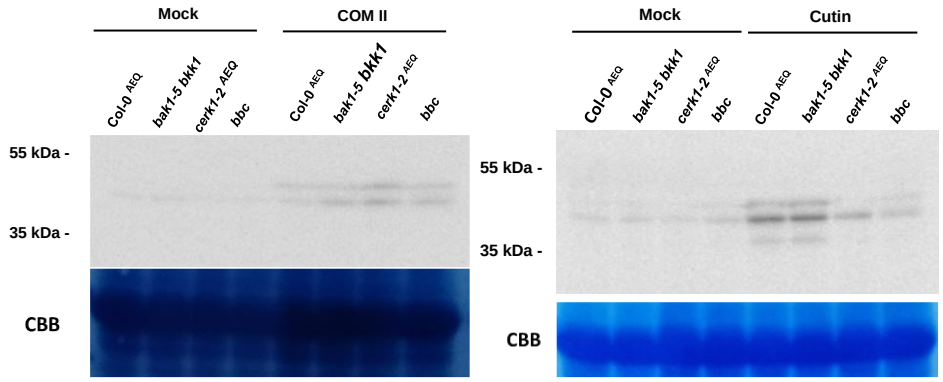

Figure S4 – Western blot evaluation of MAPK activation in 14-day-old *Arabidopsis thaliana* seedlings from wild type Col-0 and the *bak1-5 bkk1, cerk1-2 and bbc* mutants, upon treatment with 3 mg/mL of COM II or cutin against the corresponding mock control.

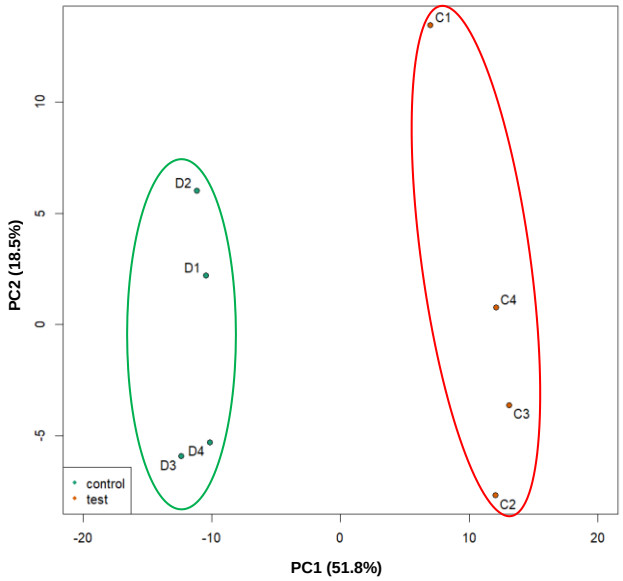

Figure S5 – Principal components analysis performed to all eight samples used for the RNA-seq experiment. The figure depicts the first two main components. Ellipses enclose the regions of the space comprising the four biological replicates of each treatment: COM (C1-C4) and 0.5 % DMSO in water – mock control (D1-D4).

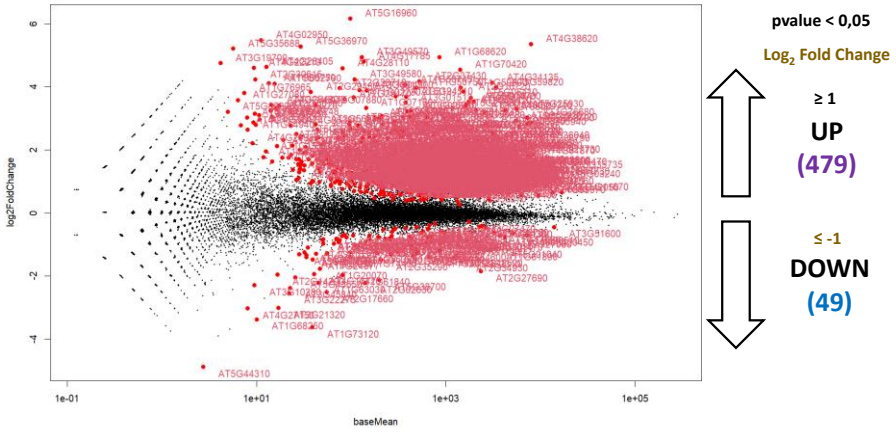

Figure S6 – MA plot representing the statistically significant (adjusted *p*value < 0,05) differentially expressed genes (Log_2 fold change ≤ -1 or ≥ 1), in *Arabidopsis thaliana* Col-0 plants upon treatment with COM for 30 min.

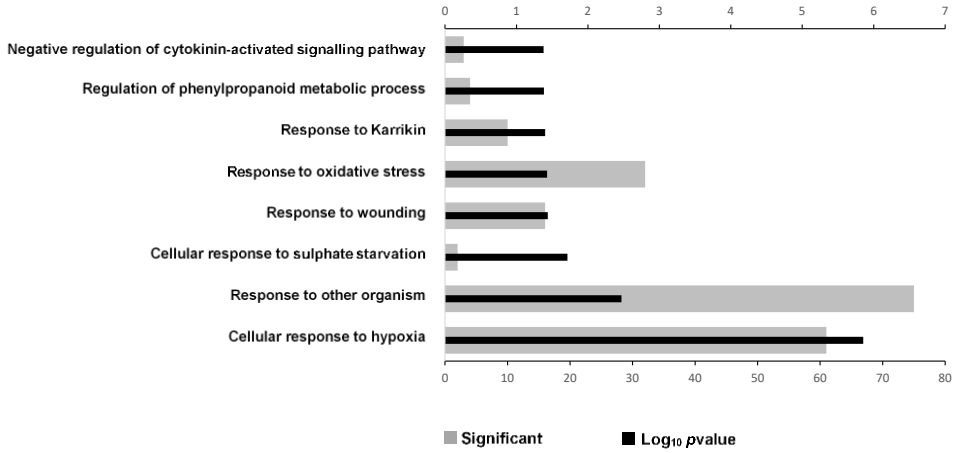

Figure S7 – GO term enrichment analysis performed for the genes that showed upregulation upon treatment with COM for 30 min.

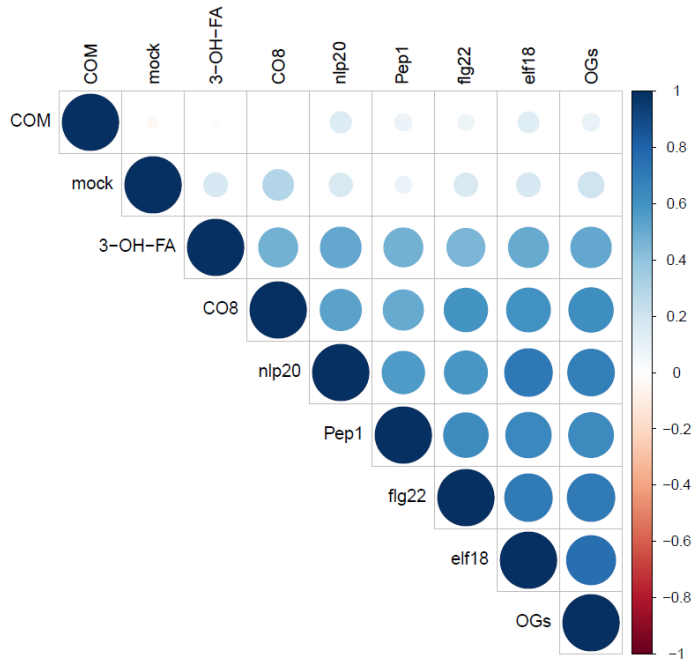

Figure S8 – Correlation plot depicting changes in gene expression between all the elicitors evaluated in the comparative analysis: all transcriptomes compared at 30 min post treatment.

Table S3 – List of genes uniquely induced by the COM treatment after comparison with seven other different elicitors of plant immunity, but also induced by one or more different of abiotic stress conditions. Genes for which there was no attributed name or description on the TAIR database were labelled as NA, and genes which were either not represented on the ATH1 microarray or were represented by a probe with multiple gene matches are labelled ND.

Gene	Log_2 FC	padj	ASI	Name	Short Description
AT3G27880	3.3280	5.38E-66	1	NA	Hypothetical protein
AT3G04200	3.0262	3.89E-03	1	NA	C2H2-type zinc finger family protein
AT2G20670	2.3084	1.01E-05	1	NA	Sugar phosphate exchanger
AT5G65790	2.1720	1.12E-09	1	ATMYB68	Putative MYB transcription factor.
AT2G27010	2.0167	8.85E-11	1	CYP705A9	Member of CYP705A
AT1G67030	1.8268	3.82E-06	1	ZFP6	Zinc finger protein containing only a single zinc finger.
AT1G31050	1.7533	2.28E-05	1	PFA1	Pericycle factor type-a 1
AT4G21510	1.7418	4.24E-14	1	ATFBS2	F-box family protein
AT1G58170	1.6905	1.11E-02	1	NA	Disease resistance-responsive family protein
AT5G42580	1.5640	3.99E-02	1	CYP705A12	Member of the cytochrome P450 family
AT1G22110	1.5603	2.04E-05	1	NA	Structural constituent of ribosome
AT2G36050	1.4361	2.24E-09	1	ATOFP15	Ovate family protein 15
AT1G67340	1.4226	1.19E-07	1	NA	HCP-like superfamily protein with MYND-type zinc finger
AT1G35515	1.3600	9.30E-03	1	HOS10	Nuclear localized R2R3-type MYB transcription factor
AT2G17080	1.2715	1.55E-04	1	NA	Hypothetical protein
AT3G14660	1.1079	8.28E-05	1	CYP72A13	Putative cytochrome P450
AT1G17360	1.0928	9.71E-05	1	NA	Protein phosphatase 1 regulatory subunit-like protein
AT5G07870	3.5385	7.84E-83	2	NA	HXXXD-type acyl-transferase family protein
AT5G05220	3.2064	4.63E-02	2	NA	Hypothetical protein
AT3G28740	2.6127	1.80E-04	2	CYP81D11	Member of the cytochrome p450 family.
AT5G07860	2.6096	3.66E-59	2	NA	HXXXD-type acyl-transferase family protein
AT4G34138	2.3470	8.31E-11	2	UGT73B1	UDP-glucosyl transferase 73B1
AT3G49690	1.9282	2.73E-07	2	ATMYB84	Putative homolog of the Blind gene in tomato.
AT1G54120	1.7080	7.66E-04	2	NA	Hypothetical protein
AT2G39330	1.5299	2.13E-02	2	JAL23	Jacalin-related lectin 23
AT1G02205	1.4895	3.06E-02	2	CER1	Gene associated with production of stem epicuticular wax
AT5G48010	1.4732	5.37E-05	2	AtTHAS1	Oxidosqualene cyclase involved in the biosynthesis of thalianol.
AT3G13310	1.4728	3.88E-13	2	DJC66	Chaperone DnaJ-domain superfamily protein
AT3G03840	1.3663	4.61E-03	2	SAUR27	SAUR-like auxin-responsive protein family
AT5G67420	1.2773	8.30E-03	2	ASL39	LOB-domain protein involved in nitrogen metabolism and leaf morphogen
AT5G53500	1.2322	1.54E-16	2	NA	Transducin/WD40 repeat-like superfamily protein
AT1G18330	1.2301	8.86E-03	2	EPR1	Early phytochrome responsive 1
AT1G68440	1.2035	6.49E-19	2	NA	Transmembrane protein
AT3G16800	1.1923	9.57E-03	2	EGR3	Regulates microtubule organization
AT1G15550	1.1772	1.52E-02	2	ATGA3OX1	Involved in the gibberellic acid biosynthetic pathway
AT4G05070	1.0033	1.73E-03	2	WIP2	Member of the wound-induced polypeptide (WIP) family
AT3G59940	2.7494	8.68E-21	3	KFB50	Member of the F-box KISS ME DEADLY (KMD) protein family
AT1G68360	1.7719	2.77E-02	3	GIS3	Nuclear localized member of the C2H2 family of transcription factors
AT2G30130	1.6642	1.55E-05	3	ASL5	Gene similar to asymmetric leaves (AS)/lateral organ boundary (LOB) ger
AT5G16600	1.5649	3.06E-03	3	ATMYB43	Putative transcription factor (MYB43)
AT3G47600	1.5635	1.87E-09	3	ATMYB94	Putative transcription factor (MYB94)
AT1G78600	1.5492	3.70E-05	3	BBX22	Light-regulated zinc finger protein
AT1G21680	1.4751	1.29E-03	3	NA	DPP6 N-terminal domain-like protein
AT5G01820	1.3611	1.60E-03	3	ATCIPK14	CBL-interacting serine/threonine protein kinase
AT5G63970	1.2545	7.16E-04	3	RGLG3	Calcium-dependent phospholipid-binding protein
AT3G24310	2.5638	2.05E-08	4	ATMYB71	Snapdragon myb protein 305 homolog (myb)
AT5G54230	2.3699	3.64E-10	4	AtMYB49	Putative transcription factor (MYB49)
AT3G48510	1.9524	9.78E-04	5	AITR2	ABA-induced transcription repressor acting as feedback regulator in ABA
AT2G47890	1.5210	1.02E-07	5	NA	B-box type zinc finger protein with CCT domain
AT4G25480	3.4252	4.48E-04	6	ATCBF3	Member of the DREB subfamily A-1 of ERF/AP2 transcription factor famil
AT1G05100	2.6703	2.87E-17	6	MAPKKK18	Member of the MEKK subfamily
AT5G35688	5.2093	3.42E-03	ND	NA	Small protein with evidence of transcription or purifying selection
AT4G22210	4.6102	1.81E-02	ND	LCR85	Member of a family of small, secreted, cysteine rich proteins.
AT2G30615	4.2291	2.97E-03	ND	NA	F-box/LRR protein
AT1G10220	3.2335	2.69E-06	ND	ZCF37	NA
AT4G15248	3.0468	7.29E-03	ND	BBX30	B-box type zinc finger family protein
AT1G72490	2.3606	2.59E-09	ND	DRO1	Member of the IGT gene family with unknown function
AT2G26370	2.2571	2.03E-02	ND	NA	MD-2-related lipid recognition domain-containing protein
AT5G63595	2.1890	2.26E-10	ND	ATFLS4	Flavonol synthase 4
AT4G37700	1.9244	1.77E-02	ND	NA	Hypothetical protein
AT1G64950	1.7784	5.54E-18	ND	CYP89A5	Member of CYP89A
AT5G65030	1.7624	3.92E-02	ND	NA	Nitric oxide synthase-interacting protein
AT2G28160	1.6114	3.29E-03	ND	ATBHLH029	Putative transcription factor regulating iron uptake responses
AT2G30230	1.3264	1.96E-03	ND	NA	6,7-dimethyl-8-ribityllumazine synthase
AT2G23690	1.3238	1.10E-03	ND	NA	HTH-type transcriptional regulator
AT4G06534	1.0011	3.85E-02	ND	NA	Transmembrane protein
AT4G02950	5.4744	1.15E-04	ND	NA	Ubiquitin family protein
AT5G23360	2.4024	6.64E-05	ND	NA	GRAM domain-containing protein / ABA-responsive protein-related
AT5G23350	1.9571	4.41E-04	ND	NA	GRAM domain-containing protein / ABA-responsive protein-related
AT1G05660	1.3890	1.14E-02	ND	NA	Pectin lyase-like superfamily protein

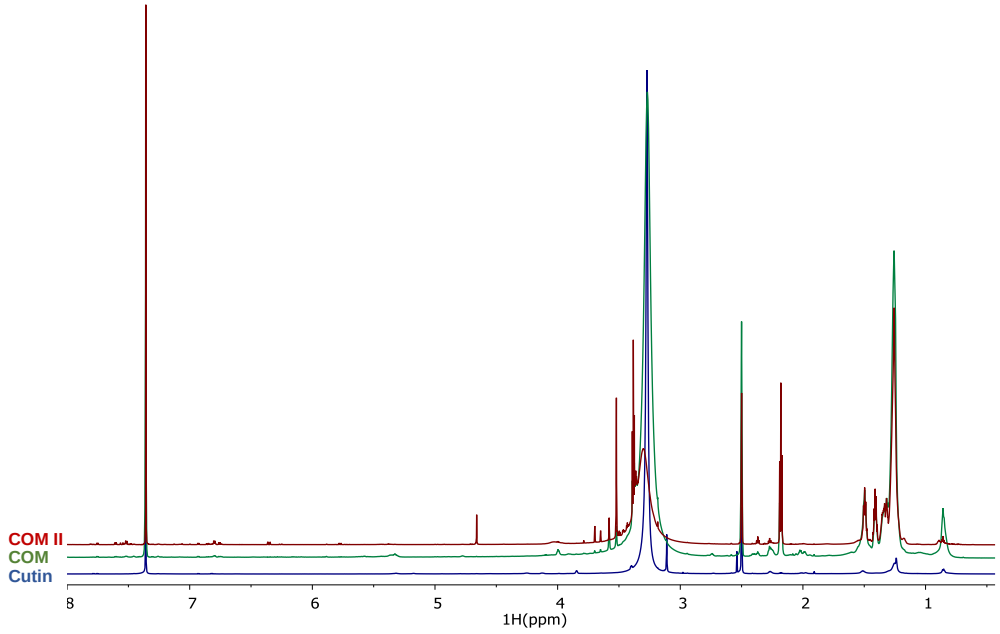

Figure S9 – Wide-ranging ^{1}H NMR spectral characterization of cutin and cutin oligomeric mixtures.

Table S4 – Chromatographic characterization of cutin and cutin oligomeric mixtures. Rf values of fractions separated on TLC plates were calculated for each sample after revelation with two different staining solutions. Images of the plates after staining are presented to illustrate differences between samples.

Compound	Bromocresol Green	Phosphomolybdic acid	UV (254/365 nm)
Cutin	-	-	-
COM	0,70 ± 0,07 0,45 ± 0,02 0,07 ± 0,00	0,75 ± 0,02 0,56 ± 0,02 0,46 ± 0,02 0,36 ± 0,04 0,27 ± 0,02 0,12 ± 0,00	0,75 ± 0,02 **0,58 ± 0,02** 0,51 ± 0,00 **0,41 ± 0,02** 0,35 ± 0,02 0,20 ± 0,00 0,11 ± 0,00
COM II	0.07 ± 0.00	-	**0,56 ± 0,02** **0,45 ± 0,01** 0,33 ± 0,05 0,22 ± 0,03 0,13 ± 0,00

CUT COM COM II

CUT COM COM II

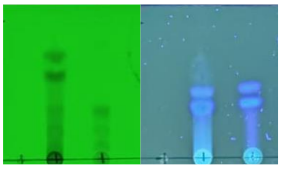

CUT COM COM II CUT COM COM II

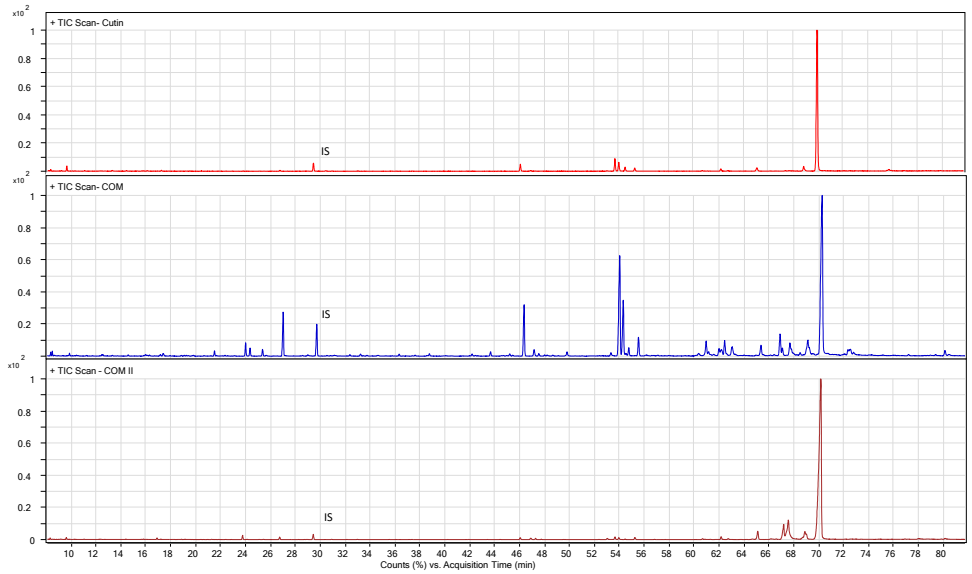

Figure S10 – GC-MS characterization of cutin and cutin oligomeric mixtures. Representative chromatographic profile of each sample after total depolymerization and derivatization. The peak corresponding to the internal standard (hexadecane) is labelled as IS.

CHAPTER V

Chapter V contains an integrated discussion of the contents of this thesis.

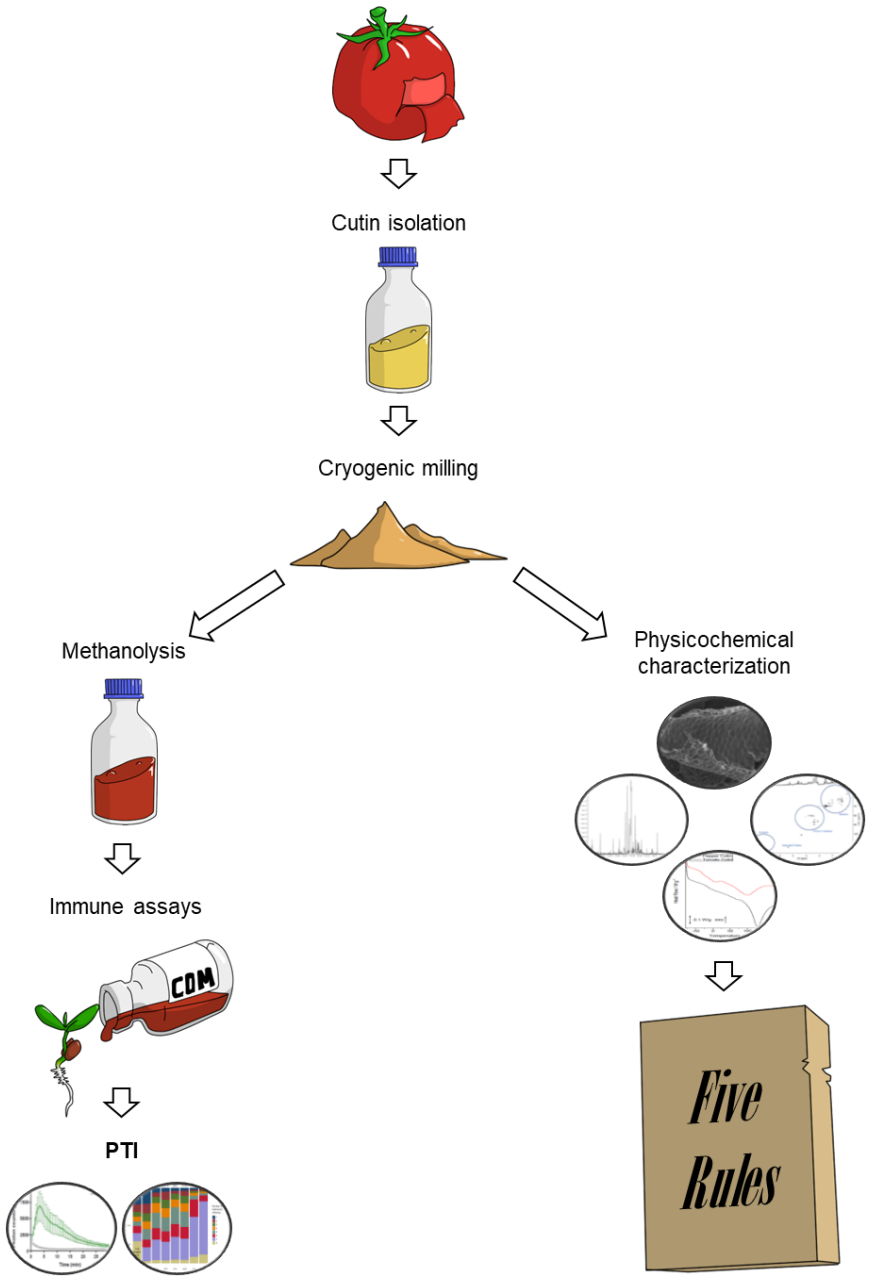

Discussion and Future Perspectives

The first goal of this project was to establish a straightforward method to purify cutin preserving a near native polymeric backbone and devoid of cross contamination with unbound cell wall constituents. The traditionally accepted gold standard methods – enzymatic digestion of polysaccharides and solvent-based dewaxing - are time consuming (days to weeks). Also, the removal of the polysaccharides may alter the cutin polymer; an increasingly relevant aspect due to recent reports suggesting that cutin might be anchored to the cell wall by chemical bonding to specific polysaccharides[1]. Notably, **the ionic liquid-based process developed in this thesis can be applied to rapidly isolate a cutin (hours) with similar quality to a cutin obtained through conventional methods**[2] (Chapter II). The ionic liquid capacity to hydrolyze different types of ester-containing compounds is very limited (Chapter II and III). Accordingly, we hypothesize that the liquid crystal environment created by the ionic liquid at 100 °C, results in the swelling of the plant cell walls, and hence separation of the cutin and the polysaccharide domains, with the latter being washed out together with all unbound components. This process was successfully used to purify cutin from tomato and pepper peels (Chapter II, III and IV).

Setting up an alternative cutin extraction method is inspiring new developments. For example, we are currently testing the suitability of this methodology to isolate cutin directly from industrial tomato pomaces (Rita Escórcio, PhD student). One important bottleneck of the industrial exploitation of natural polymers is that the heterogeneity of the raw material needs to be surpassed. Cutins isolated using the ionic liquid process display high chemical similarity, regardless of great chemical differences observed in the raw materials, currently provided by agro-industries located in Portugal and France. Current efforts focus on the exploitation of these cutins as a source of antimicrobial oligomers. In addition, the ionic liquid process showed great flexibility: following simple changes it can be applied to isolate different

plant polyesters from very distinct plant sources (Chapter III). The specificity of each plant polyester, namely type and degree of esterification of the polymer, anchoring in the cell wall and tissue localization, determines the isolation of polymeric particles (suberin from cork and potato peel) or the isolation of a polymeric continuum (cutin from tomato and pepper peels).

While the chosen ionic liquid – cholinium hexanoate – is not available commercially and its synthesis is costly, it constitutes a greener alternative compared to organic solvents used in the dewaxing process, which have negative ecological impacts. With the goal of reducing the ecological footprint of cutin industrial exploitation (used *e.g.* for coatings), our lab is testing the process scalability. Cholinium alkanoates were previously shown as environmentally benign and biodegradable, which added to their good solvent properties, makes them very attractive for industrial exploitation[3]. The usage of 'green' solvents for the valorization of industrial residues is aligned with the vision of the European Commission Green Deal (*e.g.* on recyclability and sustainable industrial development) and the United Nations Sustainable Development Goals (*e.g.* sustainable communities, responsible resource consumption and industrial innovation).

Inspired by approaches used for studying lignocellulosic materials[4], we decided to **use cryogenic milling to reduce the crystallinity and the particle size of cutin**. This strategy was applied systematically to the ionic liquid isolated cutins (Chapter II, III and IV) as well as directly to tomato peel (Chapter II). The cryogenically milled materials were then solubilized in DMSO-d_6, which allowed **for the first time to acquire solution NMR spectra of cutin**. The ability to look inside the macromolecular structure of cutin constitutes a remarkable achievement (*n.b.* a magnet of 800 MHz was used) allowing higher resolution than the previously used methods such as solid-state NMR and FTIR (discussed in Chapter I). Paradoxically it was through the use of such solid-state methodologies that we first collected information on the polymer esterification and reticulation levels that were

suggestive of the potential of the ionic liquid to obtain a near native cutin (Chapter II). However, clear evidence that the ionic liquid did not alter cutin structure was established only through the use of solution NMR, first through comparison of cutin upon and prior its isolation (Chapter II) and secondly through analysis of the ester-cleavage kinetics in model compounds (Chapter III). Importantly, the ability to solubilize directly cutin from a plant source (without any extraction) allows a direct analysis of the polymer as it exists *in planta*. In the particular case of cutin, alterations provoked by the ionic liquid seems virtually null; hence, our gold standard for cutin analysis still favors its isolation with the ionic liquid (reducing the interference by unbound components in its subsequent analysis) followed by structure analysis by NMR and monomeric analysis by GC-MS. We further **improved the NMR method to reach absolute quantification of esters** – the most critical linkage for the 3D organization of the polymer (Chapter III). The improvement of the sensitivity allowed us to detect and assign the signal corresponding to the secondary esters in both tomato and pepper cutin. Moreover, the use of an internal standard (benzene) allowed direct comparison of samples and precise quantification of total and secondary esters. Furthermore, the use of ^{31}P NMR allowed us to systematically compare the absolute quantities of free OH aliphatics associated with specific mutations, affecting cutin biosynthesis. This led to the observation that an increase in the free OH aliphatic content directly correlates with a decrease in the secondary ester content in cutins isolated from peels of Micro-Tom tomatoes.

The gold standard method used for the characterization of plant polyesters, indifferently of their plant source, developmental stage or tissue is GC-MS. Analyses of the hydrolysates, deal with major limitations: (i) there are regions of the polymer that cannot be hydrolyzed, and (ii) the fraction that is hydrolyzed comprises several non-assigned peaks. Despite these limitations, GC-MS still constitutes a powerful technique to identify building blocks and guide the identification of precursors (essential *e.g.* for the assignment of biosynthetic genes). Advances on mass spectrometry applicable for the study

of complex polymers will further support this technique as gold standard for answering specific questions[5] (some of which relevant for Chapter IV). However, it is known that compositional alterations in the polymer generated, for example, through mutations in particular genes, do not alter the GC-MS fingerprint, while they alter barrier properties. Such behavior can only be related to two main factors: the polymer macro-molecular arrangement is completely different, or the polymer is anchored in a different way to the underneath epidermal cell walls. Both aspects are increasingly relevant for plant scientists interested in understanding cutin multifunctionality *in planta*.

The methods I have established will certainly help to answer how the polyester is anchored to the cell wall; one aspect that was not fully explored on this thesis, but of which some initial steps were given. In collaboration with Rita Escórcio, we aim to identify the link, if any, between cutin and cell wall polysaccharides. For this, we are performing sequential isolation reactions of cutin from tomato pomace combining enzymatic reactions and different ionic liquids (*n.b.* some ionic liquids result in a cutin showing a WAXS diffractogram devoid of crystalline cellulose). The polysaccharide content in ionic liquid extracted cutins can be evaluated by different methods, *e.g.* as presented in Chapter III by means of immunoblotting or colorimetric detection after hydrolysis with a specific kit for total carbohydrate quantification. Both quantification strategies demonstrate a similar trend, including between wild-type and mutant genotypes of the Micro-Tom cutins, but their absolute levels are very dissimilar. This discrepancy makes evident that future efforts need to focus on the establishment of an improved methodology, guiding the discovery of the true nature of the polysaccharides associated with cutin. Yet, with either method, the results might be influenced by self-assembly events (which are concentration and time dependent) and by the heterogeneity of the material. These events may interfere with a direct detection by immunoblotting or upon their hydrolysis. Ana Tomé (undergrad fellow in the lab, who has helped me with the GC-MS analyses included in this thesis), is setting up derivatization methods for polysaccharides detection by GC-MS. In line with

this, a different angle is also preliminary being pursued in the lab, focusing on the role played by flavonoids covering the hypothesis that covalent bonds and/or strong entanglement of these chemical compounds with the cutin matrix might exist.

I trust that the isolation strategy and the quantitative solution NMR methods developed in this thesis for cutin analysis, in combination with GC-MS analyses of hydrolysates, will soon become the gold standard approach to dissect the chemical plasticity of cutin in different sources, including fine characterization of the impact of specific mutations (Chapter II and III). This has attracted substantial interest by several groups, some of which initiated collaborations with the Silva Pereira's group on very distinct topics in either cutin or suberin. As an example, the lab is analyzing suberin extant in the roots of several different plant sources, confirming the potential of our workflow to disclose its *in situ* polymeric organization, despite of a low abundance in roots.

We have decided to stretch the potential of our workflow to (maybe) a limit – ionic liquid extraction, cryogenic milling of the resultant polymer and NMR analysis, by focusing on sporopollenin. The biopolymer sporopollenin is present, for example, in the outer wall of pollen grains and shares reported chemical similarities to cutin. The aim is to disclose its true chemical nature, especially as we noticed that the sporopollenin chemical fingerprint is modified when isolated using the conventional process (acetolysis). This study is currently being pursued by Lúcia Albano (MSc student in the lab).

While I have not become an expert on NMR during this thesis, I have learned how to prepare samples of very complex polymers for NMR analysis. I learned the importance of some technical modifications that greatly improve the analytical resolution: (i) the use of a cryoprobe (increases sensitivity; confirm some assignments by HMBC), (ii) fine adjustment on the acquisition times and temperatures (increases the signal resolution), (iii) use of internal standards (absolute quantification of specific bonds), and (iv) labelling specific groups (*e.g.* free OH groups reactive to phosphorylation agents) – all of which

help us to setup a matchless quantitative approach for the analysis of the structure of plant polyesters. I observed the start of the adventure of using solution NMR for suberin. This was instrumental and inspirational, largely defining the way I have approached Chapters II and III of my thesis. The NMR workflows that were established for either plant polyesters, are helping other studies focusing plant polymers and extractives. Taken as example, NMR is being used to fingerprint the diversity of resin acids in Portuguese pine trees, before and after their biotransformation by fungi (PhD student Ângela Pinheiro) and to characterize woody outer barks (Post-Doc Artur Bento).

The data generated for cutin on this thesis was gathered with data focusing on suberin to define the **rules of thumb for the quantification of the structure-property relationships of plant polyesters** (Chapter III). It is relevant to state that we have detected distinctive chemical features in pepper cutin (*e.g.* presence of epoxide groups); we have not explored this aspect further, but it provides another cutin structural variant for future tests focusing its multifunctionality *in planta*. These rules make possible to use the macromolecular arrangement information of a given plant polyester to anticipate the thermal and crystalline properties of the ensuing materials. This creates unprecedent opportunities to use solution NMR to screen different raw materials or industrial residues to decide the best route for their valorization. Additionally, it may help deciding on strategies to combine different materials and guide selection based on unique chemical features, favoring *e.g.* a specific thermal behavior. Although this was not central for my thesis, I think it will be extremely useful for projects focusing applied research on bio-based materials. Besides, since cutin builds a defensive barrier *in planta*, it may be anticipated that the opposite route is also very relevant, *i.e.* use measurements of specific physical properties of the plant material to predict key chemical characteristics of the composing polyester (*e.g.* presence/number of epoxides and free OH in cutin).

Conditions were set to pursue the final aim of this thesis: test the **potential of cutin-derived oligomeric molecules to induce pattern-triggered immunity (PTI), acting as damage-associated molecular patterns (DAMPs)**. The opening hypothesis is in line with the identification of other DAMP molecules originating from the cell wall polysaccharides (*e.g.* OGs and cellobiose) that are of oligomeric nature[6]. The focus on cutin arose naturally by a series of reasons: it covers the aerial tissues of most land plants, constituting a defensive shield and compared to suberin presents lower chemical complexity at the level of the diversity of monomeric constituents. Through the course of this thesis, I verified that the ionic liquid process for purification of cutin was easy, time-efficient and with high recovery yields, securing our option of focusing on cutin.

Results obtained in the initial screening comprising cutin as well as cutin oligomeric mixtures (COM), supported the hypothesis that **mild cleavage of cutin generates chemical signals able to initiate immune responses in plants** (Chapter IV). The fact that we were able to observe immune responses elicited in three different model plants, belonging to two different families, ensured us that the response was not plant-specific. To perform a systematic characterization of the potential of cutin oligomeric molecules to induce first line immune responses, such as a ROS burst and calcium influx, we chose *Arabidopsis thaliana* as our model. The choice was based on the fact that most of the immune assays are already efficiently established on this plant. Moreover, the possibility to explore a number of specific mutants to try to identify families of receptors involved in the perception of such signals supported our choice. The **ability of COM to activate MAP kinases and transcriptional reprogramming was observed**. Collectively, the results gathered in Chapter IV suggest that the **COM consists of a mixture of different molecules, comprising monomers and oligomers but the main elicitor is likely oligomeric**. All tested cutin monomers – either generated through extensive depolymerization of cutin or pure compounds – systematically failed to induce any of the measured

immune outputs, irrespective that the conditions were similar to those used for testing the COM. Nevertheless, the fact that pure monomers were already reported as inducers of ROS production and of differential expression of defense genes[7], still needs to be taken in consideration. Measuring ROS was one of the biggest challenges of Chapter IV. Under the conditions tested, we could only observe a ROS response when testing cutin with minor degree of cleavage. This could be indicative that when the polymer is cleaved, specific groups are exposed that might react with the HRP enzyme, depleting its action, and hence preventing luminescence measurements. The TLC data suggest that phenolic compounds are present in our COMs. This could explain the loss of signal observed after co-treatment with flg22 and COM, as phenol oxidation is reported to inactivate the HRP enzyme[8]. This aspect needs to be revisited after measuring the concentration of phenolic compounds in COM, as the inhibition of HRP depends on the enzyme: inhibitor ratio. These observations also suggest that future efforts should consider the possibility that the activity of the elicitor molecule might depend on an aromatic group linked to one or more aliphatic monomers. In Chapter III, we synthesized a model compound, built by a monomer linked to an aromatic acid (ethyl 4-hydroxy-3-methoxy-cinnamate) and this will be one of the compounds to test in the future for the same set of immune outputs explored in Chapter IV. Another possibility is to label phenolic compounds present in COMs, allowing a precise quantification of these chemical features by solution NMR. This will be the future focus, exploring the labeling of phenolic groups already established in the lab or alternative ones, such as the use of iodide for specific NMR techniques[9].

The biggest challenge continues to be the fact that we are dealing with a heterogeneous mixture. Moreover, the results indicate that we might be searching for a low molecular weight oligomer. This was confirmed by preliminary MALDI-TOF MS analysis of COM (not presented on this thesis), which revealed the presence of molecules resulting from two or three monomers linked together, as well as the presence of other unknown chemical

features. Adding to this, a third challenge is presented: the production of sufficient amounts of the COMs to allow activity guide fractionation. Currently, we are exploring this using size exclusion chromatography techniques, with the aim of understanding the degree of polymerization of the molecules present in our mixtures. Preliminary tests are already running to allow the precise identification of the molecular weight of molecules present in our samples. Subsequent steps will include combining this analysis (and the abovementioned analytical methods) with TLC-guided fractionation of our mixtures followed by tests on the immune eliciting activity of each resulting fraction. Objectively, we want to get more homogeneous and active fraction(s), and then study the chemical identity of the active molecule by LC-MS.

Gas chromatography-based characterizations of the COMs made evident their chemical complexity, although less heterogeneous than the cutin from which they originated. Such complexity hinders any attempt to infer what are the true differences between both COMs, solely by GC-MS. Nonetheless, NMR spectra of COMs clearly show that oligomers are present in these mixtures, due to the presence of both linear and secondary esters. Direct comparison of the two COMs by TLC points to a decrease in complexity in COM II. This decrease of complexity suggests an enrichment of this mixture in the active molecule, which is supported by its stronger activation of a Ca^{2+} response. Moreover, the 'intact' cutin shows two peaks of activation of Ca^{2+} influx; this may be indicative that more than one active molecule exist in cutin, one of which is enriched in the COMs. As such, a winning strategy might be based on this kind of comparisons between complex mixtures, followed by their chromatographic fractionation and testing Ca^{2+} influx and/or MAP kinase activation. In the latter case, we observed that both cutin and COM are able to induce MAP kinase activation after 10 min of treatment, compared to the mock control. In the case of COM II, it seems that the same trend can be observed, but the tests still need to be repeated to confirm this observation.

Getting to the chemical identity of a 'pure' eliciting molecule would allow, among other things, to overcome the technical difficulties experienced with ROS measurements, or look for alternative ways of testing such response. Alternatives might include DAB staining, already tested for long-term accumulation of intracellular ROS after treatment with cutin monomers[7], or the use of genetically-encoded ROS sensors[10]. Such achievement will also have a tremendous impact on the evaluation of the potential of this molecule to induce transcriptional reprogramming. In this thesis, a first look into this effect was possible after treatment of *Arabidopsis thaliana* seedlings with COM. For this first snapshot, we used a single time-point and performed a direct comparison with mock treatment. The selected time-point demonstrates the potential of the mixture to induce transcriptomic alterations in the plant, confirming that the responses triggered are common to other reported elicitors of immunity. Moreover, a degree of uniqueness could be detected in the triggered effect, comparable in degree to potent elicitors such as flg22, despite the lower number of induced genes. The possibility to test a pure molecule could confirm if this uniqueness is even stronger, and could help better dissecting the effect on some cellular processes shown to be responsive to COM treatment. Having a pure compound would also allow us to test additional outputs such as the ability to induce resistance against specific pathogens. In fact, this was preliminarily tested by Marta Bjornson (Post-Doc in the Zipfel's Lab). Initial tests failed likely due to the presence of aggregates in water that induced wounding upon infiltration. This is one the questions we will need to revisit once pure compounds are available to be tested.

A last challenge that remains, even after obtaining the chemical identity of the eliciting molecule, will be the identification of the receptor for this DAMP. In fact, an initial effort was made by testing MAP kinase activation, in different mutants of common co-receptors from the SERK and CERK families. These mutants were however still responsive to treatment, suggesting that the elicitor(s) present in COM is/are perceived by PRRs other

than LRR and LysM families of receptors. This **clearly points out to a yet non-described perception pathway for COM** that may or may not share steps with other immune signaling pathways of known DAMPs. Future efforts may also include a refining of the transcriptome analysis, concerning the establishment of a time course analysis with our pure elicitor molecule. This could be used to guide the selection of uncharacterized genes with reported receptor domains to generate specific mutant lines to help the identification of the receptor of cutin oligomers.

Finally, it would also allow to assess the safeness of such molecule for soil and agronomical environments, opening new opportunities to explore such molecules for their use in prophylactic plant treatments to prevent specific pests. This strategy is also aligned with the European Commission Green Deal principles and the United Nations Sustainable Development Goals, previously mentioned on this discussion.

References

1. Xin, A. & Fry, S. C. Cutin:xyloglucan transacylase (CXT) activity covalently links cutin to a plant cell-wall polysaccharide. *J. Plant Physiol.* **262**, 153446 (2021).
2. Moreira, C. J. *et al.* An ionic liquid extraction that preserves the molecular structure of cutin shown by nuclear magnetic resonance. *Plant Physiol.* pp.01049.2020 (2020) doi:10.1104/pp.20.01049.
3. Petkovic, M. *et al.* Novel biocompatible cholinium-based ionic liquids—toxicity and biodegradability. *Green Chem.* **12**, 643 (2010).
4. Karinkanta, P., Ämmälä, A., Illikainen, M. & Niinimäki, J. Fine grinding of wood – Overview from wood breakage to applications. *Biomass and Bioenergy* **113**, 31–44 (2018).
5. Li, M. & Wang, X. R. Peak alignment of gas chromatography–mass spectrometry data with deep learning. *J. Chromatogr. A* **1604**, (2019).
6. de Azevedo Souza, C. *et al.* Cellulose-derived oligomers act as damage-associated molecular patterns and trigger defense-like responses. *Plant Physiol.* **173**, 2383–2398 (2017).
7. Park, J. H., Suh, M. C., Kim, T. H., Kim, M. C. & Cho, S. H. Expression of glycine-rich protein genes, AtGRP5 and AtGRP23, induced by the cutin monomer 16-hydroxypalmitic acid in Arabidopsis thaliana. *Plant Physiol. Biochem.* **46**, 1015–1018 (2008).
8. Mao, L., Luo, S., Huang, Q. & Lu, J. Horseradish Peroxidase Inactivation: Heme Destruction and Influence of Polyethylene Glycol. *Sci. Reports 2013 31* **3**, 1–7 (2013).
9. Kagawa, N., Suzuki, M., Kogure, N. & Toume, K. Characterization of organic iodides with iodine-127 nuclear magnetic resonance spectroscopy. *Tetrahedron Lett.* **56**, 5795–5798 (2015).
10. Anjum, N. A., Amreen, Tantray, A. Y., Khan, N. A. & Ahmad, A. Reactive oxygen species detection-approaches in plants: Insights into genetically encoded FRET-based sensors. *J. Biotechnol.* **308**, 108–117 (2020).